

A Novel, Free-Space Broadband Dielectric Measurement Technique

Yaqiang Liu

Supervisor: Dr. Paul O'Leary

**Submitted in partial fulfilment of the requirements for the degree of
DOCTOR OF PHILOSOPHY**



**Department of Engineering Technology
Waterford Institute of Technology
Main Campus Cork Road, Waterford City, Ireland.
Submitted to Waterford Institute of Technology, May 2014**

Abstract

Frequently, when free-space electromagnetic waves pass through a material, there will be some form of interaction between the wave and the material. Measuring this change forms the basis of free-space, dielectric material measurement, where the variations will be attenuation and a phase change relative to the wave when the material was not present and are typically recorded over a broadband range of frequencies.

In this work a new technique is presented to accurately perform free-space broadband material measurement to calculate the dielectric response of materials of unknown electrical length. (In this thesis, the electrical length means that while the physical length of the path is known, the number of wavelengths in the material is unknown, due to the unknown permittivity. This unknown number of wavelengths is described as the electrical length both here and also in many other works.) The technique is eventually applied to a more difficult form of material to measure, which is material in the form of powders and liquids. Powders and liquids present a particularly difficult challenge in that they must also be contained in a container of uniform shape and sufficient cross-section to guarantee that the entire received wave has passed through the same amount of material. The technique presented works for containment vessels with no or some dielectric response (respectively being relatively easy analysis and very difficult for dielectric analysis).

Much of the work is devoted to the development of a test infrastructure and also a new vector network analyser (VNA) calibration technique that would be more appropriate to this infrastructure and kind of measurement than existing techniques. In terms of the latter point, to minimise measurement errors a free-space, broadband Thru-Reflect-Line/Match (TRL/M) calibration technique was developed. The challenge of a test structure for materials with an unknown electric length was met by offering the ability to vary the thickness of material through which the probing wave passes. Moreover, the range over which the thickness could vary was quite large (3 mm up to 18 cm) to accommodate

materials of unknown electrical length with dielectric constant values over a wide range (2 to 80).

Two measurement techniques are presented based on horizontal and vertical probing wave propagation, both of which allow for a series of measurements to be taken where the varying parameter is thickness of material under test. However, the horizontal propagation measurements required an extra containment layer (to contain the powder/liquid on both sides normal to the propagation, rather like a large, slim fish tank), compared to the vertical propagation measurement, but had significant mechanical and also the computational difficulties mentioned earlier. The vertical propagation measurements on the other hand show more promise, both in terms of mechanical containment and also in the inversion of the measured S-parameters to arrive at the complex electric permittivity.

The measurements were performed in a large hall and also in a Radio Frequency (RF) anechoic chamber (optimal test range of approximately 500 MHz – 18 GHz).

Several diverse solid materials were tested initially in developing the test infrastructure including double glazed standard and low emissivity windows, common building materials, house insulation materials and automobile glass. Once the platform and calibration technique were completed to a satisfactory level, measurements intended for dielectric analysis were carried out on commercial glass panes, water and household plain flour. All measurements were subsequently published in various conferences and workshops, hosted by the IEEE, IEEE Communications Society, IET, the European Association on Antennas and Propagation (EurAAP) and the Royal Irish Academy's research Colloquium on Communications and Radio Sciences workshop.

Declaration

I hereby declare that this document is entirely my own work and does not contain material previously published by any other author, except where due reference or acknowledgment has been made. Furthermore, I declare that this document has not previously been submitted to any other institution for any other academic award.

Signed: _____

Yaqiang Liu

W20018753

Acknowledgement

Firstly I would like to thank Dr Paul O’Leary, who is my PhD supervisor. Without him, I would never finish this PhD. He guided me throughout this PhD and always offered me advice and support. He was patient to correct and advise with all of the small mistakes in my thesis and in my research life. To me, Dr Paul O’Leary is not only a supervisor, but my life mentor.

Furthermore it was a pleasure to work with my former colleagues Dennis Stolhofer and Youssef Elgholb. They gave me good support on my research and they will always be my good life time friends.

Last, but not least, I would like to thank my family for providing me with their trust and support to me and for offering their endless love to me. To them I dedicate this thesis.

In addition I would like to thank everyone who supported me during this research.

Table of Content

1	INTRODUCTION	2
1.1	Dielectric analysis	2
1.2	Motivation	2
1.3	Approach and novelty	3
1.4	Applications	3
1.5	Thesis layout	4
2	ELECTROMAGNETIC PROPERTIES OF MATERIALS	7
2.1	Dielectric material research	7
2.2	Material research at microwave frequencies	9
2.3	General electromagnetic properties of materials	9
2.3.1	Electron energy bands	10
2.3.2	Dielectric	11
2.3.3	Dipole Moment	14
2.3.4	Reflection and transmission	15
2.3.5	Electromagnetic wave propagations in materials	17
2.4	Dielectric material properties	18
2.4.1	Electromagnetic material interaction Mechanisms	18
2.4.2	Debye relaxation time	22
2.5	Literature review of measurement techniques	25
2.5.1	Reflection method	27
2.5.2	Transmission/reflection method	29
2.5.3	Conversion techniques	30
2.6	Selection of Technique	36
2.7	Matrix calculation	38
2.8	Conclusion	38

3	DEVELOPMENT OF MEASUREMENT ENVIRONMENT	39
3.1	Measurement components	39
3.1.1	Vector network analyser	40
3.1.2	Calibration kit for VNA	41
3.1.3	Precision Total Station	42
3.1.4	Cable	43
3.2	Antenna	43
3.3	Antenna radiation pattern	44
3.3.1	Standing Wave Ratio (SWR)	45
3.3.2	Two antenna gain method	46
3.3.3	Mounting height over the ground	48
3.4	Antenna near and far field boundary theories	49
3.4.1	Large hall	55
3.4.2	Flexible thickness container design	57
3.4.3	Anechoic chamber	59
3.5	Wireless propagation testing	62
3.5.1	Energy efficient windows	63
3.5.2	Building materials	64
3.5.3	Vehicle glass and window tints	65
3.6	Conclusion	66
4	PERMITTIVITY AND PERMEABILITY PARAMETER EXTRACTION	
	ALGORITHMS	67
4.1	Nicolson-Ross-Weir technique (NRW)	68
4.2	NIST iterative technique	71
4.3	New non-iterative technique (NNI)	73
4.4	Free space measurement technique	74
4.5	ABCD matrix conversion	77
4.6	Conclusion	81
5	MEASUREMENT RESULTS AND ANALYSIS	82
5.1	Antenna measurements	82

5.1.1	Voltage Standing wave ratio (VSWR)	82
5.1.2	Antenna radiation pattern	85
5.2	Calibration	87
5.2.1	Standard calibration	87
5.2.2	Self-calibration techniques	88
5.3	Anechoic chamber validation	90
5.4	Coated window measurement	92
5.5	Standing wave analysis	95
5.6	Building material measurement	102
5.7	Vehicle window & tints measurement	104
5.8	Dielectric material measurement and analysis	105
5.8.1	Solid glass dielectric constant	106
5.8.2	Dielectric powder and liquid measurements	109
5.8.3	Horizontal setup disadvantages	114
5.8.4	Vertical measurement proposal	115
5.8.5	Uncertainty terms analysis	117
5.9	Conclusion	118
6	CONCLUSION & FUTURE RESEARCH	119
APPENDICES		121
Publications		121
Relevant documents		146
BIBLIOGRAPHY		155

List of Figures

Figure 1-1 Applications of free space dielectric analysis	4
Figure 2-1 a) Non-polar material; b) Polar material [3].....	8
Figure 2-2 Energy band for different types of materials (modified from [8])	10
Figure 2-3 Dielectric dipolar change under the external electric field.....	13
Figure 2-4 Molecular dipole moment	14
Figure 2-5 Incident transverse electromagnetic field (TEM-Wave) reflected by and transmitted through a material boundry [14]	15
Figure 2-6 Incident waves transfer from air to materials, with corresponding equations....	17
Figure 2-7 Electromagnetic frequency response of water with key interaction mechanisms	19
Figure 2-8 Random dipole vector movement (two dimension)	19
Figure 2-9 Dipolar (orientation) polarisation [15]	20
Figure 2-10 Debye relaxation of water, Methanol and Ethanol at 20° C descriptions.....	23
Figure 2-11 Wave transmission and reflection example, as wave passes the boundary of two different materials	26
Figure 2-12 Open circuit reflection method with a coaxial cable.....	27
Figure 2-13 Short circuit reflection method [20]	28
Figure 2-14 A two-port network with input wave “ <i>a</i> ”s and output wave “ <i>b</i> ”s.....	29
Figure 2-15 Sample transmission line of Transmission/reflection of electromagnetic wave	30
Figure 2-16 Free space measurement simple structure	34
Figure 3-1 Measurement system setup diagram	39
Figure 3-2 Rhode & Schwarz vector network analyser ZVB-20.....	40
Figure 3-3 Modified Pentax Total Station for antenna mounting	43
Figure 3-4 Antenna pattern measurement structure	45
Figure 3-5 Diagram of two antenna gain method	47
Figure 3-6 Ground wave reflection between 1 m and 1.5 m antenna height	48
Figure 3-7 Position of the earliest ground reflection at transmitter antenna heights of 1 m and 1.5 m for all test frequencies	49
Figure 3-8 Antenna near field and far fields [45]	49

Figure 3-9 Phase error at the edges of a test antenna in the far-field when illuminated by a spherical wave [19]	51
Figure 3-10 Impedance of E and H-fields moving away from the antenna	53
Figure 3-11 Different far field boundaries for Schwarzbeck BBHA 9120.....	54
Figure 3-12 Far field boundaries for second pair of antennas 7.5GHz to 15 GHz measurement setup	55
Figure 3-13 Custom-built test frame, was built by PhD candidate and used in WIT. Unit: mm	56
Figure 3-14 Free space test structure, was used in the National Institute of Standards and Technology (NIST) in Boulder, Colorado, USA [46]	56
Figure 3-15 Test structure with glass tank placed.....	57
Figure 3-16 Glass tank assembly	57
Figure 3-17 Horizontal design of glass tank container with a flexible thickness	58
Figure 3-18 Horizontal design structure of glass tank container with a flexible thickness, in the picture indicated position of glass pane and spacer, which control the material thickness.....	59
Figure 3-19 WIT Anechoic chamber, which this PhD candidate was involved in the designing building and characterising work	60
Figure 3-20 Measurement of attenuation at the door (normal incidence).....	61
Figure 3-21 Measurement of attenuation at the sidewall (normal incidence).....	61
Figure 3-22 Measurement of attenuation through the door (normal incidence)	62
Figure 3-23 Energy efficient window measurement.....	63
Figure 3-24 Building materials tested	65
Figure 4-1 Cancellation leading to a small S_{11} value	70
Figure 4-2 ϵ_r versus frequency for a PTFE sample.	71
Figure 4-3 Two-port transmission network	79
Figure 5-1 Published SWR data of horn antenna Schwarzbeck BBHA 9120 LF (A) [51] .	83
Figure 5-2 Measured SWR of the horn antenna Schwarzbeck BBHA 9120 LF (A).....	84
Figure 5-3 Measured VSWR of the horn antenna Schwarzbeck JXTXLB-90-20-C.....	84
Figure 5-4 Measured E-plane antenna pattern (Schwarzbeck BBHA 9120 LF (A)).....	85
Figure 5-5 E and H-plane antenna pattern (JXTXLB-90-20-C)	86
Figure 5-6 VNA reference plane explanation	87
Figure 5-7 TRL/M free space calibration standard, developed by PhD candidate Yaqiang Liu	90

Figure 5-8 E-plane anechoic chamber validation, Green is reference line and red/blue are signal attenuation	92
Figure 5-9 S_{11} validation for WIT anechoic chamber, the reference line is taken from the S_{11} data from the roof (blue). The red trace is where the antenna pointing to the wall inside chamber	92
Figure 5-10 Different glass attenuation compare at 5m from large hall	93
Figure 5-11 Propagation results from anechoic chamber at 1.65m	94
Figure 5-12 Glass propagation measurements due to the different thickness of plain glass, from [52]	94
Figure 5-13 TiO ₂ /Ag/TiO ₂ coating transmittance and reflectance [53].....	94
Figure 5-14 Normal 4mm glass transmission attenuation result with trend line	96
Figure 5-15 Normal 4mm glass transmission phase change result (with angle wrapping at 180°).....	97
Figure 5-16 Multiple standing wave	98
Figure 5-17 Standing wave chart from cable calibration	98
Figure 5-18 DFT result of cable validation.....	99
Figure 5-19 DFT chart converted to distance response chart	101
Figure 5-20 100mm concrete blocks S_{21} results at 5m separation, frequency range: 800MHz to 6GHz	102
Figure 5-21 Natural Slate (1m by 1m) on 8mm plywood board S_{21} Results at 5m separation	103
Figure 5-22 Synthetic Slate (1m by 1m) on 8mm plywood board S_{21}	103
Figure 5-23 Foil backed insulation, graphite-impregnated polystyrene insulation, rockwool and plain polystyrene sheet sample results. (The results of graphite-impregnated polystyrene insulation, rockwool and plain polystyrene are similar and all close to 0 dB, therefore, only two lines are shown in the chart)	104
Figure 5-24 Three different car window tint film S_{21} results at 1.65m measurement distance (the losses of light smoke and limo black tints are very close to zero, therefore, only two lines are shown in chart)	105
Figure 5-25 Dielectric constant of glass pane with different thickness glass	107
Figure 5-26 Plain flour dielectric constant.....	110
Figure 5-27 Tap water dielectric constant.....	112
Figure 5-28 Lens effect caused by insufficient container rigidity	114
Figure 5-29 Lens effect in salt test (deliberate misalignment reconstructions).....	115
Figure 5-30 Misalignment reconstruction tests.....	115
Figure 5-31 Candidate vertical measurement system, in WIT anechoic chamber.....	116

Figure 5-32 Vertical measurement system, photo shoot in WIT anechoic chamber 116

List of Tables

Table 2-1 Relaxation parameters at 20°C 24

Table 2-2 Relaxation parameters at 25°C 24

Table 2-3 Comparison between different conversion techniques explanation 36

Table 3-1 Range criteria for far field boundary definition..... 54

Acronyms

EMC:	Electromagnetic Compatibility
MUT:	Material under Test
NIST:	National Institute of Standards and Technology
NNI:	New Non-Iterative technique
NRW:	Nicholson, Ross and Weir
OSM:	Open, Short and Match
OSLT:	Open, Short, Line and Through
RF:	Radio Frequency
TRL:	Thru-Reflect-Line
TRL/M:	Through-Reflect-Line/Match
VNA:	Vector Network Analyser
VSWR	Voltage Standing Wave Ratio
WIT:	Waterford Institute of Technology

1 Introduction

This work presents a novel approach to a well-studied area of material analysis, namely dielectric analysis. In dielectric analysis, materials which exhibit dielectric properties will interact with incident electromagnetic fields and the manner and scale of the interaction can be measured and analysed to determine those very dielectric properties.

1.1 Dielectric analysis

Some materials interact significantly with incident electromagnetic waves and the manner of their interaction can be used to gain useful information about the materials themselves. This thesis examines interactions for one such category of materials, namely dielectrics. Dielectrics are defined by their interaction with electric, magnetic or electromagnetic fields. In a dielectric, electric field influence can be brought to bear, not alone to cause electronic transfer (electronic polarisation), but also through displacement of anions and cations in ionic crystals (ionic polarisation) and finally also by realignment of molecular permanent dipoles (orientation polarisation). The dielectric's electrical response is often defined as the material permittivity and importantly this response is frequency dependent.

1.2 Motivation

Dielectric material measurement research can be carried out as a branch of electromagnetic wave propagation research. In this regard, some of the early work described here, involved developing a test platform, and thus simply focussed on measuring the propagation attenuation caused by different materials, such as domestic energy insulation materials. The technique developed was eventually applied to a more difficult form of dielectric material to measure, which is material that is difficult to contain uniformly as it is in the form of powders or liquids. Powders and liquids present a particularly difficult challenge in that they must also be contained in a container of uniform shape and sufficient cross-

section to guarantee that the entire received wave has passed through the same amount of material.

1.3 Approach and novelty

Dielectric measurements were taken at more than one Material under Test (MUT) thickness, so that the electrical length ceases to be an analysis variable (detailed in Chapters 4 and 5). In the case of powders and liquids, this means either having multiple containers or a single container whose thickness can be varied in a controlled manner. The latter approach was adopted in this work, whereby initial measurements were on a fixed container in order to prove aspects of the measurement technique. Subsequently the container was replaced with a second more elaborate and therefore also more flexible one, also capable of use in the measurements of powders and liquids. At least two or, in some cases, three different thickness of MUT are required for the new approach. This novel platform design initially consisted of a flexible container made of glass panes, which can be collectively used to set the thickness of test materials.

In addition, a new vector network analysers (VNA) calibration technique was developed, that would be more appropriate to this infrastructure and kind of measurement than existing calibration techniques. In terms of the latter point, to minimise measurement errors, a free-space, broadband TRL/M calibration technique was developed. The challenge of a test structure for materials with an unknown electric length was met by offering the ability to vary the thickness of material through which the probing wave passes.

1.4 Applications

This research work can be applied to several areas (Figure 1-1), such as in,

1. Moisture determination, applies to solid and powders
2. Energy transfer: drying wood, glue production and food heating efficiency
3. Structure analysis: drug powder homogeneity, tablet compression phase

4. Environmental contamination: ground contamination measurement, as the underground penetration
5. Applications in high-speed electronics design (power and signal integrity), where an understanding of the dielectric variation with frequency, for example clock frequency, is vital
6. In Telecommunications, for example in antenna design



Figure 1-1 Applications of free space dielectric analysis

1.5 Thesis layout

This PhD thesis presents a novel, feasible approach to measurement of dielectric properties for materials with an unknown electric length.

In the initial work a test platform was developed to measure microwave propagation through the increasingly popular energy efficient glass windows. This work leads, via modifications to the test structure, to non-destructive material testing, by measuring the amplitude and phase variations in microwave signal propagation through various materials. A VNA is used to measure scattering parameters from the test structure.

This thesis is structured as follows:

- Chapter 2 is the related literature review of dielectric material characterisation. It describes the fundamentals of dielectrics and its complex permittivity and also its dependence on frequency and materials. Also, some important wave-guiding transmission lines and their field descriptions will be discussed as well as resonators due to their relevance in measurement setups;
- Chapter 3 describes the test platforms developed in the course of this work in WIT; for propagation testing (including materials such as energy efficient glass, building materials and vehicle glass), development of a far field definition to define the actual measurement field, characterisation of the two antenna pairs, simple and progressively more elaborate VNA calibration, horizontal and vertical propagation measurement techniques, construction of several test frames, construction and qualification of an RF anechoic chamber, development of an ability to measure variable material thicknesses for both the horizontal and vertical techniques. For each of these points, the selection parameters are explained and justified and a description is offered of the various problems encountered and solutions attempted.
- Chapter 4 presents the various algorithms that can be used to extract the permittivity and permeability values from measured S-parameters, as well as the S-matrix algorithms that can be used in permittivity calculation. The four algorithms listed here are Nicholson-Ross Weir (NRW), National Institute of Standards and Technology (NIST) iterative, the New Non-Iterative (NNI) techniques and the Free-space technique. In this thesis, the free- space technique is used for calculating the dielectric constant. To conquer the unknown electrical length problem, a propagation constant is treated as a complex number and with the test platform's controlled variable material thickness possibility, the dielectric constant can be calculated.
- Chapter 5 presents all the measurements and data analysis results; from the early propagation test results to the subsequent complete dielectric measurement results and analysis. For the early propagation tests, energy efficiency glass, building materials, insulation materials and vehicle windows are examined. From these results it can be seen that some of those type of materials have a very strong attenuation to RF signals. For dielectric materials, glass, water and plain flour are

tested. The permittivity results are close to the published values. The horizontal test structure was used for most test setups, but some final results presented were taken from a new vertical set-up.

- Chapter 6 outlines the work proposed for future work. A newer design of the vertical structure is presented, overcoming many of the disadvantages of the current measurement structure.

2 Electromagnetic Properties of Materials

2.1 Dielectric material research

Some materials interact significantly with incident electromagnetic waves and the manner of their interaction can be used to gain useful information about the materials themselves. This thesis examines interaction one such category of materials, namely dielectrics. Dielectrics are defined by their interaction with electric, magnetic or electromagnetic fields. In a dielectric the electrons are tightly bound, thus there are no conductive properties. However, the dielectric molecules may have a polar moment, due to positional charge imbalances, although overall the molecule has no net charge [1]. In the presence of an external electric field, a dielectric exhibits certain electrical properties not present in other non-conducting materials. For example, many non-metallic crystals are of this nature. There are two broad types of dielectric, defined in *Polar Molecules* in 1929 [2]:

- 1) Non-polar molecular dielectrics. The molecular electron cloud is distributed with spherical symmetry relative to the positively charged centre. Therefore, in the absence of an external electric field, the positive and negative charge centres are coincident, so that the dipole moment $\vec{P}=0$. For example, the ground state of the hydrogen (H), carbon dioxide (CO_2) molecules and so on are all non-polar dielectrics.
- 2) Polar molecular dielectrics. The distribution of the molecular electron cloud is not distributed with spherical symmetry relative to the positively charged centre and the positive and negative charge centres do not coincide, so that each molecule has a dipole moment \vec{P} , for example, CO , HCl , H_2O , etc.

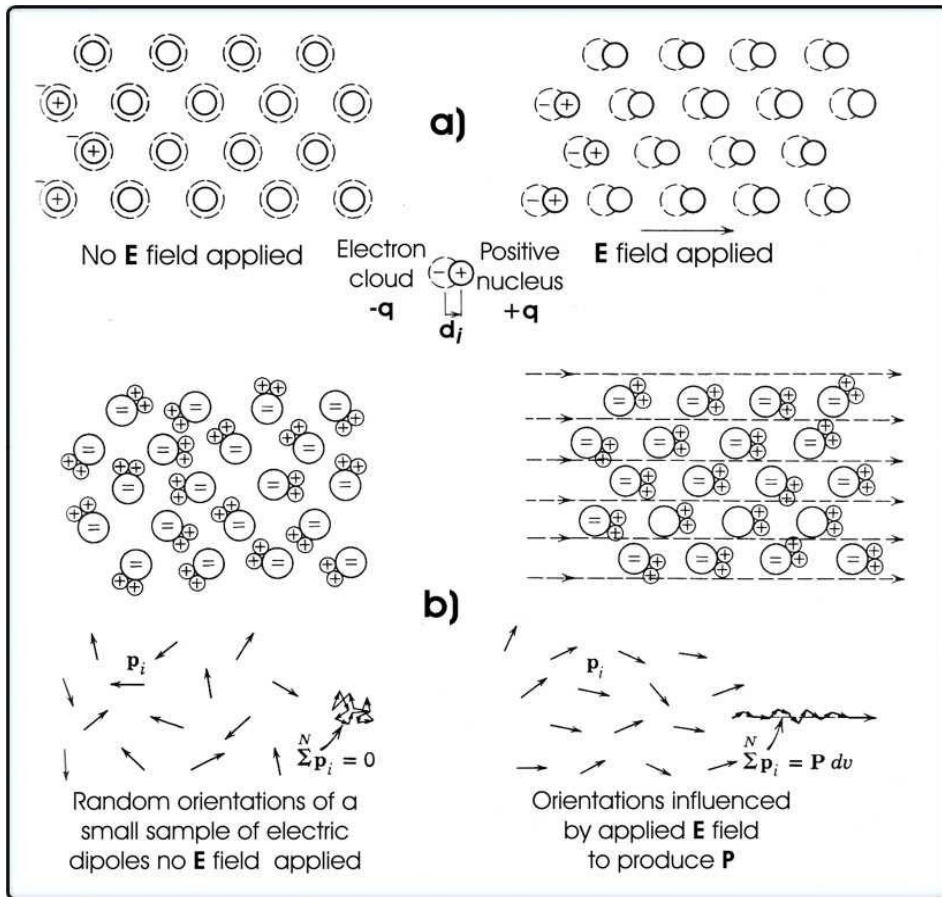


Figure 2-1 a) Non-polar material; b) Polar material [3]

Although each dielectric molecule has an inherent electric dipole moment, however, in a normal state, since the molecular thermal vibrations are random, the orientation of this electric moment is also random. Therefore within a volume, the vector value of all molecules' electric moment is typically zero, as long as no external electric field is present. If, on the other hand, there is an external electric field and if the externally applied field is time-varying, then the response of the dielectric material depends on the ability of the material's polar moment to respond to that varying field. This ability to respond, especially as the frequency varies, is known as the dielectric response of the material. Given that dielectrics do have characteristic responses that vary with frequency, this work looks at developing a reliable, flexible test platform to characterise a subset of dielectric materials, namely powders and liquids. Solid dielectrics can and have been tested, but a key development in the test technique is to test the same material repeatedly, for various

material thicknesses. Therefore a test platform, which can contain powders and liquids and whose sides can be widened, was a design requirement for this work.

2.2 Material research at microwave frequencies

Microwave frequencies are often of interest in engineering, for example in the analysis and heating of materials, conveying higher data rates in telecommunications, developing higher speeds in electronic design and in medical or security imaging. Examples of these engineering opportunities at microwave frequencies can be presented in four distinct (but not exhaustive) areas.

- 1) The knowledge gained from microwave frequency material measurements contributes to understanding both microscopic properties, through molecular interaction, and macroscopic properties, usually via a large-scale collective molecular interaction. The work described here fits into this area.
- 2) Microwave frequency communications play an increasingly important role in industrial [4], military [5] and civilian lives. The need for higher data rates, in particular, has led to the use of the microwave range of frequencies, where wider bandwidths are typically available.
- 3) As electronic design has increased in clock speeds, it is now common to examine the microwave properties of individual components, complete circuits and electronic packaging [6]. Detailed examination also requires knowledge of both permittivity and permeability of the printed circuit board and even the local environment.
- 4) Microwave frequency energy is used to dry materials such as wood, to cure materials such as epoxies and ceramics and, for material non-destructive testing, such as, for example, tumour detection in the body [7].

2.3 General electromagnetic properties of materials

Materials are often classified according to their response to externally applied energy, an area of measurement generally classified as spectroscopy. Classifications such as opaque

or transparent, conductor or insulator, are helpful in understanding certain material qualities. Although texts often refer to dielectrics as insulators, this classification is crude and even misleading in the case of applied alternating fields. While dielectrics are indeed non-conducting in terms of direct current, a dielectric is more correctly any liquid, gas or solid that will polarise in the event of an electric field being externally applied [1].

The following section elaborates on the distinctions between conductors and insulators and between insulators and dielectrics.

2.3.1 Electron energy bands

A material's response to an externally applied electric field will be considered in terms of free electrons and polar moments. The former considers the atomic or molecular electron energy bands, i.e. the discrete energy levels of the molecular electron orbits. While this approach is not directly related to an explanation of dielectric qualities, it serves as a useful starting point, by defining materials, which are generally classified as insulators.

For simplicity only atomic electron energy bands in a solid are discussed here.

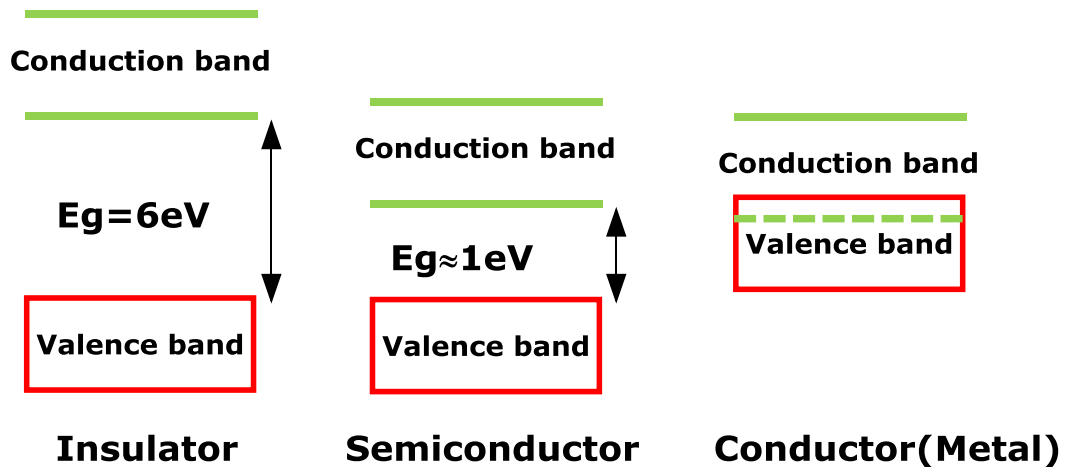


Figure 2-2 Energy band for different types of materials (modified from [8])

The highest energy band occupied by electrons at 0K is the valence band, which may be filled with electrons, either completely or partially. The conduction band is the energy band above the valence band. The electrons in the conduction band are free to move. However, there is an energy gap between these two bands. If the gap is large, there will be

no free electrons, such as in an insulator, and vice versa for a conductor. According to the band gap size between the valence and conduction bands, a material can be classified as an insulator, conductor or semiconductor. There is no band gap separating the valence and conduction bands in a conductor [9].

For insulators, the conduction band is completely empty and there is a large band gap (typically more than 2eV). When an external electric field is applied, it does energise the valence band electrons, but at low levels of external field, the new electron energy is not usually sufficient to cause it to jump the band gap and so there is no conduction of electricity. However, if the externally applied field is increased to sufficiently energise the electron, then conduction will occur, such as occurs in insulator electric breakdown. It should be no apparent that this should really be called insulator rather than dielectric breakdown, as is unfortunately the norm. At room temperature, the thermal energy (kT) of valence band electrons is much less than the band gap energy. For example, diamond is a (so-called perfect) insulator having a band gap of 5.5eV (at 300K) [10].

2.3.2 Dielectric

This thesis is, however, interested in a class of insulators, called dielectrics. A dielectric is an electrical insulator whose constituents can have an electric dipole structure under the influence of an externally applied electric field. Arthur R. Von Hippel stated that *"Dielectrics... are not a narrow class of so-called insulators, but the broad expanse of non-metals considered from the standpoint of their interaction with electric, magnetic, or electromagnetic fields. Thus we are concerned with gases as well as with liquids and solids, and with the storage of electric and magnetic energy as well as its dissipation [11]."*

In a dielectric, electric field influence can be brought to bear, not alone to cause electronic transfer (electronic polarisation), but also through displacement of anions and cations in ionic crystals (ionic polarisation) and finally also by realignment of molecular permanent dipoles (orientation polarisation). The dielectric's electrical response is often defined as the material permittivity and importantly this response is frequency dependent.

Ideal dielectrics have zero DC conductivity. When an external electric field is applied to them, the field tends to have some force on and between the molecules and also on their

individual components, although there is no free movement of electrons from molecule to molecule. Hence they do not have a net change in molecular charge, and tend instead to simply stretch and rotate. For simplification purposes, an assumption is made that our material is homogeneous, isotropic, source-free, free of charges and time invariant. This may be an over-simplification and in future work the possibility of a dielectric component with non-zero conductivity should be borne in mind.

Most dielectric measurement techniques focus on solid materials, whereas the technique developed here can be applied also to liquids and gases. When placing a dielectric in an electric field, positive and negative molecules orientate themselves along the electric field lines. This effect is known as polarisation [12].

Before the external electric field is applied, the molecules that make up the dielectric are typically in random orientations, so there should be no net electric field in the dielectric, even though, on a molecular level, there are many individual electrical dipole moments. When an external electric field is applied to the dielectric molecules, it will change the balanced condition, in a manner that depends on both the electric field and also the internal dipole moments. In the case of the externally applied electric field, different frequencies applied provoke different responses depending on the collective response of the dipole moments at those frequencies.

As mentioned earlier, the dielectric's electrical response is often defined as the material permittivity. Permittivity is usually expressed as

$$\varepsilon(f) = \varepsilon^*(f) = \varepsilon_o \varepsilon_r(f) \quad (2-1)$$

where

ε_o is the permittivity of free space

ε_r is the relative permittivity of the material

The (f) is included to highlight the frequency dependency of permittivity, but for convenience will be dropped hereafter.

The permittivity of free space may be represented as follows

$$\varepsilon_o = 8.85 * 10^{-12} F/m \quad (2-2)$$

In the materials considered in this research, the electric and magnetic properties are mainly determined by the material's permittivity (ϵ) and the permeability (μ). Moreover, as permeability defines the interaction when a magnetic field is applied the relative permeability is hereafter assumed equal to one ($\mu_r=1$), as it can be assumed the materials considered exhibit no significant magnetic properties and also that induced eddy currents are negligible. This assumption is tested and validated in the analysis of the results later. Electric and magnetic fields interact with the material in two ways: temporary energy storage and energy conversion into heat, which as it is energy removed from the travelling wave, is described henceforth as an *energy loss*. This is a correct term describing energy from the perspective of the travelling wave and not intended literally.

The relative permittivity is more conveniently expressed in complex form to represent the two mechanisms of energy storage and energy loss. Therefore (complex) permittivity may be written as [13]

$$\epsilon^* = \epsilon' + j\epsilon'' \quad (2-3)$$

This may also be represented, in terms of relative permittivity, as

$$\epsilon = \epsilon_r' \epsilon_0 + j\epsilon_r'' \epsilon_0 \quad (2-4)$$

The real part of the permittivity is usually called the *dielectric constant* and this determines both the velocity of electromagnetic wave propagation and also how much energy is stored in the material. The imaginary part represents the amount of energy that is lost to the wave. The complex value ϵ_r also captures the phase change or delay of the signal, due to passage through the dielectric.

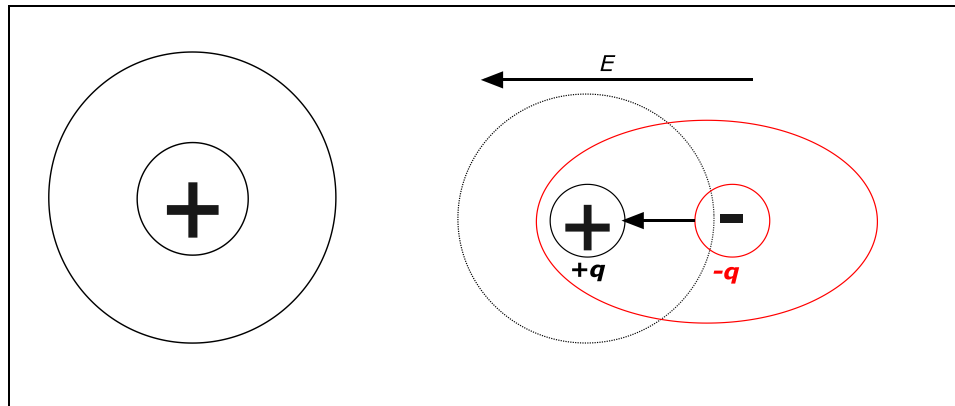


Figure 2-3 Dielectric dipolar change under the external electric field

It was mentioned earlier that the dielectric response depends in part on the nature of the electric field. This explanation here is simplistic, dealing as it does with only internal dipolar rearrangement, as shown in Figure 2-3. In fact there are other charge rearrangements that can occur, although the underlying reason is the same. The other mechanisms are significant at different electric field frequencies, as depicted later for water in Figure 2-7. Hence, their permittivity or dielectric response will change in a frequency dependent manner.

2.3.3 Dipole Moment

In a field-free environment, the total charge on a molecule is zero; however, the nature of chemical bonds is that the positive and negative charges do not completely overlap in most molecules.

The dipole moment depends partly on the separation between positive and negative charges. By taking two point dipoles as an example, the electric dipole moment for a pair of opposite charges of magnitude $+q$ and $-q$ is defined as the product of the magnitude of the charges and the distance between them, \vec{d} . The defined direction is toward the positive charge.

$$\vec{p} = \vec{d}q \quad (2-5)$$

where \vec{d} is the displacement vector pointing from the negative charge to the positive charge, as shown in Figure 2-4.

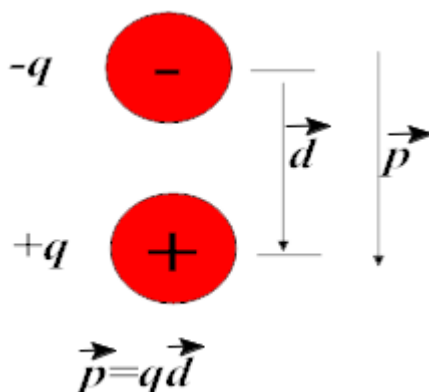


Figure 2-4 Molecular dipole moment

It is a useful concept in atoms and molecules (and dielectrics) where the effects of charge separation are measurable, but the distances between the charges are too small.

The Debye (D) is the unit for the dipole moment. The conversion of D is:

$$1D \approx 3.33564 \times 10^{-30} C.m \quad (2-6)$$

2.3.4 Reflection and transmission

When an electromagnetic wave hits a boundary between two materials at a normal angle, one part is reflected and one part is transmitted. The amplitudes of the reflected and transmitted waves can be calculated.

Consider a wave in air with E_i and H_i , arriving at a dielectric material interface. The wave will be reflected as E_r and H_r and transmitted as E_t and H_t at the boundary (as in Figure 2-5). The reflected and transmitted waves can be expressed, at the boundary, in terms of the incident wave combined with a reflection coefficient, Γ_b , and a transmission coefficient, T_b .

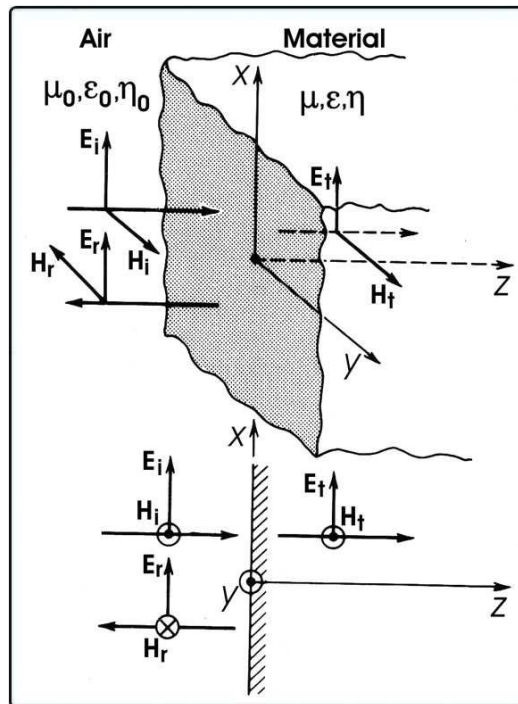


Figure 2-5 Incident transverse electromagnetic field (TEM-Wave) reflected by and transmitted through a material boundary [14]

$$\Gamma_b = \frac{E_r}{E_i} = -\frac{H_r}{H_i} = \frac{\eta - \eta_0}{\eta + \eta_0} \quad (2-7)$$

where, η_0 is the characteristic impedance of air,

η is the characteristic impedance of the dielectric material through which the wave is passing.

The relationship between free-space and material impedance, permittivity and permeability can be shown to be

$$\eta_0 = Z_0 = \sqrt{\frac{\mu_0}{\epsilon_0}}, \eta = Z = \sqrt{\frac{\mu_0 \mu_r}{\epsilon_0 \epsilon_r}} \quad (2-8)$$

And the reflection coefficient Γ_b at boundary can be shown to be a function of the impedance mismatch

$$\Gamma_b = \frac{Z - Z_0}{Z + Z_0} = \frac{\sqrt{\mu_r/\epsilon_r} - 1}{\sqrt{\mu_r/\epsilon_r} + 1} \quad (2-9)$$

The relationship can also be shown between the characteristic impedances, the reflection and transmission coefficient T_b

$$T_b = \frac{2\eta}{\eta + \eta_0} = 1 + \Gamma = \frac{\eta}{\eta_0} \times \frac{H_t}{H_i} \quad (2-10)$$

At the distance L from the boundary, T_b can be written as

$$T_b = e^{-\gamma L} \quad (2-11)$$

where γ is the material propagation constant

Note that henceforth in this work, T_b , will simply be referred to as T and also the propagation distance through the material will be referred to as d :

$$T = e^{-\gamma d} \quad (2-12)$$

Relating to dielectric constant, the higher ϵ_r , the higher the reflection coefficient and more energy is reflected from the surface [15].

2.3.5 Electromagnetic wave propagations in materials

Many aspects of wave propagation are dependent on material permittivity and permeability. Since the impedance of the wave in the material Z is different (lower) than the free space impedance Z_0 , an impedance mismatch occurs at the boundary causing part of the energy to be reflected from the material while the rest of energy transmits through the material. Once in the material, the wave velocity v_m is slower than the speed of light c . As the frequency does not change, then the wavelength in the material, λ_m , is shorter than the wavelength λ_0 in free space according to the equations given in Figure 2-6. The scale of reduction in wave energy after passage through the material is commonly known as attenuation or insertion loss.

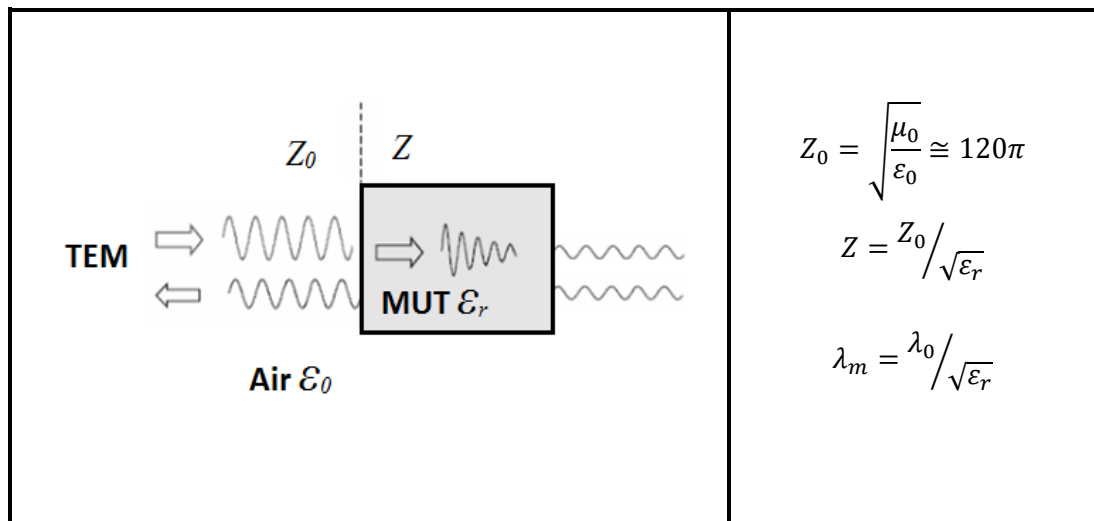


Figure 2-6 Incident waves transfer from air to materials, with corresponding equations.

2.4 Dielectric material properties

2.4.1 Electromagnetic material interaction Mechanisms

The response of materials to electromagnetic fields may be defined at microscopic or macroscopic levels. The macroscopic response is typically defined by the dimension and shape of an object made from that material.

The microscopic response is defined by the individual atoms or electrons in the material. At this scale, it is possible, for example [12], to analyse the interaction of an applied electromagnetic field, of frequency, ω , with a material's atomic parameters, such as electronic density per volume, n_e , and electronic resonance frequency, ω_e . This analysis produces an expression for the complex dielectric permittivity for the material, as a function of the applied electromagnetic frequency, ω . The microscopic electromagnetic field is represented by the microscopic electric field strength, e , and the microscopic magnetic flux density, b , and each magnetic dipole is represented by a small electrical current loop. However, as the focus of this thesis is the bulk examination of a material's dielectric response, the thesis analysis will focus primarily at the macroscopic level.

Figure 2-7 shows the different polarisation mechanisms that define many molecules' dielectric response and the frequency regions in which each mechanism is dominant [14]. Each of the three types of polarisation is a function of the frequency of the applied electric field. When the frequency of the applied electric field is sufficiently low, all polarisation types shown in Figure 2-7 have time to reach the value they would attain at steady field equal to the instantaneous value of alternating field. But with increasing frequency, some polarisation types no longer have time to reach their steady peak value. First the orientation polarisation is affected. This type of polarisation takes a time typically of the order of 10^{-12} to 10^{-10} sec to reach its equilibrium value in liquids and solids with moderately small molecules. Hence, at room temperature when the applied electric field has a frequency of 10^{10} to 10^{12} Hz, dipolar (orientation) polarisation can fail to reach its equilibrium value and will thus contribute less and less to the total polarisation as frequency increases further.

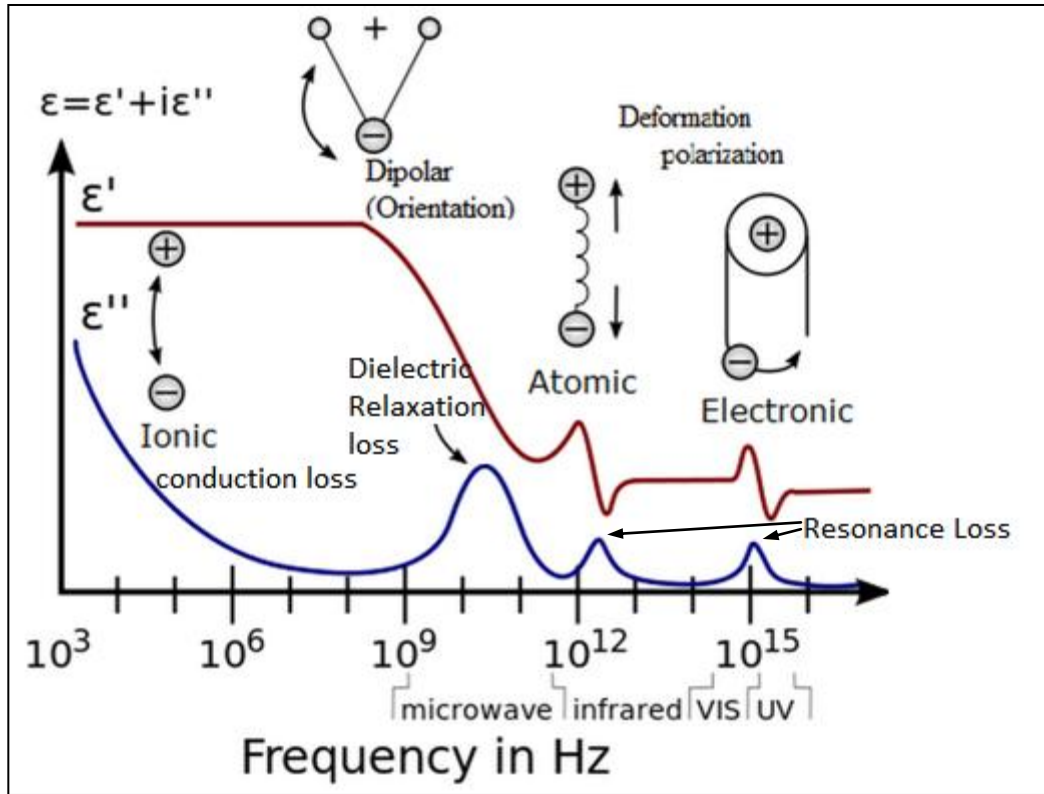


Figure 2-7 Electromagnetic frequency response of water with key interaction mechanisms
 In Figure 2-7, the dipolar (orientation) polarisation for the H_2O molecule is shown to decrease after 10^8 Hz and has minimum at about 10^{11} Hz.

1) Dipolar (Orientation) polarisation

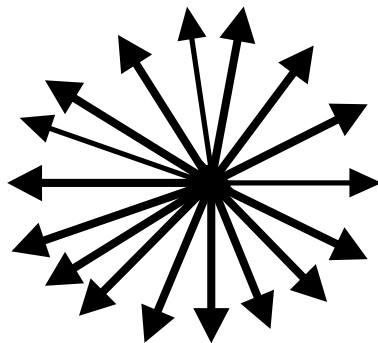


Figure 2-8 Random dipole vector movement (two dimension)

In the case of dipolar polarisation the material has permanent natural dipoles which are independent of each other, i.e. they can rotate freely. Under an external electric field at microwave frequencies, dipoles rotate to align with the field. As the stimulating

electromagnetic fields in this work are in the microwave region, then the material characterisation is more correctly called the material's dipolar polarisation response. Dipolar (Orientation) polarisation is mostly limited to liquids with electric dipoles.

Moreover, the net orientation polarisation changes all the time as molecules move. It is possible to draw all vectors from a common origin, and then the sum of all vectors should be zero, if the dipoles are randomly oriented (as shown in Figure 2-8). An example of this is liquid water, for which every water molecule is independent and free to move.

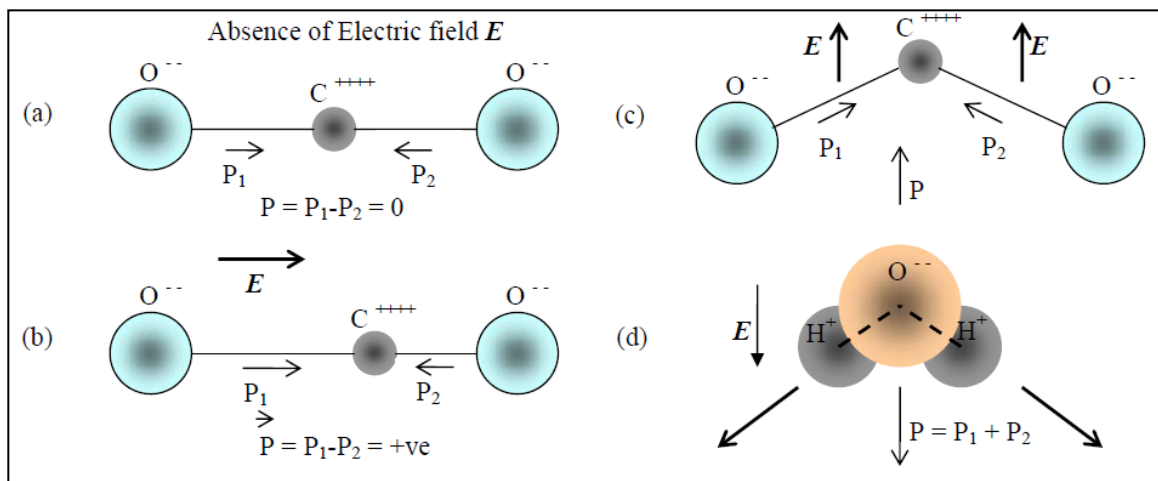


Figure 2-9 Dipolar (orientation) polarisation [15]

The linear $O-C-O$ arrangement in CO_2 results in a non-polar molecule. The resulting dipole moment of a molecule depends on the shape of the molecule and direction of applied electric field. The dipole moment of each bond is added as vectors, to obtain the resultant overall polarisation, as shown in Figure 2-9, from (a) to (c).

The asymmetry of the water molecule leads to a dipole moment in the symmetry plane pointed toward the more positive hydrogen atoms. The magnitude of this dipole moment in a single water molecule is

$$P = 6.2 \times 10^{-30} C.m \quad (2-13)$$

If an external electric field is applied, the dipoles would have a tendency to align themselves along a field line of the external field.

2) Ionic polarisation

In chemistry, as the name suggests, ionic polarisation occurs in ionic materials. It occurs when an electric field is applied to an ionic material then *cations* and *anions* get displaced in opposite directions, giving rise to a net dipole moment. For example, the most common table salt is Sodium Chloride, *NaCl*. Each Na^+ and Cl^- pair forms a dipole. When there is no externally applied electric field, the *NaCl* molecules form a structure where the individual dipoles not alone effectively cancel each other, but they also cannot rotate; their orientations are fixed. After applying an external electric field, the ions experience an extra force in the direction, which can cause the dipole to stretch and thereby to change each individual dipole moment.

3) Deformation polarisation

Deformation polarisation includes two distinct forms of polarisation, namely electronic polarisation and atomic polarisation. Electronic polarisation occurs in atoms, when the electron cloud is moved out of the equilibrium trajectory by an applied steady or alternating electric field. Electrons respond to an externally applied electric field very quickly, so electronic polarisation occurs right up to ultraviolet frequencies [16]. Atomic polarisation, on the other hand, is the displacement of atoms in a molecule. Atomic polarisation occurs when adjacent positive and negative ions “stretch” under an applied electric field. For most dielectric materials, atomic and electronic polarisations are the dominant polarisation mechanisms at microwave frequencies, although their exclusive domination occurs at frequencies far beyond the microwave region.

At a molecular scale, several dielectric mechanisms contribute to dielectric behaviour. Dipole (orientation) and ionic conduction interact strongly at microwave frequencies. Water molecules, which are permanent dipoles, rotate to follow an external electric field. These mechanisms are quite lossy, which explains why food heats in a microwave oven. Atomic and electronic mechanisms are relatively weak and usually constant over the microwave region. Each dielectric mechanism has a characteristic “cut-off frequency” As frequency increases, the slow mechanisms drop out in turn, the faster ones to contribute to ϵ_r . The loss factor (ϵ_r'') will correspondingly peak at each critical frequency. The magnitude and “cut-off frequency” of each mechanism is unique for different materials.

Water has a strong dipolar effect at low frequencies, but its dielectric constant rolls off dramatically around 20GHz.

2.4.2 Debye relaxation time

Peter Debye [2] introduced a relaxation model as a further means of characterising dielectric materials. His model defines the response delay of a dielectric to an externally applied electric field. The Debye relaxation time, τ , is a measure of the mobility of a material's molecules (dipoles). It is the characteristic time for a distribution of electrons in a dielectric returning to an equilibrium state, after a disturbance is removed and, as such is a function of the dielectric polarisation. Liquid and solid materials have molecules that are in a condensed state with some limits in the freedom to move when an electric field is applied. Collisions, commonly known as internal friction, restrict movement so that the molecules turn slowly. Combined with the effort required to align the more opposed of the randomly distributed polar moments means that the material exponentially approaches the final steady state condition of complete orientation polarisation, with the relaxation time constant τ . When the applied external electric field is switched off, the sequence is reversed and random distribution is restored with the same defining relaxation time constant.

Debye proposed that the following parameters static permittivity, ϵ_s , high frequency permittivity, ϵ_∞ , and relaxation time, τ , could be used to describe permittivity. The single relaxation Debye relation for deionised water, Methanol and Ethanol is written as [34]:

$$\epsilon' = \epsilon_\infty + \frac{\epsilon_s - \epsilon_\infty}{1 + (\omega\tau)^2} \quad (2-14)$$

and

$$\epsilon'' = \frac{(\epsilon_s - \epsilon_\infty)\omega\tau}{1 + (\omega\tau)^2} \quad (2-15)$$

The relaxation frequency f_c is inversely related to relaxation time:

$$\tau = \frac{1}{\omega_c} = \frac{1}{2\pi f_c} \quad (2-16)$$

At frequencies below the relaxation frequency, the alternating electric field is slow enough that the majority of dipoles are able to keep pace with the field variations. When the polarisation is able to develop to the fully polarized condition, the energy loss (which is related to the imaginary component ϵ_r'') is depended on the frequency. As the frequency increases, ϵ_r'' continues to increase but the component that represents the energy temporarily stored in the dielectric (which is proportional to ϵ_r') begins to decrease due to the phase lag between the dipole alignment and the changing electric field. Above the relaxation frequency both ϵ_r'' and ϵ_r' drop off as the electric field is too fast to influence the dipole rotation and both the rate of collision and the amount of polar alignment/energy storage reduce [17].

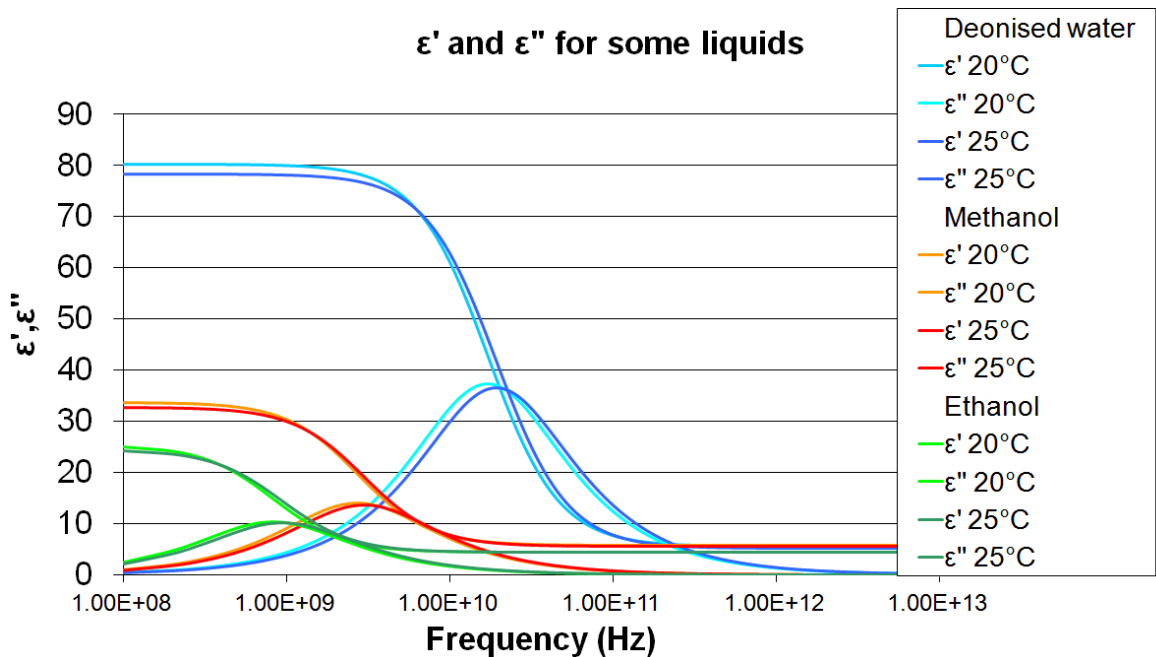


Figure 2-10 Debye relaxation of water, Methanol and Ethanol at 20° C descriptions

Microsoft Excel was used to calculate the Debye relaxation curves for liquids at 20° C, shown in Figure 2-10, where the static parameter values used are shown in Tables [17].

Table 2-1 Relaxation parameters at 20°C

Liquid	Static permittivity	Optical permittivity	Relaxation time
	ϵ_s	ϵ_∞	τ_r/ps
Deionised water	80.21	5.62	9.36
Methanol	33.65	5.76	58.75
Ethanol	25.28	4.44	192.68

Notice the temperature variations presented in the curves in Figure 2-10, which are derived from a modified Debye model, at frequencies below 100GHz and for arbitrary temperature that is given as [18]

$$\epsilon_r^* = \epsilon_\infty + \frac{\epsilon_s - \epsilon_\infty}{1 - j \frac{f}{\gamma_D}} \quad (2-17)$$

with $\gamma_D = 20.27 + 146.5\theta + 314\theta^2$, $\theta = 1 - 300 / (273.15 + T_w)$,
 $\epsilon_s = 77.66 - 103.3\theta$, $\epsilon_\infty = 0.066\epsilon_s$, f is in GHz

where T_w is the liquid temperature

Table 2-2 Relaxation parameters at 25°C

Liquid	Static permittivity	Optical permittivity	Relaxation time
	ϵ_s	ϵ_∞	τ_r/ps
Deionised water	78.36	5.16	8.27
Methanol	32.65	5.60	53.44
Ethanol	24.51	4.38	169.49

The molecular dipole moment for any material influences its permittivity and conversely measurement of the material's permittivity can be used to calculate the dipole moment. For low frequency applied electromagnetic fields of moderate intensity, all types of polarisation attain equilibrium in an isotropic polar material and the permittivity of the material is called its static permittivity ϵ_s . In investigating the material molecular structure and even in the study of high frequency dielectric behaviour, this static permittivity value is also interesting. For instance in Figure 2-7, the water dielectric constant shows considerable variation with frequency. For the upper frequency range shown ($f > 10^{14}$ Hz) the static permittivity of water has a stable value. With decreasing frequency, the

permittivity value increases until it reaches a new constant level. For some materials, this level is maintained to very low frequencies, while others show a second dispersion in microwave, UHF range or lower ranges.

Materials that exhibit a single relaxation time constant can be modelled by the Debye relation [2], which appears as a characteristic response in permittivity as a function of frequency as shown in Figure 2-10. Also, complex molecules can contain lots of different relaxation times, $\tau(n)$, or relaxation frequencies, $f_r(n)$, respectively, which can be produced from rotations of dipoles, translational vibrations between molecule clusters, rotation of molecule clouds etc. [19].

For water dielectric properties, ϵ_r' is constant, above and below the relaxation with the transition occurring near the relaxation frequency at about 22GHz. Further, the complex permittivity, ϵ_r'' is fairly small, above and below relaxation and peaks in the transition region of ϵ_r' .

2.5 Literature review of measurement techniques

The main microwave techniques for the electromagnetic characterization of materials generally fall into either resonant or non-resonant methods. Resonant methods are used to get accurate dielectric properties at a single frequency or several discrete frequencies, while non-resonant methods can be used to get the electromagnetic properties over a frequency range.

Although resonant methods can only measure material properties at a single or several discrete frequencies, resonant methods usually have higher accuracies and sensitivities than non-resonant methods [9]. In resonant methods, the MUT are tested as resonators or as a key part of a resonator, so therefore the properties of MUT are determined from the resonant properties of the resonator. This method is based on the resonant frequency and quality factor of a dielectric resonator of known dimensions, which are determined by its permittivity and permeability. By inserting the sample into a resonant cavity, these material properties can be obtained by measuring the change in both the resonant frequency and also the quality factor.

This research work uses a non-resonant dielectric material measurement method. In non-resonant methods, when an electromagnetic wave propagates from free space into the sample material, both the wave's path impedance and the wave velocity are changed. As a result of the path impedance change, there is a (partial) reflection of the incident wave at the point of change, namely at the interface between air and the material. Measurements of the both the reflected and transmitted portions of the wave provide the parameters, from which the material permittivity and permeability may be calculated.

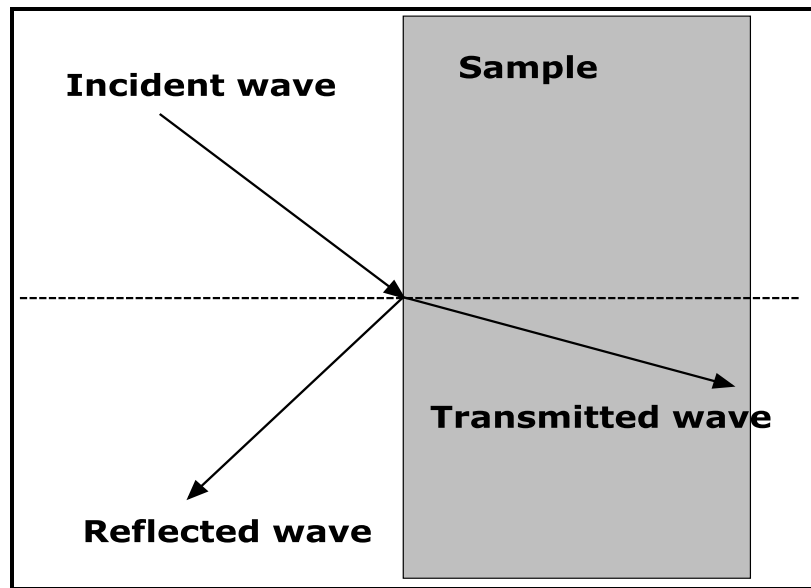


Figure 2-11 Wave transmission and reflection example, as wave passes the boundary of two different materials

Non-resonant methods mainly include reflection only measurement or both transmission and reflection measurement of the incident wave. The reflection method is based on the reflection from the test sample, while in the transmission and reflection method, the material properties are calculated from both the reflection from the material boundary and the transmission through the material. With the reflection method, electromagnetic waves are directed to the MUT, and the properties of MUT are derived from the reflection due to the impedance discontinuity caused by material presenting, so usually it is possible only to calculate either the permittivity or permeability; whereas with the transmission/reflection methods, the MUT is inserted into transmission line, and the properties are deduced on the

basis of the reflection from the material and the transmission through the material, so both the permittivity and permeability of the MUT can be calculated.

2.5.1 Reflection method

The reflection methods can be done in two ways: open circuit reflection and short circuit reflection. Assuming that the transmission line used is coaxial line.

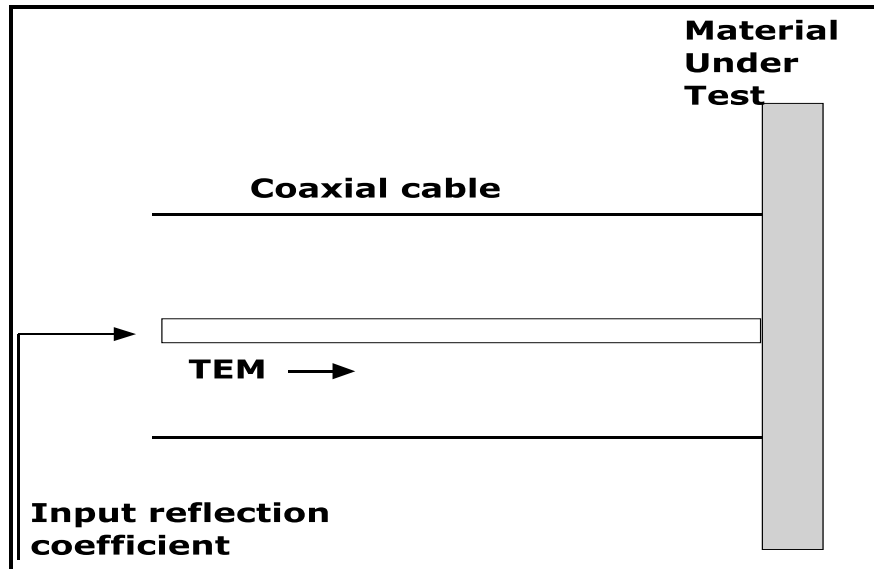


Figure 2-12 Open circuit reflection method with a coaxial cable

Figure 2-12 shows an open circuit reflection in which the co-axial cable is in contact with the MUT, when the electromagnetic wave is incident on the MUT. A weakness of this technique is that the reflected wave depends on the impedance at the material's surface, which will not be same for the entire material surface. In order to average out the influence on the impedance of surface imperfections, the reflectivity must usually be calculated at a number of positions and, if possible, the surface made uniformly even beforehand. The diameter of the MUT should be much higher than the diameter of the coaxial cable.

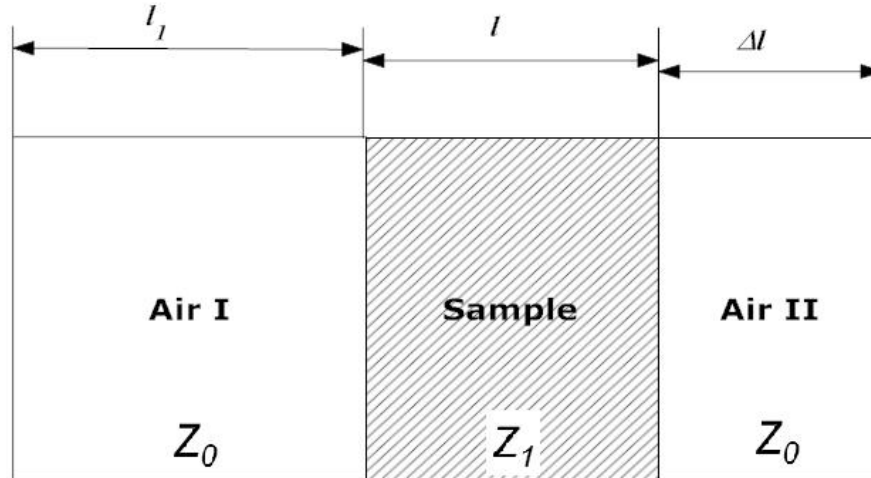


Figure 2-13 Short circuit reflection method [20]

Short circuit reflection method was introduced by Robert and Von Hippel [21]. The short circuit may either be fixed in the line or moveable. The advantage of a moving short circuit is that it allows many separate measurements at a given frequency and allows the sample to be placed in either a strong electric field or strong magnetic field region. As shown in Figure 2-13, l_1 is the distance from the calibration reference plane to the front of MUT; l is the length of the MUT, Δl is the distance from the other end of the sample to the transmission line short. While there will be a more detailed description of the calibration reference plane later in this work, at this point it will simply mean the plane which provides the benchmark position for both MUT measurements and also analysis.

This method gives the material properties depending on the material length, l , propagation constants $\gamma_{free-space}$ and $\gamma_{material}$ and the homogeneity and isotropicity of the MUT. The sample position is made depending on the type of measurements that are to be taken. The sample is inserted at the termination of the cable (after a short). It is assumed, in this case, that only the transverse electric field (no electric field in the direction of propagation) exists in this mode. At the position of the short termination in the transmission line, there should be both a low electric field and a high magnetic field, based on wave propagation theory, while at the position one quarter wavelength away from the short termination, the field should be a low magnetic field with a high electric field. Generally, a high electric field is advantageous for permittivity measurements, whereas a high magnetic field is advantageous for permeability measurements, for more sensitive measurements and better

measurement signal-to-noise ratio [11]. For the permittivity measurement the sample should be moved away from the short position, whereas for the permeability measurement the sample should be near the short [20]. As mentioned, the short circuit method can only measure either permittivity or permeability. If both permeability and the permittivity are required, the sample must be moved along the wave propagation line and new Scattering-parameters measured in the second location.

2.5.2 Transmission/reflection method

For the transmission/reflection method, an MUT is inserted into a medium, and the transmission and reflection portions which produced by an incident electromagnetic wave are measured. As mentioned earlier, using the reflection method, it is only possible to calculate either permittivity or permeability. Scattering parameters (S-parameters) are used to describe the relationship between the input waves a and output waves b .

The relationship between the input wave a and output wave b is often described by S-parameters:

$$[b] = [S][a] \quad (2-18)$$

where $[a] = [a_1 \ a_2]^T$, $[b] = [b_1 \ b_2]^T$, and

$$[S] = \begin{bmatrix} S_{11} & S_{12} \\ S_{21} & S_{22} \end{bmatrix} \quad (2-19)$$

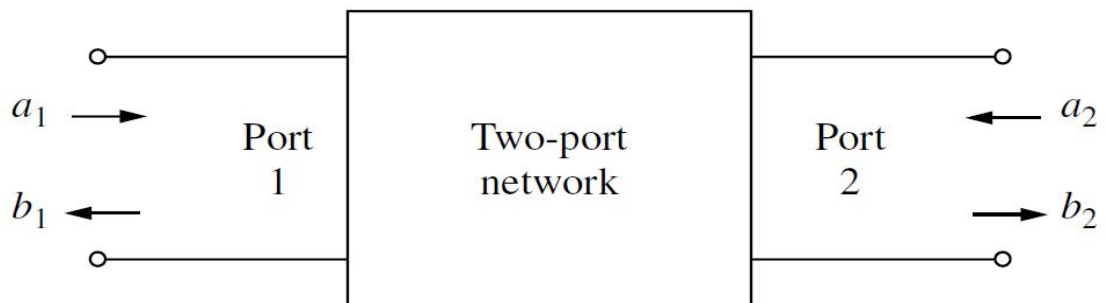


Figure 2-14 A two-port network with input wave “ a ”s and output wave “ b ”s

In the transmission and reflection method, all the four S-parameters can be obtained, so both permittivity and permeability can be calculated. The working principles for this method have been analysed in literature, such as [10], but will be outlined here now and described in detail later. In this method, the MUT is inserted into a transmission path, which may be guided (such as a wave-guide) or also free-space, as is the case in this work. As mentioned all the four S-parameters can be measured. By using these four parameters, it is possible to calculate both the material's permittivity and permeability. Figure 2-15 shows a typical configuration for a transmission/reflection method [20].

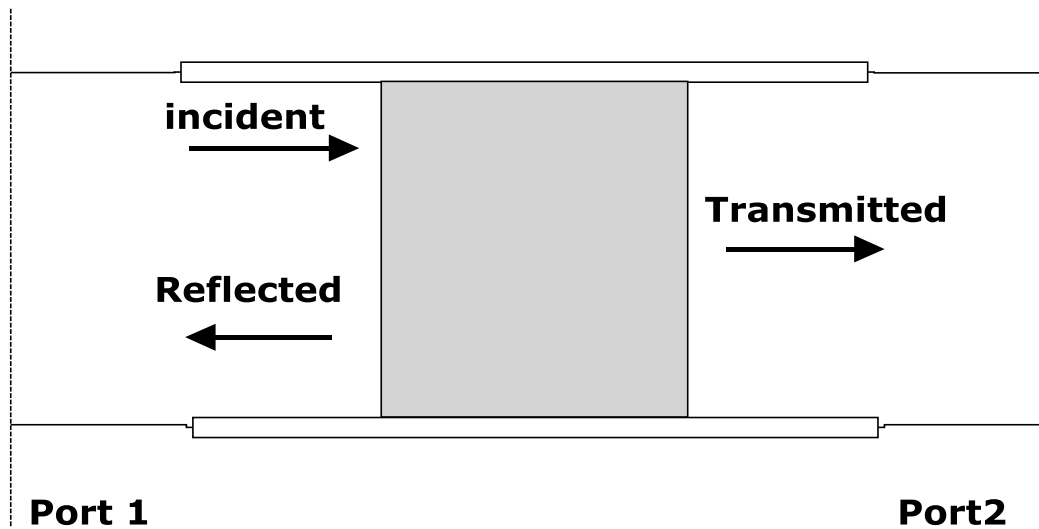


Figure 2-15 Sample transmission line of Transmission/reflection of electromagnetic wave

2.5.3 Conversion techniques

Various techniques to convert S-parameters into dielectric properties have been proposed. The Nicholson, Ross [22] Weir [23] (NRW) technique is popular and uses two or all four S-parameters, depending on the measurement technique. However it does not produce accurate results at sample sizes that are integer multiples of the incident beam's half wavelength, something which is increasingly likely when the measurement range of frequencies is broadband, such as the range 800-6000MHz used in this work. The NIST Iterative technique was first proposed by Baker-Jarvis in 1990 [24] and uses NRW as a starting point and then the Newton-Rapheson to solve for the dielectric parameters. This technique is more elaborate than NRW, but overcomes the NRW weakness, as it is

accurate at sample sizes that are integer multiples of the incident beam's half wavelength. The technique known as the New Non-Iterative (NNI) technique is based on a simplified version of the NRW technique [25]. It is suitable for permittivity calculation for the case that the permeability $\mu_r=1$, which will be the case for non-magnetic materials in which there are also no currents induced by the applied electromagnetic field.

In early 1966, R. M. Redheffer [26] was the first researcher to suggest a free-space method for dielectric measurement. In his report, he pointed out that “free-space methods are non-destructive and contactless techniques which are especially suited for dielectric measurement of materials”. In 1971, Harold L. Basset first measured the complex permittivity using a free-space method. The equipment he used was a pair of spot-focusing antennas at a fixed frequency of 9.4GHz [27].

Nowadays, the tests for complex dielectric properties are usually carried out using a Vector Network Analysers (VNA), which simultaneously measures the reflected and transmitted waves amplitudes and phases, with sufficient accuracy. The VNA amplitude and phase measurements are usually taken in the form of S-parameters. There are different methods to calculate permittivity and permeability from S-parameters. The four main conversion techniques just mentioned are now described in more detail.

1) Nicolson-Ross-Weir technique (NRW)

NRW is a popular method to calculate permittivity and permeability from at least two measured S-parameters, S_{11} (the reflection wave measurement) and S_{21} (the transmitted wave measurement). It generally uses two functions, shown in Chapter 4, which allow using S_{11} and S_{21} , which can be obtained directly from a vector network analysers (VNA) to calculate the two unknown quantities of permittivity and permeability. Both reflection coefficient and transmission coefficients require all four S-parameters, however, in a symmetrical measurement environment, only two S-parameters (S_{11} , S_{21}) are needed, as the reverse S-parameters are assumed equal to the forward S-parameters [22] [23]. The measurement environment in this PhD paper is based on symmetrical structure, therefore, only two S-parameters (S_{11} , S_{21}) are used, an assumption that was easily verified through measurement of the forward and reverse S-parameters.

It will be shown later (Chapter 4) in more detail how the reflection and transmission coefficients, Γ and T , are related through several parameters, including propagation constants, wavelength and group delay of the wave and how this is important in the analysis of measured S-parameters to arrive at the desired dielectric properties.

The NRW technique is highly sensitive to small values of the S-parameter, S_{11} . This parameter is based on the reflected wave's strength, which is usually smaller than the propagated wave's strength and thus can be small at some frequencies in the measurement range. For a small S_{11} value the uncertainty in the measurement of the phase of S_{11} can be very large, which can cause consequent large uncertainties in the calculated values. This effect can be mitigated somewhat by reducing the sample length.

The NRW technique does offer some advantages including:

- Fast, non-iterative
- Applicable to free-space, but also to waveguides and coaxial line measurements

There are however some disadvantages with the NRW technique:

- Instability at frequencies corresponding to multiples of $\lambda/2$, one half of the probing wavelength. This means it is not suitable for low loss dielectric materials; because in low loss materials, all frequency related to integer multiples of $\lambda/2$ will necessarily also have one very small S-parameter ($S_{11} \approx 0$). This in turn leads to an instability in the NRW calculation
- Thin samples of the MUT should be used to avoid the latter instability problem, but even this is not guaranteed success, as high dielectric MUTs will shorten the wavelength in the material by an appreciable amount (the $\lambda/2$ instability occurs earlier, in wavelength terms, than may have been expected).

There are two methods to calculate the complex dielectric properties using the NRW method: one is by assuming an initial value for the permittivity and permeability of the material, followed by determining the value of n (where n is the number of complete wavelengths in the material). Once the value of n is determined, both permittivity and permeability can be calculated, (more detailed analysis of this calculation is presented in Chapter 4). Another useful approach is to analyse the group delay, since the group delay of

a propagating wave does not depend on the wavelength of the particular wave, but is instead dependent on the sample length of the dielectric material and its permittivity.

2) NIST iterative technique

This technique performs a calculation based on the NRW technique, but also uses the Newton-Rapheson's root finding technique. The NIST iterative technique avoids the instability peaks that exist in the NRW technique when the sample thickness is an integer multiple of one half wavelength ($n\lambda_g/2$). By extension, unlike the NRW technique, it is also suitable for long samples and for characterizing low loss materials. A stable permittivity result over the entire frequency measurement spectrum can be obtained from the S-parameters. By assuming permeability $\mu_r=1$, this technique minimizes the instability in the NRW method (divergence and limitation of sample length problems). However, with this assumption, only non-magnetic materials and materials where there are no induced currents can be calculated by using this technique [24].

The advantages of the NIST iterative technique include

- Smooth permittivity results, no instability when the sample thickness is an integer multiple of one half wavelength, particularly when testing low loss materials
- Accurate
- Arbitrary thickness of samples can be used
- Robust for both low loss and high loss materials

The disadvantages of the NIST iterative technique will include: applicable for permittivity measurements only and will need an initial guess of the permittivity value.

3) New non-iterative technique

The new non-iterative technique (NNI) technique has the advantage of being stable over a whole range of frequencies for an arbitrary sample length. The NNI technique is based on a simplified version of the NRW technique and no divergence is observed at frequencies corresponding to multiples of one-half wavelength in the sample. It does not need an initial estimation of permittivity and can perform the calculation very quickly. The accuracies are comparable to the NIST iterative technique. The NNI technique uses a slightly different formulation from the NRW technique and it can be easily extended to other measuring methods, for example those using micro-strip or co-planar lines to propagate the probing

wave. NNI also yields both the permittivity and permeability in the expression of the effective electromagnetic parameters.

The main advantages of the new non-iterative technique may be summarised as

- Smooth permittivity results, no divergence
- Accurate
- Arbitrary length of samples can be used
- Fast, non-iterative
- No initial guess needed

A disadvantage of the new non-iterative technique is that once again it is applicable for permittivity measurements only.

4) Free space measurement technique

From the late 20th century, research increased into free-space techniques for dielectric measurements, for example, the research work shown in D.K Ghodgaonkar's paper [28].

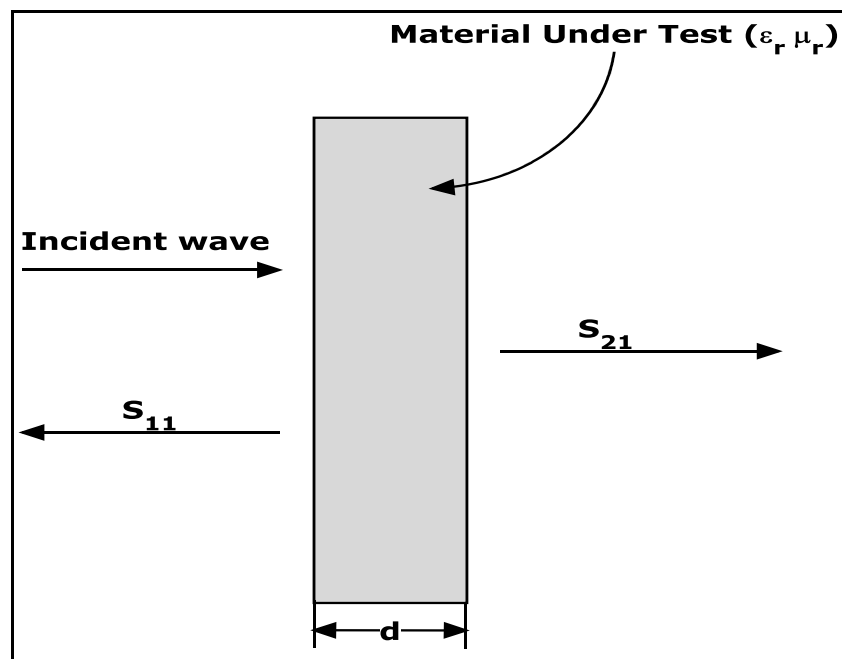


Figure 2-16 Free space measurement simple structure

The free space technique is non-destructive, contact-free and less restrictive on MUT thickness or even shape, as long as the probing beam can be guaranteed to pass through a uniform thickness of homogenous MUT. Moreover, as long as the latter condition can be met, it is also suitable for the non-solid dielectric material characterization, such as liquids or powder material, which cannot maintain the uniform thickness condition without the addition of a container and are the primary focus of this work. This condition can, in some circumstances, also be met by a waveguide, but in a waveguide the frequency range is much more restricted (only frequencies higher than the waveguide cut-off frequency can be used) than in free space. Also, for the free space technique the MUT does not have to match the waveguide cross section, is easier to guarantee uniform sample distribution and, once contained appropriately, liquids can be measured.

The inaccuracies in dielectric measurements using free space methods are mainly due to

- 1) The diffraction effects from the edge of the sample (and container, if required) and signal leakage from the whole test environment or, if not taken in an isolated environment, spurious signal interference.
- 2) Standing waves in the test environment between the antennas and the multiple surfaces of the MUT (including the container, if required), and which cannot be completely calibrated out.

The research work reported here uses the free-space technique. A VNA calibration process is performed to reduce the impact of standing waves and edge diffraction from the sample. Also, in order to reduce the impact of diffraction, hard edges were rounded and/or had graphite-impregnated foam placed on them. The calculation algorithm to arrive at the material dielectric values from the measured S-parameters is a free-space conversion method that is similar to the NRW method.

For different materials, shapes and test frequencies, each method can be more appropriate than the others. The decision on which method to use could be considered by material shape, dielectric properties or sample length. Both transmission/reflection method and free space method are mainly used for the broadband applications. In order to remove

extraneous effects and to establish a benchmark for the measurement, the first step is usually to carry out a calibration for each method before measuring the S-parameters.

Table 2-3 Similarities and minor differences between conversion techniques

Conversion techniques	S-parameters	Dielectric properties
NRW	$S_{11}, S_{21}, S_{12}, S_{22}$ Or S_{11}, S_{12}	ϵ_r, μ_r
NIST iterative	$S_{11}, S_{21}, S_{12}, S_{22}$ Or S_{11}, S_{12}	$\epsilon_r, \mu_r = 1$
New non-iterative	$S_{11}, S_{21}, S_{12}, S_{22}$ Or S_{11}, S_{12}	$\epsilon_r, \mu_r = 1$
Free Space conversion	$S_{11}, S_{21}, S_{12}, S_{22}$ Or S_{11}, S_{12}	$\epsilon_r, \mu_r = 1$

2.6 Selection of Technique

Resonant methods have much better accuracy and sensitivity than non-resonant methods [29] and are generally applied to the characterization of low-loss materials. However, in a recent study, resonant methods are also applicable to high-loss materials, if very small samples are prepared or higher volume cavities are constructed [30]. A major disadvantage both for resonant and also waveguide techniques is that they require precise sample preparation so that the MUT is an exact fit, with no air-gaps. In addition, for an analysis over a broadband frequency, a new measurement setup (a cavity) must be made, which is not feasible in a practical point of view. Tuneable resonators can be used for a wider frequency band measurement and analysis. However, they are expensive, require multiple sample preparation and also an increase in the frequency bandwidth accompanies a decrease in the measurement accuracy [31]. Non-resonant methods have relatively higher accuracy over a broad frequency band and usually necessitate less sample preparation compared to resonant methods. As a type of non-resonant method, the various

transmission-reflection methods are widely utilized for material characterization. This method has the advantage of simplicity, broad frequency coverage, and high accuracy over the range [22] [23] [18] [32].

Permittivity measurements of thin dielectric materials can be performed by using non-destructive methods such as open-ended waveguide and coaxial methods [33] [34]. The sample must be sufficiently thick so that the interaction of the electromagnetic field with the non-contacting boundaries or sample holder is negligible. Furthermore, one more disadvantage is, any bad contact present between the waveguide or coaxial aperture and the sample surface may degrade the accuracy of measurements [35]. Finally, for open-ended waveguides and coaxial probes with a lift-off distance, thin samples may sag and the theoretical calculations are more complex [36].

Free space methods, as another non-destructive method, do not have very strict requirements on the shape of samples. However, they can suffer from diffraction at the edges of the sample or sample container. In order to reduce this effect, the size of the sample can be selected sufficiently large, or by selecting proper calibration method. However, for thin materials, such solutions may decrease the performance of measurements as a result of sagging or as was the case in some early powder measurements in this work by bulging. Also as another solution, spot focusing horn-lens antennas can be employed [37]. In this case, however, the bandwidth of the focused antenna system is limited. To address some of these challenges, a calibration procedure, which takes into account the diffraction and other effects can be incorporated into the measurement process. However, the accuracy of such a calibration process may not be high if the sample is placed in the antenna's far field, a concept that will be elaborated on later [38]. A further challenge of most analysis methods is that for most materials, the material electrical length is unknown, simply because the permittivity is initially unknown. Therefore, it is not possible to directly obtain the dielectric constant without resorting to a compromise, such as an estimate of the electrical length or material wavelength (detailed in Chapter 4).

An alternative approach to this latter problem is to take measurements at more than one MUT thickness, so that the electrical length ceases to be an analysis variable. In the case of

powders and liquids, this means either having multiple containers or a single container whose thickness can be varied in a controlled manner. The latter approach was adopted in this work, whereby initial measurements were on a fixed container in order to prove aspects of the measurement technique. Subsequently the container was replaced with a second more elaborate and therefore also more flexible one, also capable of use in the measurements of powders and liquids.

Further details are included in Chapters 4 and 5, where at least two or in some cases three different thickness of MUT are required for the new approach. The new platform design will consist of a flexible container made of glass panes, which can be collectively used to set the thickness of test materials.

2.7 Matrix calculation

For the free space dielectric measurement, the MUT is usually sandwiched between two plain glass panes (thicknesses tested at 4mm, 6mm and 12mm). So the glass container structure can be described as a glass-sample-glass assembly. By using the known S_{11} and S_{21} of the whole structure and the permittivity and thickness of the glass, the S-parameter of MUT can be obtained by using the matrix calculation [20] [28]. Further detailed algorithms are listed in Chapter 4.

2.8 Conclusion

This chapter is related to a review of the published literature relating to dielectric material characterisation. It describes the fundamentals of dielectrics, its complex nature and also its dependence on frequency and materials. Finally, some important free-space and guided wave propagation measurement techniques was discussed, as well as techniques using resonance to provide a wider context for possible measurement setups.

3 Development of Measurement Environment

A considerable effort was required to develop a reliable, prototype test infrastructure, including site selection, test frame construction, antenna holders, integration with a Total Station for fine angular measurements and isolation from unwanted signal interference. The setup of the prototype system is drawn in Figure 3-1.

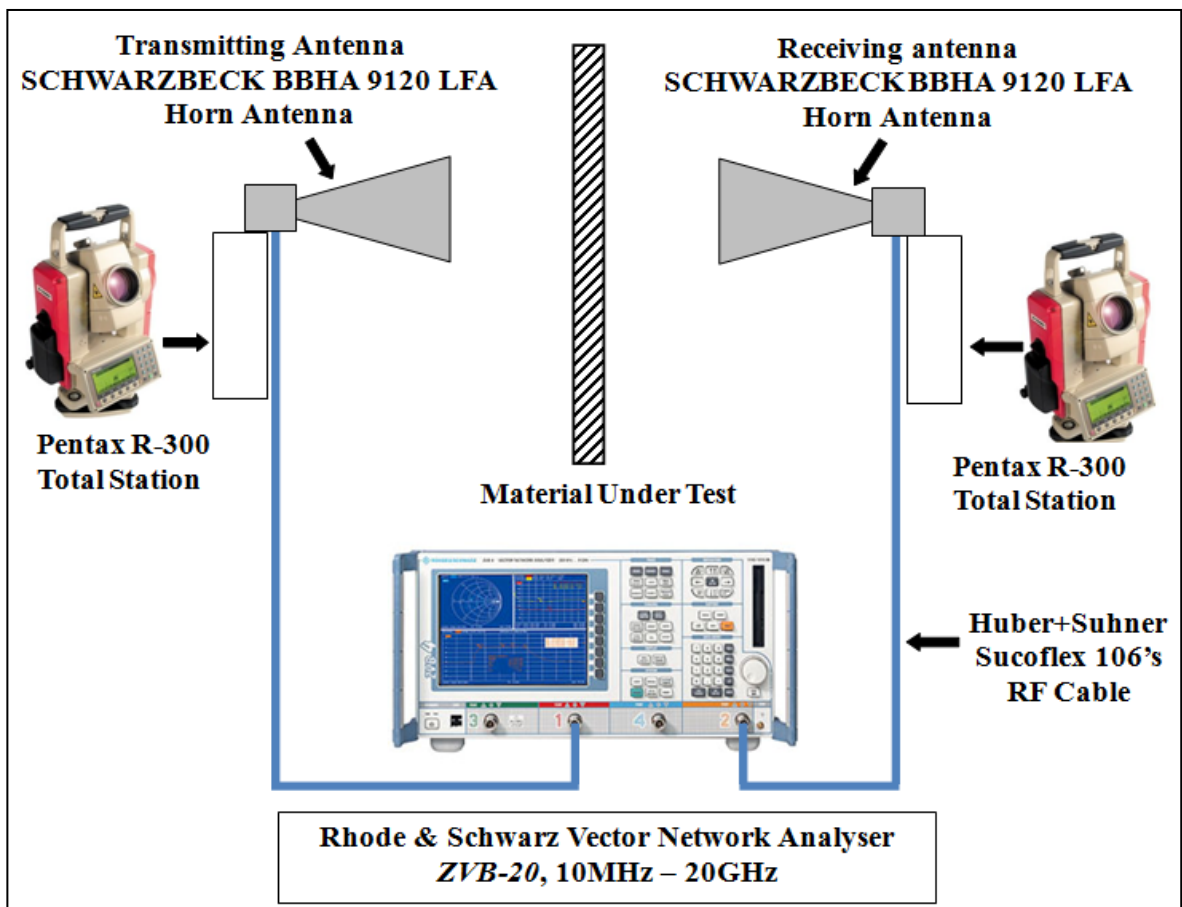


Figure 3-1 Measurement system setup diagram

3.1 Measurement components

For all dielectric measurements, the principle piece of equipment used to accurately measure the required S-parameters was a vector network analyser (VNA).

For experimental accuracy and repeatability, the cables from the VNA to the antennas were specially chosen for their phase constancy (even if moved during a measurement phase) and their overall low loss. Sometimes the transmitting antenna had extra measurement requirements, so it was mounted on a modified PENTAX Precision Total Station, shown in Figure 3-3, for accurate distance, height and angle measurements. The modifications required the specification and commissioning of a suitable antenna holder and adapter to fit in place of the handle on the top of the Total Station.

3.1.1 Vector network analyser

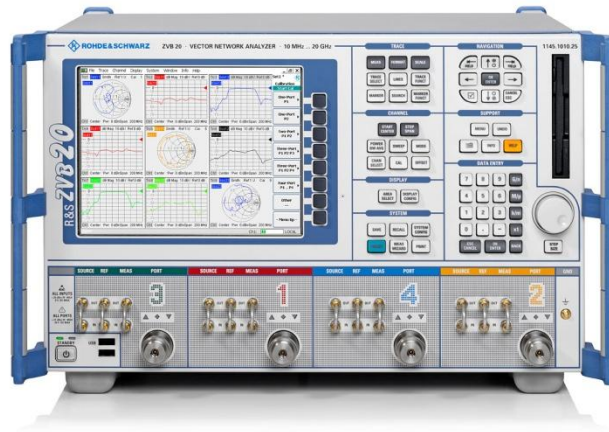


Figure 3-2 Rhode & Schwarz vector network analyser *ZVB-20*

While early glass propagation measurements used a vector signal generator on the transmit side and a spectrum analyser on the receive side, such a setup is only suitable for amplitude variations in the propagation path. Dielectric analysis also requires phase change measurements, and, for asymmetrical test set-ups, the ability to convert the transmitter to a receiver and vice versa. Therefore a two-port bi-directional Vector Network Analysers (VNA) was the obvious choice.

Also, for high frequency free space measurement, it is very difficult to measure the current or voltage, so S-parameters are usually measured instead. S-parameters are related to return loss, reflection and transmission coefficients. Measuring S-parameters can simply be obtained from the VNA. The results are formatted to EXCEL readable files, and can even be converted to H, Y, Z parameters or ABCD matrix, with the latter conversion being of

potential use when matrix inversion is required, which is considered in more detail later for glass tank containment of powders and liquids.

As mentioned measuring phase variation is an important feature of a VNA. For the purpose of dielectric analysis, both magnitude and phase results are needed to obtain dielectric properties. By using VNA, it is able to achieve both of these values in one single test.

This PhD research work used a Rhode & Schwarz four - port VNA, the *ZVB-20*, with a frequency range from 10 MHz to 20GHz, although the bulk of the work was carried out over the narrower range of 800-6000MHz, defined by one of the available horn antenna pairs. The minimum frequency resolution was 1Hz and all magnitude results were stored in linear format, and phase measurements were saved using degrees.

3.1.2 Calibration kit for VNA

For each new test setup, there were changes in the experimental environment, any of which, could affect the measurement results. For instance, a change in the antenna separation distances, the height of the two test antennas or other similar changes to the environment. A VNA calibration kit can be used to reduce the impact of such effects, by moving the measurement reference plane from the VNA itself to the calibration points. The calibration should take place at the VNA ports themselves or, even more practically, at the cable ends (at the antenna junction) and their influence in the VNA readings calibrated out. The calibration kit used here is the *ZV-Z32* from Rhode & Schwarz, which has exact Open, Short and Match (OSM) connectors over the VNA operating frequency.

An alternative calibration technique, the Through-Reflect-Match/Line (TRL/M) is described in Chapter 5 that moves the reference plane even further along the measurement propagation path by including the antennas, the propagation path to the target, the MUT and the test structure. This calibration technique requires a reflection plane to be placed in front of the MUT target, which is the same size as the target. While it is not expected to reduce the subtle unwanted signals, such as spurious cable reflections, to the same extent as the VNA calibration kit, it nonetheless will allow immediate understanding of the changes in propagation and reflection due to the MUT. A TRM calibration means replacing the “Line” in the widely used TRL calibration by a “Match” standard. The

“match” can be achieved in this free-space technique by placing RF absorber foam, with the same size as the MUT, in the same place as the reflector, thereby effectively absorbing all transmitted power, just as a matching load would do. The Thru standard is simply achieved by direct (without MUT) transmission between the two antennas. The reflected power will be the benchmarks for the minimum reflected power and the maximum transmitted power. In the case of the reflector, the VNA S_{11} results will be the benchmark for the maximum reflected power, while the S_{21} results will be the benchmark for propagated power that does not pass through the MUT (diffracted or stray reflections). When using the absorb foam, ideally, S_{11} would remain the same as when performing the Thru calibration, however, in reality the absorber foam still will reflect a small portion. In the Match calibration, the measured S_{21} value is similar to the measured S_{21} value from the reflector calibration, or more correctly, both should be similarly low. The Match value should be slightly higher as of the absorber foam will not have a strong diffraction or target edge effect. The reflection and Match calibrations are used to determine the diffraction from the edges of the MUT.

3.1.3 Precision Total Station

A modified Total Station (PENTAX R-300, pictured in Figure 3-3) was used as part of the antenna mounting, using a custom made adapter/holder. The angular accuracy of the Total Station is ± 5 seconds [39], which is of benefit in particular for the antenna gain measurements. Moreover, with a Total Station, it is possible to precisely control the height and separation of both transmitting and receiving antennas. According to antenna far field theory, the modified Total Station setup can thus help confirm that the minimum required separation between two antennas is always attained. When measuring the antenna radiation patterns, this Total Station was used to control the antenna movement, with a step size of 2° . In addition, for most of the measurements, the two antennas have to face each other, and the incident wave should be perpendicular to the MUT surface, so that the incident wave is normal to the material.



Figure 3-3 Modified Pentax Total Station for antenna mounting

3.1.4 Cable

To get accurate results for the measurements it is important that the cables are well shielded against surrounding effects and that they don't change their properties if physically perturbed. The chosen cables to meet these criteria are 7.62m long *Sucoflex* 106 from *Huber+Suhner* [40]. These cables have good phase maintaining qualities, if moved during measurements and is low loss over 0.9 to 18GHz frequency range, which encompasses the measurement range described here [40].

3.2 Antenna

Two sets of antennas are used for the measurements, which are:

- 800MHz to 6GHz Horn antenna, Schwarzbeck BBHA 9120 LFA
- 8.2GHz to 12.4GHz Horn antenna, Schwarzbeck JXTXLB-90-20-C

However, Voltage Standing Wave Ratio (VSWR) bandwidth tests (antenna mounted on a flat roof and pointing skywards) for the latter antenna showed a higher usable bandwidth,

of 7.5GHz to 15GHz, taking the usable bandwidth as the region, where the VSWR (Voltage Standing Wave Ratio) ≤ 2 [41]. VSWR (Voltage Standing Wave Ratio) ≤ 2 means that about one third of the incident wave is reflected at the antenna interface and two thirds is transmitted. VSWR is a measure of how much power is delivered to an antenna. This does not mean that the antenna radiates all the power it receives. Hence, VSWR measures the potential to radiate. VSWR is a good estimate of radiated power, needing only the antenna itself and the VNA for the measurement. A low VSWR means the antenna is well-matched, but does not necessarily mean the power delivered is also radiated. The power can be *either* absorbed (as losses) or radiated away. A second reference antenna in an anechoic chamber or other radiated antenna test is required to determine the actual radiated power, although this test is not directly carried out here. The Two Antenna test, which has been carried out, could be used to distinguish between VSWR and actual radiated power, assuming the antennas are identical.

Alternative approaches to defining a working antenna bandwidth, not followed here, include using the S_{11} = -6dB or -10dB bandwidths, where the bandwidth is defined relative to the peak S_{11} value. S_{11} is a measure of how much power the antenna "accepts".

3.3 Antenna radiation pattern

In each case the antenna radiation pattern was measured to confirm the manufacturer's graphs. As the two antennas were identical, the Two Antenna Gain method described in Section 3.3.2 was used, with the Total Station providing the required angular accuracy. Of course the measured antenna pattern is only two-dimensional, whereas an actual antenna pattern is three-dimensional. A three-dimensional test is very hard to complete, needs dedicated equipment for precise three dimensional rotation and also usually needs a lot of time. A two-dimensional measurement can be converted into an approximate three-dimensional measurement, by measuring the E- and the H-plane radiation patterns separately. Each measurement is obtained by fixing one of the antennas, while varying the angle of the other, a technique known simply as the *Two Antenna Gain method*. One of the antenna mounting tripods has the freedom to rotate and, by using the Total Station, can accurately measure over a 360° range. The antenna under test can be measured in

transmitting or in receiving mode because of the reciprocity theorem [19], which states that an antenna has the same behaviour whether transmitting or receiving.

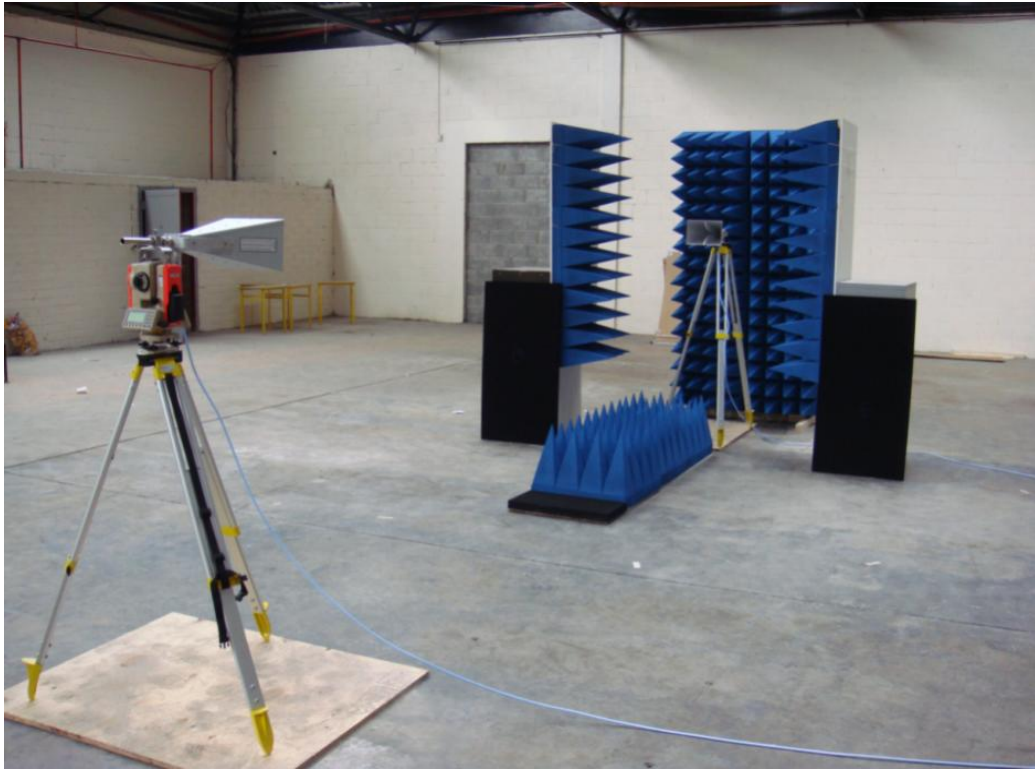


Figure 3-4 Antenna pattern measurement structure

The pattern for each antenna, for E- and H- planes, was measured in a large hall, starting at the normal incidence and then measuring up to 90° to each side. The step width was 2° and was monitored by the Total Station. The distance between the antennas was 5m, so the measurement occurred in the far field for these antennas. Pyramidal absorbent foam was placed around the measurement, to reduce the effect of the ground wave and any reflected wave from behind the receiver, as shown in the photograph in Figure 3-4. The antenna height was set at 1.60m to also reduce the effect of any ground reflected waves.

3.3.1 Standing Wave Ratio (SWR)

The ability of an antenna to accept power from a source is determined by the input impedance that the antenna presents, or more correctly, the impedance mismatch it presents relative to the source impedance. In most cases source impedance is 50Ω over the chosen frequency range, so ideally, the antenna impedance is expected to be 50Ω over the

same range. Maximum power transfer will occur for all frequencies for which the antenna impedance matches the output impedance of the source. In reality the range of frequencies for which an antenna achieves this is limited, even for the broad band antennas used in this work. When the match is not perfect some of the source energy will be reflected and a standing wave will be generated in the line. This mismatch is measurable as the VSWR and it is expressed as [19]

$$VSWR = \frac{1 + |\Gamma|}{1 - |\Gamma|} \quad (3-1)$$

where $|\Gamma|$ is the reflection coefficient and is simply S_{11} (magnitude and in linear form).

In addition, reflection which is caused by impedance mismatch can also happen once the antenna has transmitted the power, when the signal ceases to pass through air (impedance is 120π , approximately 377Ω) and encounters an obstacle with an impedance different to air. Such an effect is desirable in free space dielectric measurement, as long as the signal interacts only with the dielectric, which is impossible if tests are carried out in the antenna far field (see Section 3.4), as was the case in some of the measurements in this work. Free space, far field measurement therefore also introduces unwanted reflections as well as other unwanted interferences, such as diffractions, testing structure edge effects, etc. However, if an appropriate calibration technique is applied and good care taken, while making the free space antenna measurements, the extra interferences can be reduced to a minimum. This calibration is presented in much more detail in Section 5.2.

While normal incidence on RF absorbent foam would be a possible technique to measure the VSWR, the method used here was to point the antenna to the sky, from the roof of Waterford Institute of Technology (WIT), so any reflected power measured by the VNA may be assumed as coming from the impedance mismatch. The measured VSWR results for both pairs of antenna will present in Chapter 5.

3.3.2 Two antenna gain method

There are different methods to measure antenna gain. In this research work, the method used is valid only where two antennas are identical [19] [42]. Identical antennas mean both

antennas are of the same type and dimensions and should have, therefore, very similar gains.

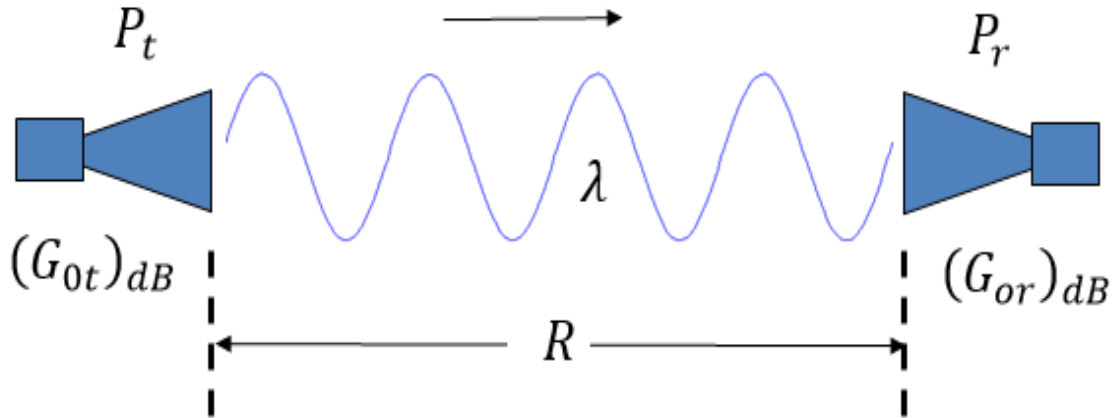


Figure 3-5 Diagram of two antenna gain method

The two-antenna method may be represented by

$$(G_{0t})_{dB} = (G_{or})_{dB} = \frac{1}{2} \left[20 \log_{10} \left(\frac{4\pi R}{\lambda} \right) + 10 \log_{10} \left(\frac{P_r}{P_t} \right) \right] \quad (3-2)$$

where

$(G_{0t})_{dB}$ = the gain of the transmitting antenna (dB)

$(G_{or})_{dB}$ = the gain of the receiving antenna (dB)

P_r = receiving power (W)

P_t = transmitting power (W)

R = antenna separation (m)

λ = operating wave length (m)

By using the initial (normal incidence) measurement as the reference, all subsequent measurements can be taken relative to this measurement. This offers the distinct advantage of not needing to include the antenna separation loss (the first term in (3-2)) in the radiation pattern calculation.

3.3.3 Mounting height over the ground

The height of the antenna is 1.5 m above the floor to avoid ground reflections. It was initially thought that it would be better to transmit at a height of 1m over the ground so that the incident wave is at the middle of window. The chosen antennas have a published (and verified here through tests) half power beam width that varies from 30° at 1 GHz to less than 10° at 6 GHz.

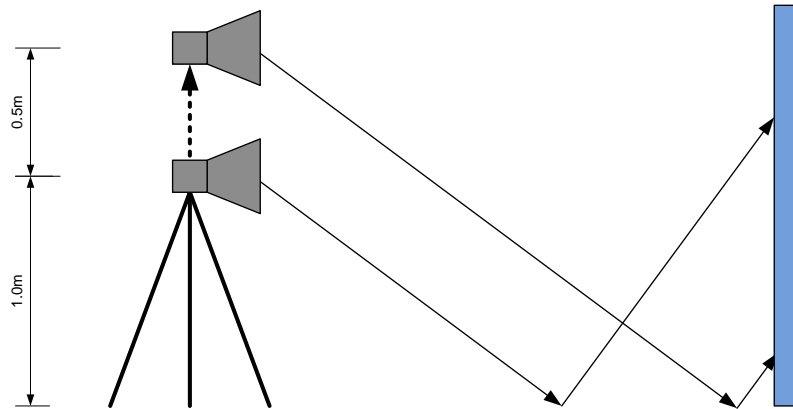


Figure 3-6 Ground wave reflection between 1 m and 1.5 m antenna height

The nearest ground reflection to the transmitter is defined by the lowest frequency, the half power beam width angles and also by the height of the transmitter above ground. Figure 3-7 shows at which distance the beam hits the ground the first time. Therefore, increasing the height of antenna from 1m to 1.5m will minimise the ground reflection [44], with the central beam now 0.5m higher than initially considered. This latter point is not of importance here as the window is simply that large. For later dielectric work, the target and receive antennas are simply elevated to accommodate the new height.

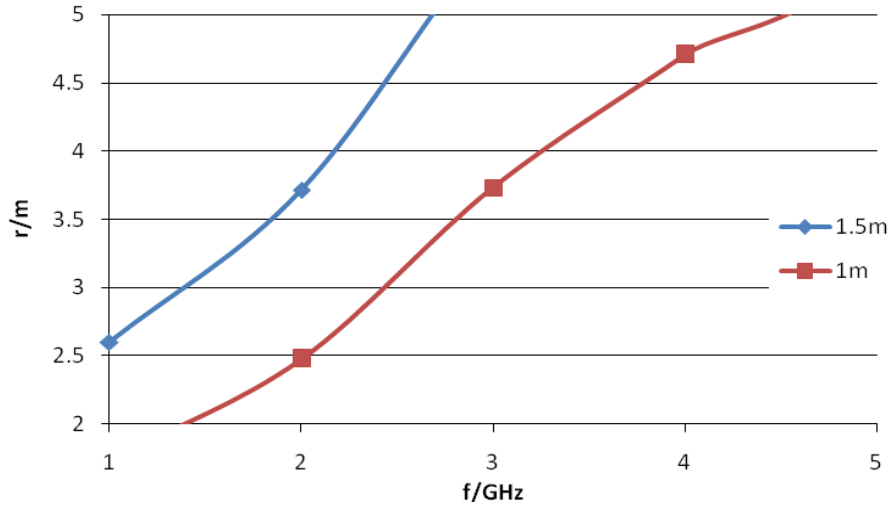


Figure 3-7 Position of the earliest ground reflection at transmitter antenna heights of 1 m and 1.5 m for all test frequencies

3.4 Antenna near and far field boundary theories

After a literature review on the near and far field boundary [43], very few published papers were found that delve into this topic [44], specifically papers, which uniquely define the far field boundary criterion.

In antenna measurement, the far field boundary can be an important condition. Near and far describe the nature of fields surrounding an antenna or an electromagnetic radiation source. The far field region is defined as “that region of the field of an antenna where the angular field distribution is essentially independent of the distance from the antenna [44]”.

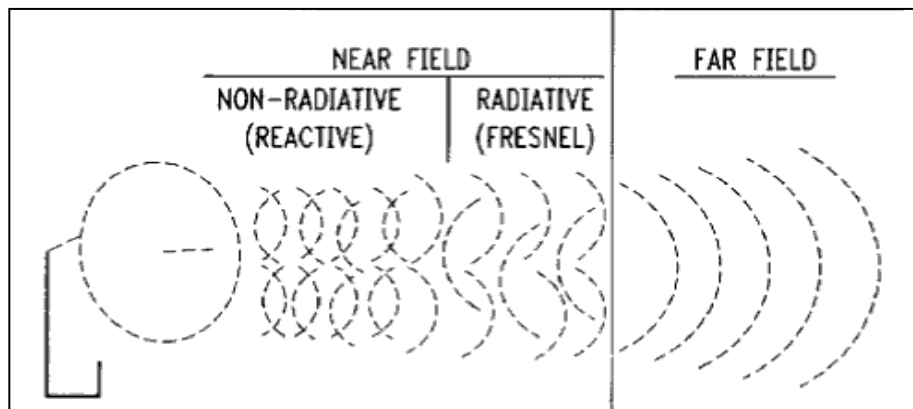


Figure 3-8 Antenna near field and far fields [45]

In fact, the regions around an antenna can be divided into three fields: reactive near field, radiating (Fresnel) near field and far (Frauenhofer) field as depicted in Figure 3-8. These three fields don't change abruptly from one field to the next, but every field may be defined by its own qualities.

The Reactive Near field region is defined as “that portion of the near field region immediately surrounding an antenna wherein the reactive field predominates” [19]. The radius of the outer boundary from this field is typically given by:

$$R_1 = 0.62 \sqrt{\frac{D^3}{\lambda}} \quad (3-3)$$

The radiating near field (Fresnel) region depends on the antenna parameter D . If the overall dimension D is not large compared to the wavelength, this region may not exist [43]. The inner boundary is shown in equation (3-3) and the outer boundary criterion is accepted by many as

$$R_2 \geq \frac{2D^2}{\lambda} \quad (3-4)$$

This boundary criterion is based on a maximum phase error of 22.5° from a simple dipole antenna. As the radiation pattern from a dipole antenna is spherical, it is easy to quantify the radiated wave's phase difference between the centre and the edge of receiving antenna. A phase difference that is accepted as standard is 22.5° ($\pi/8$), as shown for the horn antenna radiation pattern incident on a simple dipole receiver, in Figure 3-9. Other accepted standards use even smaller phase differences, if more precise measurements are required. For example, a tighter phase difference that is also used would be less than 1° , which requires a much greater separation of $R_2 \geq \frac{50D^2}{\lambda}$ [43].

In the case of 22.5° maximum phase difference, there will be a small difference in the measured wave between the edge and the centre of antenna in both amplitude and phase. However, the technique used compared the difference between two sets of results, with and without the MUT, but always at the same antenna separation. So this plane wave approximation over the entire antenna should not influence the results.

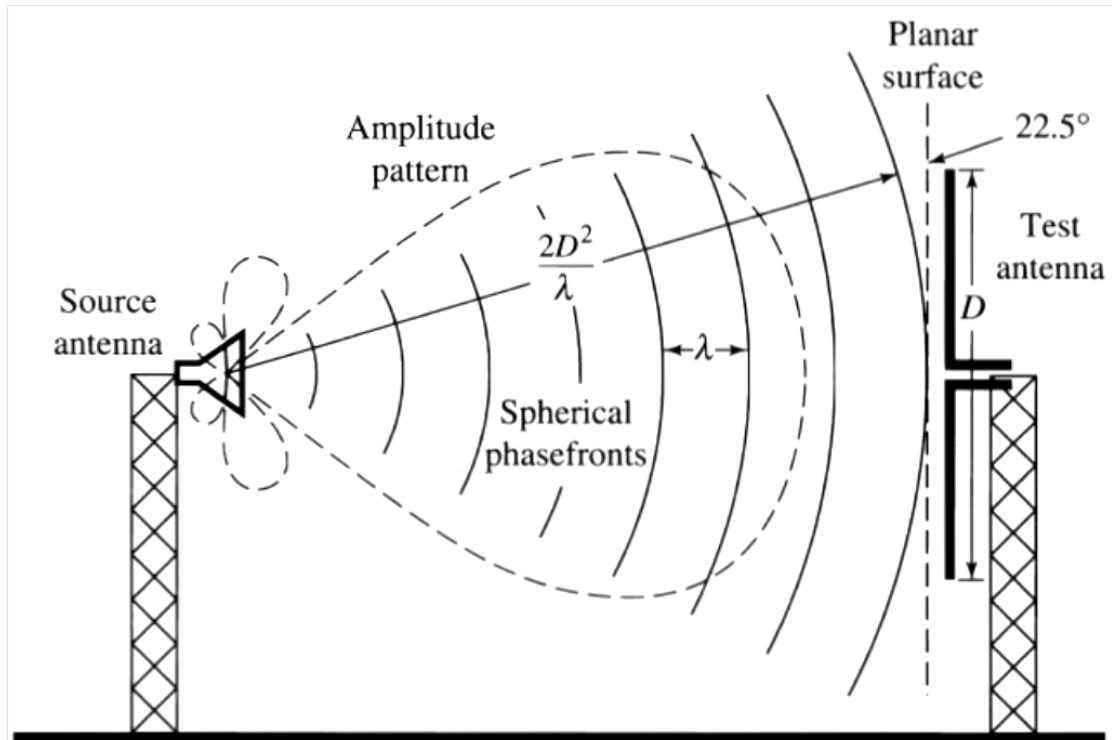


Figure 3-9 Phase error at the edges of a test antenna in the far-field when illuminated by a spherical wave [19]

It is possible to make similarly accurate measurements in the near field. In general near field measurement techniques can be expensive and very exacting, due to strict orientation and location requirements. However, in the case of dielectric analysis the near and far fields vary in the same manner (all fields are inversely proportional to the dielectric properties of the medium). The early work described in this report is derived from measurements in a large hall where the far field for the antennas was realisable, whereas later measurements were in the more confined environs of an RF anechoic chamber and were therefore restricted to the antennas near field region.

In measurements using antennas, there are other standards, apart from the two phase difference standards mentioned, to define the far field boundary. For example, the far field region is also defined as the region where the vectors H and E are perpendicular to each other. Therefore, in this region, the angle between the vectors H and E is independent of the radial distance from the radiating source. There are several criteria therefore in

determining an antenna's far field threshold and three of these conflicting criteria are listed below, with explanations as to how each is determined.

- 1) The phase difference criteria yield, for 22.5° and 1° respectively

$$R_2 = \frac{2D^2}{\lambda} \text{ and } \frac{50D^2}{\lambda} \quad (3-5)$$

- 2) Based on the point after which the electric and magnetic fields are always perpendicular to each other,

$$R_2 = 3\lambda \quad (3-6)$$

- 3) Equation (3-7) is used when the far field threshold is very large compared to the antenna size D (written as $r \gg D$, which is simplified to $r \geq 5D$). This criterion relates to an amplitude approximation ($\pi/16$ relates to the phase approximation).

$$R_2 = 5D \quad (3-7)$$

The boundary depends on the antenna dimension D and/or the operating wavelength, λ . For those criteria, there are different tests where each is deemed more appropriate.

When the radiation wave reaches the far field, the electric and magnetic fields are perpendicular to each other. The second far field separation criterion is determined by wave impedance. If using this criterion, it is necessary to find out where the angular field distribution is essentially independent of distance from the source.

This criterion is particularly important in Electromagnetic Compatibility (EMC) measurements, because the wave impedance is assumed constant at 120π (approximately 377Ω on the graph). Figure 3-10 shows the plot of electric and magnetic impedances versus normalised distance from the antenna. The horizontal axis shows the normalised distance, which is simply r/λ (distance from the antenna over wavelength). This boundary is defined in wavelengths, implying that the boundary moves in space with the wavelength (frequency) transmitted from the antenna.

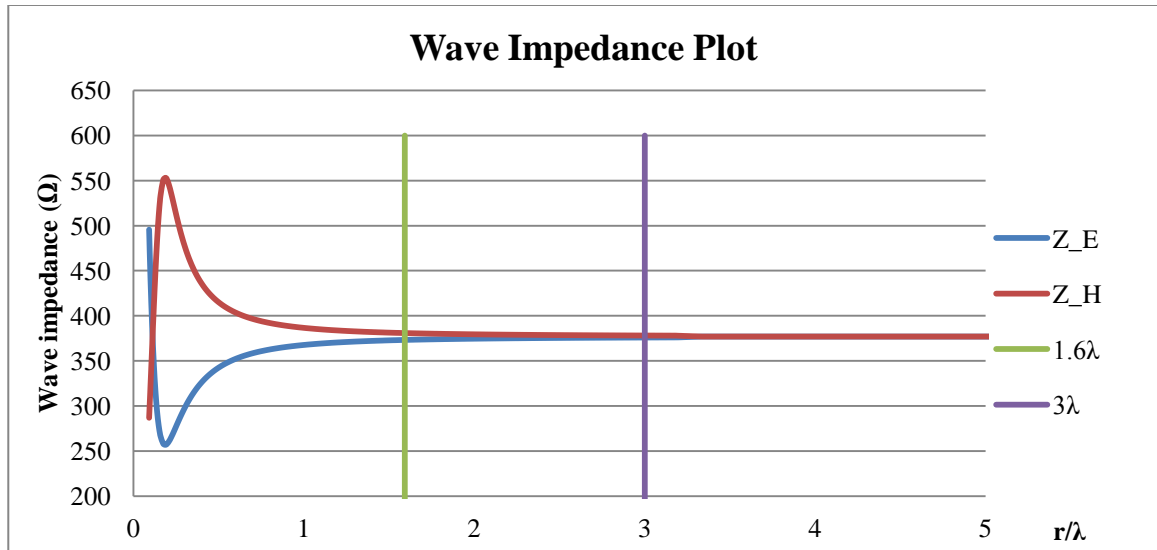


Figure 3-10 Impedance of E and H-fields moving away from the antenna

From the chart, Z_E is the electric field impedance and is defined as the ratio of two of the spherical geometry solutions to Maxwell's equations for the antenna, namely the electric field and magnetic field strengths, E_θ and H_ϕ , and, similarly, Z_H is the magnetic field impedance and is the ratio of E_ϕ and H_r .

From the plot, it can be seen that as the distance increases, both tend towards the same constant value of 377Ω or $120\pi\Omega$, which is the wave impedance of free space and can be derived as the plane wave solution to Maxwell's equations. Depending on test requirements, there are two possible selections for distance to the far field boundary. When 1.6λ is selected ($r/\lambda \approx 1.6$, shown as a green, vertical line on the graph), this occurs when both Z_E and Z_H are within 1% (or 3.77Ω) of 377Ω . However, when r/λ is roughly equal to 3 (purple, vertical line on the graph), for this criterion, the antenna spacing r is 3λ , and now both Z_E and Z_H are within 1Ω of 377Ω . More detailed analysis of the far field boundary criteria are attached in the appendix.

In summary, the different conditions and which criteria are most appropriate are shown in.

Table 3-1 Range criteria for far field boundary definition

Antenna dimension D	Appropriate minimum separation Equation
$D < \lambda/3$	$R_2 = 3\lambda$
$\lambda/3 < D < 2.5\lambda$	$R_2 = 5D$
$D > 2.5\lambda$	$R_2 = 2D^2/\lambda$

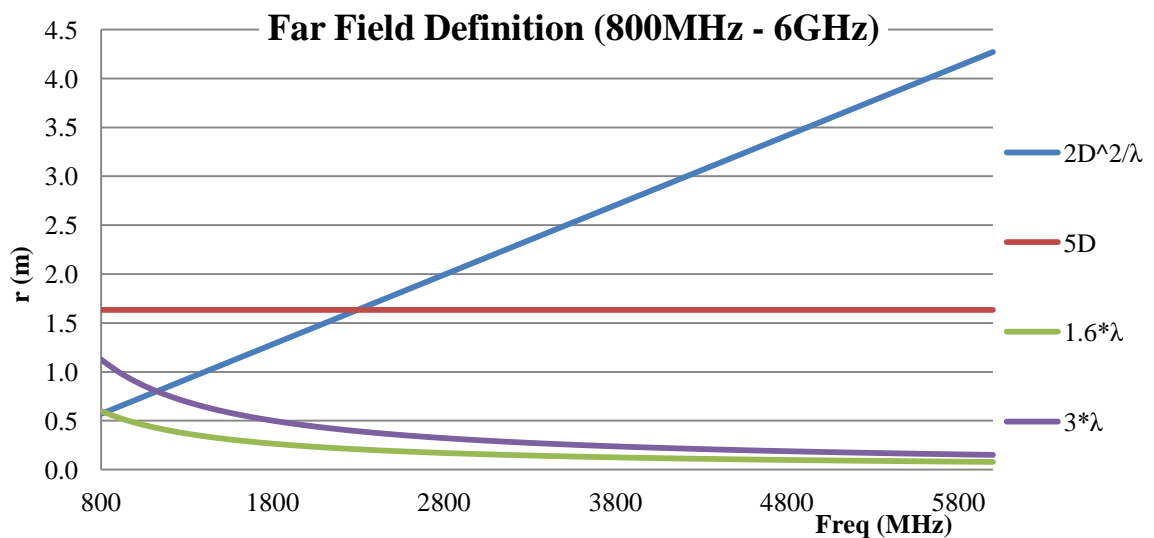


Figure 3-11 Different far field boundaries for Schwarzbeck BBHA 9120

Some of the far field criteria are plotted against their 800-6000MHz measurement range, in Figure 3-11 for the Schwarzbeck BBHA 9120 LFA Horn Antenna used in this research measurement and for which $D=0.33\text{m}$. This plot indicates a recommended antenna separation of 4.35m for far field measurements for this antenna over the entire range. In fact a separation of 5m was used for most early stage far field measurements. (This corresponds to a separation from $10-100\lambda$, for the frequencies used, if considering the other far field criteria). For the other pair of antennas (SchwarzbeckJXTXLB-90-20-C), the

primary antenna dimension $D=0.25\text{m}$, so the far field criteria can be plotted as shown in Figure 3-12. This indicates a minimum recommended antenna separation of 12m for far field measurements [41].

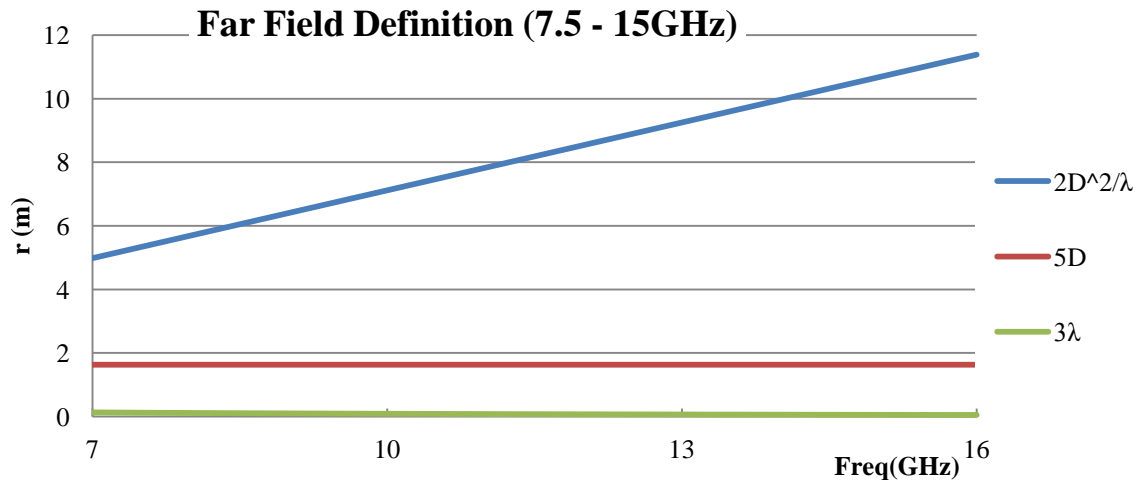


Figure 3-12 Far field boundaries for second pair of antennas 7.5GHz to 15 GHz measurement setup

The calculations here are based on a self-developed TRL/M calibration technique, which works for both the near and far field measurements. With this calibration a new near field antenna separation distance of $D=0.50\text{m}$ was also used for some of the later measurements. This separation allows the measurement system from the large hall to be deployed inside the smaller confines of the WIT RF anechoic chamber, which is a more confined space than the large hall used for the far field measurements.

3.4.1 Large hall

Due to the far field requirements, these tests were performed in a big hall (approximately 45m x 30m x 8m). A custom-built wooden frame (2.1m x 1.1m cross-section), with rounded edges to reduce diffraction effects, (Figure 3-13) was created to hold the glass under test in a position normal to the propagating wave. A similar technique was used in the National Institute of Standards and Technology (NIST) in Boulder, Colorado, USA, shown in Figure 3-14.

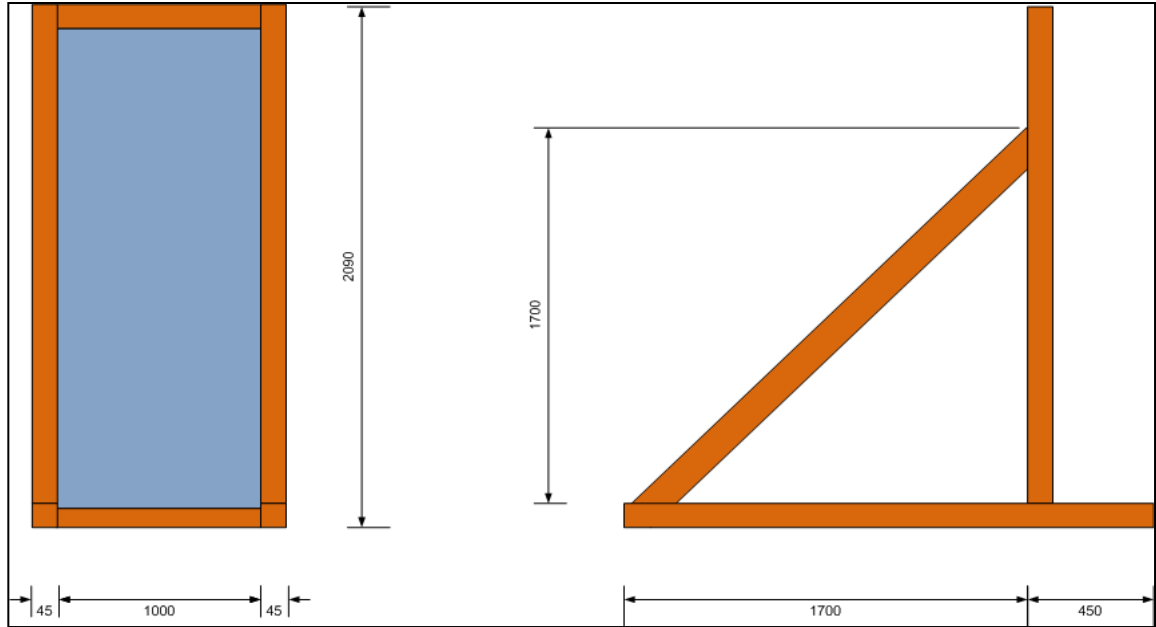


Figure 3-13 Custom-built test frame, was built by PhD candidate and used in WIT. Unit: mm

Figure 3-15 and Figure 3-16 show the first custom-built glass tank, for liquid and powder dielectric property measurements. This first tank was later improved to introduce the ability to vary dielectric powder or liquid thickness.

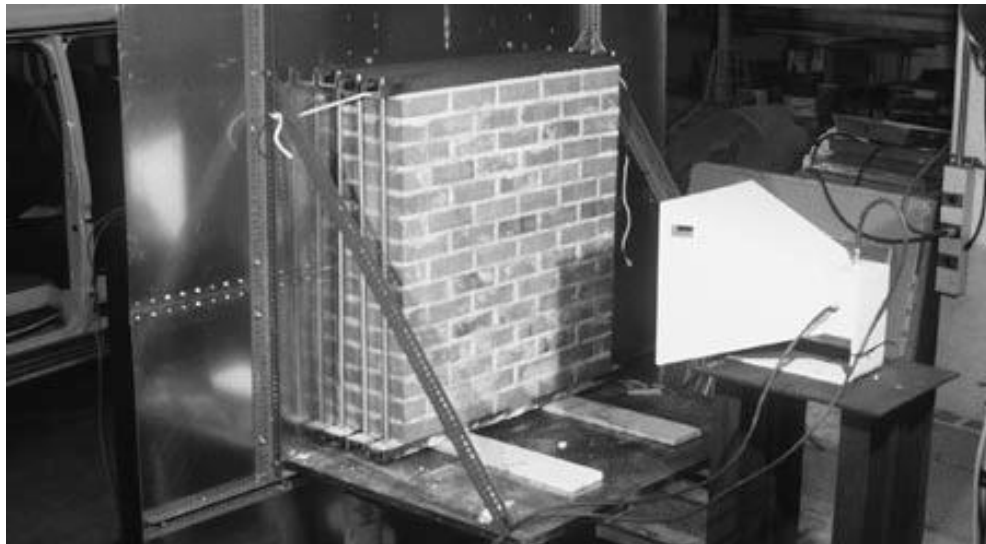


Figure 3-14 Free space test structure, was used in the National Institute of Standards and Technology (NIST) in Boulder, Colorado, USA [46]

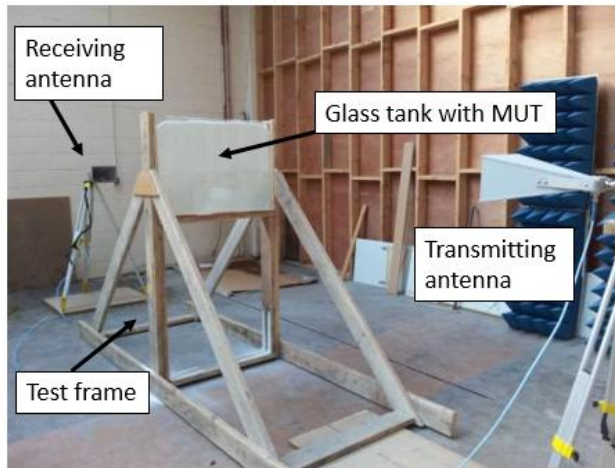


Figure 3-15 Test structure with glass tank placed

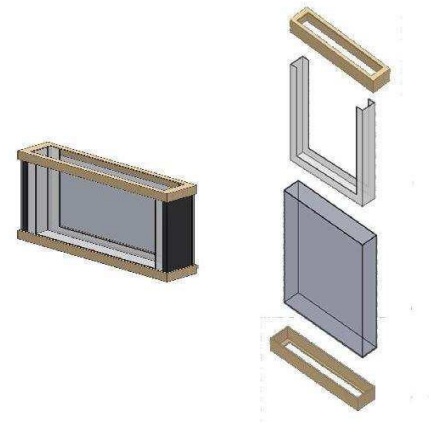


Figure 3-16 Glass tank assembly

3.4.2 Flexible thickness container design

The dielectric tests were carried out initially on standard glass panes and then on some non-solid materials (salt, sugar and tap water).

In order to test the dielectric materials (powder and liquids), a prototype glass container was made that could hold a fixed 50mm of material in the propagation path. The other tank dimensions were 1000mm by 500mm and it could be easily filled with powder or liquid material. A free space measurement technique for dielectric property calculation was applied to this prototype glass container. As mentioned earlier in Chapter 2, this technique is non-destructive, and is also suitable for the non-solid dielectric material characterization, such as liquids or powder material, as long as the probing beam can be guaranteed to pass through a uniform thickness of homogenous MUT. More detail of free space techniques conversion algorithm will be introduced in Chapter 4.

For unknown dielectrics, a modified approach was applied to overcome the unknown permittivity value. In this case a newer container was developed with the ability to control the container thickness d_i . The new platform consisted once again of a container made of glass panes, whose uniform separation could be controlled. A block diagram representation is shown in Figure 3-17, where spacing can vary from a minimum value of $d_l = 3\text{mm}$ to a

maximum value of $d_2 = 18\text{cm}$, the latter figure having been chosen simply to place an upper limit on the material tested. This means there is a lot of flexibility in MUT thickness, so the MUT can either be made electrically thin or, for wide spacing, could have sufficient material loss that the multiple reflections between the two containing glass surfaces can be neglected. Glass is not perfectly rigid, so the 18cm maximum thickness also helped to reduce the effects of sample thickness variation. The low value for d_1 was selected to facilitate uniform packing of powder, reduce the impact of thickness variation due to slight imperfections or bulging in the glass and to measure phase variation directly for low valued dielectrics [47].

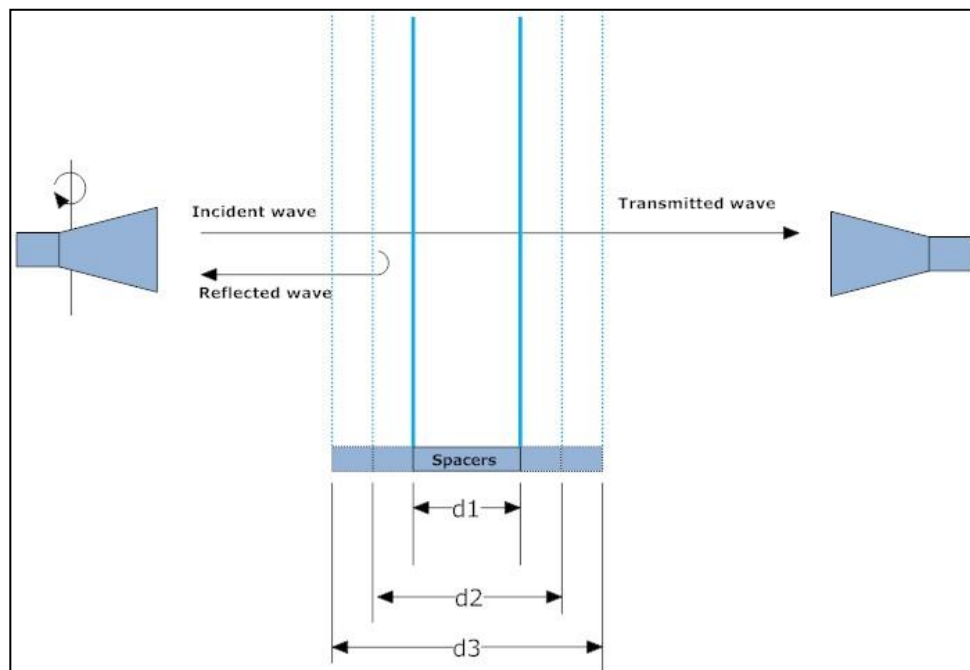


Figure 3-17 Horizontal design of glass tank container with a flexible thickness

During testing, two more tanks were developed with two different sizes of 60cm by 40cm and 40cm by 30cm, to help isolate errors associated with container misalignment, a topic that will be addressed in section 5.8.3.

Five different thickness glass panes, of 4mm, 6mm, 8mm, 12mm and 15mm, were tested individually and then as the walls to contain powder dielectrics,. The flexible tank was made from two panes of identical thickness glass as a sandwich structure, although Perspex and hard plastic boards were also tested.

Several different powders and liquids were tested in the tank, including household powders such as plain flour, white sugar and table salt. The powders were tested at thicknesses including 3mm, 8mm, 30mm and as large as 36mm.

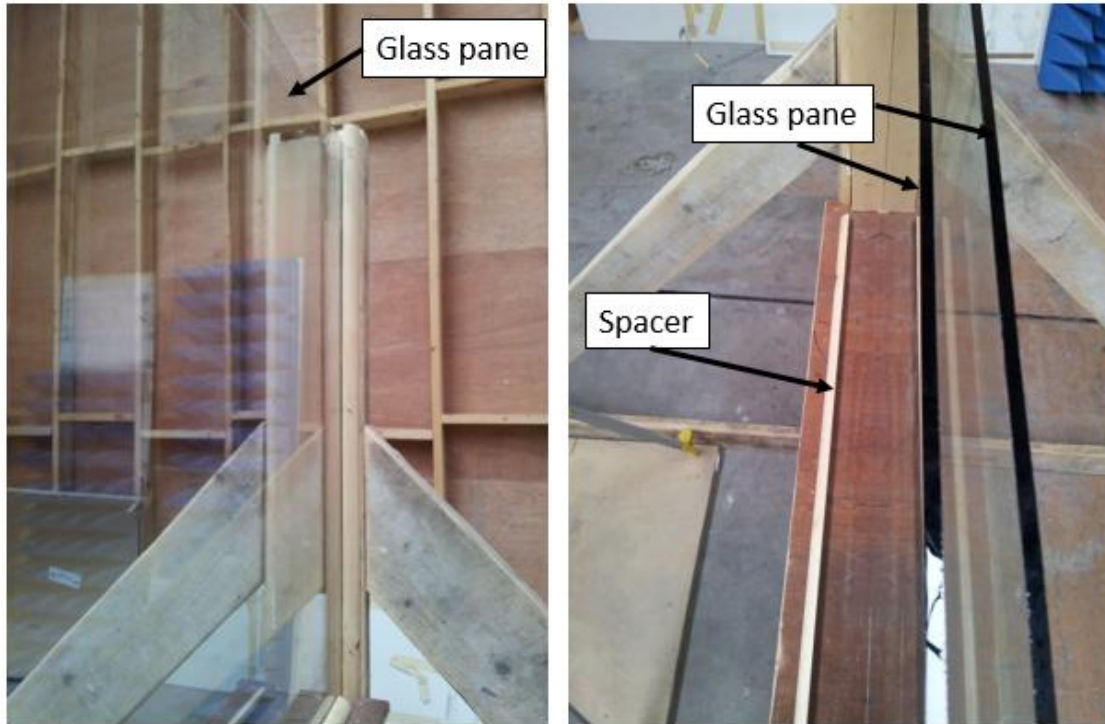


Figure 3-18 Horizontal design structure of glass tank container with a flexible thickness, in the picture indicated position of glass pane and spacer, which control the material thickness

3.4.3 Anechoic chamber

Fully anechoic RF chambers have all surfaces covered with resistive foam pyramid absorbers. The foam absorbers are impregnated with graphite powder and are usually pyramidal or even better conical in shape in order to maximise the path of an incident wave. Maximising the path increases the amount of signal incident on the graphite powder, thereby transferring more energy from the wave into the powder. The function of a fully anechoic test chamber is to copy or mimic free space by using absorbers that have ‘*progressive impedance*’; this is, to prevent reflectivity by gradually absorbing the energy. A fully anechoic chamber can be of any size depending on the requirement. The outer skin is normally metal, where the high conductivity is an effective shield against electric fields (Faraday cage). Ideally the metal would also have a high magnetic permeability, to provide

a low reluctance path around the room, to slow-varying or static magnetic fields. The WIT RF chamber is enclosed in sheet steel for these reasons.

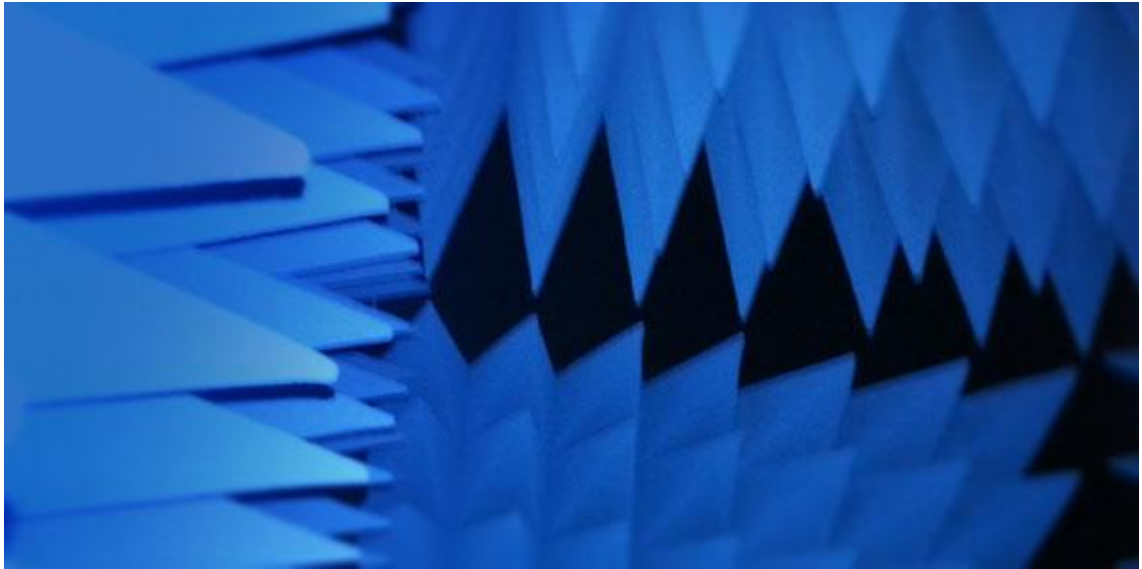


Figure 3-19 WIT Anechoic chamber, which this PhD candidate was involved in the designing building and characterising work

The WIT RF anechoic chamber foam was fitted out by this PhD candidate, the supervisor and an exchange student. The pyramid absorber foam used is the *APM 45* from Siepel, which has a claimed attenuation from -25 to -50dB in the frequency range 500MHz to 40GHz [48]. It has been used for some tests outside of the chamber, such as the large hall mentioned in Section 3.3).

Figure 3-20 and Figure 3-21 show the tests carried out for the qualification of the chamber and its pyramidal RF absorbers, using a VNA. Chamber qualification results are also presented in Chapter 5. For now, it is simply worth mentioning that the RF absorbent foam reflection results for normal incidence were similar to the manufacturer's claimed values, at the measurement frequency range of 800MHz to 6GHz and the signal leakage from or into the chamber was about -70dB.

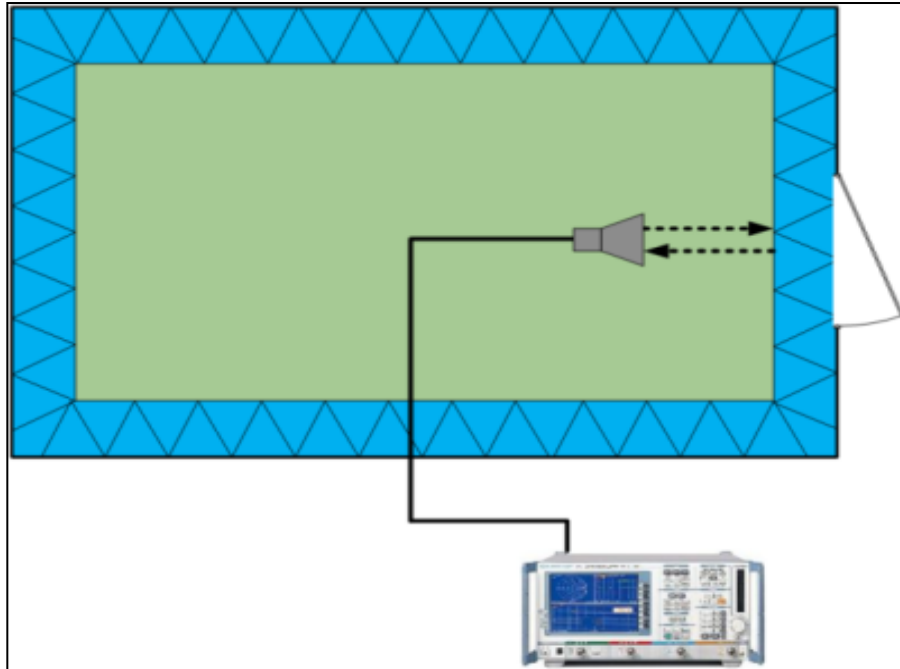


Figure 3-20 Measurement of attenuation at the door (normal incidence)

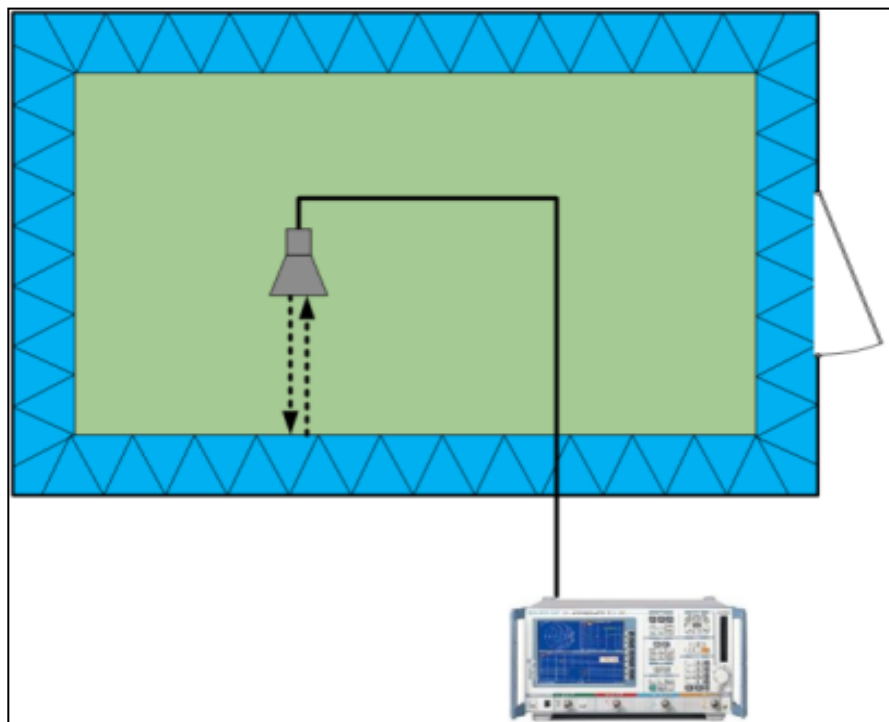


Figure 3-21 Measurement of attenuation at the sidewall (normal incidence)

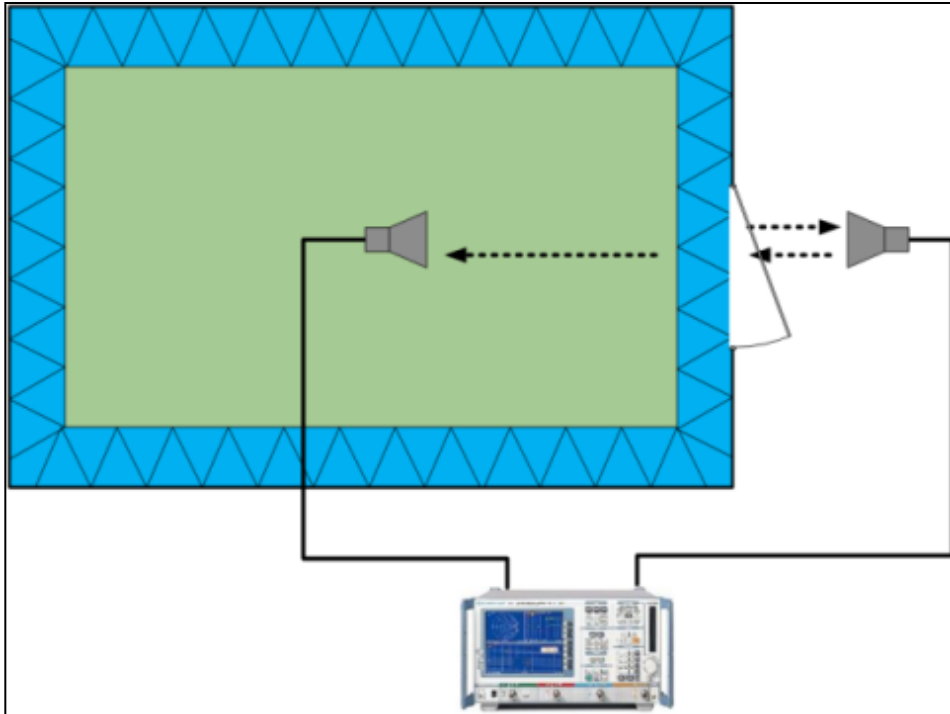


Figure 3-22 Measurement of attenuation through the door (normal incidence)

In addition, with the principle of the Faraday cage it is possible to create a non-interference area inside the chamber. That means that no signals propagate from outside to inside (e.g. RF waves). In Figure 3-22 the test setup is to verify that there is no leakage of any consequence from the chamber.

3.5 Wireless propagation testing

Early work described here focussed on examining wireless propagation through various materials to build up an understanding of the requirements of free space measurement, especially free space calibration. Various calibration techniques were used throughout the work, but in the early stages the calibration plane was simply at the cable end, just before the antennas, with measurements normalised to show the change in performance due to the introduction of the MUT. The wooden test frame mentioned in Section 3.4.1 was built to hold the MUTs, which varied in size, shape and density and included double glazed energy efficient windows, insulating building materials, vehicle transparent glass and vehicle window tints.

3.5.1 Energy efficient windows

Transparent conductors (TCs) are gaining widespread acceptance in glass manufacture, as a means of controlling the energy leaving (or entering, in warmer climates) buildings. Legislation has been introduced to encourage this, such as Germany's *Verordnung über energiesparenden Waermeschutz und energie sparende Anlagentechnik bei Gebaeuden (Energiesparverordnung - EneV)*, which states that the energy demand shall be reduced by over 30% and in a further step by the year 2012 by a further 30%, compared with previous legislated levels [49].

The industry response has focussed primarily on the use of TC coatings, usually on one of the inward facing sides in a double glazed unit. The aim of applying thin coats of TC is to reduce heat transfer across a vertically mounted window. However, this coating also reduces the wireless signal propagation. The initial research was to exam the attenuation of these coated energy efficient window. This work was published at the European Wireless Conference, Lucca. A copy of the paper is in the Appendices.

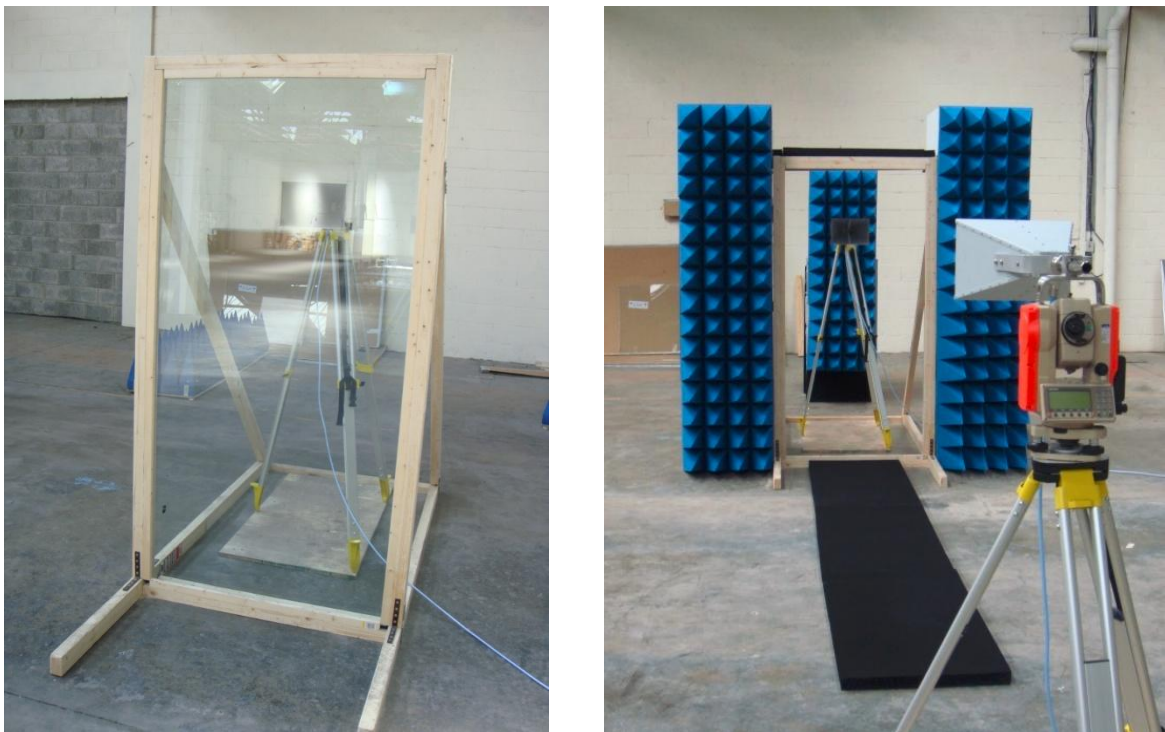


Figure 3-23 Energy efficient window measurement

3.5.2 Building materials

In the modern energy conscious world, energy efficient materials are widely used as part of building heat retention. According to previous research on the propagation measurement of traditional building materials (such as block, solid concrete, wood, bricks, etc.), wireless propagation through building walls can be strongly attenuated [46]. For this reason, the principle propagation path into buildings has been through the building openings, namely external doors and windows. However, the international demand for improved energy efficiency has led to an examination of building openings in terms of their poor ability to retain heat within the building. As mentioned in the previous section, this has in turn led to the manufacture of windows that are much better at retaining heat, but with a significant negative consequence for wireless, with measured attenuation of up to -30dB, (results presented in Chapter 5).

The final significant access opportunity into a building is via the roof. There are many different materials used in roofing, including natural slate and engineered slate, wood, concrete tiles and (internally) insulation. This work therefore examined the signal attenuation for various materials used in both roof and wall construction. It also recorded the dielectric response of each material for future use in material dielectric analysis.

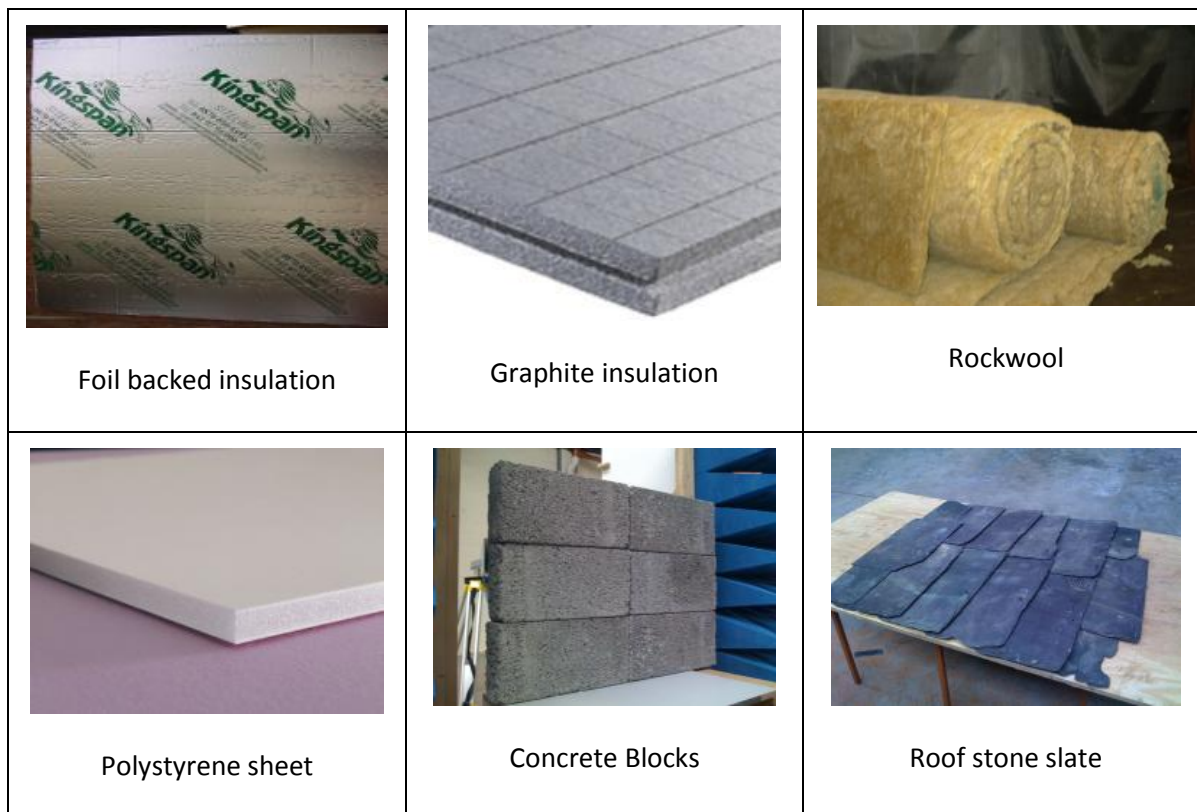


Figure 3-24 Building materials tested

Results from this work were accepted at the *IET Colloquium on Antennas, Wireless and Electromagnetics*, Loughborough, UK, 2013. A copy of the presentation is included in the Appendices.

3.5.3 Vehicle glass and window tints

Signal transmission into and out of a vehicle is also a modern issue in wireless communications. Apart from the metal structure, which will not permit passage to any appreciable signal strength, the question to be answered in this part of the research is whether the vehicle glass causes any significant attenuation of the wireless signals.

In particular most vehicle rear windows which have integrated heating wire are a potential risk to signal propagation. In addition, some vehicles with front window heating wire should also be taken into account. Although not widely used on vehicles, four different types of vehicle window tint film were also measured. Results are presented in Chapter 5.

3.6 Conclusion

Chapter 3 described the test platforms developed in the course of this work in WIT. For propagation material tests (including tests on materials such as energy efficient glass, building materials and vehicle glass), various accepted far field definitions were presented to help select the actual measurement separation distance. In terms of the test setup, the chapter describes the characterisation of the two antenna pairs, simple and progressively more elaborate VNA calibration methods, horizontal and vertical propagation measurement techniques, construction of several test frames, construction and qualification of an RF anechoic chamber and, finally, the development of an ability to measure variable material thicknesses for both the horizontal and vertical techniques. For each of these points, the selection parameters were explained and justified and a description was offered of the various problems encountered and solutions attempted.

4 Permittivity and permeability parameter extraction algorithms

The VNA S-parameter measurements produce results that represent the probing signal's amplitude and phase variations depending on the dielectric material's permittivity and permeability. Several algorithms have been proposed to extract that material permittivity and permeability data from the S-parameter measurements. As mentioned in Chapter 2, the four most important of these algorithms will be discussed here, namely Nicolson-Ross-Weir (NRW), NIST iterative, the New non-iterative (NNI) techniques and Free-space techniques.

All the techniques listed in this chapter are based on a symmetrical test setup, where the same results should be obtained if transmitter becomes receiver and vice versa. Therefore, in terms of the S-parameters $S_{11}=S_{22}$, $S_{21}=S_{12}$.

The Nicholson-Ross-Weir (NRW) technique is popular and uses either two or all four S-parameters. However, it does not produce accurate results at sample sizes that are integer multiples of the incident beam's half wavelength, something which is increasingly likely when the measurement range of frequencies is broadband, such as the range 800-6000MHz used in this work. The NIST Iterative technique uses NRW as a starting point and then the Newton-Rapheson method to solve for the dielectric parameters. This technique is more elaborate than NRW, but overcomes the NRW weakness, as it is accurate at sample sizes that are integer multiples of the incident beam's half wavelength. The technique known as the New Non-Iterative (NNI) technique is based on a simplified version of the NRW technique. It is suitable for permittivity calculation for the case that the permeability $\mu_r = 1$, which will be the case for non-magnetic materials in which there are also no currents induced by the applied electromagnetic field. Free space measurements are non-destructive and contact-free. They usually use NRW as starting point and introduce complex propagation constant to solve complex permittivity and so is also as the starting point used in this PhD work.

4.1 Nicolson-Ross-Weir technique (NRW)

NRW is popular and uses two or all four S-parameters, depending on the measurement technique. The reflection and transmission coefficients are related to the S-parameters and given by:

$$S_{11} = \frac{\Gamma(1 - T^2)}{1 - \Gamma^2 T^2} \quad (4-1)$$

$$S_{21} = \frac{T(1 - \Gamma^2)}{1 - T^2 \Gamma^2} \quad (4-2)$$

Those parameters (S_{11} and S_{21}) can be easily and accurately obtained using a VNA, a technique described in Chapter 3.

The reflection coefficient, Γ , can be obtained by inverting equations (4-1) and (4-2) and is given by

$$\Gamma = X \pm \sqrt{X^2 - 1} \quad (4-3)$$

where $|\Gamma| < 1$ is required for finding the correct root value.

$$X = \frac{S_{11}^2 - S_{21}^2 + 1}{2S_{11}} \quad (4-4)$$

Similarly, an expression for the transmission coefficient, T , can be obtained:

$$T = \frac{S_{11} + S_{21} - \Gamma}{1 - (S_{11} + S_{21})\Gamma} \quad (4-5)$$

The free space wavelength, λ_0 , and the cut off wavelength, λ_c , are related to the transmission and reflection coefficients by the equation

$$\frac{1}{\Lambda^2} = \left(\frac{\epsilon_r \times \mu_r}{\lambda_0^2} - \frac{1}{\lambda_c^2} \right) \quad (4-6)$$

where Λ is a unitless factor. In addition, for a coaxial line or for free space, $\lambda_c = \infty$.

After solving the equation and relating it to the sample length and the transmission coefficient, equation (4-7) can be arrived at,

$$\frac{1}{\Lambda} = - \left[\frac{1}{2\pi L} \ln \left(\frac{1}{T} \right) \right]^2 \quad (4-7)$$

As in equation (4-7), there is an infinite number of roots. The imaginary part of the complex number T is equal to the angle of the complex value plus $2\pi n$, where n is an integer. The value of n relates to the unknown material electrical length.

So, the permittivity and the permeability can be derived from the above equations,

$$\epsilon_r = \frac{\lambda_0^2}{\mu_r} \left(\frac{1}{\lambda_c^2} - \left[\frac{1}{\lambda_0} \ln \left(\frac{1}{T} \right) \right]^2 \right) \quad (4-8)$$

$$\mu_r = \frac{1 + \Gamma}{\Lambda(1 - \Gamma) \sqrt{\frac{1}{\lambda_0^2} - \frac{1}{\lambda_c^2}}} \quad (4-9)$$

However, NRW becomes unstable when the sample thickness is an integer multiple of one half wavelength ($n\lambda/2$) of the probing beam. Clearly this is a particular problem when the probing beam is broadband, as is the case in this work, as the instability will recur in the derived dielectric constant. The value of S_{11} becomes very small or zero [50] at this point. The reason is the interference and partial cancellation of the reflected wave from the back surface and the reflected wave from the front surface, which leads to very small values of the measured reflection S_{11} measured what is shown in Figure 4-1.

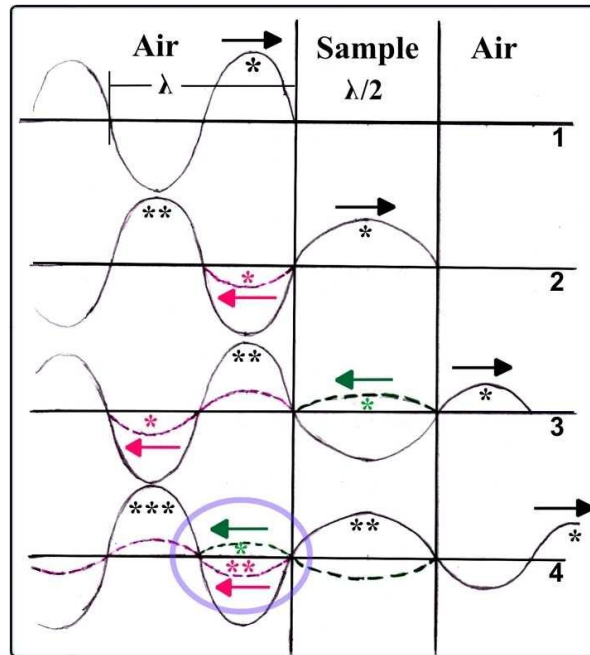


Figure 4-1 Cancellation leading to a small S_{11} value

These small values produce peaks in the term $1 + \Gamma / 1 - \Gamma$ from the NRW Equation (4-9), and therefore peaks in the permittivity curve, as Boughriet *et al.* [25] have demonstrated. Figure 4-2 shows the variation in ϵ_r' versus frequency for a PTFE sample. This displays the resulting inaccurate peaks from cancellation of the reflection from the back surface and the reflection on the front surface. The solid line shows the result for ϵ_r' by using the NRW model and the dashed line shows the iterative solution from using the NIST model, which uses an initial guess from NRW equations. This $\lambda/2$ problem appears at measurement wavelengths, which are integer multiples of $\lambda/2$ sample lengths [18].

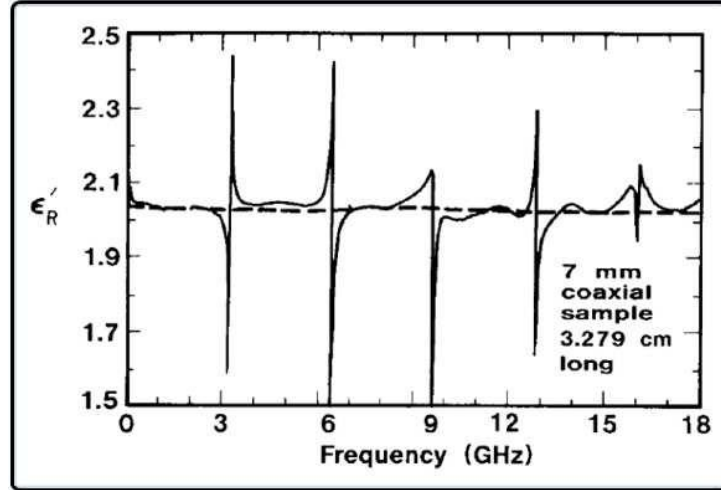


Figure 4-2 ϵ_r' versus frequency for a PTFE sample.

4.2 NIST iterative technique

The NIST iterative technique uses the NRW technique to obtain the initial values. This technique then uses the Newton-Rapheson root finding technique, thereby overcoming the weakness of NRW. As described in Chapter 2, the NIST technique overcomes the instability peaks that exist in NRW technique when the sample thickness is an integer multiple of one half wavelength ($n\lambda/2$). It is suitable for long samples and characterizing low loss materials. However, if the approximate permittivity value of the material is known, then the reflection and transmission coefficient can be deduced from the following equations:

$$\Gamma = \frac{\frac{\gamma_0}{\mu_0} - \frac{\gamma}{\mu}}{\frac{\gamma_0}{\mu_0} + \frac{\gamma}{\mu}} \quad (4-10)$$

where γ_0 is the propagation constant in air. It can be defined as

$$\gamma_0 = j \sqrt{\left(\frac{\omega}{c}\right)^2 - \left(\frac{2\pi}{\lambda_c}\right)^2} \quad (4-11)$$

And the propagation constant in material γ can be defined as

$$\gamma = j \sqrt{\frac{\omega^2 \mu_r \epsilon_r}{c^2} - \left(\frac{2\pi}{\lambda_c}\right)^2} \quad (4-12)$$

Then the reflection and transmission coefficient are (for the case where $\mu_r=1$)

$$\Gamma = \frac{\frac{Y_0}{\mu_0} - \frac{Y}{\mu}}{\frac{Y_0}{\mu_0} + \frac{Y}{\mu}} = \frac{Y_0 - Y}{Y_0 + Y} \quad (4-13)$$

$$T = e^{(-\gamma L)} = e^{-jL \sqrt{\frac{\omega^2 \mu_r \epsilon_r}{c^2} - \left(\frac{2\pi}{\lambda_c}\right)^2}} \quad (4-14)$$

After solving those equations, a function of permittivity, $F(\epsilon_r)$ is arrived at:

$$F(\epsilon_r) = S_{11}S_{22} - S_{21}S_{12} - [e^{-2\gamma_0(L_{air}-L)}] \frac{T^2 - \Gamma^2}{1 - \Gamma^2 T^2} \quad (4-15)$$

$$F(\epsilon_r) = \frac{S_{21} + S_{12}}{2(1 - T^2 \Gamma^2)} - T(1 - \Gamma^2) e^{-2\gamma_0(L_{air}-L)} \quad (4-16)$$

Apply the Newton-Rapheson numerical method for the roots calculation of $F(\epsilon_r)$. To determine the roots by the Newton method, a Jacobian matrix is calculated [24].

$$J = \begin{pmatrix} \frac{f_1(\epsilon' + h, \epsilon'') - f_1(\epsilon' - h, \epsilon'')}{2h} & \frac{f_1(\epsilon', \epsilon'' + h) - f_1(\epsilon', \epsilon'' - h)}{2h} \\ \frac{f_2(\epsilon' + h, \epsilon'') - f_2(\epsilon' - h, \epsilon'')}{2h} & \frac{f_2(\epsilon', \epsilon'' + h) - f_2(\epsilon', \epsilon'' - h)}{2h} \end{pmatrix} \quad (4-17)$$

Where, $F(\epsilon_{r1}) = f_1(\epsilon', \epsilon'')$, $F(\epsilon_{r2}) = f_2(\epsilon', \epsilon'')$

Then the conversion process can be presented as,

$$\epsilon_{r(new)} = \epsilon_r + \Delta\epsilon_r \quad (4-18)$$

where $\Delta\epsilon_r$ is the change that brings the permittivity value close to the desired value.

This technique depends on the initial guess of the permittivity. This technique is suitable where the permittivity value of the material is known approximately. However, if the material properties are unknown, then the NIST technique can also be unstable.

4.3 New non-iterative technique (NNI)

The new non-iterative technique has the advantage of being stable over a whole range of frequencies for an arbitrary sample length. The NNI technique is based on a simplified version of the NRW technique and no divergence is observed at frequencies corresponding to multiples of one-half wavelength in the sample. The NNI technique uses a slightly different formulation from the NRW technique and it can be easily extended to other measuring methods. From Equation (4-3) the reflection coefficient can be written as

$$\Gamma = X \pm \sqrt{(X^2 - 1)} \quad (4-3)$$

where $|\Gamma| < 1$ is required for finding the root.

As mentioned early in this chapter, the tests performed were based on a symmetrical setup, where the transmit and receive antenna could swop roles, without effecting the outcome. This was verified throughout the testing, for example during the propagation tests on the energy efficient windows, where the roles of transmitting and receiving antenna when switched still gave almost identical results.

In terms of the S-parameters, based on this symmetrical test setup, X from Equation (4-4) was defined as:

$$X = \frac{S_{11}^2 - S_{21}^2 + 1}{2S_{11}} \quad (4-4)$$

The transmission coefficient from Equations (4-5) and (4-6) is also reproduced for convenience here

$$T = \frac{S + S_{21} - \Gamma}{1 - (S_{11} + S_{21})\Gamma} \quad (4-5)$$

$$\frac{1}{\Lambda^2} = \left(\frac{\epsilon_r \times \mu_r}{\lambda_0^2} - \frac{1}{\lambda_c^2} \right) = - \left(\frac{1}{2\pi L} \ln \left(\frac{1}{T} \right) \right)^2 \quad (4-6)$$

where λ_0 is free space wavelength and λ_c is the cut off wavelength.

As in waveguide measurement for dielectric analysis, the wavelength is

$$\lambda_{og} = \frac{1}{\sqrt{\frac{1}{\lambda_0^2} - \frac{1}{\lambda_c^2}}} \quad (4-19)$$

Then the material's electromagnetic parameters are defined as

$$\mu_{eff} = \frac{\lambda_{og}}{\Lambda} \left(\frac{1 + \Gamma}{1 - \Gamma} \right) \quad (4-20)$$

$$\varepsilon_{eff} = \frac{\lambda_{og}}{\Lambda} \left(\frac{1 - \Gamma}{1 + \Gamma} \right) \quad (4-21)$$

With the result of the calculation for Γ , these electromagnetic parameters can easily be determined.

Therefore it can be deduced that

$$\mu_r = \mu_{eff} = \frac{\lambda_{og}}{\Lambda} \left(\frac{1 + \Gamma}{1 - \Gamma} \right) \frac{1}{\sqrt{\frac{1}{\lambda_0^2} - \frac{1}{\lambda_c^2}}} \quad (4-22)$$

$$\varepsilon_r = \left(1 - \frac{\lambda_0^2}{\lambda_c^2} \right) \varepsilon_{eff} + \frac{\lambda_0^2}{\lambda_c^2} \frac{1}{\mu_{eff}} \quad (4-23)$$

If the MUT is purely non-magnetic, with no induced currents, then $\mu_r = 1$, so

$$\varepsilon_{eff} = \varepsilon_{eff}(\mu_{eff})^n = \left(\frac{1 - \Gamma}{1 + \Gamma} \right)^{n-1} \left(\frac{\lambda_{og}}{\Lambda} \right)^{n+1} \quad (4-24)$$

where n=1 is for new non-iterative technique.

4.4 Free space measurement technique

The free space technique is non-destructive, contact-free and less restrictive than NRW, NIST and NNI techniques on MUT thickness or even shape as long as the probing beam can be guaranteed to pass through a uniform thickness of homogenous MUT. The free space technique can apply to broadband tests and can be used for testing a wide range of

materials, such as gases, solids, liquids and powers. Similar to the NRW technique, the reflection and transmission coefficients are related to the scattering parameters and given previously by Equations (4-1) to (4-5):

$$S_{11} = \frac{\Gamma(1 - T^2)}{1 - \Gamma^2 T^2} \quad (4-1)$$

$$S_{21} = \frac{T(1 - \Gamma^2)}{1 - T^2 \Gamma^2} \quad (4-2)$$

Once again, those parameters can be easily directly measured with a properly calibrated VNA.

The reflection coefficient, Γ , is given by

$$\Gamma = X \pm \sqrt{X^2 - 1} \quad (4-3)$$

where

$$X = \frac{S_{11}^2 - S_{21}^2 + 1}{2S_{11}} \quad (4-4)$$

The transmission coefficient, T , is:

$$T = \frac{S_{11} + S_{21} - \Gamma}{1 - (S_{11} + S_{21})\Gamma} \quad (4-5)$$

The chosen of the plus or minus is defined by $|\Gamma| < 1$. Then

$$\varepsilon = \frac{\gamma}{\gamma_0} \left(\frac{1 - \Gamma}{1 + \Gamma} \right) \quad (4-25)$$

$$\mu = \frac{\gamma}{\gamma_0} \left(\frac{1 + \Gamma}{1 - \Gamma} \right) \quad (4-26)$$

The magnitude of the material propagation constant can be written as

$$\gamma = \frac{[\log_e(1/T)]}{d} \quad (4-27)$$

where d is the thickness of MUT.

Since T is a complex number, the complete equation for the material propagation constant can be written as

$$\gamma = \frac{[\log_e(1/|T|)]}{d} + j \left(\frac{2\pi n - \phi}{d} \right) \quad (4-28)$$

where $n=1, 2, 3\dots$

The real part is single valued, but the imaginary part may have multiple values. So,

$$\text{imaginary part of } (\gamma) = \text{phase constant } (\beta) = 2\pi/\lambda_m \quad (4-29)$$

$$\frac{d}{\lambda_m} = n - \frac{\phi}{2\pi} \quad (4-30)$$

When $n=0$ and $-2\pi < \phi < 0$, d/λ_m is between 0 and 1. If the thickness d is less than λ_m , there will be a unique value for the complex permittivity and permeability.

When $d > \lambda_m$, one solution is to make the measurements on two different thicknesses of the MUTs.

If the thickness $d < \lambda_m$, then $i=0$, however, if $d > \lambda_m$, the value of n varies. Because the electrical lengths of the MUT are unknown, developing a new tank design was required with a flexible thickness to help overcome this problem. A detailed explanation follows below.

Equation (4-30) is the key to solving for propagation in a dielectric material. However, solving the imaginary part presents a challenge, unless the material width, d , happens to be smaller than the material wavelength, λ_m . This is difficult to guarantee, even for low values of permittivity, over the range of frequencies tested so far (wavelength in air falls from 37.5cm down to 5cm). As the future work will also include higher frequencies (wavelength in air ranging from 5cm down to 1.5cm), it is then impossible to guarantee this condition.

For any material thickness, d_i , the measured phase change, ϕ_i , and the material wavelength, λ_m , are related by:

$$d_i = n_i \lambda_m + \frac{\phi_i}{2\pi} \lambda_m, 0 < \phi_i < 2\pi \quad (4-31)$$

The material thickness, d_i , and the phase change, ϕ_i , can be measured, but neither the material wavelength, λ_m , nor the number of wave periods in the material, n_i , are known. Both are required in the solution of equation (4-31).

Therefore, a new flexible tank can be designed based on this free-space technique.

The next step is to control the variation in the thickness d_i , when measuring the dielectric response of powders and liquids. This controlled increase will also allow the experimenter to avoid a situation where the new thickness is an integer multiple of material wavelengths more than the previous thickness. Clearly this will then yield two linear equations, where the thicknesses and phase changes can be measured; leading to an easy solution for the material wavelength, λ_m , and the number of wave periods in the material, n_i is the new tank design.

4.5 ABCD matrix conversion

Before introducing the ABCD matrix to the calculation, the matrix of the measurement set up first of all may be represented as;

$$[A] = [A_g] \cdot [A_{MUT}] \cdot [A_g] \quad (4-32)$$

where

A_g is the matrix of glass

A_{MUT} is the matrix of testing sample

A is the matrix of the whole assembly

When the free space method is used, two sets of results can be obtained. One set is based on the calibration, with only glass present; therefore, there is no material sample in the structure.

$$[A] = [A_g] \cdot [A_{air}] \cdot [A_g] \quad (4-33)$$

If it is desired to avoid using a matrix in this calculation, the propagation attenuation change between A_g and A_{air} should be linear. As there are several impedance mismatches

between this multilayer structure, the change between A_g and A_{air} are not linear, which has been confirmed in the results captured using the VNA.

As the permittivity and thickness of the glass pane are known, the ABCD matrix of glass plates is as follows [28]

$$[A_g] = \begin{bmatrix} \cosh(\gamma_g d) & Z_g \sinh(\gamma_g d) \\ \frac{1}{Z_g} \sinh(\gamma_g d) & \cosh(\gamma_g d) \end{bmatrix} \quad (4-34)$$

where

$\gamma_g = j \frac{2\pi\sqrt{\epsilon_g}}{\lambda_0}$ is the propagation constant in glass

d and ϵ_g is the thickness and relative permittivity of glass respectively

λ_0 is the free space wavelength

Z_g is the impedance of the glass plate

$$Z_g = \sqrt{\frac{\mu_0 \mu_g}{\epsilon_0 \epsilon_g}} \quad (4-35)$$

As ϵ_0 and μ_0 is the permittivity and permeability of free space respectively. Assuming for a non-magnetic medium, $\mu_g=1$, then,

$$Z_g = \sqrt{\frac{\mu_0}{\epsilon_0 \epsilon_g}} = \sqrt{\frac{\mu_0}{\epsilon_0}} \frac{1}{\sqrt{\epsilon_g}} \quad (4-36)$$

$$Z_g = Z_0 \frac{1}{\sqrt{\epsilon_g}} \quad (4-37)$$

This is then followed by calculating the MUT S-matrix by re-arranging equation (4-32)

$$[A_{MUT}] = [A_g]^{-1} \cdot [A] \cdot [A_g]^{-1} \quad (4-38)$$

S-parameters are most widely used in microwave measurements of 2-port networks, as they describe the relationship between the reflected and incident power waves at each of the ports.

$$S = \begin{pmatrix} S_{11} & S_{12} \\ S_{21} & S_{22} \end{pmatrix} \quad (4-39)$$

However, other parameters are also at times convenient, for example, if the system has more than one 2-port network, it is convenient to use the transmission line $ABCD$ (or T -) parameters.

In the case of a glass tank holding powder or liquid, this means for free space measurements, treating the tank as a cascade of two 2-ports. The two sheets of glass can be simply treated as one 2-port and the powder/liquid is the other 2-port.

The T -parameters are described by:

$$\begin{pmatrix} V_1 \\ I_1 \end{pmatrix} = \begin{pmatrix} A & B \\ C & D \end{pmatrix} \begin{pmatrix} V_2 \\ -I_2 \end{pmatrix} \quad (4-40)$$

where I_2 is directed away from the port.

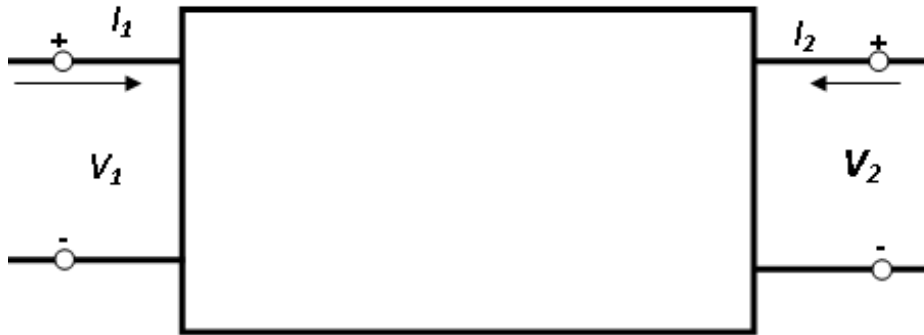


Figure 4-3 Two-port transmission network

Two (or more) 2-ports in series may be combined by simply multiplying the individual $ABCD$ matrices [50].

$$A = \frac{(Z_{01}^* + S_{11}Z_{01})(1 - S_{22}) + S_{12}S_{21}Z_{01}}{2S_{21}\sqrt{R_{01}R_{02}}} \quad (4-41)$$

$$B = \frac{(Z_{01}^* + S_{11}Z_{01})(Z_{02}^* + S_{22}Z_{02}) - S_{12}S_{21}Z_{01}Z_{02}}{2S_{21}\sqrt{R_{01}R_{02}}} \quad (4-42)$$

$$C = \frac{(1 - S_{11})(1 - S_{22}) - S_{12}S_{21}}{2S_{21}\sqrt{R_{01}R_{02}}} \quad (4-43)$$

$$D = \frac{(1 - S_{11})(Z_{02}^* + S_{22}Z_{02}) + S_{12}S_{21}Z_{02}}{2S_{21}\sqrt{R_{01}R_{02}}} \quad (4-44)$$

where

Z_{01} and Z_{02} are the complex impedances of ports 1 and 2, respectively; similarly, Z_{01}^* and Z_{02}^* are the complex conjugates of the respective impedances.

The values R_{01} and R_{02} are the real parts of port impedances Z_{01} and Z_{02} .

For the glass pane, it can be assumed, because of symmetry and uniform construction, that $S_{11}=S_{22}$ and $S_{21}=S_{12}$ and $R_{01}=R_{02}$, $Z_{01}=Z_{02}$.

$$A = \frac{(Z_{01}^* + S_{11}Z_{01})(1 - S_{11}) + S_{21}^2Z_{01}}{2S_{21}R_{01}} \quad (4-45)$$

$$B = \frac{(Z_{01}^* + S_{11}Z_{01})^2 - S_{21}^2Z_{01}^2}{2S_{21}R_{01}} \quad (4-46)$$

$$C = \frac{(1 - S_{11})^2 - S_{21}^2}{2S_{21}R_{01}} \quad (4-47)$$

$$D = \frac{(1 - S_{11})(Z_{02}^* + S_{11}Z_{02}) + S_{21}^2Z_{01}}{2S_{21}R_{01}} \quad (4-48)$$

In order to derive the equations used by Ghodgaonkar [37], it is necessary to show that the input impedance is Real $Z_{01}^*=Z_{01}=R_{01}$ [29]. If permittivity and permeability is real, then material is low loss. There are:

$$A = \frac{(1 + S_{11})(1 - S_{11}) + S_{21}^2}{2S_{21}} \quad (4-49)$$

$$B = \frac{R_{01}((1 + S_{11})^2 - S_{21}^2)}{2S_{21}} \quad (4-50)$$

$$C = \frac{(1 - S_{11})^2 - S_{21}^2}{2S_{21}R_{01}} \quad (4-51)$$

$$D = \frac{(1 - S_{11}^2) + S_{21}^2}{2S_{21}} \quad (4-52)$$

4.6 Conclusion

Chapter 4 presents the various algorithms that can be used to extract the permittivity and permeability values from the measured S-parameters, as well as the S-matrix algorithms that can be used in permittivity calculation. The four algorithms listed here are Nicholson-Ross Weir (NRW), National Institute of Standards and Technology (NIST) iterative, the New Non-Iterative (NNI) techniques and the free-space technique. In this thesis, the free-space technique is used to measure and calculate the dielectric constant. To conquer the unknown electrical length problem, the propagation constant is treated as a complex number and when combined with the test platform's controlled variable material thickness possibility, the dielectric constant can be calculated without the traditional estimation required when the electrical length is unknown.

5 Measurement results and analysis

This chapter presents antenna characterisation results, propagation results for dielectric analysis for various materials under test, from glass windows to concrete blocks, and dielectric analysis for glass various powder materials and tap water.

5.1 Antenna measurements

First of all, to qualify the testing infrastructure, an antenna characterisation was performed, with bandwidth (VSWR) and radiation pattern measurements, both of which were also compared with published manufacturer data.

5.1.1 Voltage Standing wave ratio (VSWR)

The roof (non-reflection) VSWR test examined the usable bandwidth of the Schwarzbeck antennas to be used for dielectric testing. The published and measured data are quite close to each other, shown in Figure 5-1 and Figure 5-2. In general, if the VSWR is under 2 the antenna match is considered very good and little would be gained by impedance matching, although this can be considered to extend the VSWR range. In the manufacturer's data, the VSWR value does not go over a value of 2, between 800MHz and 6GHz. However, in the measured results, the VSWR value slightly exceeds this threshold, once, at a value of 2.03 at 5GHz.

At this point it is worth commenting briefly on the meaning of the threshold and also therefore the consequences of testing with an antenna, whose VSWR exceeds the threshold, albeit once only and by the margin in this case.

Recall the VSWR definition from Equation (3-1)

$$VSWR = \frac{1 + |\Gamma|}{1 - |\Gamma|}$$

where Γ is the reflection coefficient and is simply S_{11} (linear not in dB).

It's clear from this equation that the threshold of 2 refers to one third of power is reflected. This in turn implies one third of the power intended for transmission through the antenna is in fact being reflected back due to impedance mismatch at the cable antenna interface. Implicit in this is that two thirds of the power is transmitted. So a minor VSWR= 2 threshold overshoot at an individual frequency is not significant.

It's also worth considering here how much wider a bandwidth can be considered for testing. A quick glance at either the published or measured data shows how quickly the impedance mismatch prevents expansion into frequencies lower than the lower working frequency. On the other hand there is a real, albeit unfathomed in the measured or published data, prospect of working beyond the upper test frequency of 6GHz. However, the focus on this work will remain instead on developing the technique and proving it in the manufacturer's published bandwidth of 800-6000MHz.

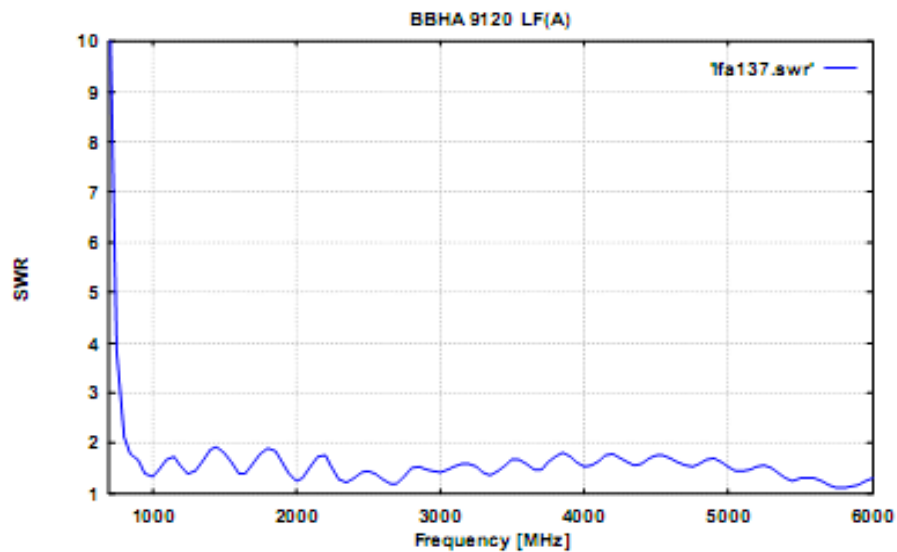


Figure 5-1 Published SWR data of horn antenna Schwarzbeck BBHA 9120 LF (A) [51]

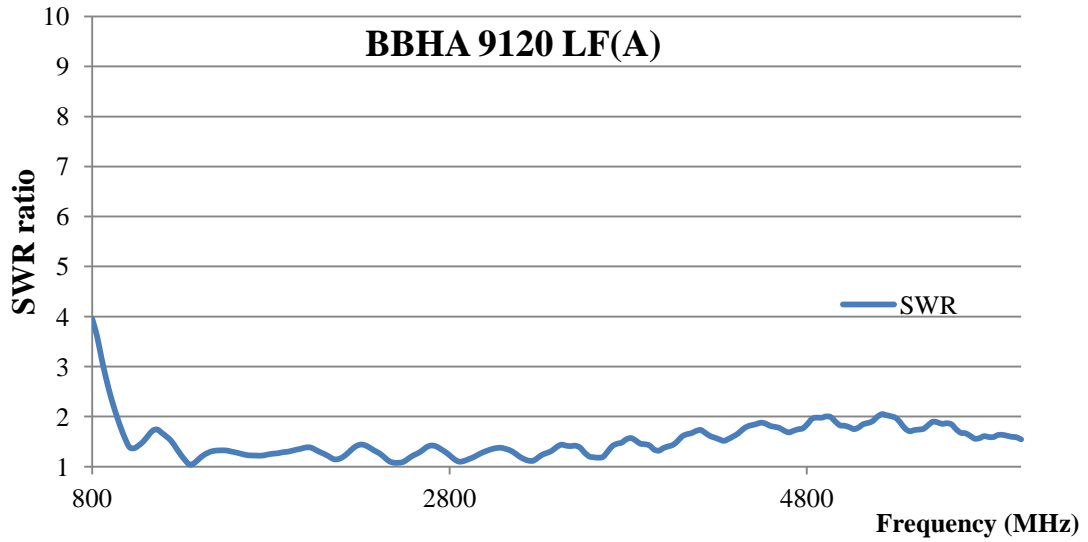


Figure 5-2 Measured SWR of the horn antenna Schwarzbeck BBHA 9120 LF (A)

A second pair of horn antennas (Schwarzbeck JXTXLB-90-20-C) was also evaluated with a view to future work in dielectric analysis outside of the band used in this thesis, at frequencies between the manufacturer's specifications of 8.2 to 12.4GHz.

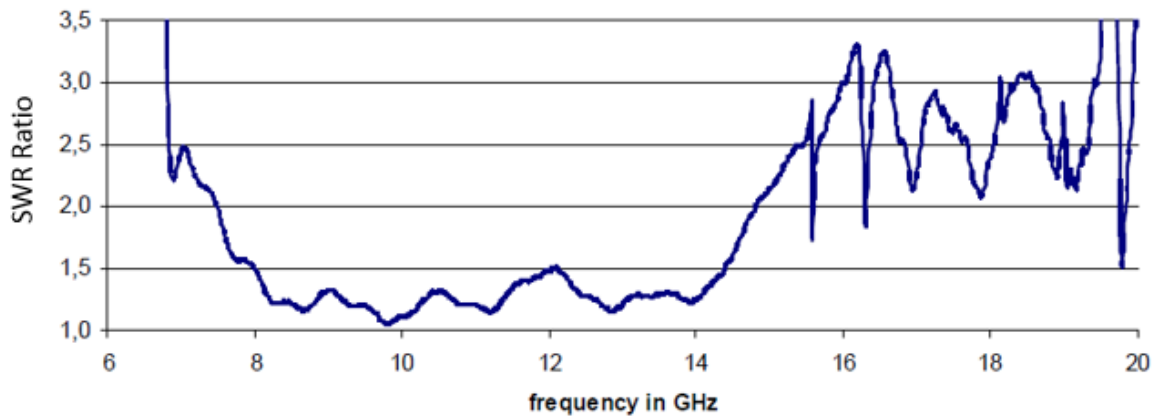


Figure 5-3 Measured VSWR of the horn antenna Schwarzbeck JXTXLB-90-20-C

As shown in Figure 5-3, the VSWR of the JXTXLB-90-20-C horn antenna performs better than the manufacturer's specified frequency range of 8.2 to 12.4GHz. The actual testing range could be expanded to cover a range from 7.6 to 15GHz.

5.1.2 Antenna radiation pattern

The antenna radiation pattern was measured in the large hall, starting at the normal and then up to 90° in steps, to either side. The step width was 2° and was controlled by the operator using readings from the Total Station.

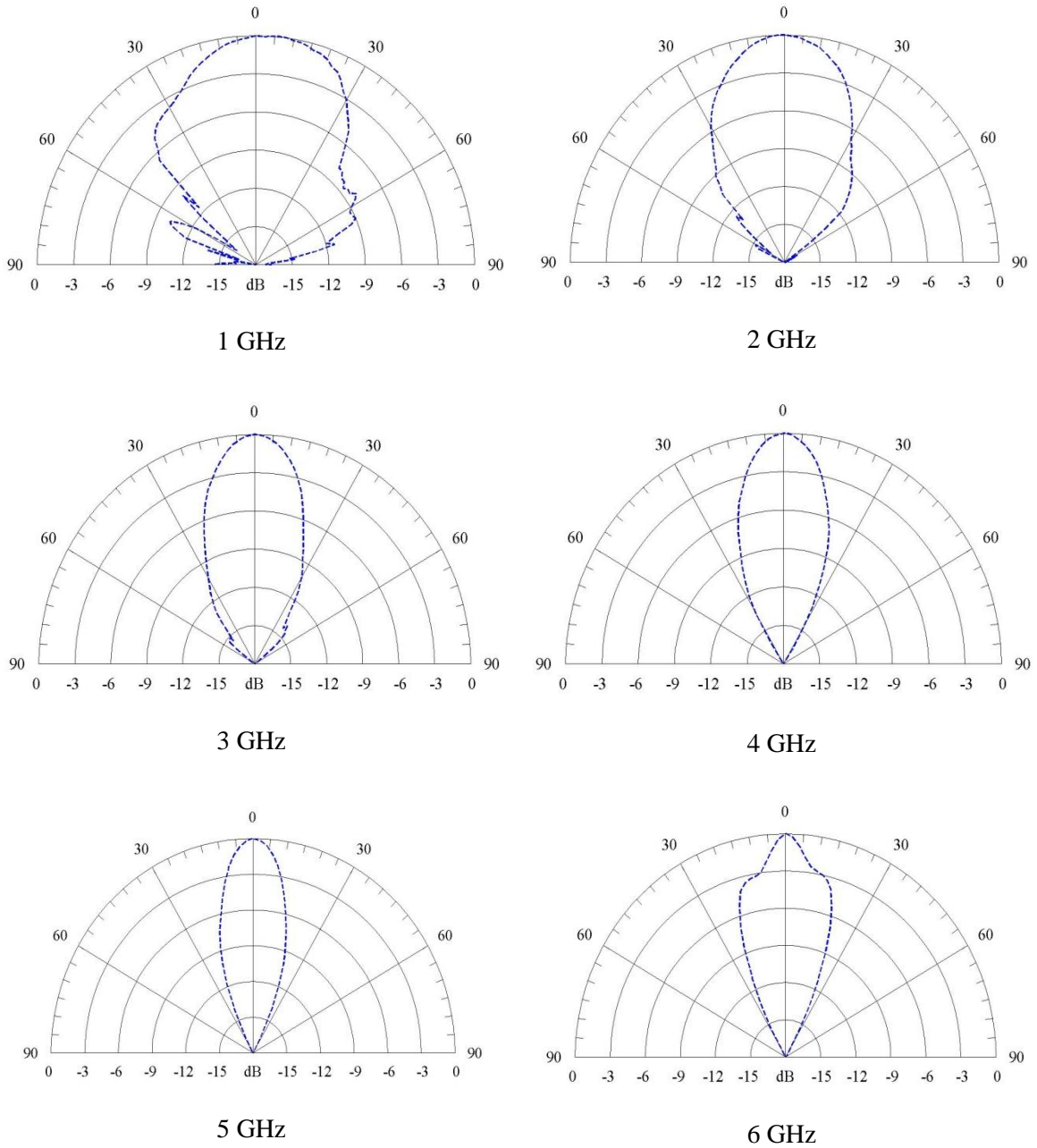


Figure 5-4 Measured E-plane antenna pattern (Schwarzbeck BBHA 9120 LF (A))

The distance between the two antennas was 5m, to ensure the measurement was performed in the far field for all frequencies, although this is not strictly required. The results presented here are for the E-plane only. H-plane measurements were also made, and are broadly similar to the E-plane results. Figure 5-4 was for the first pair of Schwarzbeck (800MHz to 6GHz) horn antennas. The comparison of those published results and measured data shows that the Half Power Beam Width (HPBW) is almost identical.

For the second pair of antennas (JTXTLB-90-20-C, 8.2GHz to 12.4GHz) validation, the same two antenna gain method was used. The measurements are performed in the E-plane and H-plane. The results [41] are shown below; both E and H-plane are selectively presented here.

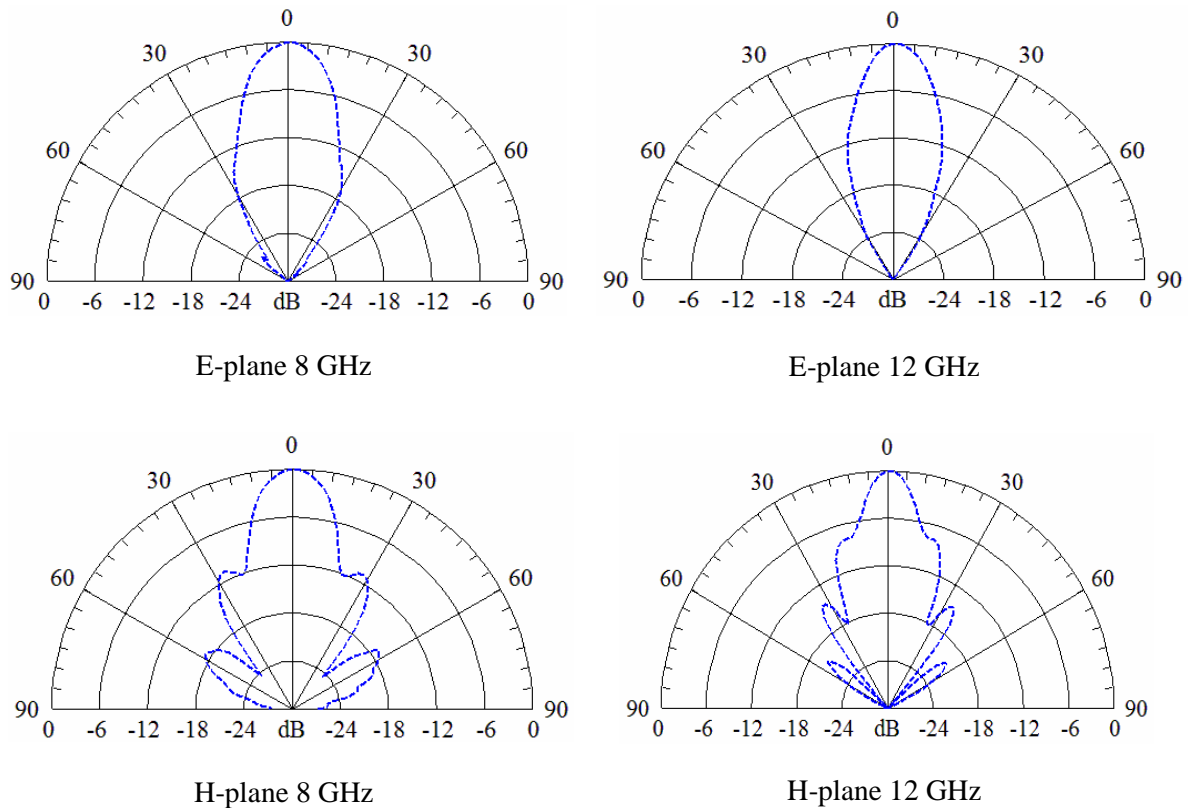


Figure 5-5 E and H-plane antenna pattern (JTXTLB-90-20-C)

5.2 Calibration

A VNA is different from the other microwave equipment available to do this work, in that it achieves highly accurate measurements by correcting the systematic errors in the instrument, the characteristics of cables, adapters and even the test structure. The process of error correction, commonly called experimental calibration, is an entirely different process, compared to manufacturer calibration, and may be performed by an engineer several times during testing.

5.2.1 Standard calibration

Standard calibration using manufacturer supplied kits is widely used to move the measurement reference plane from the VNA front end to position right before or after the device or component being tested.

This was the case when an Open Short Load (OSL) was performed, using the calibration kit ZV-Z32. Hence the signal propagation through the cable is calibrated out so that the end of the cable is the new reference plane. This means simply that all phase and amplitude variations caused by subsequent testing are relative to a notional plane at the end of the cables. This standard calibration technique is the most common type of a VNA calibration, as it is excellent for individual device or component measurements. However, this method offers less accuracy in the case of free-space measurement, so that at other calibration techniques have to be also considered [52]

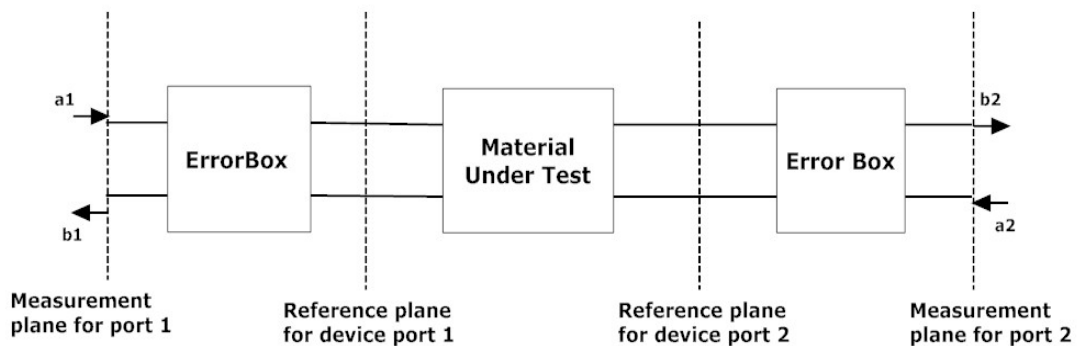


Figure 5-6 VNA reference plane explanation

In the early tests on window propagation, a one-port, two-path Open Short Load Thru (OSLT) calibration was performed to move the reference plane to the testing window, so that the attenuation losses and phase changes are only due to the window itself.

5.2.2 Self-calibration techniques

Self-calibration techniques can be used on free space measurements, where of course it is not possible to use discrete standards. As this method applies to free space it offers more potential to this work than the OSM calibration method [37] [38].

As powders and liquids, which are contained in the plane of propagation by two glass sheets, are the target materials, there are still known challenges such as composition variation, due to non-uniform packing or density. By measuring two or three sample thicknesses, this should be less of an issue, especially if care is taken to ensure no air pockets (powders). As the containing glass sheets are inserted individually and independent of each other, calibration at their plane should be possible, even relatively easy, as should be the measurement of reflection and propagation characteristics of the glass sheet itself. The elimination of errors due to multiple reflections between the glass sheets, using the Thru-Reflect-Line (TRL) [37] and the dual separation [53] calibration techniques can also be easily achieved with this test platform.

The TRL calibration is more commonly used than OSLT method in VNA measurements of free space propagation. While TRL shares the Thru and Line measurements of OSLT, TRL doesn't rely on precisely known standards, which are required for Open and Short over all testing frequencies, but only needs three relatively simple steps to complete the calibration process.

In Figure 5-7, the three steps of the typical TRL calibration are presented. A calibration technique developed by this PhD candidate will be detailed in the following.

- Thru: Antennas facing each other normally. Distance between antennas has to match the selected relevant distance, in both far field and near field testing. and the material holder must be empty. This establishes a reference for the propagation or S_{21} measurement once the material has been added.

- Reflect: Insert a metal reflector the same size as the glass containment sheet and in the same position as the MUT. This establishes a maximum for the reflected component, S_{11} and also for the diffracted contribution to the propagation measurement, S_{21} from the edges of the test set-up and therefore energy that did not pass through the MUT.
- Line: Antennas moved by up to $\pm\lambda/4$ longer than Thru, at the centre frequency of the swept frequencies, to avoid a singularity. Ratio of start-stop frequencies should be less than 8:1. And measuring the response of the empty material holder. The antennas are repositioned to their original location as the Thru calibration standard

By applying the TRL calibration in the measurement, most systematic errors can be removed. The metal reflector is the same size as the MUT; therefore this step can remove edge diffraction and signal leakage from the test frame (by measuring the propagated signal, as well as the reflected signal). However, to perform a TRL calibration, focused antennas (horn antennas with additional lens components) are needed, because when performing the “Thru” and “Line” standards, ideally all of the signal should be transmitted from transmitting antenna to the receiving antenna. In other words, this TRL calibration requires that the receiving antenna get the same amount signal for both Thru and Line standards. Otherwise because the “Line” standard required a movement over a short distance, in practise the small movement will cause some change in the amount of received signal. This change would not occur if the received power remained constant in spite of the move and is the reason the TRL calibration technique is favoured by systems which include a focussing lens in the propagation path. Without the lens, this term cannot be easily separated from the VNA results. It would thus cause a new error term within the calibration process. In addition, a precise positioning system should also be used for TRL, so that the antennas can be repositioned after the “Line” calibration.

When it is very difficult to achieve the Line part of the TRL calibrations, one of the alternate approaches is to use the Thru-Reflect-Match (TRM) calibration, which is identical to the TRL calibration except for “Line” being replaced by a “Match” standard. The Match standard can be achieved by simply placing absorber foam in the sample holder. If one recalls early engineering classes, where Matching loads simply absorb all

delivered power then the introduction of high quality absorbent foam achieves the same effect (without needing to match to the source impedance). When using the TRM calibration, antennas can remain fixed, unlike the Line part of TRL, so that focused antennas and precise position system are no longer required.

In the case of calibration:

- 1) Stored calibration values and zeroing the VNA now
- 2) Match: This establishes the $S_{11} = 0$ and $S_{21} = 0$ condition
- 3) Line: This establishes the $S_{11} = 0$ and $S_{21} = \text{maximum}$ condition

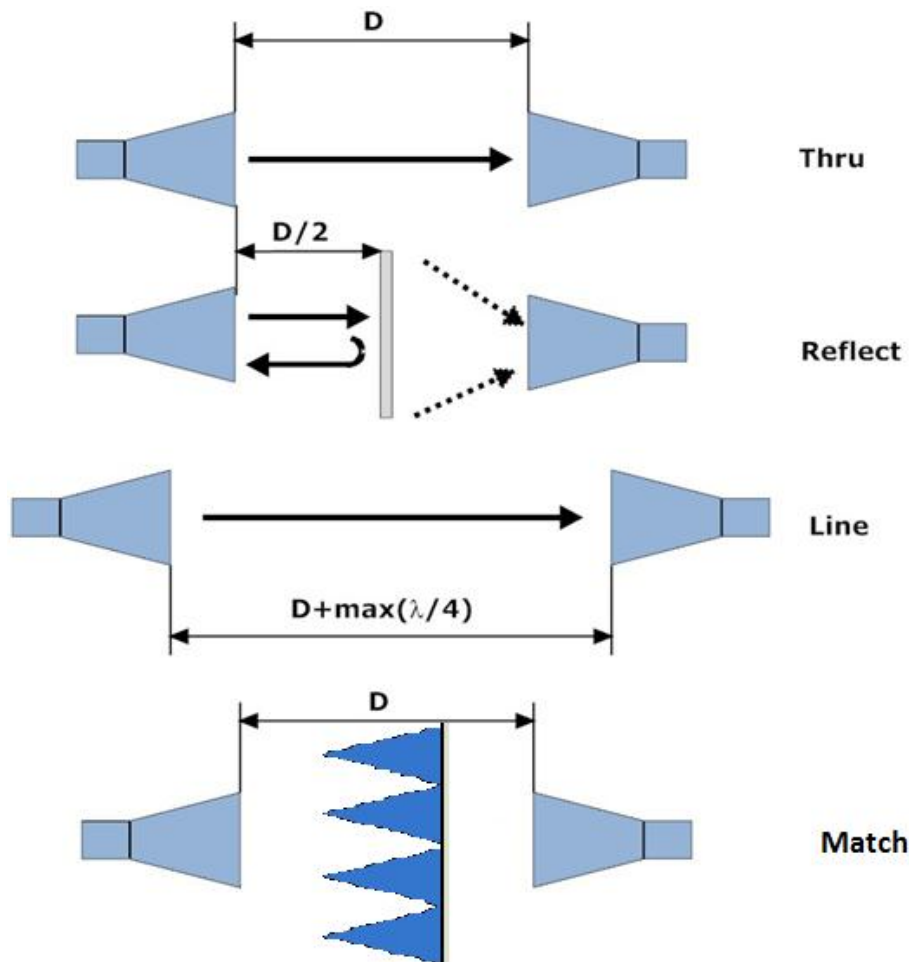


Figure 5-7 TRL/M free space calibration standard, developed by PhD candidate Yaqiang Liu

5.3 Anechoic chamber validation

As the WIT anechoic chamber was to be used for some of the experimental work, it was decided that it should be validated as part of this work. The validation of the WIT anechoic chamber was performed in two ways. First, the chart in Figure 5-9 shows the signal leakage from inside to outside of the chamber. The receiving antenna was placed outside the chamber to capture the signal transmitted from within, with the door closed. Figure 5-8 shows the leakage from outside to inside, again of course with the door closed. Both tests were performed in both the E-plane and H-plane. In order to comply with the far field boundary requirements [43], the test setup separation was 4.44m. The reference data was created by a bidirectional Thru calibration and the two antennas were facing each other through the closed chamber door, which was considered the point of highest signal leakage.

The results shown here are for the E-plane only, although the H-plane results are similar. From Figure 5-8, the inside-outside attenuation of the chamber is around -60dB. Given the signal levels measured in the course of this work, it was thus assumed that there is no external disturbance from outside or signal leakage from inside the anechoic chamber.

The chamber walls were also validated as a reflection test inside the chamber was also performed, with the results displayed in Figure 5-9. This chart compares the chamber reflection results to the rooftop VSWR test results and it can be seen that there is practically no difference (Figure 5-9). This indicates that over the test range the reflected power is dominated by the antenna cable impedance mismatch and that the chamber wall has no significant impact even for normal incidence. In fact when the chamber is used the transmitting antenna is very close to the receiver antenna and both are facing each other, so the amount of power going to the chamber wall will be very small.

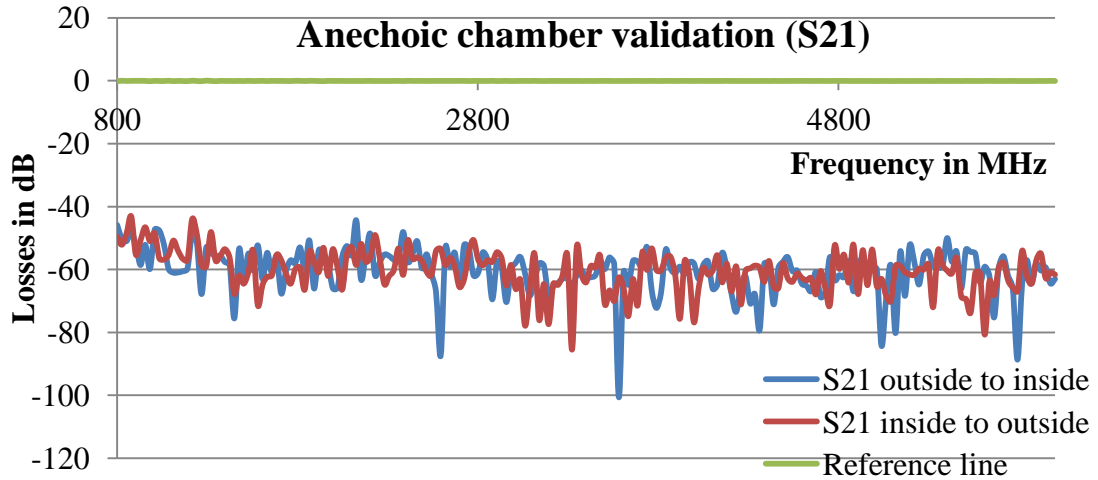


Figure 5-8 E-plane anechoic chamber validation, Green is reference line and red/blue are signal attenuation

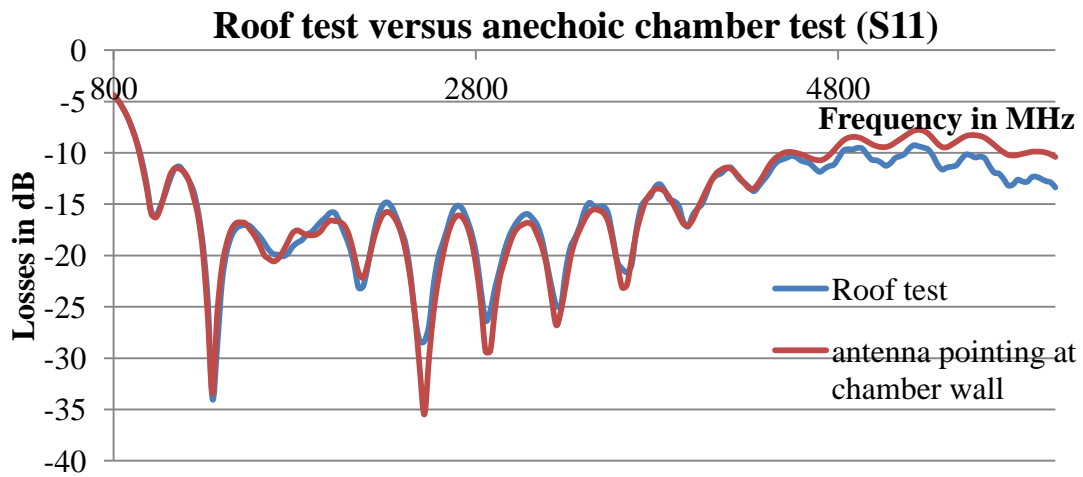


Figure 5-9 S_{11} validation for WIT anechoic chamber, the reference line is taken from the S_{11} data from the roof (blue). The red trace is where the antenna pointing to the wall inside chamber

5.4 Coated window measurement

The initial propagation measurements were carried out on glass windows and building materials. The results are presented in this and the following section. The test infrastructure developed and calibration procedures for these initial measurements were later successfully

modified for the permittivity measurements of powders and liquids. The results provided were made using the Schwarzbeck (800MHz to 6GHz) horn antenna only. This work was published in European Wireless Conference, presented [54] by in Lucca by the PhD candidate.

The windows being tested were two different brands of double glazed energy efficient (low emissivity- i.e. with one side of one of the two panes also coated with a selectively reflective surface, with the intention of retaining Infrared radiation within a building, thereby reducing heat loss) glass (Glass A: 2m x 1m, Glass B: 1m x 0.3m). The calibration procedure is a “line-through-line calibration”, a one-path two-port procedure for the VNA. In addition to comparing the attenuation from those coated glass windows, a normal plain single layer glass (4mm) was also measured, in the same test structure, simply for comparison purposes. The measurements were repeated at separations of 7m and 1.65m (test range reduced to 1 to 2GHz) and similar results were obtained.

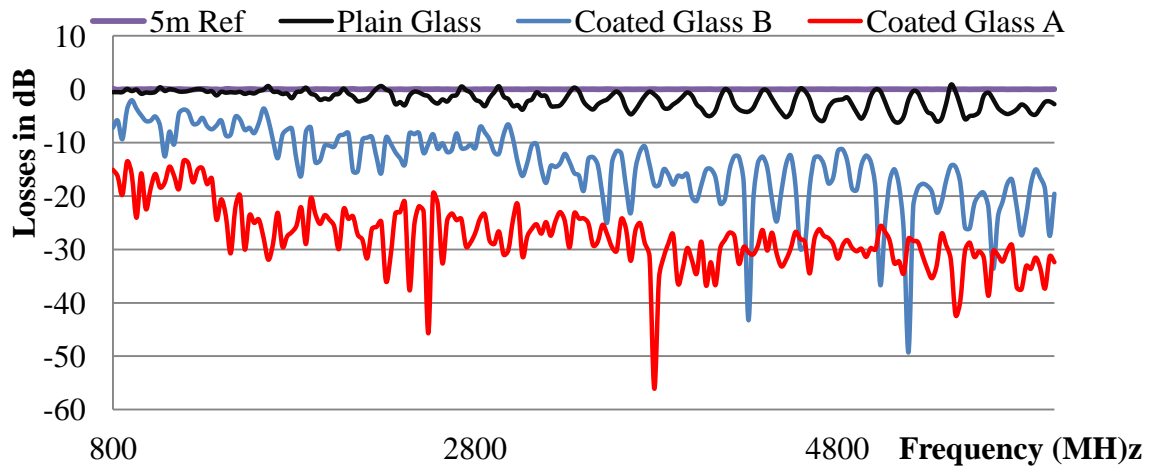


Figure 5-10 Different glass attenuation compare at 5m from large hall

The same glass was then tested in the WIT anechoic chamber. In order to observe the far field criteria mentioned earlier, the test range was limited to 1-2GHz. In this range, the antenna separation can be 1.65m, for the chosen antennas. The results are presented in Figure 5-11

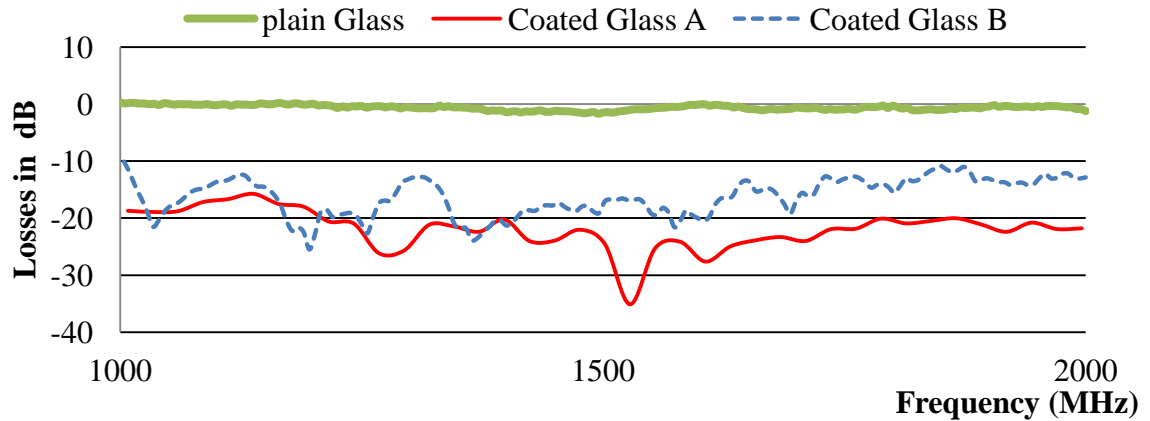


Figure 5-11 Propagation results from anechoic chamber at 1.65m

The RF propagation results for the 4mm thick plain glass are always better than -3dB and correspond well with other published results [46]. There is a gradual increase in propagation losses, as reported by, for example, NIST [46]. For coated glass, the propagation can fall as low as -30dB and these results correspond well with previous work carried out by the research group, associated with this thesis [55].

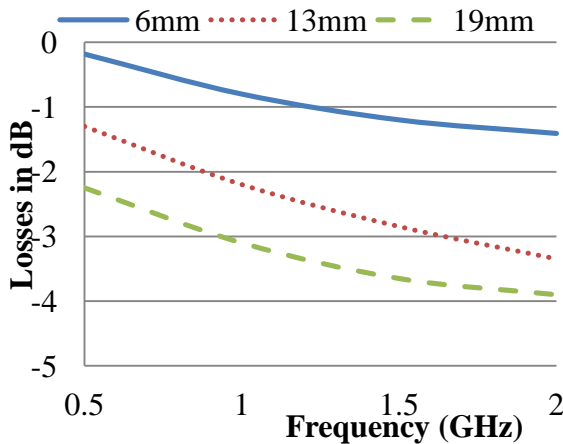


Figure 5-12 Glass propagation measurements due to the different thickness of plain glass, from [52]

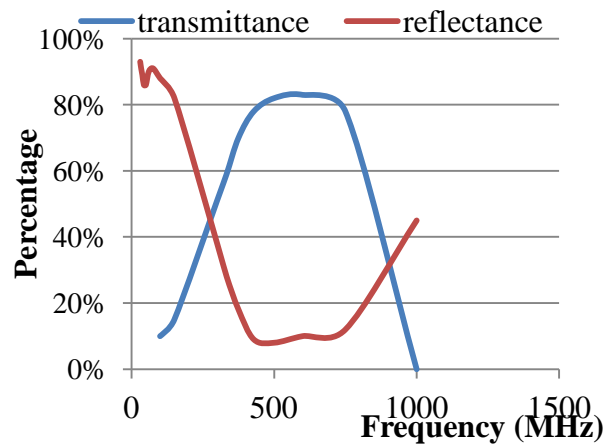


Figure 5-13 TiO₂/Ag/TiO₂ coating transmittance and reflectance [53]

Although neither the actual coating material nor the coating thickness nor even the uniformity of deposition is known for the coated glasses under test, certain conclusions may nonetheless be drawn. Figure 5-13 shows a transmittance reflectance curve for a

coated glass, which, from the perspective of RF propagation, may be assumed to be fairly indicative of the coating influence. (The graph may not be representative entirely of the glass measured here, in that the amount of transmittance/reflectance depends on material, thickness, anti-reflection material and nature of deposition).

Those energy efficient windows are coated with transparent conductors (TCs) to access the controlling of the energy entering or leaving buildings. The heat transfer can be reduced from about $3-1.5 \text{ Wm}^{-2}\text{K}^{-1}$ to as low as $0.4 \text{ Wm}^{-2}\text{K}^{-1}$ for double glazing, principally by reducing the radiative energy loss for frequencies beyond (wave length lower than) the visible part of the spectrum. By using TCs, it could ensure the light transmittance in the visible part of the electromagnetic spectrum, as shown in Figure 5-12. Although published TC data measurements typically stop at about wavelengths of $3\mu\text{m}$ and the work here covers RF wavelengths from 5 to 37.5cm, it may be expected from the published graphs that the RF propagation would be quite low, which is indeed confirmed by the glass test result. The plasma frequency for TCs lies in the infra-red region. Below the TC plasma frequency, it acts as a conductor and reflects incident light [56]. Above the TC plasma frequency, it passes or absorbs light, acting like a dielectric. This conductor-like reflection behaviour is observed also at RF frequencies, which are much lower than those normally measured by those interested in TC development or those interested in window manufacture.

Both coated windows offer significantly poorer RF propagation paths compared to standard glass. The results from the anechoic chamber, in Figure 5-11, are consistent with the large hall measurements, in Figure 5-10, albeit showing even poorer propagation. The higher propagation results for the hall may be due to some small signal leakage, in spite of the protective, RF absorbent foam shroud created for the receiver.

5.5 Standing wave analysis

The early test platform development also produced an interesting side analysis into the interpretation of the VNA output. As mentioned the initial VNA calibration technique calibrated to the cable ends, using the manufacturer supplied standard. A baseline antenna to antenna propagation measurement without MUT in the transmission path was then

recorded. When the material was then introduced, subsequent measurements were compared to the baseline and variations assumed to be due to the material's introduction. While this technique is simple, it has flaws, some of which are addressed in the improved calibration technique. One flaw is that there will be some fluctuations in the measurements, caused by unavoidable standing waves. These standing waves are due to the introduction of the MUT and are inevitable with this technique, whether carried out in the large hall or the anechoic chamber. As the MUT is placed perpendicular to the antenna radiation path due to the impedance mismatches some of the wave will be reflected. It should be clear that due to the introduction of the material the impedance mismatches are no longer the same as when no material was present. This also means that at various frequencies, standing waves will be created between each component of the test set-up including antennas and the MUT.

An interesting aspect of this new impedance mismatch appears as a standing wave superimposed on the S_{21} measurement, an example of which is shown for 4mm thick plain glass in Figure 5-14. The standing wave issue will affect both the attenuation and phase patterns. The wave is influenced by the position of the impedance mismatch in the propagation path for the S_{21} measurement.

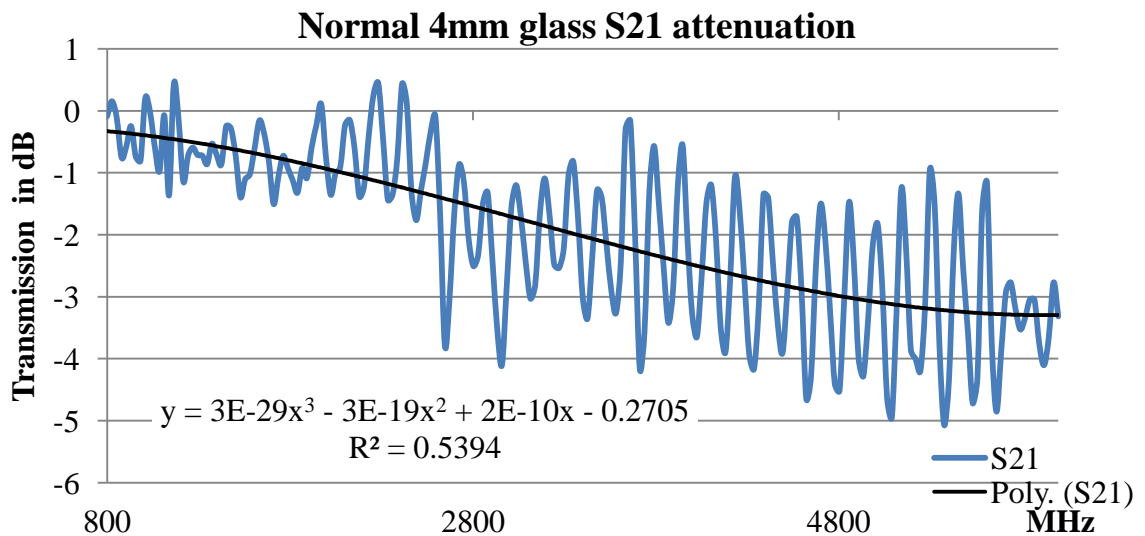


Figure 5-14 Normal 4mm glass transmission attenuation result with trend line

In dielectric material measurements, this standing wave will sometimes cause the S_{21} measurement to be over 0dB, which may not at first seem possible as it is even bigger than the reference (no MUT) value (see Figure 5-14). Standing wave was caused by the insertion of MUT that cannot be removed. So these error values will mislead the test results in calculation. Therefore, a data smoothing technique is required, which before putting VNA data into calculation.

The smoothing technique chosen here is from EXCEL Trend line function. By using the polynomial trend line and the equation it shown, we are able to provide the data of a trend line. For example in Figure 5-14, the equation shows the 3rd order of a polynomial trend line of the standing wave. The R^2 values for 3rd, 4th and 5th order polynomial fitting are 0.53, 0.54 and 0.55, which are quite close to each other. Therefore, 3rd order was chosen for smoothing the selected data. Same techniques are applied to VNA phase results as well, after unwrapping the phase (degree) data.

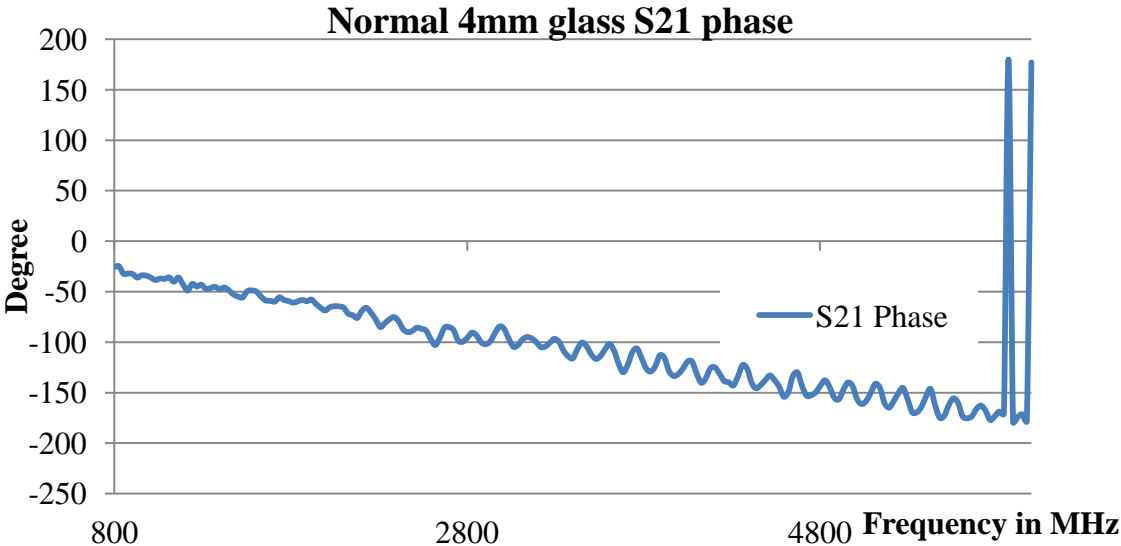


Figure 5-15 Normal 4mm glass transmission phase change result (with angle wrapping at 180°)

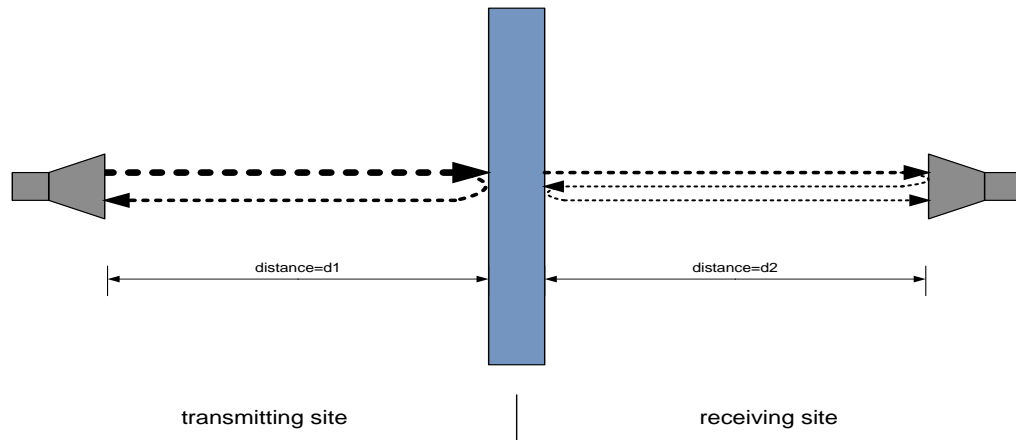


Figure 5-16 Multiple standing wave

Clearly the MUT will introduce standing waves, which cannot be easily removed by conventional calibration. It is proposed that these standing wave can be analysed, by, for example, applying Fourier analysis to the VNA output. The basis for this analysis is outlined below. It can be shown that the VNA repeat patterns are each defined by a fundamental standing wave. For instance, Figure 5-17 shows a close-up of the VNA output for a single 7.65m cable. This pattern is usually calibrated out before MUT measurements.

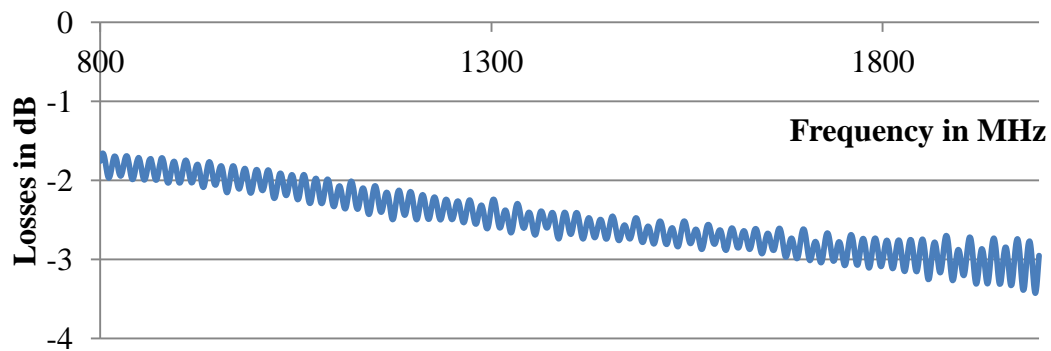


Figure 5-17 Standing wave chart from cable calibration

By selecting points where peaks occur, here at 817MHz and 968MHz, the integer number of peaks between these two points can be counted and found to be 10. The individual peak separation for constructive interference in the VNA output, can thus be calculated as $(968\text{MHz} - 817\text{MHz}) / 10 = 15.1\text{MHz}$. To confirm the pattern is associated with the cable, if we presume the speed of light in the RF cable is (according to the manufacturer) at 77% of the speed of light in a vacuum [40], then the fundamental standing wave wavelength is

$$\lambda' = \frac{c'}{\Delta f} = \frac{2.31 \times 10^8}{15.1 \times 10^6} = 15.29\text{m} \quad (5-1)$$

If this does indeed correspond to a standing wave then the fundamental wavelength should be double the distance travelled in the cable (one half of wavelength to the impedance mismatch at the cable end and the other half in the length back. In which case the calculated cable length is $\lambda'/2 = 7.645\text{m}$, which closely matches the actual length of 7.65m [40].

This concept could be taken further by examining the Fourier transform of the same VNA cable results, shown in Figure 5-18. The strong low frequency value may be ignored; as it is due to the VNA results being all positive (absolute values were taken, so there is a strong DC or average component).

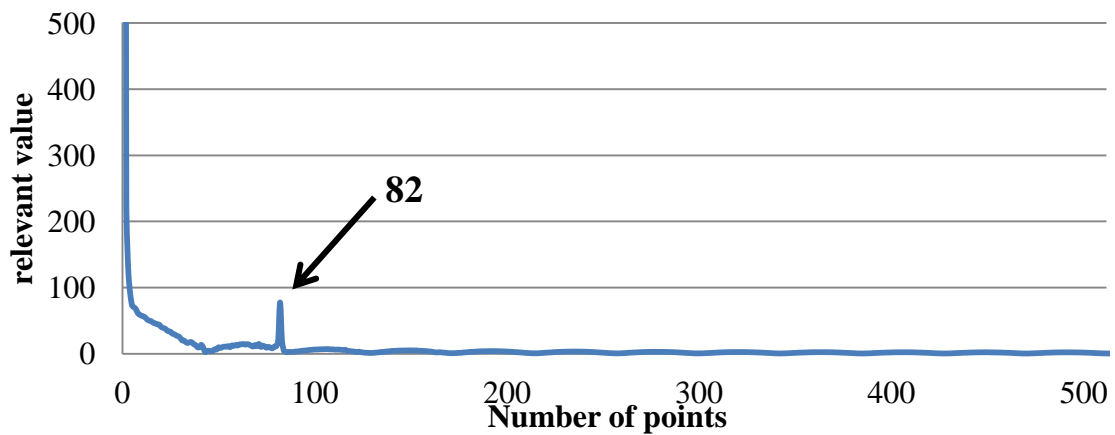


Figure 5-18 DFT result of cable validation

The original swept frequency range was 800-2000 MHz, with 1000 sampling points, so the resolution of the VNA output is

$$\Delta F = \frac{2000\text{MHz} - 800\text{MHz}}{(1000 - 1)\text{points}} = 1.2\text{MHz per point} \quad (5-2)$$

As considering the ten periods from the peak at 817MHz to the peak at 968MHz, (range of 151MHz). The number of samples between point 817MHz and 968MHz is $(151\text{MHz}/1.2\text{MHz/point})=125.8$. There are ten periods in this range. The number of samples per period is equivalent to the ratio of frequency to sampling frequency in a conventional DFT. In a conventional DFT representation, the horizontal axis is from Zero Hertz to half the

sampling frequency in Hertz (assuming only half of the spectrum is displayed). The ratio described above defines the actual position of any individual frequency on the DFT spectrum. For convenience, the 1000-point VNA output was zero padded up to 1024 points, so a radix-2 FFT could be performed. The ratio can be calculated and then used to predict where the peak should appear on the 1024-point DFT of the VNA output:

$$\begin{aligned}
 ns &= \frac{\textit{selected number of points}}{\textit{selected periods}} = \frac{125.8}{10} \\
 &= 12.58 = \frac{\textit{sampling points}}{\textit{VNA period}}
 \end{aligned}
 \tag{5-3}$$

$$\textit{DFT point} = \frac{N}{ns} = \frac{1024}{12.58} \approx 82
 \tag{5-4}$$

Referring to Figure 5-18, the relevant point on the Fourier transform is also 82.

Of course, to have real value the DFT output needs to be translated into distance, so that the interface causing the standing wave may be determined. In this case there is only one interface (the end of the cable), but in a real system, more than one standing wave may appear in the VNA output, due to the presence of multiple interfaces. In this case, the number of samples is 1024.

The fundamental standing wavelength λ' is

$$\lambda' = C \times \frac{f}{N} \times \frac{ns(\textit{No. of Sample})}{\Delta f(\textit{Selected Frequency Span})}
 \tag{5-5}$$

$$\begin{aligned}
 \frac{ns}{\Delta f} &= \frac{\textit{Total No. of VNA points} - 1}{\textit{Total Frequency Span}} \\
 &= \frac{1000 - 1}{2000\text{MHz} - 800\text{MHz}} \\
 &= \frac{999}{1200\text{MHz}} \\
 &= 0.8325
 \end{aligned}
 \tag{5-6}$$

Therefore, $\frac{\textit{Total No. of VNA points} - 1}{\textit{Total Frequency Span}}$ is a constant, which will be called k here. So then,

$$\lambda' = f \times \frac{C}{N} \times k \tag{5-7}$$

where

f is the number of points in the DFT (1, 2, 3,..... f)

N is the total number of sample points (usually 1024)

If there is only one period in this range, number of samples per period equals to 1024. The number of sample per period in this range is defined as $1024/DFT$ points. As two points from the VNA outputs were picked, the number of samples between these two points is 127. So the relevant period can be defined as $127/ns$. The difference between the select two points is 15.1MHz.

Consider the results in Figure 5-19. There is a reflection response at $x = 7.645m$, which as mentioned earlier corresponds to the cable length.

Analysing the more detailed output from a full MUT measurement would equally supply distance confirmation, as in the example above, but also, more importantly, a relative comparison of the impedance mismatches from various surfaces, by examining the amplitudes. If care is taken in choosing the VNA frequency range and the number of sampled points, it should be possible to even distinguish between the two different reflection coefficients in the energy efficient double glazed windows. As this technique is not core to the present PhD research, merely an interesting and possibly promising related topic, it can be easily pursued in some future work.

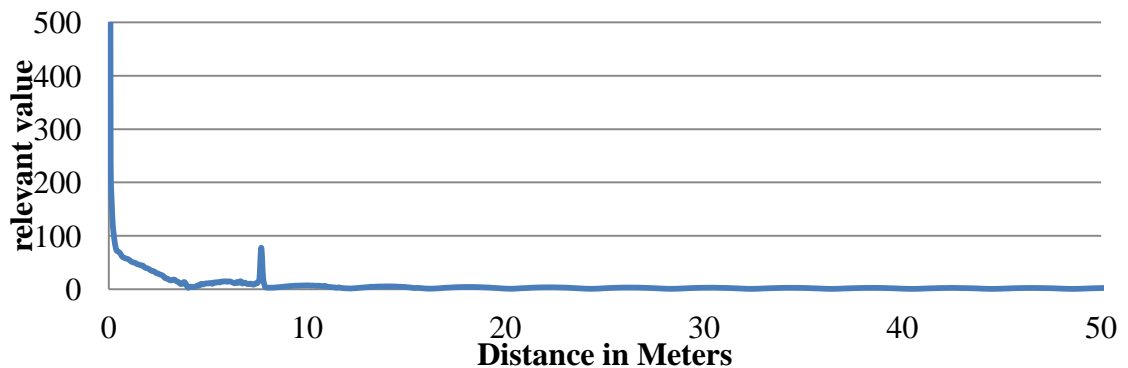


Figure 5-19 DFT chart converted to distance response chart

5.6 Building material measurement

The RF propagation measurements on energy efficient glass proved useful in developing both a test platform and appropriate calibration techniques for future dielectric analysis. On completion of the energy efficient glass tests, it was decided to confirm the techniques and to examine the requirements for various material thicknesses and consistencies to try to refine the requirements for variable thickness powder and liquid measurements. Several other building materials were therefore tested, such as concrete blocks, natural and synthetic slate and four different popular types of thermal building insulations. These fulfilled the requirements for variable thicknesses, consistencies and shapes and also completed the analysis of RF penetration into energy efficient buildings, relevant papers were published in the Royal Irish Academy URSI [57] and IET Colloquium [58]. In order to guarantee the antenna far field boundary (800MHz - 6GHz range), the distance between the two antennas for all tests was maintained at 5m. All measurements are presented relative to no MUT and consequently phase and attenuation measurements represent changes due to the MUT.

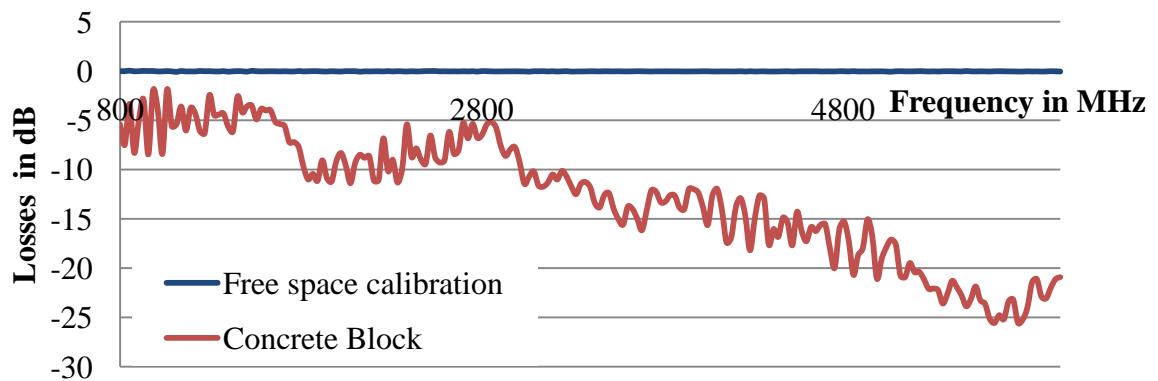


Figure 5-20 100mm concrete blocks S_{21} results at 5m separation, frequency range: 800MHz to 6GHz

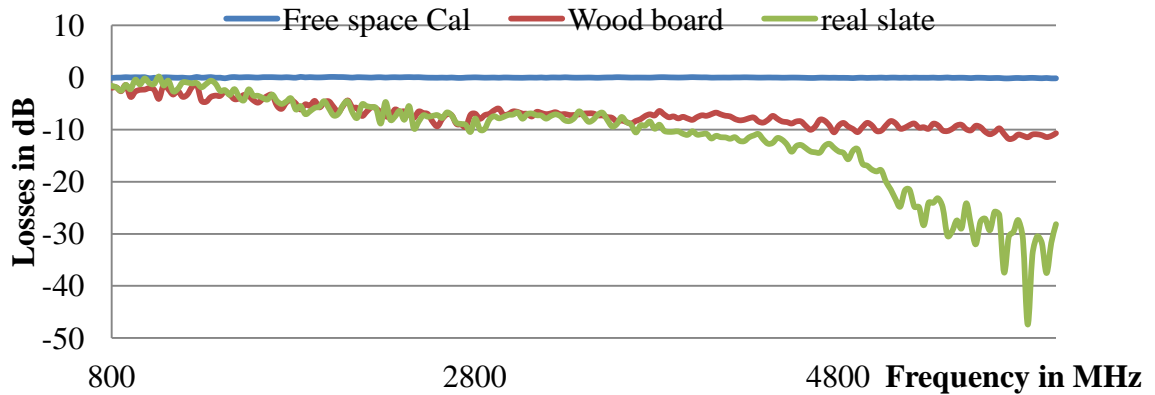


Figure 5-21 Natural Slate (1m by 1m) on 8mm plywood board S_{21} Results at 5m separation

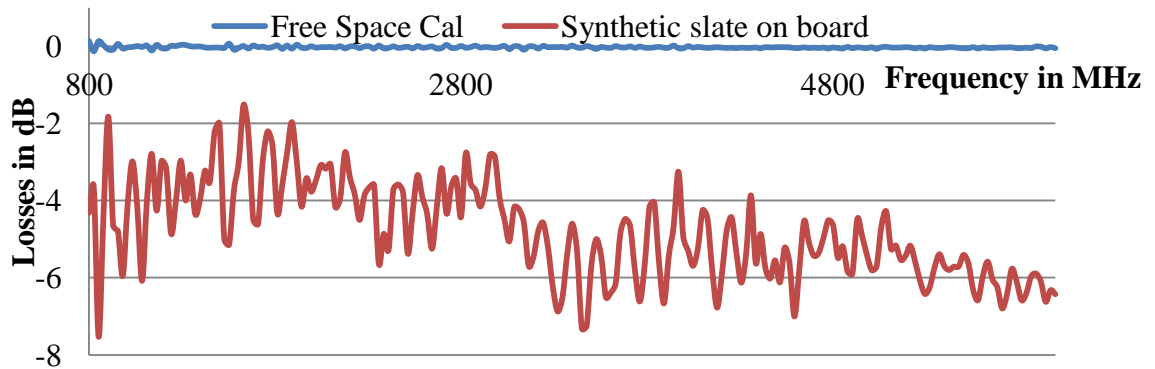


Figure 5-22 Synthetic Slate (1m by 1m) on 8mm plywood board S_{21}

For the four types of insulation tested, their size was initially relatively small compared to the antenna separation (5m) required to guarantee far field measurement over the range of frequencies 600MHz to 6GHz, with the chosen horn antennas. In order to reduce the ground effect and signal scattering, as well as increasing the proportion of signal passing through the target, the distance was reduced to 1.65m, at which the far field frequency range reduces down to 1 - 2GHz (Figure 5-23).

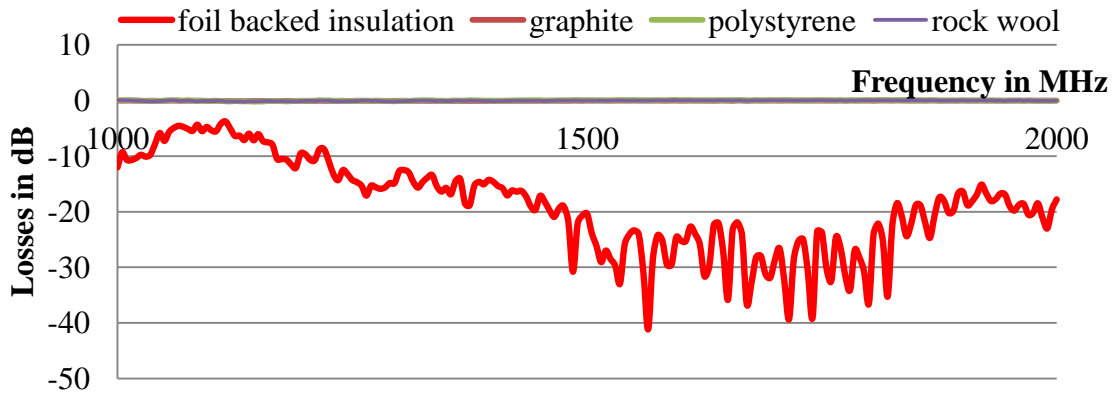


Figure 5-23 Foil backed insulation, graphite-impregnated polystyrene insulation, rockwool and plain polystyrene sheet sample results. (The results of graphite-impregnated polystyrene insulation, rockwool and plain polystyrene are similar and all close to 0 dB, therefore, only two lines are shown in the chart)

It is clear that the foil backed insulation allows the least amount of signal to propagate. Given that this type of insulation is now the norm in cavity walled constructions, coupled with the results for the energy efficient windows and the cavity blocks, one wonders how wireless communication will function in the future, particularly for mobile handheld devices (other devices, such as the television may have wires passing from the outside to the inside, thereby penetrating through this energy-efficient RF screen).

5.7 Vehicle window & tints measurement

In addition to the building materials tests, car windows and window tint films were also measured as these are unusual shapes and sizes and required a lot of thought in relation to the test set-up.

The result is that for a range of automotive glass (front heating glass, rear heating glass and side window glass) propagation results are quite similar, in that they all have nearly -5dB attenuation.

Three different car window tint films were also tested, which are limo black, light smoke and silver reflector. These films were also the thinnest materials tested in the course of this work. The attenuation of the silver reflector tint is significant, as much as -20dB, where the

other two films was lower than -5dB. Therefore, most RF propagation can pass through those two films, including mobile phone, and GPS wireless signals. Cars using the silver tint on the other hand suffer considerable attenuation to their RF signals, including GPS and mobile phones.

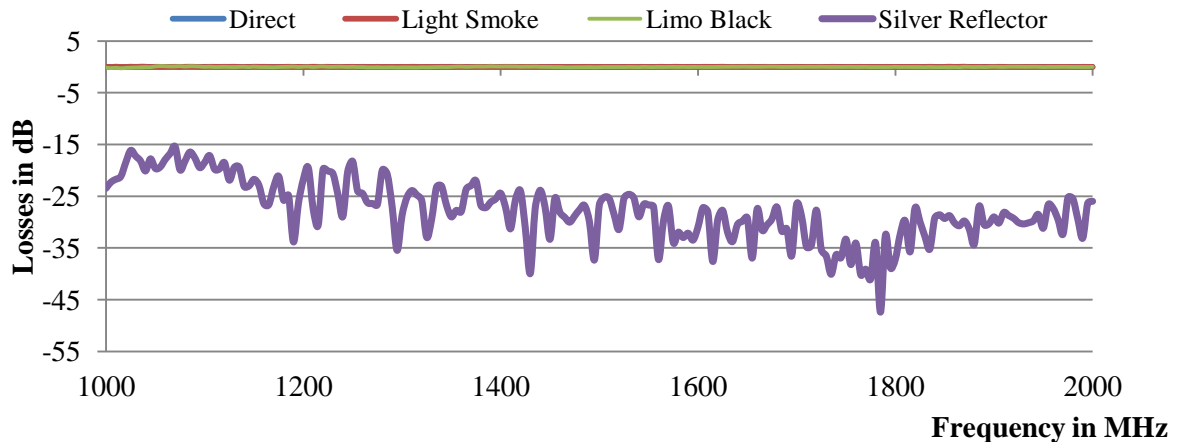


Figure 5-24 Three different car window tint film S_{21} results at 1.65m measurement distance (the losses of light smoke and limo black tints are very close to zero, therefore, only two lines are shown in chart)

5.8 Dielectric material measurement and analysis

The wireless propagation measurements initially carried out focussed on attenuation and ignored phase variations caused by the materials. This research then moved on to include phase measurements for dielectric analysis using RF propagation. Solid glass was the first material to be tested for its dielectric properties. When powders and liquids were later considered, then various thicknesses of standard glass were used for the container walls, even though its permittivity presented an inversion challenge in the dielectric calculations. It offered the advantage, however, of visible examination of material distribution (in the case of powders) and also a fairly good rigidity of containment of the MUTs. Glass was later replaced with an opaque plastic whose permittivity constant was approximately one over the measurement band, so that the inversion requirement was no longer required. Dielectric analysis work on model design and some results has been published in presentation and poster at an IEEE Workshop in Taiwan [59]. In addition, the first

successful results are also accepted by EUCAP (8th European Conference on Antennas and Propagation) in The Hague, Netherlands, in April 2014.

5.8.1 Solid glass dielectric constant

In the early testing stage of the system, the first results presented are for solid glass at thicknesses of 4mm, 6mm, 8mm, 12mm and 15mm. Glass was chosen due to its availability and previously published data. Due to confidentiality reasons, the ingredients of each glass could not be obtained from the manufacturers.

Also the glass panes were possible candidates as walls for containment purposes in the final horizontal propagation path system, offering rigidity and ease of material inspection at the early stages of development. Furthermore, the permittivity of glass can be calibrated out in the vertical (proposed) propagation path system, as only a single containment (i.e. not a sandwich) layer is required in such a system.

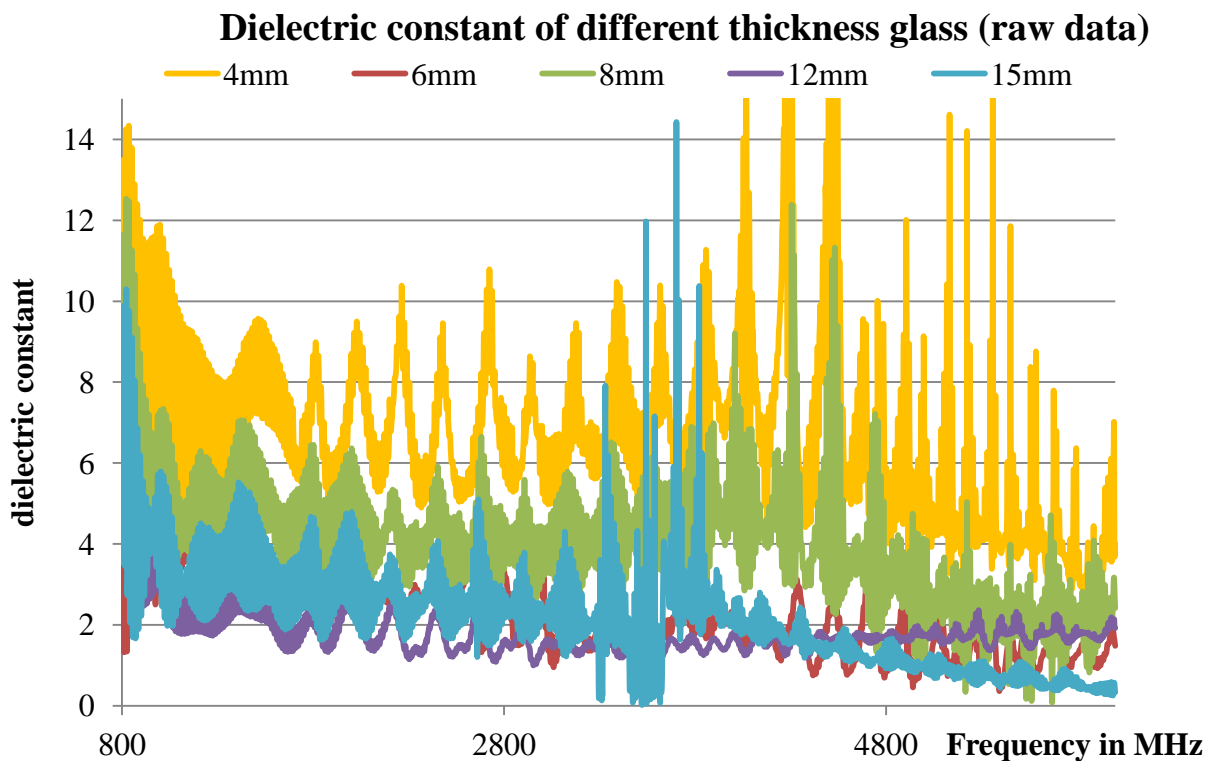


Figure 5-25 Dielectric constant of glass pane with different thickness glass raw data

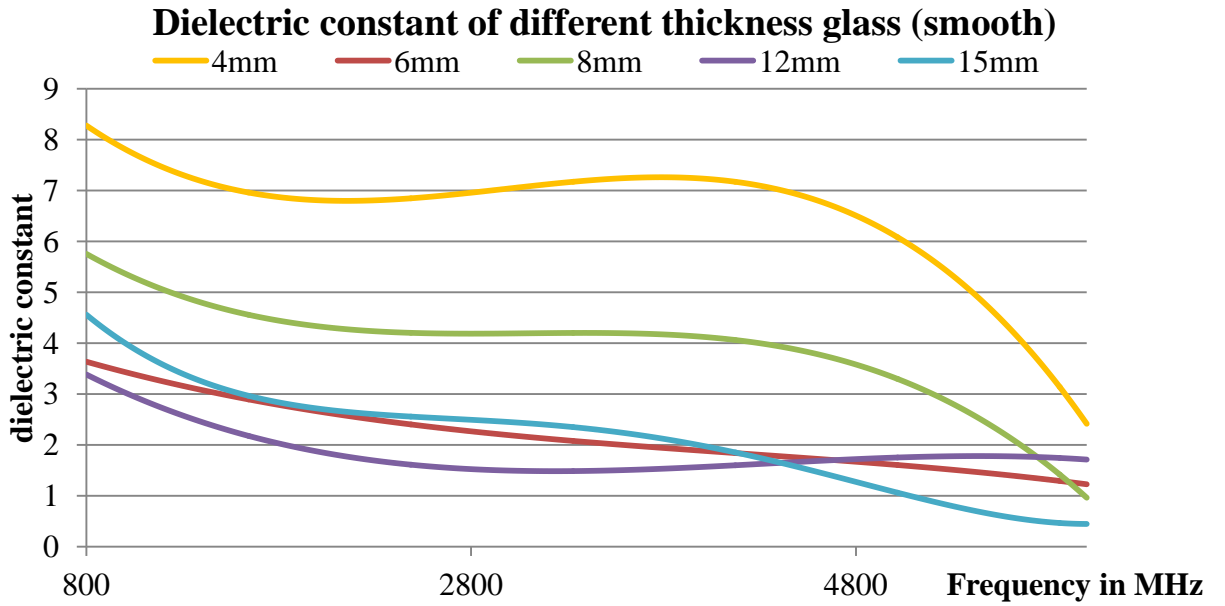


Figure 5-26 Dielectric constant of glass pane with different thickness glass (smooth)

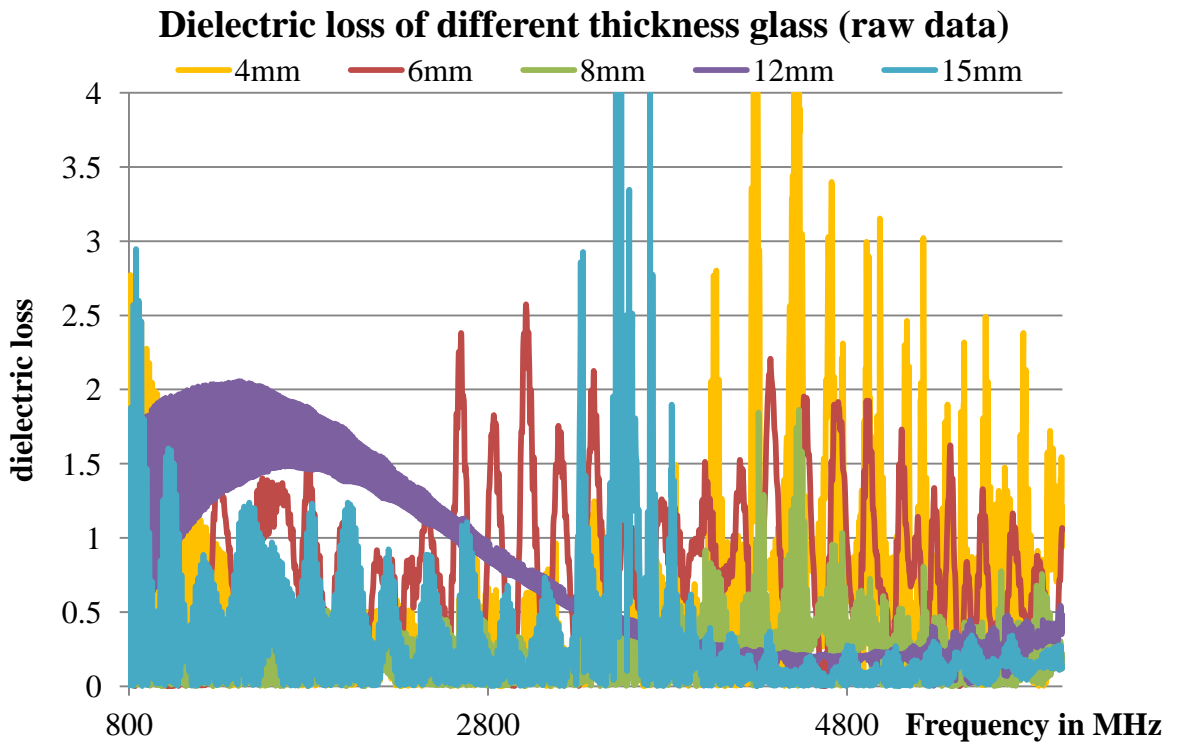


Figure 5-27 Dielectric loss of glass pane with different thickness glass raw data

The results show reasonable agreement with each other and with the published values of permittivity constant for glass (from 2 to 15 dielectric constant figures), taking into account that the glass is from different manufacturers.

Several measurements are performed in different days for certain glass, with the aim to confirm testing results. The variation in results may be attributed to different glass compositions, although the existence of such composition differences in the glass used has not been possible to confirm. The five panes of glass used in testing, were ordered directly from the distributor, but it was not possible to purchase the various required thicknesses from the same manufacturers. Silica (SiO_2), sodium oxide (Na_2O), boric oxide (B_2O_3), alumina (Al_2O_3) and magnesia (MgO) are the main constituents of different types of glass (especially silica) and each have different dielectric properties [60]. The percentage compositions may vary depending on the intended glass usage. The overall glass dielectric properties will be different, depending on the different percentages of each of these ingredients. The permittivity of the mixtures fell between the predictions of two classical mixing rules: the Maxwell Garnett formula and the Bruggeman formula. [61] [62] [63], according, for example to the Landau-Lifschitz formula or the several modifications introduced thereafter. For example,

- Fused quartz is primarily composed of SiO_2 , although this is not a very common glass, due to its high glass transition temperature of over 1200 °C
- Sodium carbonate (Na_2CO_3 , "soda"), can be used to lower the glass transition temperature. However, soda glass alone is water soluble.

Calcium oxide (CaO), Magnesium oxide (MgO) and aluminium oxide (Al_2O_3) are added for better chemical durability. The resulting glass contains about 70 to 74% silica by weight and is called a soda-lime glass. Soda-lime glass accounts for about 90% of manufactured glass. For different glass usage purposes, the chemical composition of each glass pane would be expected to vary. For instance, thin 4mm glass is very brittle and needs extra reinforcement and thus would typically contain more aluminium. For use in windows different thicknesses need different thermal expansion capability and, importantly, good optical transparency.

Although the components and their percentage volumes of certain glass is usually confidential information, the assumption is the higher dielectric constant of the 4mm glass pane compared to other thickness glass is due to the different composition of each glass pane, as outlined in this section.

5.8.2 Dielectric powder and liquid measurements

As mentioned in Chapters 3 and 4, a test platform was developed that was initially used to qualify wireless propagation through energy efficient windows, and building materials. Subsequently, the setup was modified, through the addition of a bespoke tank to facilitate the dielectric analysis of powders and liquids. The tank fitted into the original structure and had a fixed, inflexible thickness design. This tank was later replaced with a second more elaborate and also more flexible tank, also capable of use in measurements of powders and liquids.

1) Plain Flour

Published dielectric constant results of plain flours are between 2.5 to 3 at room temperature. In one measurement, standard household plain flour was tested. Four thicknesses of flour were tested, 3mm, 8mm, 30mm and 36mm.

When the thickness is very small (3mm and 8mm), the wavelength in flour is bigger than the thickness of the flour sample, therefore less than one probing wavelength is present in the flour, so n in equation (4-31) is equal to zero. However, when the thickness is up to 30mm or 36mm, n is then considered greater than zero.

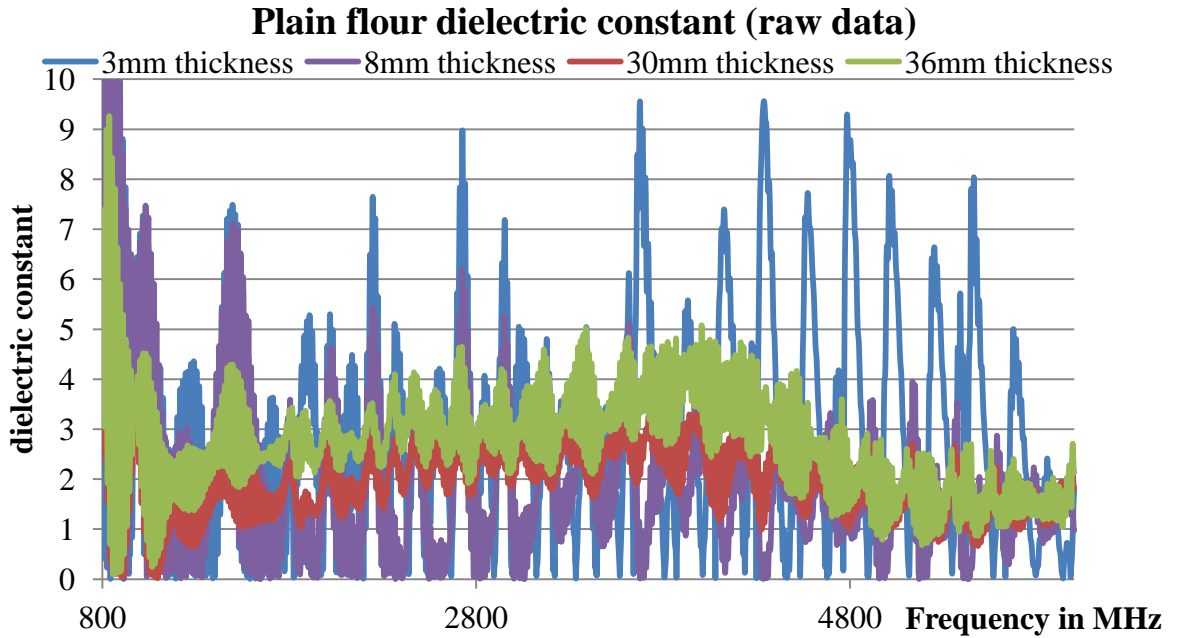


Figure 5-28 Plain flour dielectric constant raw data

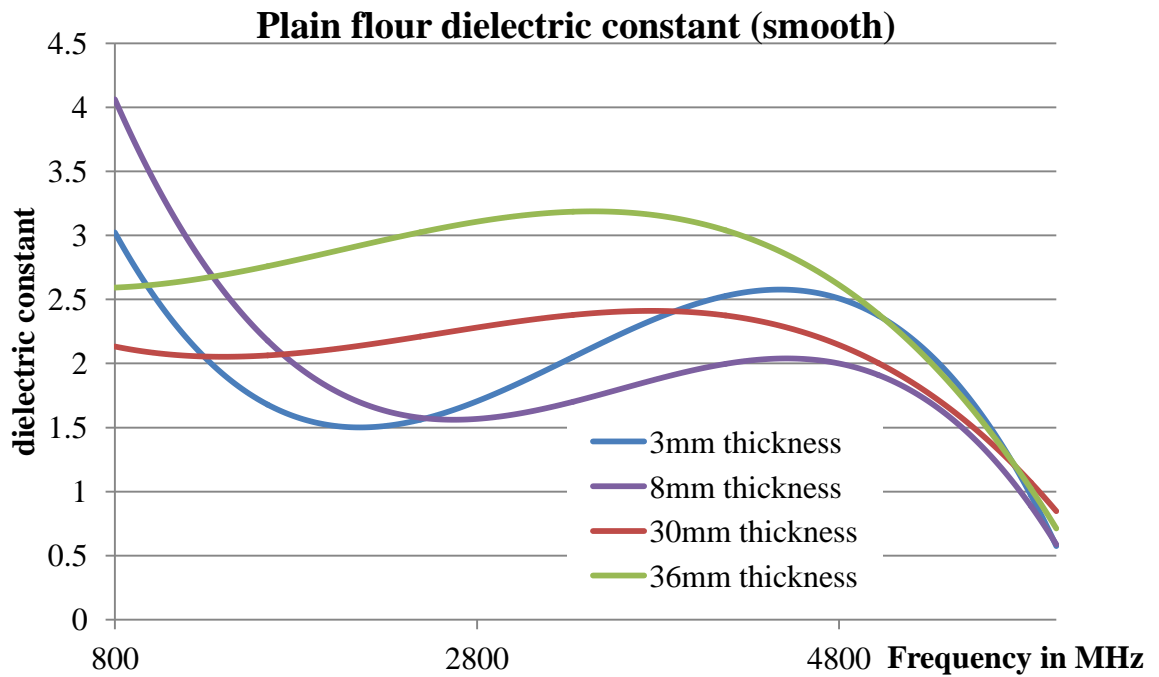


Figure 5-29 Plain flour dielectric constant (smooth)

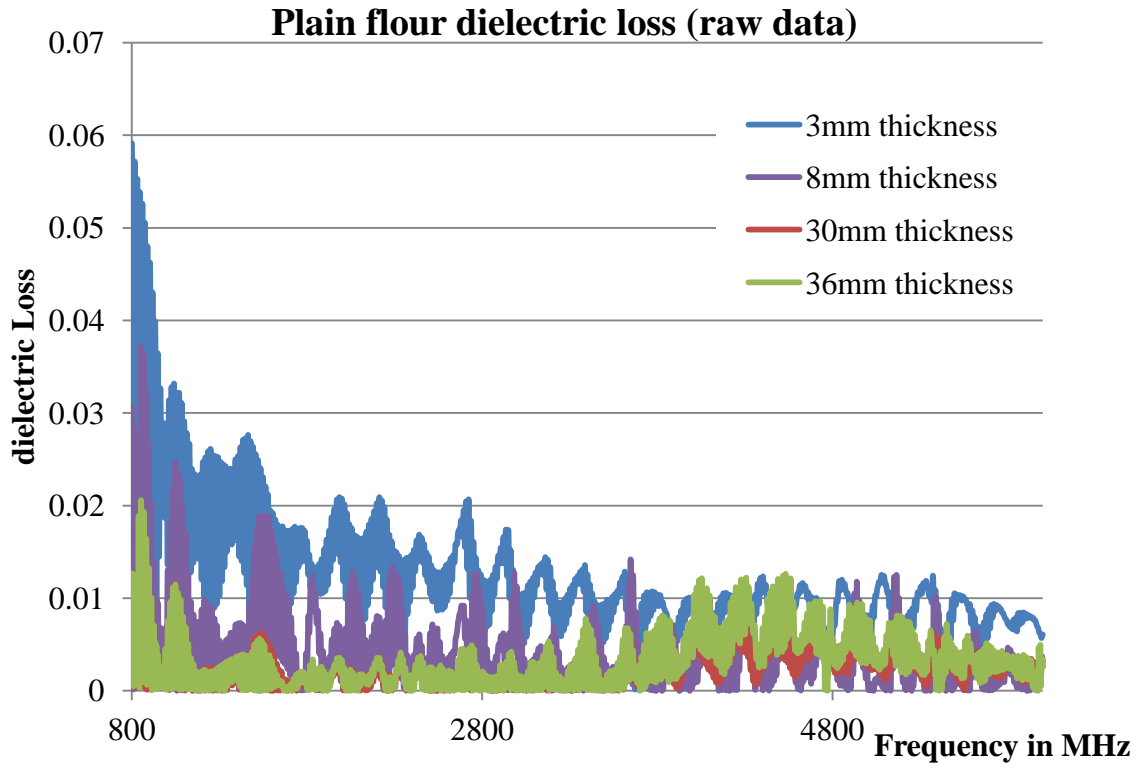


Figure 5-30 Plain flour dielectric loss raw data

2) Water

The water tested here was normal tap water. Thickness was controlled using the flexible tank. Measurement was performed in room temperature (25 to 30 °C).

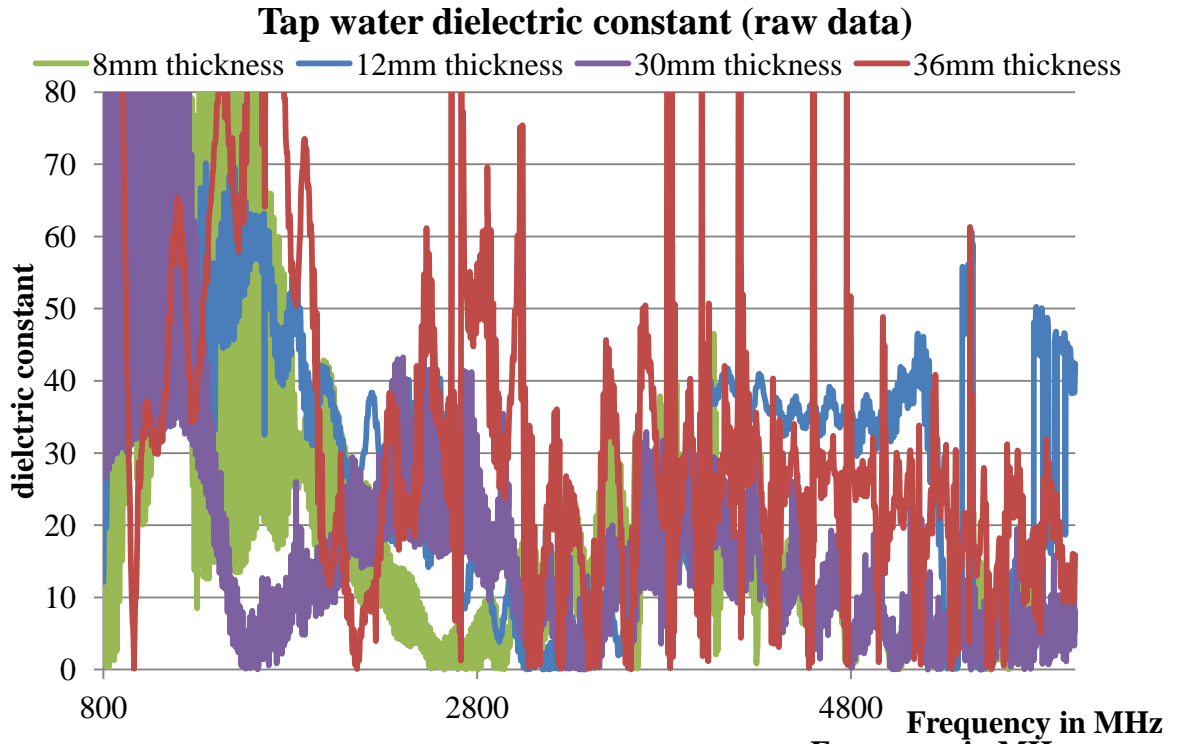


Figure 5-31 Tap water dielectric constant raw data

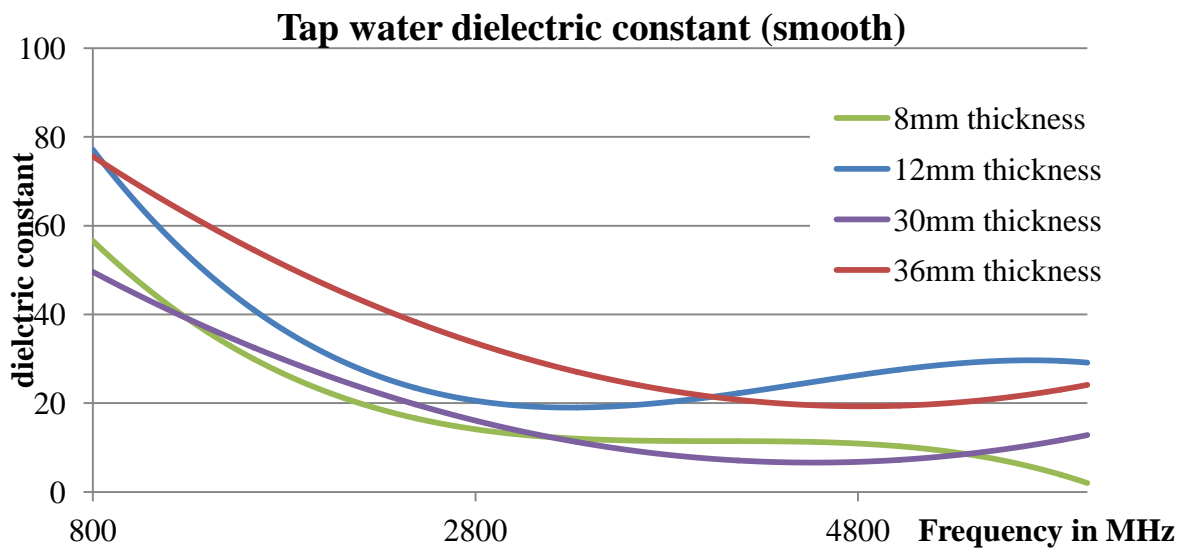


Figure 5-32 Tap water dielectric constant (smooth)

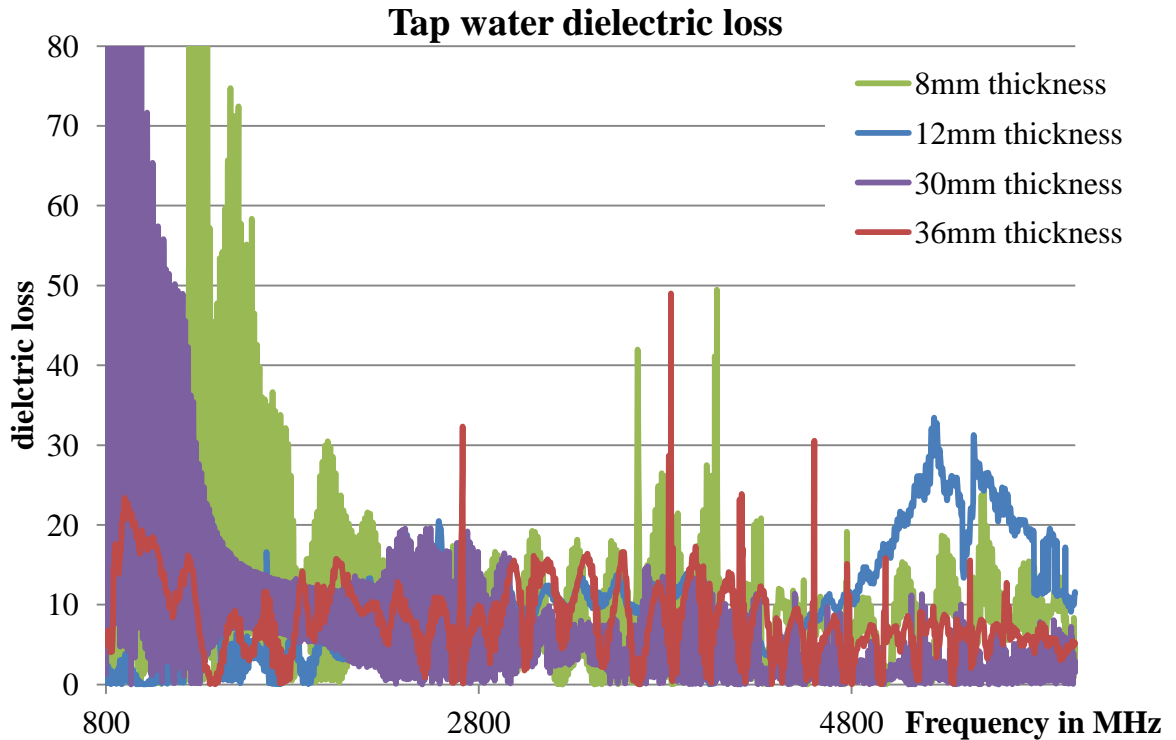


Figure 5-33 Tap water dielectric loss raw data

All of the water dielectric constant results show a decreasing trend for all the samples (From 800MHz to 6GHz). The decrease is fairly rapid at lower frequency range. The decrease of dielectric constant with increasing frequency is a normal dielectric behaviour for all materials tested here, which is also observed by other researchers [64]. A glass containment system is considered as a heterogeneous material that can experience interfacial polarisation as predicted by Maxwell and Wagner [19] [20]. Their work explains that for the lower microwave frequency region used in tests described here, that the movement of charge carriers trapped in the interfacial region is caused by inhomogeneous dielectric structure. Of the materials tested they typically are lossless in the low-frequency region (of the test range used here), and usually exhibit higher losses at high frequencies (of the test range used here). The imaginary part of the permittivity has its maximum value at the critical frequency (refer to the water example in Figure 2-7, the blue trace, albeit at frequencies outside the test range used here). Recall from Section 0 on

Dielectric material properties that at a molecular scale, several mechanisms contribute to define dielectric behaviour. With increasing the frequency, the dominant mechanism contributing to the dielectric constant is the polarisations that still have time to reach their steady peak value. The slower mechanisms drop out in turn as frequencies rise, the faster ones, however, continue to contribute to ϵ_r . Recall that the loss factor (ϵ_r'') will peak at each critical frequency. The magnitude and “cut-off frequency” of each mechanism is unique for different materials. Water, for example, has a strong dipolar effect at low frequencies, but its dielectric constant rolls off dramatically around 20GHz (beyond the testing range of this research).

5.8.3 Horizontal setup disadvantages

It became obvious early on in the development of the horizontal test structure that the combined rigidity and flexible depth requirements were very difficult to meet, especially when glass is considered for the containment. Perfect rigidity was difficult, even with 12mm thick glass. Values lower than this thickness exhibited a lens effect, shown in block diagram form in Figure 5-34 and in a measurement of table salt (Figure 5-35). One consequence of this is surprisingly large values of S_{21} at some frequencies, even when the lens effect is not so obvious to the human eye.

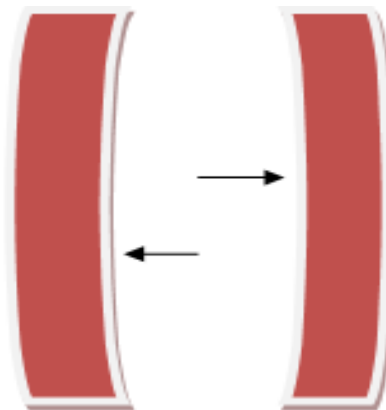


Figure 5-34 Lens effect caused by insufficient container rigidity



Figure 5-35 Lens effect in salt test (deliberate misalignment reconstructions)

The requirements to measure materials at several thicknesses also presented challenges of misalignment of container walls. These produced apparently anomalous results until deliberate misalignment reconstructions were measured to confirm misalignment as the source of the anomalies.



Figure 5-36 Misalignment reconstruction tests

5.8.4 Vertical measurement proposal

Although a vertically aligned test infrastructure presents particular structural challenges in particular in stability, normal incidence and alignment; some benefits are immediately apparent compared with the horizontal structure. Immediately, the containment

requirement is simpler and the flexible depth to allow variable MUT thickness is also much more straightforward.

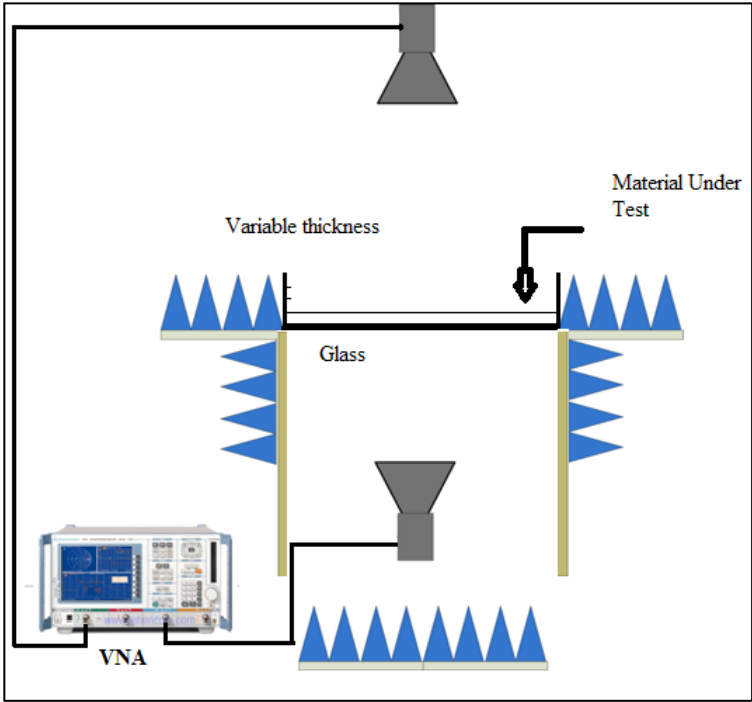


Figure 5-37 Candidate vertical measurement system, in WIT anechoic chamber



Figure 5-38 Vertical measurement system, photo shoot in WIT anechoic chamber

Figure 5-37 Figure 5-38 illustrates a proposed structure to implement a vertically aligned measurement in an anechoic chamber. This structure consists of one layer of glass beneath the material instead of the two layers required in the horizontal structure, which also allows an easier inversion (no ABCD matrix requirements) in the permittivity calculations. Once fixed in place, it also permits normal incidence of the waves with more accuracy. It is excellent for high permittivity values (short electrical length, as the MUT can easily be a depth of 5mm or less, with one limitation now being accurate of depth measurement. It also provides simple and easy measurements of MUT thickness variation (powders) and is particularly easy to test liquids [65].

5.8.5 Uncertainty terms analysis

Expressions of constitutive parameters of liquid / powder samples were derived using an asymmetric cell from reference-plane invariant S-parameters. However, the effect of sample holder properties on the measurement accuracy and on the performance of the proposed method was not considered. Toward this end, in this section, an uncertainty analysis was performed to consider the effect of some parameters on the accuracy level of measurements. Several factors contribute to the uncertainty in permittivity and permeability determination in free-space measurements namely:

- 1) The uncertainty in measured S-parameters
- 2) Errors in the sample and holder lengths
- 3) The uncertainty in reference-plane positions
- 4) Mismatches
- 5) Air gaps between the internal surface of the sample (holder) and inner walls of container

Care can be given to limit the uncertainties due to calibration, misalignments, and mismatches by using appropriate free-space calibration techniques and machining the sample holder with no scratches, nicks, or cracks [24].

Because part of MUT in our problem is the liquids, and because liquid samples occupy the container where they are poured, there will not, in essence, be any air gap between container walls and the sample. About the powder MUT, if well taken care when added in

to container, air gap can also be eliminated. On the other hand, utilizing low-loss sample holders as for holding the liquid sample (i.e., glass pane), small air gaps (if any) between the MUT and container walls will not much change the measurement results.

5.9 Conclusion

This chapter presented all the measurement results and data analysis, from the early propagation test results to the subsequent complete dielectric measurement results and analysis. For the early propagation tests, energy efficiency glass, building materials, insulation materials and vehicle windows were examined. From these results it can be seen that some of those type of materials have a very strong attenuation to RF signals. For dielectric materials, glass, water and plain flour were tested. The permittivity results are close to the published values. The horizontal test structure was used for most test setups, but some final results presented were taken from a new vertical set-up.

6 Conclusion & Future Research

This work set out to develop a novel free-space dielectric analysis technique. In dielectric analysis, materials which exhibit dielectric properties will interact with incident electromagnetic fields and the manner and scale of the interaction can be measured and analysed to determine those very dielectric properties.

The previous research work is based on wireless signal propagation through different materials, and, to use the same technology to carry out dielectric material characterisation. Non-destructive testing (NDT) for material characterisation can be performed by measuring complex permittivity and permeability using this technique. Dielectric analysis has advanced considerably and now includes several frequency and time domain techniques, in free space and also confined space, for individual frequencies and also for broadband, for both high and also low loss materials. Developments have included a reduction of the effects of multiple reflections, of diffraction from boundary edges, of initial guesses for ϵ_r , of precise sample thickness knowledge, and of phase uncertainty in reflection measurements. Many of the free space propagation measurement techniques are used or could be used on similar platforms and this concept forms the basis of the test platform design described in this work.

Although non-resonant waveguide techniques are popular and require less material, free space broadband techniques can yield useful results due to the bulk of material and a large frequency range for measurements. Reflection only free-space measurement techniques obtain the dielectric properties from the reflection coefficients, and consists of an antenna illuminating a flat-surface MUT. Although simple, such techniques can suffer if the surface is not smooth, or if the surface is in any way not a good representation of the bulk of the material (e.g. moisture content) and standard calibration techniques can be applied. Therefore, techniques that include propagation measurements offer the advantages of reduced impact of surface roughness (especially at higher frequencies), local variations in material composition can be averaged out and standard calibration techniques can also be

applied. The proposed test platform will accommodate reflection only, as well as transmission/reflection techniques. It will also be flexible in accommodating various sample thicknesses, required by some measurement techniques.

It is proposed to examine several of these techniques, in the same environment, for the same materials, by using the new vertical transmission design in the WIT anechoic chamber.

From Chapter 5, at least two or in some cases three or more different thickness of MUTs are measured for the new technique [66]. The new vertical platform design will consist of a flexible container made of one piece of glass pane. A block diagram representation, where spacing can vary from a minimum value of $d_1=3\text{mm}$ to a maximum value of $d_2=36\text{mm}$, the latter figure having been chosen simply to the size of the vertical container. This means there is also a lot of more flexibility in MUT thickness, compare to the horizontal measurements. So it is not only reduce the systematic error of the horizontal setups but also remain the MUT can either be liquids or powders. In addition, the shape of MUT is not uniform.

From the three tested material results (glass, plain flour, tap water), both dielectric constant and loss are presented in this thesis, however, in some parts of the charted results, the dielectric values are not as good as expected, in particular that some dielectric constant values are lower than 1 (impossible) and dielectric loss are close, but plain flour dielectric loss has an error of roughly ten times of published data (around 0.005 from 800MHz to 6GHz); dielectric loss value of glass is very close to published data (normal glass is around 0.2); dielectric loss of water from 800MHz to 6GHz is around 10 to 15, therefore, the calculated result from this technique is close to this value. This focus of this thesis is to develop and establish a novel testing technique for measuring dielectric constant and loss. While this has been achieved, there are nonetheless a few areas that need some improvement. These further works will be carried out in future research in the Waterford institute of Technology.

Appendices

Publications

Conference proceeding: 16th European Wireless, IEEE, Lucca, Italy, 2010

Rf Propagation Through Transparent Conductors In Energy Efficient Windows

D. Stolhofer, H. Doelecke
Elektro- und Informationstechnik
Fachhochschule Hannover
Hannover, Germany

Yaqiang Liu, P.O'Leary
Engineering Technology
Waterford Institute of Technology
Waterford, Ireland

Abstract— Windows were traditionally used as a means of building access and egress for RF signals. However, the drive towards building energy efficiency now means that windows are frequently coated with thin layers of Transparent Conductors (TCs). TCs can let visible light energy pass virtually unattenuated, but reflect longer wavelengths (typically from the infrared region), to keep buildings warmer in colder climates and cooler in warmer climates. However, the use of TCs has a negative impact on wireless propagation, which this paper reports on. Three commercially available windows are examined, with results showing that less than 1% of the signal passes in either direction. This result is taken from a series of measurement over a range of frequencies from 800 MHz to 6 GHz, both in a large hall and in the WIT anechoic chamber.

Keywords—microwave; propagation; reflection coefficient; energy efficient glass;

I. INTRODUCTION

Transparent conductors (TCs) are gaining widespread acceptance in glass manufacture, as a means of controlling the energy leaving (or entering in warmer climates) buildings. Legislation has been introduced to encourage this, such as Germany's *Verordnung ueber energiesparenden Waermeschutz und energie sparende Anlagentechnik bei Gebaeuden (Energiesparverordnung - EnEV)*, which states that the energy demand shall be reduced by over 30% and in a further step by the year 2012 by a further 30%, compared with previous legislated levels [1].

The industry response has focused primarily on the use of TC coatings, usually on one of the inward facing sides in a double glazed unit. The aim of applying thin coats of TC is to reduce heat transfer across a vertically mounted window from about $3\text{-}1.5 \text{ Wm}^{-2}\text{K}^{-1}$ to as low as $0.4 \text{ Wm}^{-2}\text{K}^{-1}$ for double glazing, principally by reducing the radiative energy loss for frequencies beyond (lower than) the visible part of the spectrum [2]. The challenge for window manufacturers, in using TCs, is to also maintain light transmittance in the visible part of the electromagnetic spectrum, as shown in the $\text{TiO}_2/\text{Ag}/\text{TiO}_2$ coated glass graph in Figure 1 (reproduced from [2]).

Quite a lot of research has gone into the development and testing of various TCs, but mainly focusing on performance in the visible and near Infra-red regions of the spectrum. This

research examines the knock-on effect for Radio Frequency (RF) propagation.

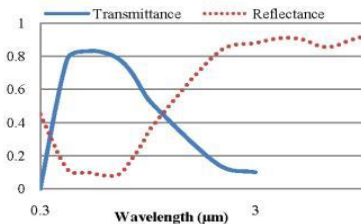


Figure 1. $\text{TiO}_2/\text{Ag}/\text{TiO}_2$ coating transmittance and reflectance (reproduced from [2])

Although published TC data measurements typically stop at about wavelengths of $3 \mu\text{m}$ and the work here covers RF wavelengths from 5 to 37.5 cm , it may be expected from the published graphs that the RF propagation would be quite low.

This large expected loss due to the coating may be contrasted with the low expected loss in passing through the silica float glass alone, as reported in [3] for the range 0.5-2GHz and reproduced here in Figure 2. The glass reported on here is 4mm thick (single pane), twice 6mm (coated double glazed unit- Glass A) and twice 4mm (coated double glazed unit- Glass B).

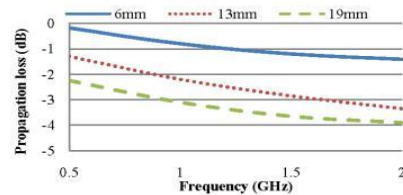


Figure 2. Glass propagation measurements from [3]

the Total Station, with each glass held in the test frame, which was placed just in front of the receiver antenna.

Results presented here are for E-plane measurements. H-plane measurements are not presented, although the results are similar.

III. RESULTS

Energy efficient windows must first and foremost pass visible light. The visible light transmittance for the two coated glass windows under test was measured and compared with a plain glass pane (4mm thick) and presented in Table I. A handheld light meter is used to measure visible light transmittance, by averaging ten readings taken in front of and behind the glass.

TABLE I. VISIBLE LIGHT TRANSMITTANCE

Glass Types	Transmittance
Coated Glass A	75%
Coated Glass B	81%
Plain glass	87%

These results are also consistent with the transmittance for the TiO₂/Ag/TiO₂ coating shown in Figure 1. No infrared source was available to measure the transition wavelength from transmitting to reflecting for the coated glasses.

The RF propagation from 800MHz-6GHz was then measured and results are compared (with respect to a reference line, when no glass under test was present) in Figure 6, for an antenna separation of 5m. The baseline data, mentioned in Section 2.2, appears as a reference line at 0dB across the range of test frequencies. Both the coated glasses show considerably reduced propagation compared with plain or no glass.

The measurements were repeated at separations of 7m and 1.65m (test range reduced to 1 to 2GHz) and similar results were obtained.

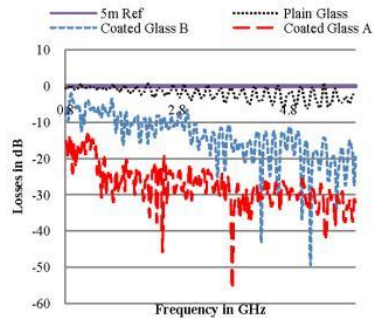


Figure6. Propagation results from large hall

The same glasses were then tested in the WIT anechoic chamber. In order to observe the far field criteria mentioned earlier, the test range was limited to 1-2GHz. In this range, the antenna separation can be 1.65m, for the chosen antennas. The results are presented in Figure 7.

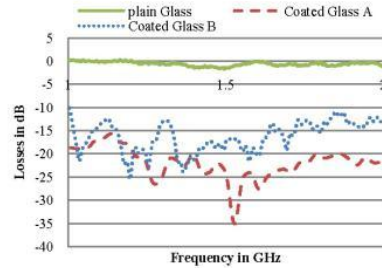


Figure7. Propagation results from anechoic chamber at 1.65m.

IV. ANALYSIS

There are two analysis produced for these measurements.

A. VNA Result Analysis

The visible light transmittance results are all quite similar, especially when taking into account that Glass A is 12mm total of glass (due to its large size, only 6mm thick glass was feasible for each pane) and Glass B is 8mm total of glass. The plain glass is 4mm thick. Glass A and B are from different manufacturers and may therefore be assumed to have different coatings.

The RF propagation results for the 4mm thick plain glass are always better than -3dB and correspond well with other published results. There is a gradual increase in propagation losses, as reported by, for example, NIST. For coated glass, the propagation can fall as low as -30dB and these results correspond well with previous work carried out by this group of researchers [4].

Although neither the actual coating material nor the coating thickness nor even the uniformity of deposition is known for the coated glasses under test, certain conclusions may nonetheless be drawn. Figure 1 shows a transmittance reflectance curve for a coated glass, which, from the perspective of RF propagation, may be assumed to be fairly indicative of the coating influence. (The graph may not be representative, in that the amount of transmittance/reflectance depends on material, thickness, anti-reflection material and nature of deposition).

The plasma frequency for TCs lies in the infra-red region. Below the TC plasma frequency, it acts as a conductor and reflects incident light [5]. Above the TC plasma frequency, it passes or absorbs light, acting like a dielectric. This conductor-like reflection behaviour is observed also at RF frequencies, which are much lower than those normally measured by those

interested in TC development or those interested in window manufacture.

Both coated windows offer significantly poorer RF propagation paths compared to standard glass. The results from the anechoic chamber, in Figure 7, are consistent with the large hall measurements, in Figure 6, albeit showing even poorer propagation. The higher propagation results for the hall may be due to some small signal leakage, in spite of the foam shroud created for the receiver.

B. VNA standing wave analysis

Although the VNA is usually calibrated to the cable ends, the fluctuations in the VNA output is caused by unavoidable standing waves, due to the introduction of the MUT, whether in the large hall or the anechoic chamber. Clearly the MUT will introduce standing waves, which cannot be easily removed by calibration. It is proposed to analyse these standing wave results in the future, as a means of confirming reflection measurements, by using Fourier analysis of the VNA output. The basis for this future analysis is outlined here.

It can be shown that the VNA repeat patterns are each defined by a fundamental standing wave. For example, Figure 8 shows a close-up of the VNA output for a single 7.65m cable itself. This pattern is usually calibrated out before MUT measurements.

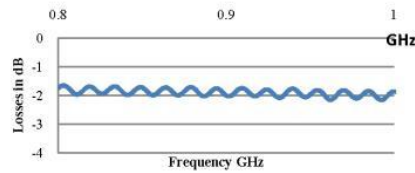


Figure8. Standing wave Chart from cable validation

The individual peak separation for constructive interference can be calculated as 15.1MHz. To confirm the pattern is associated with the cable, if we presume the speed of light in the RF cable is lower than *c*, at 77% of the speed of light in a vacuum [6], then the fundamental standing wave wavelength is

$$\lambda = \frac{c'}{\Delta f} = \frac{2.31 \times 10^8}{15.1 \times 10^6} = 15.29\text{m}$$

So the calculated cable length is $\lambda/2 = 7.645\text{m}$, which closely matches the actual length of 7.65m.

A simple example may be seen by examining the Fourier transform of VNA results shown in figure 9. The strong low frequency value may be ignored, as it is due to the VNA results being all positive (absolute values were taken).

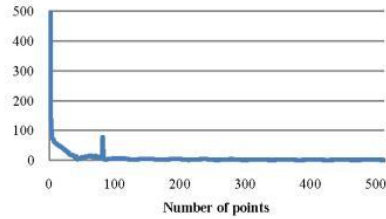


Figure9. DFT result of cable validation

The resolution of the VNA output, in this example, is

$$\Delta f = \frac{2000\text{MHz} - 800\text{MHz}}{1000 \text{ points}} = 0.12\text{MHz}$$

We calculate the number of samples between point 817MHz and 968MHz is 127. There are ten periods in this range. So, the number of sample per period is close to:

$$ns = \frac{\text{total number of points}}{\text{total periods}} = \frac{127}{10} = 12.7$$

$$f = \frac{N}{ns} + 1 = \frac{1024}{12.7} + 1 \approx 81 + 1 = 82$$

Referring to figure 9, the relevant point is 82. Therefore, by converting the DFT result into relevant distance, figure 10 is presented.

For figure 10 below, there is a reflection response at $x = 7.645\text{m}$, which is the cable length.

Analysing the more detailed output from a full MUT measurement would equally supply distance confirmation, as in the example above, but also, more importantly, a relative comparison of the impedance mismatches from various surfaces, by examining the amplitudes. If care is taken in choosing the VNA frequency range and the number of sampled points, it should be possible to even distinguish between the two different reflection coefficients in the energy efficient double glazed windows.

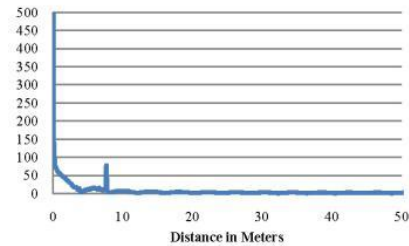


Figure10. DFT chart converted to distance response chart

V. CONCLUSION

These results require further work, with more glasses and also with glass manufacturers, so that their TC information may help widen the understanding of the phenomenon.

One further question also naturally arises from these results, namely how RF signals can penetrate buildings, if the window opening is no longer, or is at least less of, an option. Other studies, for example [3] have shown the other materials in the main building fabric to be highly attenuating. The authors are consequently currently examining some traditional and some new building materials for RF propagation. Some materials offer some hope for RF propagation, particularly in the case of domestic dwellings.

On the other hand, it may be worth mentioning that RF propagation reduction is not always a disadvantage. The use of TCs on windows also means less signal leakage from the building, thereby increasing security for the inhabitants.

ACKNOWLEDGMENT

The authors would like to acknowledge support under the TSR Strand I for Yaqiang Liu and also from Bryan Hallissey in the Building Technology Department of WIT for the Total Station.

REFERENCES

- [1] Bundesministerium fuer Verkehr Bau und Stadtentwicklung, 01 October 2009
- [2] Claes G. Granqvist, *Transparent conductors as solar energy materials: A panoramic review*. Vol.91, pp. 1529-1598, 15 October 2007.
- [3] W. C. Stone, "Electromagnetic Signal Attenuation in Construction Materials," in *NIST Construction Automation Program Report No. 3*, October, 1997.
- [4] N. Knauer, "Investigation of the Physical Effects when Electromagnetic Waves pass through various Window Types", Diploma dissertation, Fachhochschule Hannover, Germany, 2006.
- [5] R.G. Gordon, "Criteria for Choosing Transparent Conductors", *MRS Bulletin*, vol.25, no. 8, pp. 52, August, 2000.
- [6] *Data Sheet of Coaxial Cable: Sucoflex 106*. Huber+Suhner, Herisau, Switzerland, 2007.

Broadband Wireless Propagation through Various Building Materials

Yaqiang Liu, Praveen Munjampally and P.O’Leary
Waterford Institute of Technology
Cork Road
Waterford
Ireland

Abstract- Heat containment within buildings has become a major goal in recent times. Such containment can occasionally have a negative effect on wireless propagation into and out of buildings. The motivation for this work derived from a series of measurements on new energy efficient windows. The measurement results (800MHz-6GHz) highlighted very poor propagation characteristics (as low as -30dB), which will be published in [1]. Given that windows traditionally provided access/egress opportunities for wireless, this work reports on a series of measurements on typical building materials. This study also follows on from published building materials’ research, such as by NIST Ref. [2].

I. INTRODUCTION

In the modern world, energy efficient materials are widely used as part of building heat retention. According to previous research on the propagation measurement of traditional building materials (such as block, solid concrete, wood, bricks, etc), wireless propagation through building walls can be strongly attenuated [2]. For this reason, the principle propagation path into buildings has been through the building openings (or opes), namely external doors and windows. However, the international demand for improved energy efficiency has led to an examination of building opes in terms of their poor ability to retain heat within the building. This has led to the manufacture of windows that are much better at retaining heat, but with a significant negative consequence for wireless, with measured attenuation of up to -30dB [1].

The final significant access opportunity into a building is via the roof. There are many different materials used in roofing, including natural slate and engineered slate, wood, metal concrete tiles and (internally) insulation. This work qualifies the signal attenuation for various materials used in both roof and wall construction. It also records the dielectric response of each material for future use in material dielectric analysis.

This paper is divided into 4 sections, as follows. Section II describes the test configuration, error analysis and also the measurement technique. Section III is to record the test result from VNA. The results are represented in EXCEL graphic, which x-axis is frequency and y-axis is magnitude. Section IV performs an analysis based on the result.

II. MEASUREMENT METHOD

The tests were initially performed in a big hall (approximately 45m x 30m x 8m). The propagation properties are measured in the far field, which is defined, at the test frequencies (800MHz-6GHz), to be further than a

combination of 3λ , $5d$ and $2-d/2\lambda$, (where d is the biggest antenna dimension and λ is the test wavelength). For the antennas used (Schwarzbeck horn antenna BBHA 9120), $d=0.33m$. Thus the minimum far field separation, at the maximum test frequency of 6GHz, is 4.35m, which we rounded up to 5m. For some materials, measurements were also taken over a narrower, lower range of frequencies, at a separation of 1.65m. The antennas were mounted on a modified Pentax Precision Total Station (figure 3), which permitted accurate distance and angular measurements.

A. Measurement Set-Up

Materials to be tested were held by a wooden frame, sited between the transmit and receive antennas. The receive antenna is also shrouded by absorbent foam, with more foam placed between the transmit and receive antennas to reduce the ground reflected wave, as shown in Figure 1.



Figure 1 Large hall test configuration, without wooden frame



Figure 2 Modified Total Station Antenna Mount

A custom-built wooden frame (2.1m x 1.1m cross-section) with rounded edges was created to support and align the materials under test (MUT), as shown in Figure 4.

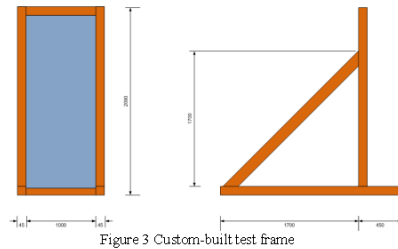


Figure 3 Custom-built test frame

B. Measurement procedure

The materials tested were four types of common heat insulators (foil backed insulation, graphite impregnated polystyrene, rock wool and polystyrene), concrete blocks, slate (natural & synthetic), plywood board.

Further tests in the near future will include other building materials, including bricks, tiles, asphalt and felt.

As a VNA was used for the propagation measurements, it was possible to easily examine the effect of the material under test alone, by doing a two-port one-path calibration. To do this both transmit and receive antennas stood in the position, which is selected for the “normal” measurement, with only the materials under test missing from the configuration. The results for S_{21} and S_{12} were stored in the VNA, as baseline data. This fundamental data was later used to remove the effects of the cables, antenna, etc, in a manner similar to a standard VNA calibration. The S_{21} and S_{12} were then measured with the material under test in place.

Each of the materials was tested for RF propagation as follows. The antennas were placed at a separation defined by the Total Station, with each material held in the test frame, which was placed just in front of the receiver antenna.

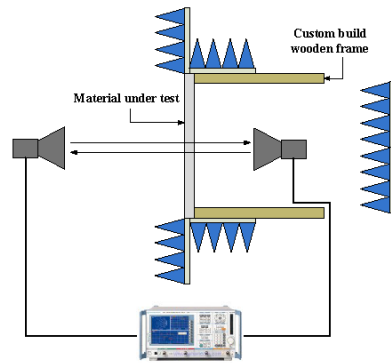


Figure 4 Measurement set-up plan view



Figure 5 Materials under Test

Results presented here are for E-plane measurements. H-plane measurements are not presented, although the results are similar.

III. RESULTS

The figures below are several results for concrete blocks, natural and synthetic slate and four insulations. The distance, in this case, between the two antennas is 5m, so the frequency range is from 800MHz to 6GHz, in order to comply with the far field requirements. All measurements are presented relative to free space and consequently phase and attenuations represent changes due to the MUT.

The VNA phase data can be used to either calculate the time delay or the dielectric response of the MUT. This is of interest for some future work in time of flight and (separately) in dielectric analysis.

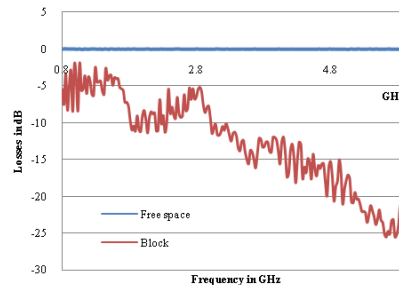


Figure 6 Concrete block attenuation at 5m

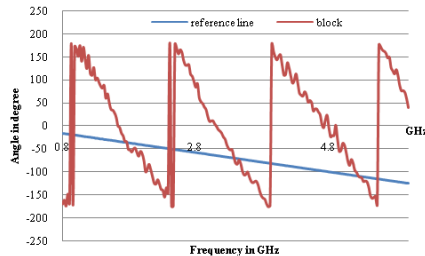


Figure 7 Phase change due to concrete blocks

As may be expected, losses are up to -25dB for 100mm of block, although they are as low as -5dB around the GSM 900MHz band.

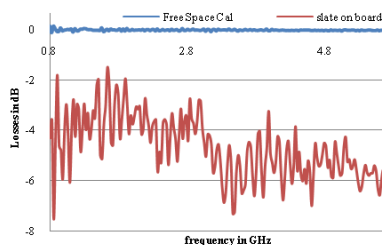


Figure 8 Synthetic slate on 8mm plywood board

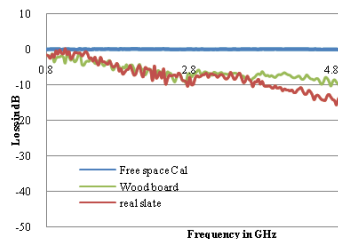


Figure 9 Natural slate (area cover 1m x 1m) on 24mm plywood board,

For the four types of insulation test, due to the size requirement, the distance was reduced to 1.65m, which the frequency range is limited down to 1 – 2GHz.

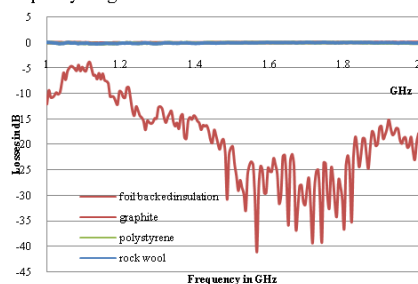


Figure 10 Four insulation test results in 1.65m

IV. ANALYSIS

It is important to initially point out that results show apparent *oscillations* in the VNA output over the entire frequency range of interest. These are easily explained and do not take anything from the validity of the results.

Consider the diagram in Figure 4, initially without the material under test, for the reference measurement and then subsequently with the material under test. The inclusion of the material under test means that there will also now be extra reflections in the measurement path (receiver antenna to material, material back to receiver, etc). This would mean that for both s21 and s11, some frequencies will constructively interfere with each other. The amplitude of the VNA output's *oscillation* depends on the impedance mismatch at the point of reflection and will be examined in future work as a means of determining impedance mismatch.

In terms of the measurement results and typical building construction, where foil backed insulation is used, wireless propagation is severely attenuated. Foil backed insulation may be used in wall cavity as well as floor/roof, in which case signal propagation is severely reduced (e.g. -15 to -50dB in a cavity wall with concrete block on inner and outer leaf).

The roof may offer more hope, in particular where insulation is not foil-backed. Here the use of synthetic slate, wood and one of the other insulation types would reduce propagation to as little as 6dB over the range of measurements, while still maintaining the building and energy integrity requirements.

However, energy efficient materials are and will be widely used in modern building techniques. A solution to the problem may lie in access through the roof area, if composite materials are used in the building fabric and no foil-backed insulation. More likely is that an external antenna will be required to bring signals from the outside (or vice versa). This proved very effective, for example, for television signals (satellite or terrestrial).

ACKNOWLEDGMENT

The authors would like to acknowledge support under the TSR Strand I for Yaqiang Liu and also from Bryan Hallissey in the Building Technology Department of WIT for the Total Station.

REFERENCES

- [1] D. Stolhofer, Yaqiang Liu, H. Doeledke and P.O'Leary, "RF Propagation Through Transparent Conductors In Energy Efficient Windows," *16th European Wireless Conference*, Lucca, Italy, April 2010.
- [2] W. C. Stone, "Electromagnetic Signal Attenuation in Construction Materials," in *NIST Construction Automation Program Report No. 3*, October, 1997.
- [3] R. Bansal, *The Far-Field: How Far is Far Enough?*, Applied Microwave & wireless, Nov 1999
- [4] C.A. Balanis, *Antenna Theory: Analysis and design*. Hoboken, N.J: Wiley-interscience, c2005.

BROADBAND WIRELESS PROPAGATION THROUGH VARIOUS BUILDING MATERIALS



Yaqiang Liu, Praveen Munjampally and P.O'Leary

Waterford Institute of Technology, Waterford, Ireland.

E-mail: poleary@wit.ie, Phone:+353-51-302630, Fax:+353-51-302666

Introduction

Energy efficient materials are widely used as part of building heat retention. Wireless propagation through building walls can be strongly attenuated. For this reason, the principle propagator path into buildings has been through the building openings (or open, nearly external doors and windows). However, the intentional demand for improved energy efficiency has led to an examination of building types in terms of their great ability to retain heat within the building. This has led to the manufacture of windows that are much better at retaining heat, but with a significant negative compromise for windows, with measured attenuation of up to 30dB.

Measurement Method

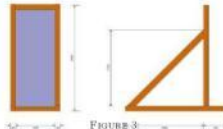


Measurement Set-Up

The tests were initially performed in a big hall (approximately 40m x 30m x 8m). The propagation properties are measured in the big hall, which is defined, at the test frequency (900MHz/925MHz), to be further than a combination of 5λ and 20λ, where λ is the biggest antenna dimension and λ is the test wavelength. For the Schwanbeck horn antenna BWA 925, this is 20cm. Thus the minimum for full separation, at the maximum test frequency of 925MHz, is 4.0m. The antenna was mounted on a modified Tripod Precision Test Station (figure 2), which permitted accurate distance and angle measurements.

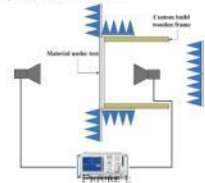


Materials to be tested were held by a wooden frame, steel between the transmit and receive antennas. The receive antenna is also identified by absorbent foam, with noise foam placed between the transmit and receive antennas to reduce the ground reflected wave, as shown in Figure 3. A custom-built wooden frame 1.1m x 1.1m (two dimensions) with rounded edges was created to support and align the materials under test (MUT), as shown in Figure 4.



Measurement procedure

The materials tested were four types of common heat insulators (full backed insulation, graphite impregnated polyurethane, cork wool and polystyrene), concrete blocks, slate (natural and synthetic), plywood board. Further tests in the same format will include other building materials including bricks, stone, asphalt and foil. As a VNA was used for the propagation measurements, it was possible to easily measure the effect of the material under test alone, by doing a two-port one-port calibration. To do this both transmit and receive antennas stand in the position, which is selected for the "normal" measurements, with only the materials under test removed from the configuration. The results for S21 and S12 were stored in the VNA, as hardware data. This hardware data was later used to remove the effect of the cables, antennas, etc, in a manner similar to a standard VNA calibration. The S21 and S12 were then measured with the material under test in place. Each of the materials was tested for RF propagation as follows. The antenna were placed at a separation defined by the Tripod Station, with each material held in the test frame, which was placed just in front of the receive antenna.



Results

Concrete Blocks, slate, insulation losses

The figures below are several results for concrete blocks, natural and synthetic slate and full insulation. The distance, in this case, between the two antennas is 4m, or the frequency range is from 900MHz to 925MHz, in order to comply with the big hall requirement. All measurements are presented relative to free space and compensating phase and attenuation reported changes due to the MUT.

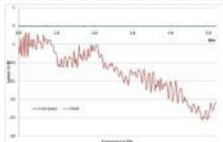


FIGURE 5:

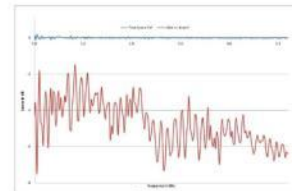


FIGURE 6:

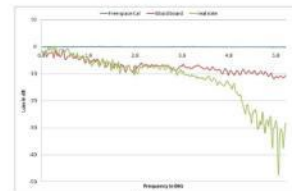


FIGURE 7:

For the four types of insulation test, due to the site requirement, the distance was reduced to 1.5m, which the frequency range is limited down to 1-2GHz.

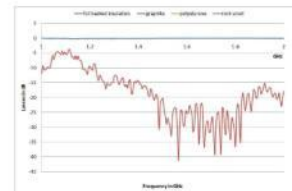


FIGURE 8:

Phase Measurements

The VNA phase data can be used to either calculate the time delay or the dielectric response of the MUT. This is of interest for some future work in use of light and (especially) in dielectric analysis.

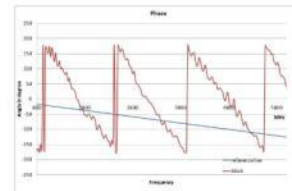


FIGURE 9:

Analysis

In terms of the measurement results and typical building construction, where full backed insulation is used, window propagation is severely attenuated. Full backed insulation can be used in wall cavity as well as floor/roof, in which case signal propagation is severely reduced (eg. 15 to 30dB) in a cavity wall with concrete block on inner and outer leaf. The roof can offer some hope, in particular where insulation is not full backed. Here the use of synthetic slate, wood and one of the other insulation types would reduce propagation to an extent as will over the range of measurements, while still maintaining the building and energy efficiency requirements. However, energy efficient materials are and will be widely used in modern building techniques. A solution to the problem may lie in access through the roof area, if composite materials are used in the building (slate and an full-backed insulation). More likely is that an external antenna will be required to bring signals from the outside (or vice versa). This proved very effective, for example, for television signals (satellite or terrestrial).

ACKNOWLEDGMENT

The authors would like to acknowledge support under the TSM Strand 1 for Yaqiang Liu and also from Ryan Railway in the Building Technology Department of WIT for the Tripod Station.

2010 Waterford Institute of Technology Research Day poster

Broadband Wireless Analysis for the Pharmaceutical and Food Sectors

¹Yaqiang Liu, Praveen Munjampally and P.O'Leary

Flexible Wireless and Large Scale Simulation Group
Waterford Institute of Technology, Waterford, Ireland.

[†]E-mail: 20018753@mail.wit.ie, Phone:+353-51-302630, Fax:+353-51-302666

Introduction

This poster describes a novel technique to measure the dielectric properties of sample materials. The properties of a wireless signal can change as it passes through walls and objects. When measured, these changes can be used to analyze the object and material composition. It was developed in WIT to accurately and efficiently measure signals to measure liquids and porous materials, such as flour, sugar, coffee, etc., used in the food processing industry and many pharmaceutical products. The new technique draws on our experience and a test platform developed by our research group, the attenuation of two-dimensional energy efficient plane waves being tested [1]. Sample results will also be presented for some solid materials, including plastics, composite materials, concrete, polystyrene and acrylic glass and test materials [2].

Measurement Method

Measurement Set-up

The tests were initially performed in a big hall (approximately 6m x 3m x 3m) (Figure 1). The propagation properties are measured as in the far field. For the Schwarzschild from antenna (SMA) with 10dB isolation. This far distance for full separation at the maximum test frequency of 9GHz, is 4.1m [3]. The antenna was mounted on a modified Pictus Precision Total Station (Figure 2), which provided accurate distance and angle measurements.



FIGURE 1
Large hall test configuration, without wooden frame



FIGURE 2
Antenna Mounting. Modified Precision Precision Total Station. 0.20X

Materials to be tested were held in a wooden frame, used between the transmit and receive antennas. The receive antenna is also shielded from a 20 dB near-field plane between the transmit and receive antennas to reduce the ground reflected wave, as shown in Figure 3. A custom built wooden frame (2.1m x 1.0m connected) with control when was mounted to support and align the material under test (MUT), as shown in Figure 4.

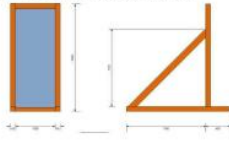


FIGURE 3
Custom-built wooden frame. Cross-section 2.1m x 1.0m

Measurement Procedure

As a VNA was used for the propagation measurements, it was possible to easily consider the effect of the material under test alone. To do this, two transmit and receive antennas placed in the position, which is selected for the "normal" measurement, with only the material under test standing from the configuration. Both antennas and plane change results for S_{11} , S_{21} , S_{12} , and S_{22} were stored in the VNA, as baseline data. This baseline data was later used to correct the effect of the cables, antennas, etc. in a custom routine for a standard VNA calibration. The S11 and S22 were then measured with the material under test in place. Each of the materials was tested by RF propagation as follows. The antenna was placed at a separation defined by the Total Station, with each material held in the test frame, which was fixed in place at the receive antenna.

New Structure Definition

A new structure is introduced for the far and field measurement. As in Figure 4, to replace the material under test to the new task structure, we are able to store profile, height and other information at a distance thickness. The task component is assembled by four parts, from top to bottom are: top wood frame, support frame, glass pane and bottom wood frame.

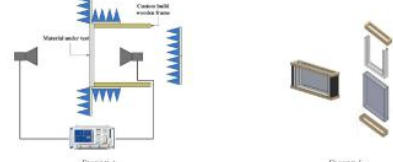


FIGURE 4
Measurement set-up plan view, receiving antenna is shielded by RF absorption frame

FIGURE 5
Task component structure for powder and liquid test

Results

Concrete Blocks, slate, insulation losses

The figures below are several examples for concrete blocks, natural insulation and dry insulation. The distance is the same, between the two antennas is 7m, as the frequency range is from 800MHz to 9GHz, in order to comply with the far field requirements. All measurements are presented relative to free space and consequently phase and attenuation responses change due to the MUT.

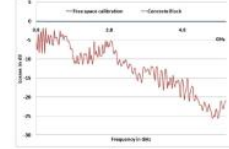


FIGURE 6
10mm concrete blocks S_{11} results at the separation, frequency range 800MHz to 9GHz

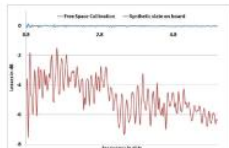


FIGURE 7
Synthetic Slate (1m x 1m) on free plywood board S_{11} Results at 7m separation.

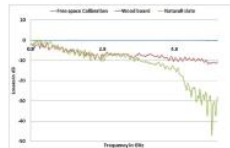


FIGURE 8
Natural Slate (1m x 1m) on 10mm plywood board S_{11} Results at 7m separation.

For the first type of insulation test, the test site equipment, the distance was reduced to 4.0m, which the frequency range is limited due to 1 - 3 GHz.

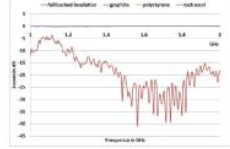


FIGURE 9
Polystyrene (1m x 1m) on 10mm plywood board S_{11} Results at 7m separation.

Phase Measurements

The VNA phase data can be used to either calculate the time delay or the dielectric response of the MUT. This is of interest for many future work in terms of high and frequency in dielectric analysis.

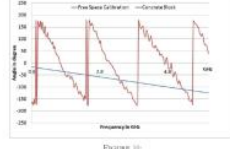


FIGURE 10
Phase results for Polystyrene (1m x 1m) on 10mm plywood board.

Dielectric Analysis and Calculation

Background

There are three main techniques to obtain the complex dielectric properties (permittivity ϵ and permeability μ) of the dielectric materials at applied frequencies [5].

- Debye Relaxation (DR)
- Natural resonant of materials technique (NMT)
- Two area dielectric technique (2AD)

The DR method is used to resolve the complex dielectric properties from the parameters, S_{11} (the reflection S_{11} transmission). It generally uses two functions, which are required to the theoretical calculation of ϵ' and ϵ'' , with the two unknown quantities of permeability and permittivity. The reflection and transmission coefficients are related through several parameters. Some of them are propagation constants, wavelength and group delay of the wave with respect to a dielectric material. There are two methods to calculate the complex dielectric properties with the DR method, one is to convert an initial value for the permeability and permittivity of the material and the other one is to search for the group delay. The group delay of a propagating wave can be defined as the wavelength of the particular wave, but is dependent on the sample length of the dielectric material and its permeability. By taking the small loss from a standard glass, S_{11} and S_{21} measurement, a phase calibration is applied before. The results are also from VNA. All data are obtained after a VNA two-point calibration.

Phase calculation

Calculations of permittivity and permeability from the parameters obtained from a normal active plane wave (NAP) test using VNA:

$$S_{11} = 0.129 + j0.029, S_{21} = 0.022 - j0.256 \quad (1)$$

Measurement central frequency

$$f = 3.072 \text{ GHz} \quad (2)$$

With the sample thickness,

$$L = 0.4 \text{ m}, \lambda_0 = 0.295 \text{ m}, \lambda = 0.055 \text{ m} \quad (3)$$

λ_0 is free space wavelength

λ is the ref. of wavelength, which are both related to the transmission and reflection coefficients.

1. The reflection coefficient calculated with the equation:

$$\Gamma = \frac{S_{11} + S_{21} \sqrt{\epsilon_r \mu_r}}{1 - S_{11} \sqrt{\epsilon_r \mu_r}} = 0.201 - j0.116 \quad (4)$$

2. Transmission coefficient

$$T = \frac{S_{21} \sqrt{\epsilon_r \mu_r}}{1 - S_{11} \sqrt{\epsilon_r \mu_r}} = 0.560 - j0.242 \quad (5)$$

3. Permittivity

$$\epsilon_r = \frac{4}{\pi^2} \frac{1}{L^2} \left(\frac{1}{|T|^2} - \frac{1}{|S_{21}|^2} \right) = 1.094 - j2.016 \quad (6)$$

4. Permeability

$$\mu_r = \frac{1 + \Gamma}{1 - \Gamma} \frac{1}{\epsilon_r} = 0.023 + j0.011 \quad (7)$$

Industrial Application



FIGURE 11
Application on food sector and pharmaceutical industry

- In food sector, this technique will improve the ability to produce new or best food product efficiently using a microwave oven and to analyze any additional food additives that may enhance the microwave heating of the food product.
- Other future work is to analyze the homogeneity of drug powder blends prior to the tablet compression phase, which will be a improvement on existing techniques [6].

Acknowledgment

The authors would like to acknowledge support under the TSB Street 1 for Yaqiang Liu and also from Praveen Balaram in the Building Technology Department of Waterford Institute of Technology for the Total Station.

References

[1] D. Sloboda, Yaqiang Liu, B. Doolin, and P.O'Leary. RF propagation through transparent conductors in energy efficient windows. *IEEE European Wireless Conference*, April 2010.
 [2] Yaqiang Liu, Praveen Munjampally, and P.O'Leary. Broadband wireless propagation through various building materials. *Wireless and an Emerging Technology*, April 2010.
 [3] W. C. Chew. The time-domain signal attenuation in concrete slab materials. *IEEE Construction Automotive Program Report*, 3, October 1987.
 [4] R. Sencel. The In-Field How to be successful? *Applied Microwave & Wireless*, 10(4).
 [5] R. Balas & Schwarz. Measurement of dielectric material properties. July 2010.

2011 Waterford Institute of Technology Research Day poster

A Novel Dielectric Measurement Technique for Material of Unknown Electrical Length

Yaqiang Liu, and P.O'Leary

Flexible Wireless and Large Scale Simulation Group
Waterford Institute of Technology, Waterford, Ireland.

E-mail: 20018753@mail.wit.ie, Phone: +353-51-302630, Fax: +353-51-302666

Introduction

The paper describes a novel non-destructive method (NNT) technique to measure the dielectric properties of sample materials. Unlike methods using TDT techniques using a probing electromagnetic wave, which is both reflected and propagated through the material under test (MUT), the NNT can be used on insulating materials whose electrical properties have a direct impact that contributes to an applied electric field, thereby identifying the insulating material as a dielectric.

Dielectrics are not a uniform class of material, but the broad spectrum of materials considered from the standpoint of their interaction with electric, magnetic, or electromagnetic fields. Thus we are concerned not just with the storage of electric and magnetic energy as well as its dissipation [1].

A new technique has been developed by IIT to accurately and efficiently measure unknown materials with dielectrics. From space non-destructive testing of material dielectric properties overcomes a difficult challenge when the electrical length of the material is unknown. Conventional techniques are based on estimation of the electrical length and then a iterative process to refine the estimate. This work presents an alternative to the conventional technique, by taking measurements over two (or more) material thicknesses. This technique is a solution for the material manufacturer and liberates the material dielectric response. The proposed technique should work well for dielectric products, batch and even and require a modification to the existing dielectric measurement structure to permit thickness variation of the material under test.

Background Review

The main objective dielectric properties are usually defined as a vector derived from the VNA. The VNA contains an internal antenna in the form of a resonant structure to convert a transmission line dielectric properties have been proposed. The Schwan, Han [2] Wang [3] [4] [5] [6] [7] [8] [9] [10] [11] [12] [13] [14] [15] [16] [17] [18] [19] [20] [21] [22] [23] [24] [25] [26] [27] [28] [29] [30] [31] [32] [33] [34] [35] [36] [37] [38] [39] [40] [41] [42] [43] [44] [45] [46] [47] [48] [49] [50] [51] [52] [53] [54] [55] [56] [57] [58] [59] [60] [61] [62] [63] [64] [65] [66] [67] [68] [69] [70] [71] [72] [73] [74] [75] [76] [77] [78] [79] [80] [81] [82] [83] [84] [85] [86] [87] [88] [89] [90] [91] [92] [93] [94] [95] [96] [97] [98] [99] [100] [101] [102] [103] [104] [105] [106] [107] [108] [109] [110] [111] [112] [113] [114] [115] [116] [117] [118] [119] [120] [121] [122] [123] [124] [125] [126] [127] [128] [129] [130] [131] [132] [133] [134] [135] [136] [137] [138] [139] [140] [141] [142] [143] [144] [145] [146] [147] [148] [149] [150] [151] [152] [153] [154] [155] [156] [157] [158] [159] [160] [161] [162] [163] [164] [165] [166] [167] [168] [169] [170] [171] [172] [173] [174] [175] [176] [177] [178] [179] [180] [181] [182] [183] [184] [185] [186] [187] [188] [189] [190] [191] [192] [193] [194] [195] [196] [197] [198] [199] [200] [201] [202] [203] [204] [205] [206] [207] [208] [209] [210] [211] [212] [213] [214] [215] [216] [217] [218] [219] [220] [221] [222] [223] [224] [225] [226] [227] [228] [229] [230] [231] [232] [233] [234] [235] [236] [237] [238] [239] [240] [241] [242] [243] [244] [245] [246] [247] [248] [249] [250] [251] [252] [253] [254] [255] [256] [257] [258] [259] [260] [261] [262] [263] [264] [265] [266] [267] [268] [269] [270] [271] [272] [273] [274] [275] [276] [277] [278] [279] [280] [281] [282] [283] [284] [285] [286] [287] [288] [289] [290] [291] [292] [293] [294] [295] [296] [297] [298] [299] [300] [301] [302] [303] [304] [305] [306] [307] [308] [309] [310] [311] [312] [313] [314] [315] [316] [317] [318] [319] [320] [321] [322] [323] [324] [325] [326] [327] [328] [329] [330] [331] [332] [333] [334] [335] [336] [337] [338] [339] [340] [341] [342] [343] [344] [345] [346] [347] [348] [349] [350] [351] [352] [353] [354] [355] [356] [357] [358] [359] [360] [361] [362] [363] [364] [365] [366] [367] [368] [369] [370] [371] [372] [373] [374] [375] [376] [377] [378] [379] [380] [381] [382] [383] [384] [385] [386] [387] [388] [389] [390] [391] [392] [393] [394] [395] [396] [397] [398] [399] [400] [401] [402] [403] [404] [405] [406] [407] [408] [409] [410] [411] [412] [413] [414] [415] [416] [417] [418] [419] [420] [421] [422] [423] [424] [425] [426] [427] [428] [429] [430] [431] [432] [433] [434] [435] [436] [437] [438] [439] [440] [441] [442] [443] [444] [445] [446] [447] [448] [449] [450] [451] [452] [453] [454] [455] [456] [457] [458] [459] [460] [461] [462] [463] [464] [465] [466] [467] [468] [469] [470] [471] [472] [473] [474] [475] [476] [477] [478] [479] [480] [481] [482] [483] [484] [485] [486] [487] [488] [489] [490] [491] [492] [493] [494] [495] [496] [497] [498] [499] [500] [501] [502] [503] [504] [505] [506] [507] [508] [509] [510] [511] [512] [513] [514] [515] [516] [517] [518] [519] [520] [521] [522] [523] [524] [525] [526] [527] [528] [529] [530] [531] [532] [533] [534] [535] [536] [537] [538] [539] [540] [541] [542] [543] [544] [545] [546] [547] [548] [549] [550] [551] [552] [553] [554] [555] [556] [557] [558] [559] [560] [561] [562] [563] [564] [565] [566] [567] [568] [569] [570] [571] [572] [573] [574] [575] [576] [577] [578] [579] [580] [581] [582] [583] [584] [585] [586] [587] [588] [589] [590] [591] [592] [593] [594] [595] [596] [597] [598] [599] [600] [601] [602] [603] [604] [605] [606] [607] [608] [609] [610] [611] [612] [613] [614] [615] [616] [617] [618] [619] [620] [621] [622] [623] [624] [625] [626] [627] [628] [629] [630] [631] [632] [633] [634] [635] [636] [637] [638] [639] [640] [641] [642] [643] [644] [645] [646] [647] [648] [649] [650] [651] [652] [653] [654] [655] [656] [657] [658] [659] [660] [661] [662] [663] [664] [665] [666] [667] [668] [669] [670] [671] [672] [673] [674] [675] [676] [677] [678] [679] [680] [681] [682] [683] [684] [685] [686] [687] [688] [689] [690] [691] [692] [693] [694] [695] [696] [697] [698] [699] [700] [701] [702] [703] [704] [705] [706] [707] [708] [709] [710] [711] [712] [713] [714] [715] [716] [717] [718] [719] [720] [721] [722] [723] [724] [725] [726] [727] [728] [729] [730] [731] [732] [733] [734] [735] [736] [737] [738] [739] [740] [741] [742] [743] [744] [745] [746] [747] [748] [749] [750] [751] [752] [753] [754] [755] [756] [757] [758] [759] [760] [761] [762] [763] [764] [765] [766] [767] [768] [769] [770] [771] [772] [773] [774] [775] [776] [777] [778] [779] [780] [781] [782] [783] [784] [785] [786] [787] [788] [789] [790] [791] [792] [793] [794] [795] [796] [797] [798] [799] [800] [801] [802] [803] [804] [805] [806] [807] [808] [809] [810] [811] [812] [813] [814] [815] [816] [817] [818] [819] [820] [821] [822] [823] [824] [825] [826] [827] [828] [829] [830] [831] [832] [833] [834] [835] [836] [837] [838] [839] [840] [841] [842] [843] [844] [845] [846] [847] [848] [849] [850] [851] [852] [853] [854] [855] [856] [857] [858] [859] [860] [861] [862] [863] [864] [865] [866] [867] [868] [869] [870] [871] [872] [873] [874] [875] [876] [877] [878] [879] [880] [881] [882] [883] [884] [885] [886] [887] [888] [889] [890] [891] [892] [893] [894] [895] [896] [897] [898] [899] [900] [901] [902] [903] [904] [905] [906] [907] [908] [909] [910] [911] [912] [913] [914] [915] [916] [917] [918] [919] [920] [921] [922] [923] [924] [925] [926] [927] [928] [929] [930] [931] [932] [933] [934] [935] [936] [937] [938] [939] [940] [941] [942] [943] [944] [945] [946] [947] [948] [949] [950] [951] [952] [953] [954] [955] [956] [957] [958] [959] [960] [961] [962] [963] [964] [965] [966] [967] [968] [969] [970] [971] [972] [973] [974] [975] [976] [977] [978] [979] [980] [981] [982] [983] [984] [985] [986] [987] [988] [989] [990] [991] [992] [993] [994] [995] [996] [997] [998] [999] [1000] [1001] [1002] [1003] [1004] [1005] [1006] [1007] [1008] [1009] [1010] [1011] [1012] [1013] [1014] [1015] [1016] [1017] [1018] [1019] [1020] [1021] [1022] [1023] [1024] [1025] [1026] [1027] [1028] [1029] [1030] [1031] [1032] [1033] [1034] [1035] [1036] [1037] [1038] [1039] [1040] [1041] [1042] [1043] [1044] [1045] [1046] [1047] [1048] [1049] [1050] [1051] [1052] [1053] [1054] [1055] [1056] [1057] [1058] [1059] [1060] [1061] [1062] [1063] [1064] [1065] [1066] [1067] [1068] [1069] [1070] [1071] [1072] [1073] [1074] [1075] [1076] [1077] [1078] [1079] [1080] [1081] [1082] [1083] [1084] [1085] [1086] [1087] [1088] [1089] [1090] [1091] [1092] [1093] [1094] [1095] [1096] [1097] [1098] [1099] [1100] [1101] [1102] [1103] [1104] [1105] [1106] [1107] [1108] [1109] [1110] [1111] [1112] [1113] [1114] [1115] [1116] [1117] [1118] [1119] [1120] [1121] [1122] [1123] [1124] [1125] [1126] [1127] [1128] [1129] [1130] [1131] [1132] [1133] [1134] [1135] [1136] [1137] [1138] [1139] [1140] [1141] [1142] [1143] [1144] [1145] [1146] [1147] [1148] [1149] [1150] [1151] [1152] [1153] [1154] [1155] [1156] [1157] [1158] [1159] [1160] [1161] [1162] [1163] [1164] [1165] [1166] [1167] [1168] [1169] [1170] [1171] [1172] [1173] [1174] [1175] [1176] [1177] [1178] [1179] [1180] [1181] [1182] [1183] [1184] [1185] [1186] [1187] [1188] [1189] [1190] [1191] [1192] [1193] [1194] [1195] [1196] [1197] [1198] [1199] [1200] [1201] [1202] [1203] [1204] [1205] [1206] [1207] [1208] [1209] [1210] [1211] [1212] [1213] [1214] [1215] [1216] [1217] [1218] [1219] [1220] [1221] [1222] [1223] [1224] [1225] [1226] [1227] [1228] [1229] [1230] [1231] [1232] [1233] [1234] [1235] [1236] [1237] [1238] [1239] [1240] [1241] [1242] [1243] [1244] [1245] [1246] [1247] [1248] [1249] [1250] [1251] [1252] [1253] [1254] [1255] [1256] [1257] [1258] [1259] [1260] [1261] [1262] [1263] [1264] [1265] [1266] [1267] [1268] [1269] [1270] [1271] [1272] [1273] [1274] [1275] [1276] [1277] [1278] [1279] [1280] [1281] [1282] [1283] [1284] [1285] [1286] [1287] [1288] [1289] [1290] [1291] [1292] [1293] [1294] [1295] [1296] [1297] [1298] [1299] [1300] [1301] [1302] [1303] [1304] [1305] [1306] [1307] [1308] [1309] [1310] [1311] [1312] [1313] [1314] [1315] [1316] [1317] [1318] [1319] [1320] [1321] [1322] [1323] [1324] [1325] [1326] [1327] [1328] [1329] [1330] [1331] [1332] [1333] [1334] [1335] [1336] [1337] [1338] [1339] [1340] [1341] [1342] [1343] [1344] [1345] [1346] [1347] [1348] [1349] [1350] [1351] [1352] [1353] [1354] [1355] [1356] [1357] [1358] [1359] [1360] [1361] [1362] [1363] [1364] [1365] [1366] [1367] [1368] [1369] [1370] [1371] [1372] [1373] [1374] [1375] [1376] [1377] [1378] [1379] [1380] [1381] [1382] [1383] [1384] [1385] [1386] [1387] [1388] [1389] [1390] [1391] [1392] [1393] [1394] [1395] [1396] [1397] [1398] [1399] [1400] [1401] [1402] [1403] [1404] [1405] [1406] [1407] [1408] [1409] [1410] [1411] [1412] [1413] [1414] [1415] [1416] [1417] [1418] [1419] [1420] [1421] [1422] [1423] [1424] [1425] [1426] [1427] [1428] [1429] [1430] [1431] [1432] [1433] [1434] [1435] [1436] [1437] [1438] [1439] [1440] [1441] [1442] [1443] [1444] [1445] [1446] [1447] [1448] [1449] [1450] [1451] [1452] [1453] [1454] [1455] [1456] [1457] [1458] [1459] [1460] [1461] [1462] [1463] [1464] [1465] [1466] [1467] [1468] [1469] [1470] [1471] [1472] [1473] [1474] [1475] [1476] [1477] [1478] [1479] [1480] [1481] [1482] [1483] [1484] [1485] [1486] [1487] [1488] [1489] [1490] [1491] [1492] [1493] [1494] [1495] [1496] [1497] [1498] [1499] [1500] [1501] [1502] [1503] [1504] [1505] [1506] [1507] [1508] [1509] [1510] [1511] [1512] [1513] [1514] [1515] [1516] [1517] [1518] [1519] [1520] [1521] [1522] [1523] [1524] [1525] [1526] [1527] [1528] [1529] [1530] [1531] [1532] [1533] [1534] [1535] [1536] [1537] [1538] [1539] [1540] [1541] [1542] [1543] [1544] [1545] [1546] [1547] [1548] [1549] [1550] [1551] [1552] [1553] [1554] [1555] [1556] [1557] [1558] [1559] [1560] [1561] [1562] [1563] [1564] [1565] [1566] [1567] [1568] [1569] [1570] [1571] [1572] [1573] [1574] [1575] [1576] [1577] [1578] [1579] [1580] [1581] [1582] [1583] [1584] [1585] [1586] [1587] [1588] [1589] [1590] [1591] [1592] [1593] [1594] [1595] [1596] [1597] [1598] [1599] [1600] [1601] [1602] [1603] [1604] [1605] [1606] [1607] [1608] [1609] [1610] [1611] [1612] [1613] [1614] [1615] [1616] [1617] [1618] [1619] [1620] [1621] [1622] [1623] [1624] [1625] [1626] [1627] [1628] [1629] [1630] [1631] [1632] [1633] [1634] [1635] [1636] [1637] [1638] [1639] [1640] [1641] [1642] [1643] [1644] [1645] [1646] [1647] [1648] [1649] [1650] [1651] [1652] [1653] [1654] [1655] [1656] [1657] [1658] [1659] [1660] [1661] [1662] [1663] [1664] [1665] [1666] [1667] [1668] [1669] [1670] [1671] [1672] [1673] [1674] [1675] [1676] [1677] [1678] [1679] [1680] [1681] [1682] [1683] [1684] [1685] [1686] [1687] [1688] [1689] [1690] [1691] [1692] [1693] [1694] [1695] [1696] [1697] [1698] [1699] [1700] [1701] [1702] [1703] [1704] [1705] [1706] [1707] [1708] [1709] [1710] [1711] [1712] [1713] [1714] [1715] [1716] [1717] [1718] [1719] [1720] [1721] [1722] [1723] [1724] [1725] [1726] [1727] [1728] [1729] [1730] [1731] [1732] [1733] [1734] [1735] [1736] [1737] [1738] [1739] [1740] [1741] [1742] [1743] [1744] [1745] [1746] [1747] [1748] [1749] [1750] [1751] [1752] [1753] [1754] [1755] [1756] [1757] [1758] [1759] [1760] [1761] [1762] [1763] [1764] [1765] [1766] [1767] [1768] [1769] [1770] [1771] [1772] [1773] [1774] [1775] [1776] [1777] [1778] [1779] [1780] [1781] [1782] [1783] [1784] [1785] [1786] [1787] [1788] [1789] [1790] [1791] [1792] [1793] [1794] [1795] [1796] [1797] [1798] [1799] [1800] [1801] [1802] [1803] [1804] [1805] [1806] [1807] [1808] [1809] [1810] [1811] [1812] [1813] [1814] [1815] [1816] [1817] [1818] [1819] [1820] [1821] [1822] [1823] [1824] [1825] [1826] [1827] [1828] [1829] [1830] [1831] [1832] [1833] [1834] [1835] [1836] [1837] [1838] [1839] [1840] [1841] [1842] [1843] [1844] [1845] [1846] [1847] [1848] [1849] [1850] [1851] [1852] [1853] [1854] [1855] [1856] [1857] [1858] [1859] [1860] [1861] [1862] [1863] [1864] [1865] [1866] [1867] [1868] [1869] [1870] [1871] [1872] [1873] [1874] [1875] [1876] [1877] [1878] [1879] [1880] [1881] [1882] [1883] [1884] [1885] [1886] [1887] [1888] [1889] [1890] [1891] [1892] [1893] [1894] [1895] [1896] [1897] [1898] [1899] [1900] [1901] [1902] [1903] [1904] [1905] [1906] [1907] [1908] [1909] [1910] [1911] [1912] [1913] [1914] [1915] [1916] [1917] [1918] [1919] [1920] [1921] [1922] [1923] [1924] [1925] [1926] [1927] [1928] [1929] [1930] [1931] [1932] [1933] [1934] [1935] [1936] [1937] [1938] [1939] [1940] [1941] [1942] [1943] [1944] [1945] [1946] [1947] [1948] [1949] [1950] [1951] [1952] [1953] [1954] [1955] [1956] [1957] [1958] [1959] [1960] [1961] [1962] [1963] [1964] [1965] [1966] [1967] [1968] [1969] [1970] [1971] [1972] [1973] [1974] [1975] [1976] [1977] [1978] [1979] [1980] [1981] [1982] [1983] [1984] [1985] [1986] [1987] [1988] [1989] [1990] [1991] [1992] [1993] [1994] [1995] [1996] [1997] [1998] [1999] [2000] [2001] [2002] [2003] [2004] [2005] [2006] [2007] [2008] [2009] [2010] [2011] [2012] [2013] [2014] [2015] [2016] [2017] [2018] [2019] [2020] [2021] [2022] [2023] [2024] [2025] [2026] [2027] [2028] [2029] [2030] [2031] [2032] [2033] [2034] [2035] [2036] [2037] [2038] [2039] [2040] [2041] [2042] [2043] [2044] [2045] [2046] [2047] [2048] [2049] [2050] [2051] [2052] [2053] [2054] [2055] [2056] [2057] [2058] [2059] [2060] [2061] [2062] [2063] [2064] [2065] [2066] [2067] [2068] [2069] [2070] [2071] [2072] [2073] [2074] [2075] [2076] [2077] [2078] [2079] [2080] [2081] [2082] [2083] [2084] [2085] [2086] [2087] [2088] [2089] [2090] [2091] [2092] [2093] [2094] [2095] [2096] [2097] [2098] [2099] [2100] [2101] [2102] [2103] [2104] [2105] [2106] [2

IEEE International workshop on Electromagnetics: Applications and Student Innovation Competition, Taipei, Taiwan, 2011

Design of Flexible Platform for Various Free-Space, Broadband Dielectric Analysis Measurement Techniques



†Yaqiang Liu and Paul O'Leary

Flexible Wireless and Large Scale Simulation Group
Waterford Institute of Technology, Waterford, Ireland.

† E-mail: 20018753@mail.wit.ie, Phone:+353-51-302630, Fax:+353-51-302666

Introduction

This poster describes a novel non-destructive testing (NDT) technique to measure the dielectric properties of sample materials. Dielectric analysis has advanced considerably and now includes several frequency and time domain techniques, in free space and also confined space, for individual frequencies and also broadband, for both high and low loss materials. Free space broadband techniques can yield useful results, due to the bulk of material and the ability to test over a large frequency range.

Measurement method

The tests were initially performed in a big hall (approximately 45m x 30m x 8m) (Figure 1). The propagation properties are measured in the far field (for the Schwarzbeck horn antenna BBHA 9120, D=0.33m, so the minimum far field separation, at the maximum test frequency of 6GHz, is 4.35m). In addition, for higher frequency measurement, a second pair of antennas is introduced, which under Standing Wave Ratio qualification tests showed a usable bandwidth, of 7.5 GHz to 15 GHz, taking the usable bandwidth as the region where the SWR2. Now D=0.27m, so the far field distance requirement increases to 11m. The antennas were mounted on a modified Pivax Precision Total Station (Figure 1), which permitted accurate distance and angular measurements.



FIGURE 1: Antenna mounting



FIGURE 2: Test platform

Materials under test (MUTs) are held by a wooden frame, aided between the transmit and receive antennas. The receive antenna is also shielded by absorbent foam, with more foam placed between the transmit and receive antennas to reduce the ground reflected wave, as shown in Figure 1. A custom-built wooden frame (2.1m x 1.1m cross-section) with rounded edges was created to support and align the MUT, as shown in Figure 2. A custom-built glass tank is used for holding non-solid samples (such as powder and liquids), therefore we are able to test powders and liquids at a uniform thickness.

Results and dielectric constant analysis

Glass measurement result

The figures below are preliminary results for the two layer, 4mm standard glass. All measurements are presented relative to free space and consequently phase and attenuation represent changes due to the MUT.

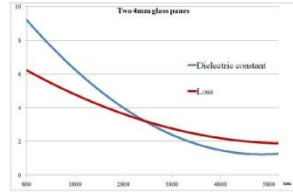


FIGURE 3: Glass dielectric results

The graph for measured and calculated glass dielectric constant matches results published by others, reinforcing confidence in the measurement infrastructure and technique. The measurement is also applied to several non-solid materials, such as salt, sugar and tap water where the sample materials are enclosed in the glass tank. For different dielectric test materials, the electrical length is unknown beforehand, complicating the dielectric constant calculation. This research work proposes a measurement structure to overcome this difficulty, by replicating the first measurement over a slightly thicker sample, where the thickness is flexibly altered in a controlled manner. By measuring the transmission and reflection coefficients of the sample over both thicknesses, we can obtain the electrical length in the sample material, and furthermore, the dielectric constant of this material can be defined.

Dielectric analysis and calculation

The parameter S_{11} and S_{21} of the sample material can be obtained by matrix calculation from the glass tank and the whole test structure measurements. The thickness of glass and its permittivity are both known, the S-parameters of the whole structure can be captured using the VNA. Because of the sandwiched nature of the glass-material under test-glass structure, it is most convenient to change from S-parameter representation to the lesser used ABCD matrix, which allows the effect of the glass, in the transmission path, to be removed.

$$[A] = \begin{bmatrix} A & B \\ C & D \end{bmatrix} \quad (1)$$

For each glass pane in the glass tank, the ABCD matrix can be measured and calculated beforehand. So the ABCD matrix of the sample $[A']$ is then given by

$$[A] = [A'] \cdot [A'] \cdot [A'] \quad (2)$$

$$[A'] = [A]^{-1} \cdot [A] \cdot [A]^{-1} \quad (3)$$

So the S_{11} and S_{21} can be obtained from equation (3)

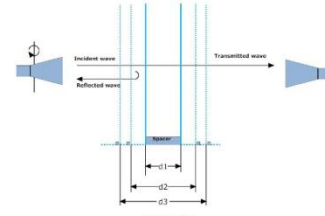


FIGURE 4: New glass tank design, with flexible thickness $d_1, d_2, d_3 \dots$

The complex electric permittivity and the complex magnetic permeability, relative to free space, are defined as

$$\epsilon = \epsilon' + j\epsilon'', \mu = \mu' + j\mu'' \quad (4)$$

By applying boundary conditions at the air-sample interfaces in Figure 7, it can be shown that the S_{11} and S_{21} parameters are related to Γ and T

$$S_{11} = \frac{\Gamma(1 - T^2)}{1 - \Gamma^2 T^2}, S_{21} = \frac{T(1 - \Gamma^2)}{1 - \Gamma^2 T^2} \quad (5)$$

where Γ , and T are the reflection and transmission coefficients of the air-sample interface. The complex propagation constant γ can be written as

$$\gamma = [\log_e(1/T)] / d \quad (6)$$

where d is the thickness of the material. We can also get

$$\epsilon = \frac{\gamma}{20} \frac{1 - \Gamma}{1 + \Gamma}, \mu = \frac{\gamma}{20} \frac{1 + \Gamma}{1 - \Gamma} \quad (7)$$

Since the parameter T is a complex number, there are multiple values for γ . Then γ can be re-written as

$$\gamma = [\log_e(1/T)] / d + j \left[\frac{2\pi n + \phi}{d} \right] \quad (8)$$

where $n=0, \pm 1, \pm 2, \dots$. The real part of γ is unique and single valued, but the imaginary part of γ has multiple values. So (8) will be given multiple values.

$$d/\lambda_m = n + \frac{\phi}{2\pi} \quad (9)$$

where λ_m is the wavelength in the material. Equation (9) is key to analysing the MUT. The material width, d , is unlikely to be smaller than the material wavelength, λ_m , even for low values of permittivity, over the range of frequencies tested so far (wavelength in air falls from 37.5cm down to 5cm, with future work using wavelengths in air ranging from 5cm down to 1.5cm). For any material thickness, d , the measured phase change, $n\lambda_m$, and the material wavelength, λ_m , are related by:

$$d_i = n\lambda_m + \phi\lambda_m/2\pi, 0 < \phi < 2\pi \quad (10)$$

The material thickness, d_i , and the phase change, ϕ_i , can be measured, but neither the material wavelength, λ_m , nor the number of wave periods in the material, n , are known. Both are required in the solution of equation (10). The future work proposed will include controlled variation in the thickness d_i , when measuring the dielectric response of powders and liquids. This controlled variation will also allow the experimenter to avoid a situation where the new thickness is an integer multiple of material wavelengths more than the previous thickness. Clearly this will then yield two linear equations, where the thicknesses and phase changes can be measured, leading to an easy solution for the material wavelength, λ_m , and the number of wave periods in the material, n . This technique is novel and overcomes the difficulties of unknown dielectric properties and, therefore, electrical length.

Applications



FIGURE 5:

Applications in drying, manufacturing and ground penetrating radar

- In the food sector, this technique will improve the ability to predict the heating efficiency of a food product in a microwave oven and the likely impact of additional food additives.
- It also can be used in wood drying or glue production (curing).
- To measure the homogeneity of drug powder blends prior to the tablet compression phase.
- To measure oil contamination in underground storage system, such as detection of petrol station oil leakage.

Acknowledgment

The authors would like to acknowledge support from Bryan Hallisey in the Building Technology Department of Waterford Institute of Technology for the Total Station.

1st IET Colloquium on Antennas, Wireless and Electromagnetics, Loughborough, UK, 2013

1st IET Colloquium on Antennas, Wireless and Electromagnetics
29 May 2013, Loughborough University, Loughborough, UK

Broadband wireless access in an energy efficient environment

Yaqiang Liu, Paul O'Leary



The Institution of Engineering and Technology
Professional Home for Life® for Engineers and Technicians

Affiliation



Waterford Institute of Technology
Cork Road, Waterford, Ireland

20018753@mail.wit.ie



The Institution of Engineering and Technology
Professional Home for Life® for Engineers and Technicians

Introduction

Wireless access into and out of buildings is a fundamental requirement of current and future successful handheld device usage. A number of factors, guided by energy efficiency, can negatively influence the successful propagation of such wireless signals through the building envelope.

This work examines commonly used building materials in terms of their attenuation on wireless frequencies from 800-6000MHz and concludes that the external doors are the final remaining wireless openings.





The Institution of Engineering and Technology
Professional Home for Life® for Engineers and Technicians

Content

- Building Materials Under Test
- Test Structure
- Far Field Selection Criteria
- Window Propagation
- Dry Building Material Propagation
- Insulation Material Propagation
- Results & Conclusion



The Institution of Engineering and Technology
Professional Home for Life® for Engineers and Technicians

Building materials under test



- Individual testing of typical building components
 - Wall and roof materials
 - Glass in window opes
 - Insulation
 - rock wool, polyisocyanurate, graphite-impregnated styrofoam

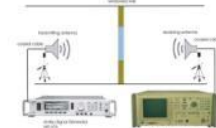


ET The Institution of Engineering and Technology **Professional Home for Life® for Engineers and Technicians**

Test structures & equipment

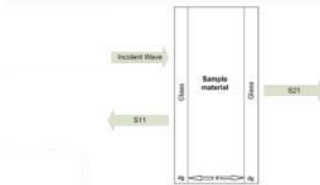


- Rohde & Schwarz ZVB-20 VNA
 - ZV-Z32 calibration kit
 - 7.62m Sucoflex 106 low-loss cables
- Anritsu 68147A signal generator
 - Anritsu MS2702A
 - Backup tests



ET The Institution of Engineering and Technology **Professional Home for Life® for Engineers and Technicians**

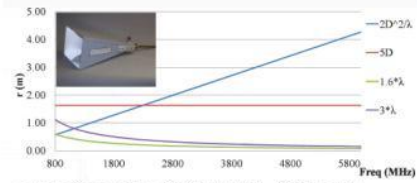
Test block diagram



- Propagated and reflected s-parameters of interest
 - Here MUT is double glazing

ET The Institution of Engineering and Technology **Professional Home for Life® for Engineers and Technicians**

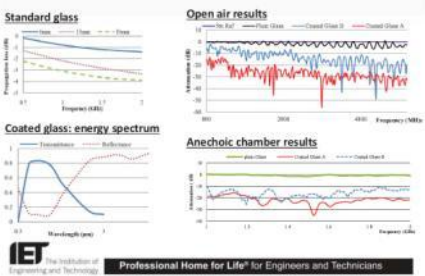
Far field selection criteria



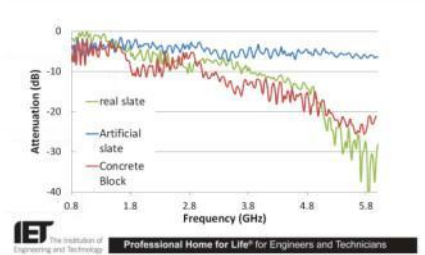
- Selection criteria: $2D^2/\lambda$, $5D$, 1.6λ , 3λ (& more)
 - Schwarzbeck BBHA 9120 LFA Horn Antenna $D=0.33m$

ET The Institution of Engineering and Technology **Professional Home for Life® for Engineers and Technicians**

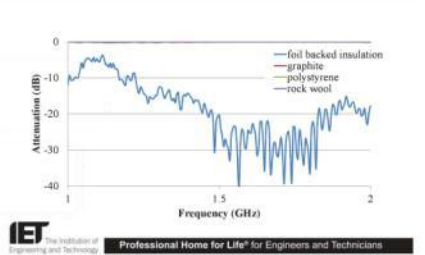
Low energy & std. window propagation



Dry building materials



Heat insulation materials



Results

- Low emissivity glass adds 10-30dB extra attenuation over standard glass
 - Standard wall/roof insulation has a negligible effect on wireless attenuation
 - More recent insulation is foil-backed
 - Adds 10-30dB attenuation depending on frequency
 - Combined with dry concrete block on edge leads to attenuations of 20-50dB
- IEE The Institution of Engineering and Technology Professional Home for Life® for Engineers and Technicians

Conclusions

- Building heat energy efficiency efforts have lead to the introduction of transparent conductors in double/triple glazing
 - Also foil-back insulation in wall cavities and in roof
 - Prevents radioactive loss (gain in hot countries) of heat energy
 - However, also impacts significantly on wireless propagation
 - Front/back doors are the final opes for wireless!



The Institution of
Engineering and Technology

Professional Home for Life® for Engineers and Technicians

Acknowledgements

The authors would like to acknowledge the support of Mr Bryan Hallissey of the WIT Department of Construction & Civil Engineering, for the use of the Total Station for the work described here and also for the directional gain tests on the antennas.



The Institution of
Engineering and Technology

Professional Home for Life® for Engineers and Technicians

References

- [1] D. Stolhofer, Yaqiang Liu and P.O'Leary, "RF Propagation Through Transparent Conductors In Energy Efficient Windows," *16th European Wireless Conference*, Lucca, Italy, April 2010.
- [2] W. C. Stone, "Electromagnetic Signal Attenuation in Construction Materials," in *NIST Construction Automation Program Report No. 3*, October, 1997.
- [3] Claes G. Granqvist, *Transparent conductors as solar energy materials: A panoramic review. Vol.91, pp. 1529-1598, 15 October 2007.*
- [4] N. Knauer, "Investigation of the Physical Effects when Electromagnetic Waves pass through various Window Types", Diploma dissertation, Fachhochschule Hannover, Germany, 2006.



The Institution of
Engineering and Technology

Professional Home for Life® for Engineers and Technicians

Technical Appendix

- The reflection and transmission coefficients are related to the scattering parameters by:

$$S_{11} = \frac{\Gamma(1 - T^2)}{1 - \Gamma^2 T^2} \quad S_{21} = \frac{T(1 - \Gamma^2)}{1 - T^2 \Gamma^2}$$

- The reflection coefficient, Γ , can be obtained by inverting these equations:

$$\Gamma = X \pm \sqrt{X^2 - 1} \quad X = \frac{S_{11}^2 - S_{21}^2 + 1}{2 * S_{21}}$$



The Institution of
Engineering and Technology

Professional Home for Life® for Engineers and Technicians

Technical Appendix (2)

- Similarly, an expression for the transmission coefficient, T , can be obtained:

$$T = \frac{S_{11} + S_{21} - \Gamma}{1 - (S_{11} + S_{21})\Gamma}$$

- The free space wavelength, λ_0 , and the cut off wavelength, λ_c , are related to the transmission and reflection coefficients by the equation:

$$\frac{1}{\Lambda} = \left(\frac{\epsilon_r \mu_r}{\lambda_0^2} - \frac{1}{\lambda_c^2} \right)$$



The Institution of Engineering and Technology
Professional Home for Life® for Engineers and Technicians

Technical Appendix (3)

- So, the permittivity and the permeability can be derived from the above equations :

$$\epsilon_r = \frac{\lambda_0^2}{\mu_r} \left(\frac{1}{\lambda_c^2} - \left[\frac{1}{2\pi L} \ln \left(\frac{1}{T} \right) \right]^2 \right)$$

$$\mu_r = \frac{1 + \Gamma}{\Lambda(1 - \Gamma) \sqrt{\frac{1}{\lambda_0^2} - \frac{1}{\lambda_c^2}}}$$



The Institution of Engineering and Technology
Professional Home for Life® for Engineers and Technicians

System for the Dielectric Evaluation of Powders and Liquids

Youssef El gholb, Yaqiang Liu and Paul O'Leary
Engineering Department, Waterford Institute of Technology, Waterford, Ireland.
Email: yelgholb@wit.ie

Abstract— A free-space broadband measurement technique is proposed to determine the dielectrics properties of powders and liquids. Two techniques are presented based on horizontal and vertical propagation, both of which allow for a series of measurements to be taken where the varying parameter is thickness of material under test (to overcome the challenge of the unknown electrical length). The horizontal propagation measurements required an extra containment layer, which had consequent mechanical and also computational difficulties. The vertical propagation measurements on the other hand show more promise, both in terms of mechanical containment and also in the inversion of the measured S-parameters to arrive at the complex electric permittivity. The measurements were performed in a large hall and also in an anechoic chamber. To minimise measurement errors a free-space Thru-Reflect-Line/Match (TRL/M) calibration technique was performed. The initial results reported here are for various glass thicknesses in the frequency range of 0.8-6 GHz, only although the application to powders and liquids will be apparent.

Index Terms— TRL/M Calibration, Non-Destructive Testing measurement, Vector Network Analyser, Dielectric Materials, Complex Permittivity

I. INTRODUCTION

Wireless signals can be used to obtain a deeper understanding of a material's nature through Non-Destructive Testing (NDT). The change in a signal's parameters because it passed through a Material Under Test (MUT) can be used to identify the material's properties, for example, if the material is to be heated in microwave ovens (such as food, adhesives, wood, plastics, etc.), or if communication signals are expected to pass through the material (for example, walls, windows, etc.).

A dielectric measurement technique has been developed which can be used to measure both solid and non-solid dielectrics. Free space non-destructive testing of material dielectric properties encounters a challenge when the electrical length of the material is unknown. Conventional techniques are based on estimates of the electrical length and then an iterative process to refine the estimate. This work presents an alternative to the conventional techniques, by taking measurements over several material thicknesses. This leads immediately to a solution for the material wavelength and thereafter the material dielectric response. The proposed technique should work well for dielectric powders, liquids and gases and requires a modification to a previously developed dielectric analysis structure [3], to permit thickness variations of the material under test. This is a broadband, free-space technique, which has advantages over alternative more frequency- and sample-limited methods using microwave probes or waveguides.

The propagating microwaves will change due to the presence of the dielectric material and this can be used to extract the material's permittivity (and permeability) values. This calculation starts by measuring the material's S-parameters by using VNA over a wide range of frequencies (here 800 to 6000MHz)

II. MEASUREMENT TECHNIQUE AND FRAMEWORK

Both the horizontal and vertical techniques presented here measure the material at various thicknesses, to overcome the uncertainty relating to electrical length. This is presented in simple form in Figure 1.

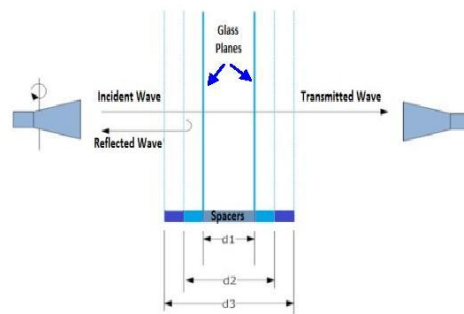


Fig. 1 Antennas mounted on a modified Pentax Precision Total Station

The reduction of errors in the measurement system was effected using the TRL/M method, shown in block diagram form in Figure 2, for free-space and is fairly easily achieved with this test platform.

In this case, TRL/M stands for,

- Thru: Antennas facing each other normally
- Reflect: Metal reflector same size and placed in the same position as the Material Under Test
- Line: Antennas moved by up to $\pm\lambda/4$ longer than Thru, at centre frequency, to avoid a singularity. Ratio of start-stop frequencies is less than 8:1
- Match: Absorbing foam at the same position as the reflector

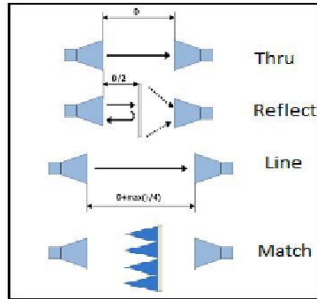


Fig. 2: TRL/M Calibration

A. Horizontal Measurement Method

Free-space broadband dielectric measurement of powders and liquids presents particular problems that originate with powder/liquid containment to present a uniform and homogenous profile to the probing electromagnetic waves. The form the containment takes also impacts the inversion challenge from measured S-parameters to complex permittivity results.

As the originally developed test framework [3] used horizontally propagating waves, this approach was also taken initially when considering the challenge of measuring powders and liquids.

The propagation properties were measured using Schwarzbeck BBHA 9120 horn antennas. The antennas were mounted on a modified Pentax Precision Total Station [7] (Figure 3), which permitted accurate distance and angular measurements. The measurements were performed with a Rohde & Schwarz ZVB-20 Vector Network Analyser (VNA). The Rhode & Schwarz calibration kit ZV-Z32 was used for the cable calibrations. The cables chosen were 7.62m long Sucoflex 106, low-loss cables from Huber and Suhner. A glass tank is developed for non-solid material test, with a variable thickness.

Horizontal measurements however, require a vertically-orientated material and in the case of free-flowing materials such as liquids and powders, this means a container is required, especially as material homogeneity and thickness is required. The challenge is exacerbated here with the need to take measurements at various material thicknesses.

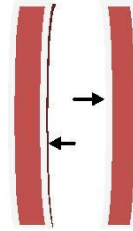


Fig. 3: Antennas mounted on a modified Pentax Precision Total Station



Fig. 4: Horizontal large hall measurements

Requirements of the containment structure include therefore that it should offer flexible, but consistent depth, and offer a wide target to improve accuracy. Ideally the containment walls should therefore be rigid, unyielding under the pressure of the MUT. The depth variability and width requirements implies a large volume of material may be required for the larger thicknesses (up to 200mm is possible with the current set-up, while the width and height are 40cm and 30cm respectively). Various thicknesses of standard glass was used initially for the container walls, even though its permittivity presented an inversion challenge in the dielectric calculations. It offered the advantage, however, of visible examination of material distribution (in the case of powders). It was later replaced with an opaque plastic whose permittivity constant was approximately 1 over the measurement band.



It became obvious early on in the development of the horizontal test structure that the combined rigidity and flexible depth requirements were very difficult to meet. Perfect rigidity was difficult, even with 12mm thick glass. Values lower than this thickness exhibited a lens effect, shown in block diagram form in Figure 5 and in a measurement of table salt in Figure 6. One consequence of this is surprisingly large values of S_{21} values at some frequencies (see Figure 8), even when the lens effect is not so obvious to the human eye.



Fig. 6: Lens effect in salt test (centre of picture)

The requirements to measure materials at several thicknesses (depth flexibility in the container) also presented challenges of misalignment of container walls. These produced apparently anomalous results until deliberate misalignment reconstructions (Figure 7) were measured to confirm this as the source of the anomalies.



Fig. 7: Misalignment reconstruction tests

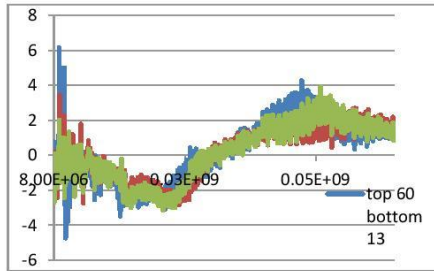


Fig. 8: Typical misalignment measurements

B. Vertical Measurement Method

Although a vertically aligned test infrastructure presents particular structural challenges in particular in stability, normal incidence and alignment, some benefits are immediately apparent compared with the horizontal arrangement. Immediately the containment requirement is simpler and the flexible depth to allow variable MUT thickness is also straightforward. Figure 11 illustrates a proposed structure to implement a vertically aligned measurement in an anechoic chamber. This structure consists of one layer of glass beneath the material instead of two in the horizontal structure, which also allows an easier inversion (no ABCD matrix requirements) in the permittivity calculations. Once fixed in

place, it also permits normal incidence of the waves with more accuracy. It is excellent for high permittivity values (short electrical length, as the MUT can easily be a depth of 5mm or less. It also provides simple and easy measurements of MUT thickness variation (powders) and is particularly easy to test liquids.



Fig. 9: Candidate vertical measurement system

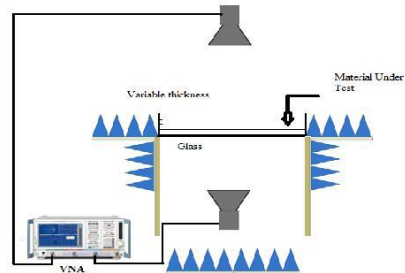


Fig. 10: Block diagram of vertical measurement system

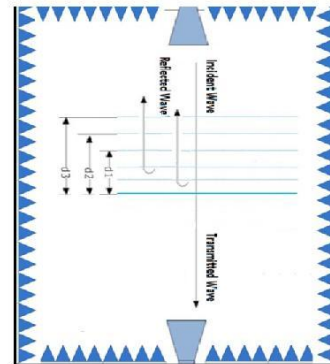


Fig. 11: Vertical anechoic chamber measurements

C. Inversion Algorithm

The calibrated scattering parameters, S_{21} and S_{11} are easily obtained using a VNA. The reflection and transmission coefficients are related to the scattering parameters:

$$S_{11} = \frac{\Gamma(1 - T^2)}{1 - \Gamma^2 T^2} \quad (1)$$

$$S_{21} = \frac{T(1 - \Gamma^2)}{1 - T^2 \Gamma^2} \quad (2)$$

Which can be inverted, so that the reflection coefficient, Γ , is and transmission coefficient, T , can be related to the permittivity, the permeability and the propagation constant by:

$$\varepsilon = \frac{\gamma}{\gamma_0} \left(\frac{1 - \Gamma}{1 + \Gamma} \right) \quad (3)$$

$$\mu = \frac{\gamma}{\gamma_0} \left(\frac{1 + \Gamma}{1 - \Gamma} \right) \quad (4)$$

$$\gamma = [\log_e(1/|T|)]/d + j \left(\frac{2\pi n + \phi}{d} \right) \quad (5)$$

where d is the thickness of material under test and $n=0, 1, 2, \dots$

The real part of the propagation constant is single valued, but the imaginary part may have multiple values. So, imaginary part of is the phase constant

$$\beta = \frac{2\pi}{\lambda_m} \quad (6)$$

$$\frac{d}{\lambda_m} = n + \frac{\phi}{2\pi} \quad (7)$$

- When $n=0$ and $0 < \phi < 2\pi$, d/λ_m is between 0 and 1. If the thickness d is less than λ_m , there will be a unique value for the complex permittivity and permeability.
- When $d > \lambda_m$, one solution is to make the measurements for at least two different thicknesses of the material under tests as first proposed in [4] and explained in more detail below.

Equation (7) is the key to solving for propagation in a MUT. However, solving the imaginary part presents a challenge, unless the material width, d , happens to be smaller than the material wavelength, λ_m . This is difficult to guarantee, even for low values of permittivity, over the range of frequencies tested so far, it is then impossible to guarantee this condition.

For any material thickness, d_i , the measured phase change, ϕ_i , and the material wavelength, λ_m , are related by:

$$d_i = n_i \lambda_m + \frac{\phi_i}{2\pi} \lambda_m, 0 < \phi_i < 2\pi \quad (8)$$

The material thickness, d_i , is known and the phase change, ϕ_i , can be measured, but neither the material wavelength, λ_m , nor the number of wave periods in the material, n_i , are known. Both are required in the solution of (8).

The control of the variation in the thickness d_i when measuring the dielectric response of the material under test

will allow the experimenter to avoid a situation where the new thickness is an integer multiple of material wavelengths more than the previous thickness. Clearly this will then yield two linear equations, where the thicknesses and phase changes can be measured, leading to an easy solution for the material wavelength, λ_m , and the number of wave periods in the material, n_i .

III. RESULTS

This is relatively early in the testing stage of the system, so the first results presented are for solid glass at thicknesses of 4, 6, 8, 12 and 15mm. Glass was chosen due to its availability, previously published data for benchmarking, possible use for containment purposes in the final system, rigidity and ease of material inspection at the early stages of development. Furthermore, the permittivity of glass will be calibrated out in the vertical system, as only a single containment (i.e. not a sandwich) layer is required.

The results presented here were measured using the horizontal system (6mm and 12mm) in a large hall, as well as the vertical system (4mm, 8mm and 15mm) in an anechoic chamber. The results show reasonable agreement with each other and with the published values of permittivity constant for glass (3-15 dielectric constant figures).

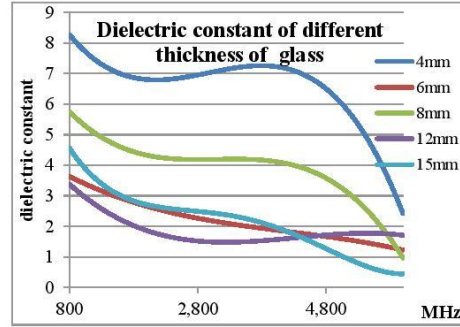


Fig. 12: Different thickness glass measurements

IV. CONCLUSION

This research work presents a new technique of measuring powder and liquid material's permittivity and permeability, using free space, broadband reflection and propagation techniques. Only initial results are at present available, but the technique shows some promise for future measurement.

V. ACKNOWLEDGMENT

The authors would like to acknowledge the support of Bryan Hallissey in the Building Technology Department of Waterford Institute of Technology for their support.

REFERENCES

- [1] R. M. Redheffer, "The measurement of dielectric constant," *Techniques of Microwave Measurements*, vol. 2, pp. 591-657, 1966.
- [2] H. L. Bassett, "A free-space focused microwave system to determine the complex permittivity of materials to temperature exceeding 2000° C," *The Review of Scientific Instruments*, vol. 42, pp. 200-204, 1971.
- [3] Yaqiang Liu, "Different definitions of Antenna far field boundary," Waterford Institute of Technology, Waterford, 2009.
- [4] D.K. Ghodgaonkar, V.V. Varadan and V.K. Varadan, "Free-space measurement of complex permittivity and complex permeability of magnetic materials at microwave frequencies," *IEEE Trans. Instrum. Meas.*, vol. 39, pp. 387-394, April 1990.
- [5] W. C. Stone, "Electromagnetic Signal Attenuation in Construction Materials," in *NIST Construction Automation Program Report No. 3*, October, 1997.
- [6] R. Zoughi, *Microwave Non Destructive Testing and Evaluation*. Dordrecht, The Netherlands: Kluwer, 2000.
- [7] Ltd Pentax Precision Co. Introduction Manual Electronic Total Station R-300 Series [Online]. <http://www.geosolution.com/download/r300x-quick-basic-english.pdf>
- [8] Yaqiang Liu, Paul O'Leary, "Design of Flexible Platform for Various Free-Space, Broadband Dielectric Analysis Measurement Techniques", IEEE International Workshop on Electromagnetic, Taipei, Taiwan, 2011
- [9] Mansor Nakkash, Yi Huang, Waleed Al-Nuaimy, and M.T.C. Fang "An Improved Calibration Technique for Free-Space Measurement of Complex Permittivity." *IEEE Transactions on Geoscience and Remote Sensing*, VOL. 39, NO. 2, February 2001

17th Research Colloquium on Communications and Radio Sciences into the 21st Century, Royal Irish Academy, Ireland, 2014

Development of a vertical method of dielectric measurement for powders and liquids

Youssef El gholb, Yaqiang Liu and Paul O'Leary

Engineering Department, Waterford Institute of Technology, Waterford, Ireland.

Email: yelgholb@wit.ie

Abstract— Two free-space broadband measurement techniques to determine the dielectrics properties of powders and liquids are presented based on horizontal and vertical propagation, both of which allow for a series of measurements to be taken where the varying parameter is thickness of material under test (to overcome the challenge of the unknown electrical length). The horizontal propagation measurements required an extra containment layer, which had consequent mechanical and also computational difficulties. The vertical propagation measurements on the other hand show more promise, both in terms of mechanical containment and also in the inversion of the measured S-parameters to arrive at the complex electric permittivity. The measurements were performed in a large hall and also in an anechoic chamber. To minimise measurement errors a free-space Thru-Reflect-Line/Match (TRL/M) calibration technique was performed.

Index Terms— TRL/M Calibration, Non-Destructive Testing measurement, Vector Network Analyser, Dielectric Materials, Complex Permittivity

I. INTRODUCTION

Wireless signals can be used to obtain a deeper understanding of a material's nature in a topic more commonly known as material characterisation through Non-Destructive Testing (NDT), by using microwave energy.

Material characterization is an important issue in many material production, processing, and management applications in agriculture, food engineering, medical treatments, bioengineering, and the concrete industry [1,2]. In literature, due to the importance of electromagnetic characterization, many techniques were proposed, each with its own constraints and advantages. Cavity resonators [3,4], parallel-plate waveguides [5], free space measurements [6,7], and transmission-line techniques (waveguide, microstrip, coaxial, etc) [8,9], and some techniques that rely on the use of open-ended probes [10,11]. Due to their relative simplicity, higher accuracy and broad frequency coverage, free space techniques been widely utilized for characterization of materials [6].

This work presents a novel free space technique to examine the dielectric response of different materials, especially liquids and powders, over a frequency range of 0.8-6 GHz. The microwave signals will change due to the presence of the dielectric material and this can be used to extract the material's permittivity and permeability values. The calculation is based on measuring the material's S-parameters by VNA. It is possible to also carry out the calibration of the test infrastructure, thereby eliminating its influence from the measurement, followed by the dielectric' measurement. The dielectric measurement technique that has been developed can be used to measure both solid and non-solid dielectrics, although the eventual benefit will be more for non-solid

dielectrics. Free space non-destructive testing of material dielectric properties encounters a challenge when the electrical length of the material is unknown. Conventional techniques are based on estimates of the electrical length and then followed by an iterative process to refine the estimate. This work presents an alternative to the conventional techniques, by taking measurements over several material thicknesses. This leads immediately to a solution for the material wavelength and thereafter the material dielectric response. The proposed technique should work well for dielectric powders, liquids and gases and required an improvement to a previously developed dielectric analysis structure [12], to permit thickness variations of the material under test.

II. MEASUREMENT TECHNIQUE AND FRAMEWORK

Both the horizontal and vertical techniques presented here measure the material at various thicknesses, to overcome the uncertainty relating to electrical length. This is presented in simple form in Figure 1.

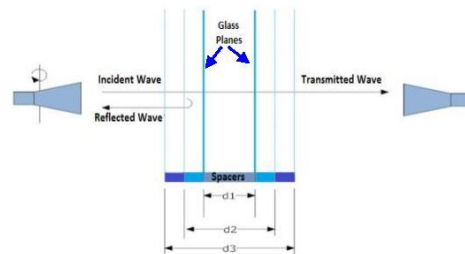


Fig. 1 Antennas mounted on a modified Pentax Precision Total Station

The removal of the structure from the measurement and the reduction of errors in the measurement system was effected using the TRL/M calibration method, shown in block diagram form in Figure 2, for free-space and is fairly easily achieved with this test platform.

In this case, TRL/M stands for,

- Thru: Antennas facing each other normally
- Reflect: Metal reflector same size and placed in the same position as the Material Under Test.
- Line: Antennas moved by up to $\pm\lambda/4$ longer than Thru, at centre frequency, to avoid a singularity. Ratio of start-stop frequencies is less than 8:1
- Match: Absorbing foam at the same position as the reflector

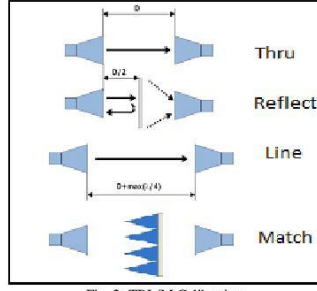


Fig. 2: TRL/M Calibration

A. Inversion Algorithm

The calibrated scattering parameters, S_{21} and S_{11} are easily obtained using a VNA. The reflection and transmission coefficients are related to the scattering parameters:

$$S_{11} = \frac{\Gamma(1 - T^2)}{1 - \Gamma^2 T^2} \quad (1)$$

$$S_{21} = \frac{T(1 - \Gamma^2)}{1 - T^2 \Gamma^2} \quad (2)$$

Which can be inverted, so that the reflection coefficient, Γ , is and transmission coefficient, T , can be related to the permittivity, the permeability and the propagation constant by:

$$\epsilon = \frac{\gamma}{\gamma_0} \left(\frac{1 - \Gamma}{1 + \Gamma} \right) \quad (3)$$

$$\mu = \frac{\gamma}{\gamma_0} \left(\frac{1 + \Gamma}{1 - \Gamma} \right) \quad (4)$$

$$\gamma = [\log_e(1/|T|)]/d + j \left(\frac{2\pi n + \phi}{d} \right) \quad (5)$$

where d is the thickness of material under test and $n=0, 1, 2, \dots$

The real part of the propagation constant is single valued, but the imaginary part may have multiple values. So, the imaginary part is the phase constant

$$\beta = \frac{2\pi}{\lambda_m} \quad (6)$$

$$\frac{d}{\lambda_m} = n + \frac{\phi}{2\pi} \quad (7)$$

- When $n=0$ and $0 < \phi < 2\pi$, d/λ_m is between 0 and 1. If the thickness d is less than λ_m , there will be a unique value for the complex permittivity and permeability.
- When $d > \lambda_m$, one solution is to make the measurements for at least two different thicknesses of the material under tests as first proposed in [6] and explained in more detail below.

Equation (7) is the key to solving for propagation in a MUT. However, solving the imaginary part presents a challenge, unless the material width, d , happens to be smaller than the material wavelength, λ_m . This is difficult to guarantee, even for low values of permittivity, over the range of frequencies tested so far, it is then impossible to guarantee this condition.

For any material thickness, d_i , the measured phase change, ϕ_i , and the material wavelength, λ_m , are related by:

$$d_i = n_i \lambda_m + \frac{\phi_i}{2\pi} \lambda_m, 0 < \phi_i < 2\pi \quad (8)$$

The material thickness, d_i , is known and the phase change, ϕ_i , can be measured, but neither the material wavelength, λ_m , nor the number of wave periods in the material, n_i , are known. Both are required in the solution of (8).

The control of the variation in the thickness d_i , when measuring the dielectric response of the material under test will allow the experimenter to avoid a situation where the new thickness is an integer multiple of material wavelengths more than the previous thickness. Clearly this will then yield two linear equations, where the thicknesses and phase changes can be measured, leading to an easy solution for the material wavelength, λ_m , and the number of wave periods in the material, n_i .

B. Horizontal Measurement Method

Free-space broadband dielectric measurement of powders and liquids presents particular problems that originate with powder/liquid containment to present a uniform and homogenous profile to the probing electromagnetic waves. The form the containment taken also impacts the inversion challenge from measured S-parameters to complex permittivity results.

As the originally developed test framework [12] used horizontally propagating waves, this approach was also taken initially when considering the challenge of measuring powders and liquids, as two containment walls were required.

The propagation properties were measured using Schwarzbeck BBHA 9120 horn antennas. The antennas were mounted on a modified Pentax Precision Total Station [13] (Figure 3), which permitted accurate distance and angular measurements. The measurements were performed with a Rohde & Schwarz ZVB-20 Vector Network Analyser (VNA). The Rhode & Schwarz calibration kit ZV-Z32 was used for the cable calibrations. The cables chosen were 7.62m long Sucoflex 106, low-loss cables from Huber and Suhner. A glass tank, with a variable thickness was developed for non-solid material test using horizontally propagating waves.

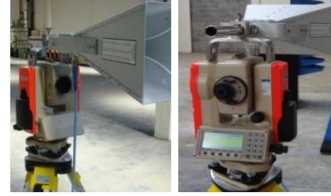


Fig. 3: Antennas mounted on a modified Pentax Precision Total Station

Horizontal measurements however, in the case of free-flowing materials such as liquids and powders, require a vertically-orientated material. This means a container is required, especially as material homogeneity and thickness is required. The challenge is exacerbated here with the need to take measurements at various material thicknesses.



Fig. 4: Container wall's misalignment



Fig. 5: Horizontal large hall measurements

Requirements of the containment structure include therefore that it should offer flexible, but consistent depth, and offer a wide target to improve accuracy. Ideally the containment walls should therefore be rigid, unyielding under the pressure of the MUT. The depth variability and width requirements imply a large volume of material may be required for the larger thicknesses. Various thicknesses of standard glass were used initially for the container walls, even though its permittivity presented an inversion challenge in the dielectric calculations. It offered the advantage, however, of visible examination of material distribution (in the case of powders). It was later replaced with an opaque plastic whose permittivity constant was approximately 1 over the measurement band.



Fig. 6: Lens effect caused by insufficient container rigidity

It became obvious early on in the development of the horizontal test structure that the combined rigidity and flexible depth requirements were very difficult to meet. Perfect rigidity was difficult, even with 12mm thick glass. Values lower than this thickness exhibited a lens effect, shown in block diagram form in Figure 5 and in a measurement of table salt. One consequence of this is surprisingly large values of S_{21} values at some frequencies (see Figure 8), even when the lens effect is not so obvious to the human eye.

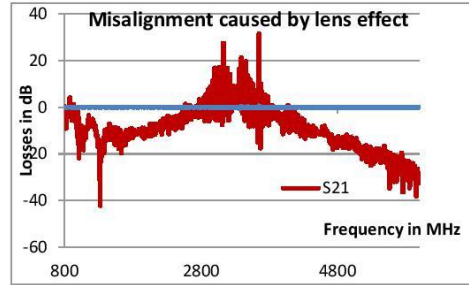


Fig 7: Misalignment of a salt measurement result caused by lens effect

C. Vertical Measurement Method

Although a vertically aligned test infrastructure presents particular structural challenges in particular in stability, normal incidence and alignment, some benefits are immediately apparent compared with the horizontal arrangement. Immediately the containment requirement is simpler and the flexible depth to allow variable MUT thickness is also straightforward. Figures 8-9-10 illustrate a proposed structure to implement a vertically aligned measurement in an anechoic chamber. This structure consists of one layer of glass beneath the material instead of two in the horizontal structure, which also allows an easier inversion (no ABCD matrix requirements) in the permittivity calculations. Once fixed in place, it also permits normal incidence of the waves with more accuracy. It is excellent for high permittivity values (short electrical length, as the MUT can easily be a depth of 5mm or less. It also provides simple and easy measurements of MUT thickness variation (powders) and is particularly easy to test liquids.



Fig. 8: Candidate vertical measurement system

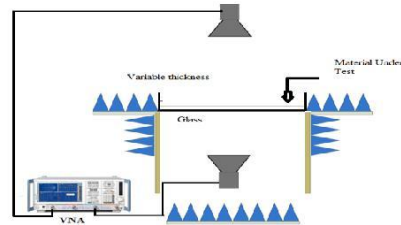


Fig.9: Block diagram of vertical measurement system

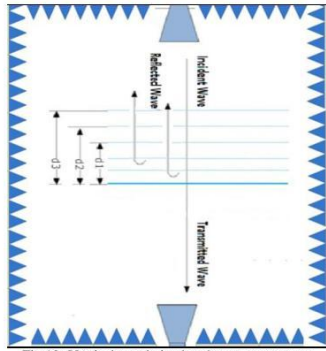


Fig.10: Vertical anechoic chamber measurements

III. CONCLUSION

This research work presents a new technique of measuring powder and liquid material's permittivity and permeability, using free space, broadband reflection and propagation techniques. Early measurements confirm the accuracy, ease-of-use and reliability of this new technique. The technique therefore shows some promise for future measurements.

IV. ACKNOWLEDGMENT

The authors would like to acknowledge the support of Bryan Hallissey in the Building Technology Department of Waterford Institute of Technology for their support.

REFERENCES

- [1] L.F. Chen, C.K. Ong, C.P. Neo, V.V. Varadan, V.K. Varadan, *Microwave Electronics, Measurement and Materials Characterization*, Wiley, West Sussex, England, 2004.
- [2] J. Blitz, *Electrical and Magnetic Methods of Non-destructive Testing*, Chapman & Hall, London, UK, 1997.
- [3] J. Blitz, *Electrical and Magnetic Methods of Non-destructive Testing*, Chapman & Hall, London, UK, 1997.
- [4] B. Kapilevich, B. Litvak, Optimized microwave sensor for online concentration measurements of binary liquid mixtures, *IEEE Sens. J.* 11 (10) (2011) 2611–2616.
- [5] H. Zhang, S.Y. Tan, H.S. Tan, An improved method for microwave non-destructive dielectric measurement of layered media, *Prog. Electromagn. Res. B* 10 (2008) 145–161.
- [6] D.K. Ghodgaonkar, V.V. Varadan and V.K. Varadan, "Free-space measurement of complex permittivity and complex permeability of magnetic materials at microwave frequencies," *IEEE Trans. Instrum. Meas.*, vol. 39, pp. 387–394, April 1990.
- [7] U.C. Hasar, Non-destructive testing of hardened cement specimens at microwave frequencies using a simple free-space method, *NDT&E Int.* 42 (6) (2009) 550–557.
- [8] A.M. Nicolson, G. Ross, Measurement of the intrinsic properties of materials by time-domain techniques, *IEEE Trans. Instrum. Meas.* 19 (4) (1970) 377–382.
- [9] K. Chalapat, K. Sarvala, J. Li, G.S. Paraoanu, Wideband reference-plane invariant method for measuring electromagnetic parameters of materials, *IEEE Trans. Microw. Theory Tech.* 57 (9) (2009) 2257–2267.
- [10] D. Misra, M. Chhabra, B.R. Epstein, M. Mirotznik, K.R. Foster, Noninvasive electrical characterization of materials at microwave frequencies using an open-ended coaxial line: test of an improved calibration technique, *IEEE Trans. Microw. Theory Tech.* 38 (1) (1990) 8–13.
- [11] U.C. Hasar, Permittivity determination of fresh cement-based materials by an open-ended waveguide probe using amplitude-only measurements, *Prog. Elec-tromagn. Res.* 97 (2009) 27–43.

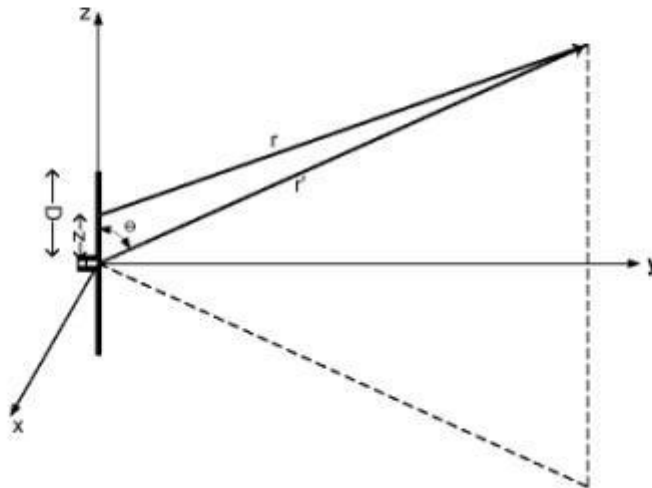
- [12] Yaqiang Liu, Paul O'Leary, "Design of Flexible Platform for Various Free-Space, Broadband Dielectric Analysis Measurement Techniques.", *IEEE International Workshop on Electromagnetic, Taipei, Taiwan, 2011*
- [13] Ltd Pentax Precision Co. *Introduction Manual Electronic Total Station R-300 Series*. [Online]. <http://www.geosolution.com/download/r-300x-quick-basic-english.pdf>

Relevant documents

Different definition of far field boundary

In a modern antenna measurement, there are several different standards on the boundary of far field. According to the most common ones, I will discuss three criteria of an antenna far field range.

The $\frac{2D^2}{\lambda}$ or wave phase criterion



As shown in the figure, we can get

$$r'^2 = r'^2 + z^2 - 2r'z \cos \theta$$

By using binomial expansion, we can write as,

$$r = r' - z \cos \theta + \frac{1}{r'} \left(\frac{z^2}{2} \sin^2 \theta \right) + \frac{1}{r'^2} \left(\frac{z^3}{2} \cos \theta \sin^2 \theta \right) \dots$$

Where in this case, $r' \gg z$, so the higher order for this expression can be neglected.

When $r' \gg z$, r and r' can be defined as parallel lines. Then we can have

$$r \approx r' - z \cos \theta$$

The third term of equation can have its maximum value, when $\theta = \frac{\pi}{2}$,

$$\frac{1}{r'} \left(\frac{z^2}{2} \sin^2 \theta \right) = \frac{z^2}{2r'}, (\theta = \frac{\pi}{2})$$

In this case, when $\theta = \frac{\pi}{2}$ the higher terms of the equation will be ignored. So this value can be approximately introduced as maximum error. In antenna theory, when D (the largest dimension of antenna) is greater than one wavelength ($D > \lambda$). If the maximum phase error is, as is often accepted in published work, to be $\frac{\pi}{8}$, (22.5°), then, applying the equation above,

$$\frac{z^2}{2r'} \leq \frac{\pi}{8}$$

As $-\frac{D}{2} \leq z \leq \frac{D}{2}$, then we can convert to

$$\begin{aligned} r' &\geq \frac{2D^2}{\lambda} \\ r &\gg D \\ r &\gg \lambda \end{aligned}$$

There is another criterion of precision antenna, which is

$$r' \geq \frac{50D^2}{\lambda}$$

In this case, we can calculate the phase error will be 0.9°, which is very small.

The 3λ and 1.6λ or wave impedance criterion

If using wave impedance to determine the boundary of far field, we need to find out when the electromagnetic field become constant.

By taking the example of infinitesimal dipole, the vector potential A is written as,

$$A(x, y, z) = \hat{a}_z \frac{\mu I_0}{4\pi r} e^{-j\beta r} \int_{-D/2}^{+D/2} dz'$$

The expression to find H_ϕ , E_θ is

$$H_\phi = j \frac{\beta I_0 D \sin \theta}{4\pi r} \left[1 + \frac{1}{j\beta r} \right] e^{-j\beta r}$$

$$E_\theta = j\eta \frac{\beta I_0 D \sin \theta}{4\pi r} \left[1 + \frac{1}{j\beta r} - \frac{1}{(\beta r)^2} \right] e^{-j\beta r}$$

Where I_0 is the wire current in amps,

β is the electrical length per meter of wavelength,

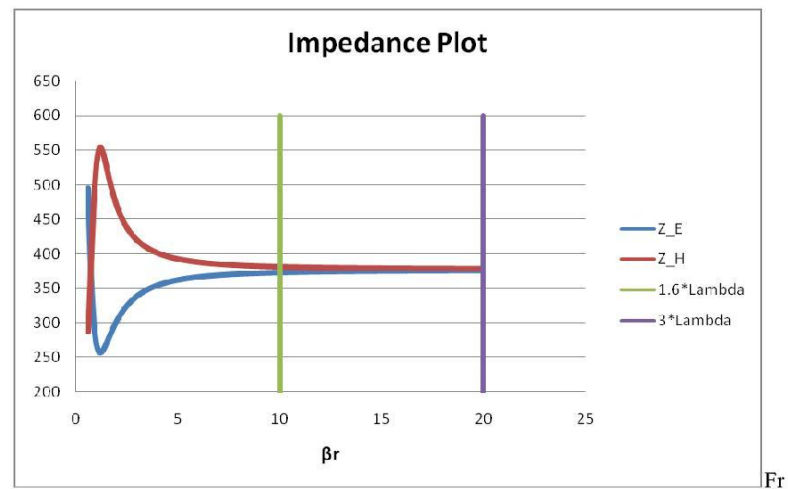
So, we can calculate the following

$$\begin{aligned}
 Z_E &= \frac{|E_\theta|}{|H_\phi|} \\
 &= \frac{\left| j\eta \frac{\beta I_0 D \sin \theta}{4\pi r} \left[1 + \frac{1}{j\beta r} - \frac{1}{(\beta r)^2} \right] e^{-j\beta r} \right|}{\left| j \frac{\beta I_0 D \sin \theta}{4\pi r} \left[1 + \frac{1}{j\beta r} \right] e^{-j\beta r} \right|} \\
 &= \eta \frac{\left[1 + \frac{1}{j\beta r} - \frac{1}{(\beta r)^2} \right]}{\left[1 + \frac{1}{j\beta r} \right]}
 \end{aligned}$$

Similar to Z_E , We can get Z_H .

$$Z_H = \eta \frac{\left[1 + \frac{1}{j\beta r} \right]}{\left[1 + \frac{1}{j\beta r} + \frac{1}{(j\beta r)^2} \right]}$$

We can use Z_E and Z_H to draw the impedance plot.



om the plot, we can tell the impedance of the wave. In this case, βr is a step value. In near field region, $\beta r \ll 1$, so

$$Z_E = \frac{-j\eta}{\beta r}$$

When the distance increasing, the ratio becomes more constant

$$Z_E = \eta = 377\Omega$$

From the graph, we can see both wave impedances are within 1% of the free space impedance from $\beta r \approx 10$, so

$$\begin{aligned}\frac{2\pi}{\lambda}r &\approx 10 \\ r &\approx \frac{5\lambda}{\pi} \\ r &\approx 1.6\lambda\end{aligned}$$

However, for the condition that both wave impedances are within 1% of the free space impedance, this occurs when $\beta r \approx 20$,

$$\begin{aligned}\frac{2\pi}{\lambda}r &= 20 \\ r &= \frac{10\lambda}{\pi} \\ r &\approx 3\lambda\end{aligned}$$

The 5D or wave amplitude criterion

As we have the far field region boundary

$$r = r' - z \cos \theta + \frac{1}{r'} \left(\frac{z^2}{2} \sin^2 \theta \right) + \frac{1}{r'^2} \left(\frac{z^3}{2} \cos \theta \sin^2 \theta \right) \dots$$

The term in this equation decrease when z increases. As we know, the condition is $z \ll r$, the denominator will only affects amplitude. We let

$$r = r'$$

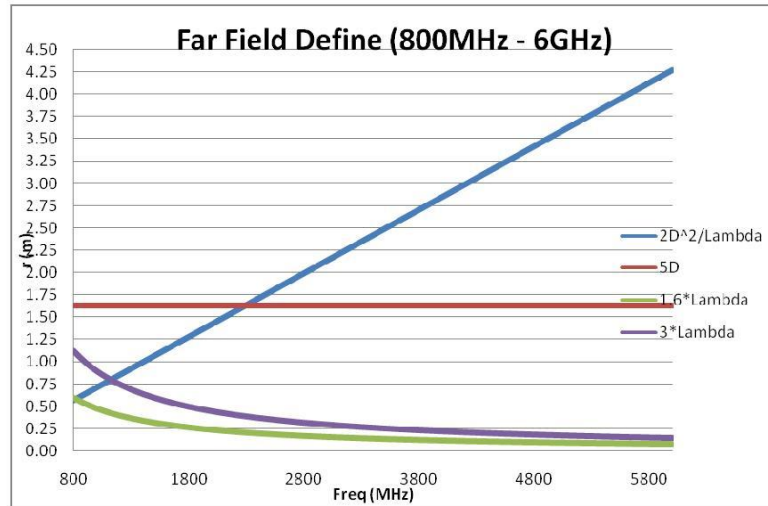
It only happens when the far field is very large compared to the antenna size D . So

$$r \gg D$$

Written as the condition $r \gg D$ (changed to $r > 5D$) and relates to the amplitude approximation ($\pi/16$ relates to the phase approximation). So, we get

$$r > 5D$$

Analysis



The antenna we choose is horn antenna. The dimension is 0.27m x 0.18m. So the largest dimension $D = \sqrt{0.27^2 + 0.18^2} = 0.327$ m.

The curve $\frac{2D^2}{\lambda}$ and $5D$ intersect at point (0.05, 1.1). When $\lambda < 0.05$, it meets $r \gg \lambda$,

$r \gg D$. SO the boundary of far field can be defined as $\frac{2D^2}{\lambda}$.

REFERENCE

1. W. L. Stutzman, G. A. Thiele: *Antenna Theory and Design*, Wiley, Second Edition, New York, 1998, Page25
2. C. Balanis, *Antenna Theory: Analysis and Design*, 2nd ed., Wiley, 1997.

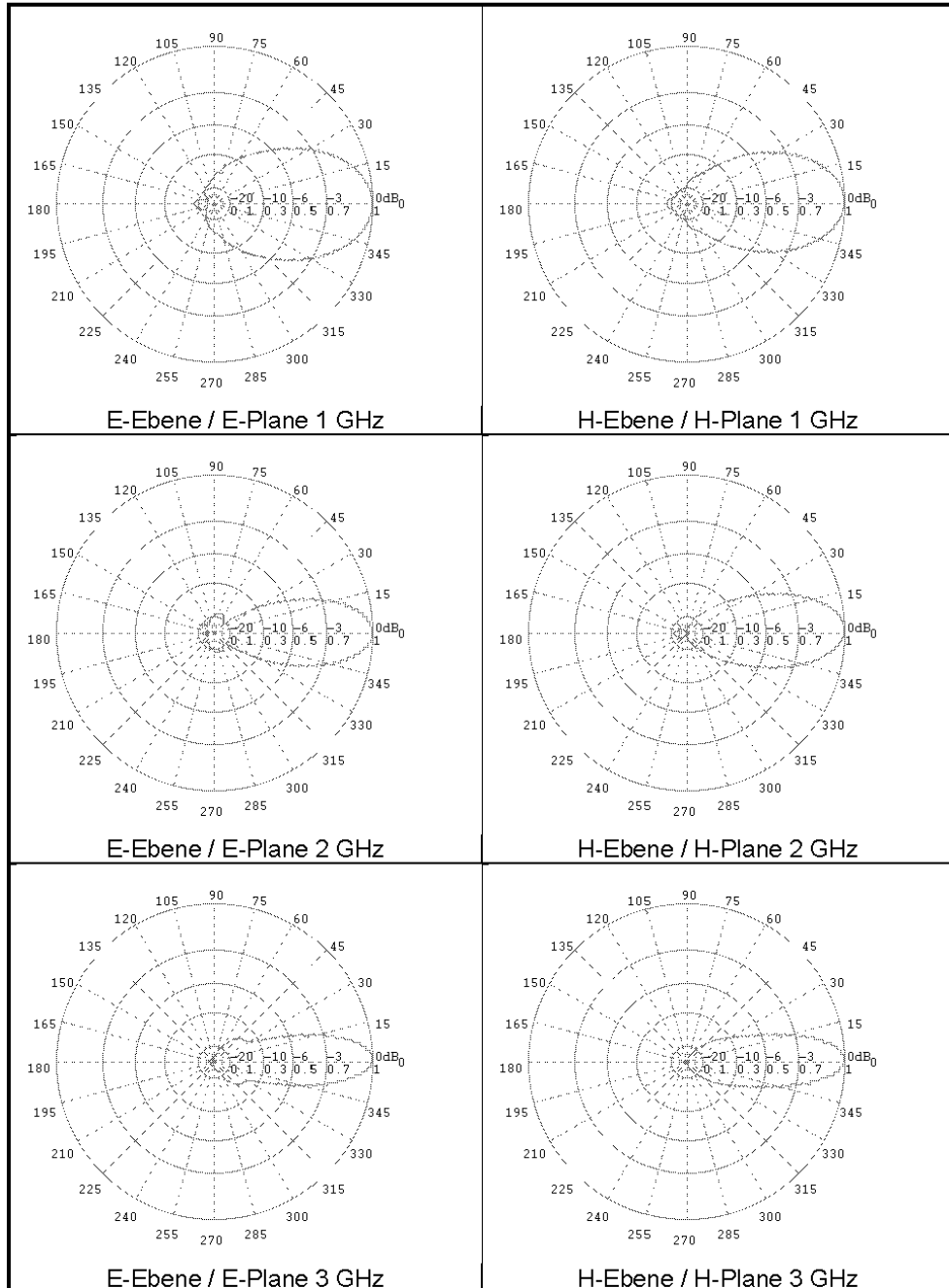
Schwarzbeck horn antenna BBHA 9120 LFA 0.7-6 GHz radiation pattern

SCHWARZBECK MESS - ELEKTRONIK

An der Klinge 29 D-69250 Schönau Tel.: 06228/1001 Fax.: (49)6228/1003

Double Ridged Broadband Horn Antenna

BBHA 9120 LFA 0.7 - 6 GHz

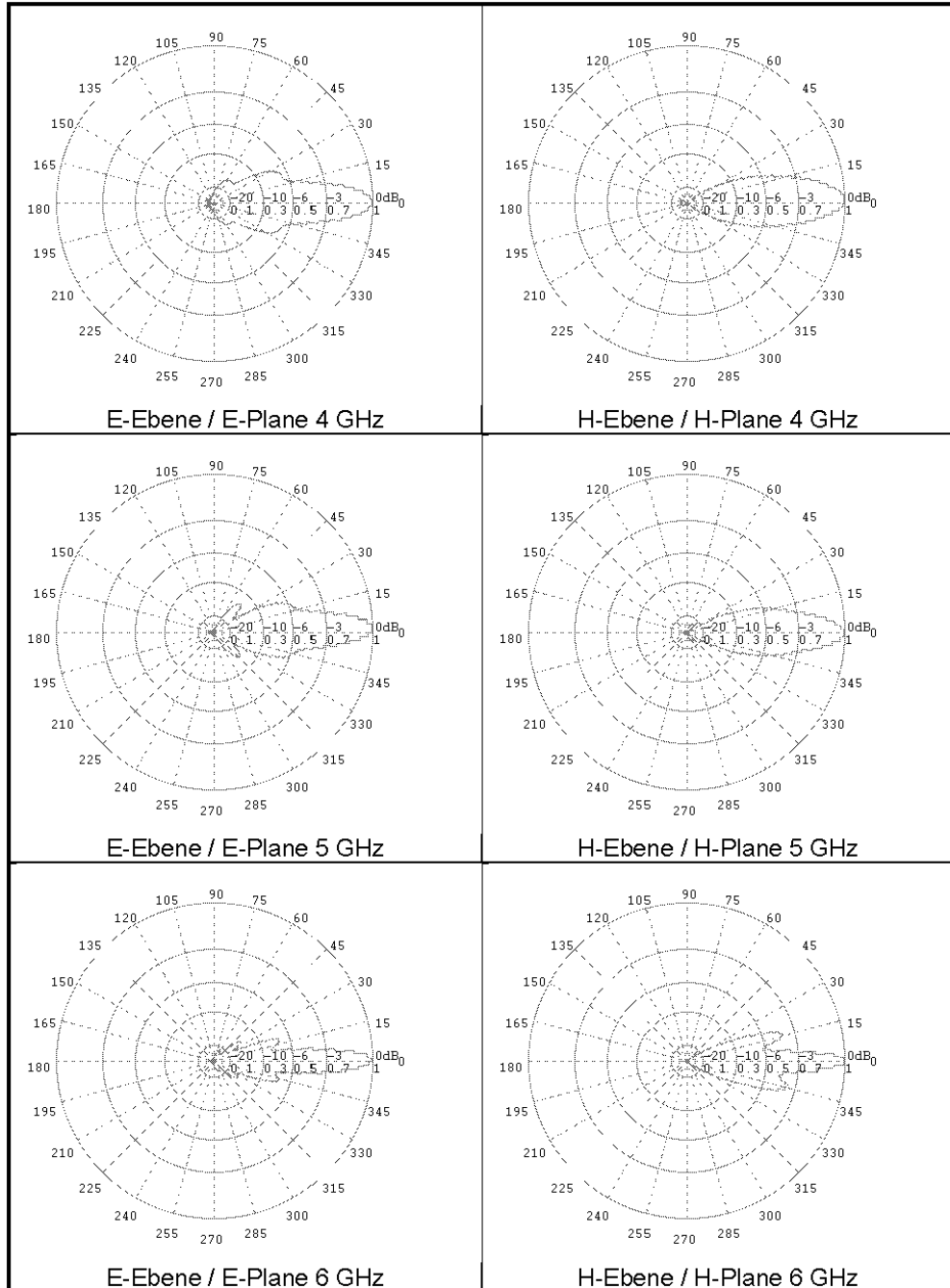


SCHWARZBECK MESS - ELEKTRONIK

An der Klinge 29 D-69250 Schönau Tel.: 06228/1001 Fax.: (49)6228/1003

Double Ridged Broadband Horn Antenna

BBHA 9120 LFA 0.7 - 6 GHz



Bibliography

- [1] A. Von Hippel, Dielectric Materials and Applications, Boston: Artech House, 1995b.
- [2] D. P., Polar Molecules, New York: NY: The Chemical Catalog Company, 1929.
- [3] C. Johnk, Engineering Electromagnetic Fields and Waves, New York: Wiley, 1988.
- [4] W. Voss, "Industrial Microwave Applications," in *4th European Microwave Conference*, Montreux, Switzerland, 1974.
- [5] Hu Zhaohu, Wei Ruixuan, Luo Jixun, Ding Jian, "Research on Kill Efficiency of Double BVR Air-to-Air Missile Fusillade in a Complex Electromagnetic Environment," in *Intelligent Human-Machine Systems and Cybernetics (IHMSC)*, Hangzhou, China, 2013.
- [6] Martínez-Olmos A, Fernández-Salmerón J, Lopez-Ruiz N, Rivadeneyra Torres A, Capitan-Vallvey LF, Palma AJ, "Screen Printed Flexible Radiofrequency Identification Tag for Oxygen Monitoring," *Analytical Chemistry*, 2013.
- [7] Anders Ahlbom, Maria Feychting, Yngve Hamnerius, Lena Hillert, "Radiofrequency electromagnetic fields and risk of disease and ill health - Research during the last ten years," Swedish Council for Working Life and Social Research, Stockholm, 2012.
- [8] W. Bolton, Electrical and Magnetic Properties of Materials, Harlow: Longman Scientific & technical, 1992.
- [9] Millman, Microelectronics, Hill Education (India) Pvt Limited, 2001.

- [10] J. Baker-Jarvis, M. D. Janezic, J. H. Grosvenor, R. D. Geyer, "Transmission/Reflection and short-circuit line methods for measuring permittivity and permeability," *NIST Technical Note 1335-R*, December 1993.
- [11] A. V. Hippel, *Dielectric Materials and Applications*, John Wiley & Sons, 1954.
- [12] G. Bekefi and A.H. Barrett, *Electromagnetic vibrations, Waves, and Radiation*, the MIT press, 1977, pp. 398-449.
- [13] *A Guide to the characterisation of dielectric materials at RF and microwave frequencie*, London: NPL, 2003.
- [14] R. Botsco and R. McMaster, "Nondestructive Testing Handbook," *ASNT*, vol. 4, 1986.
- [15] T. D.C., *Electricity and Magnetism*, Himalaya Publishers, 1988.
- [16] N. Mathis, "Soil moisture determination with TDR: Single-rod probes," A PhD dissertation submitted to the SWISS FEDERAL INSTITUTE OF TECHNOLOGY, 2005.
- [17] "Basics of Measuring the Dielectric Properties of Materials, Application Note," Agilent literature number 5989-2589EN, 2006.
- [18] Baker-Jarvis, J., Vanzura, E.J. and Kissick, W.A., "Improved technique for determining complex permittivity with the transmission/ reflection method," *IEEE Trans. Microw. Theory Tech.*, vol. 38, pp. 1096-1103, 1990.
- [19] C. Balanis, *Antenna Theory analysis and design*, Third ed., New Jersey: John wiley & Sons, 2005.
- [20] L.F. Chen et al., *Microwave electronics Measurement and Materials Characterization*, Chichester: John wiley & Sons, Ltd, 2004.

- [21] Roberts,S. and Von Hippel,A., “A new method for measuring dielectric constant and loss in the range of centimeter waves,” *J. Appl. Phys.*, vol. 7, pp. 610-616, July 1946.
- [22] A. M. N. a. G. F. Ross, “Measurement of intrinsic properties of materials by time domain techniques,” *IEEE Trans. Instrum. Meas.*, Vols. IM-19, p. 377–382, November 1970.
- [23] W. Weir, “Automatic measurement of complex dielectric constant and permeability at microwave frequencies,” *Proc. IEEE*, vol. 62, pp. 33-36, January 1974.
- [24] J. Baker-Jarvis, “Transmission/reflection and short-circuit line permittivity measurements,” *NIST tech. note 1341*, July 1990.
- [25] A.H. Boughriet., C. Legrand and A. Chapoton, “Noniterative stable transmission/reflection method for low-loss material complex permittivity determination,” *IEEE Trans. Microwave Theory Tech.*, vol. (1), no. 45, pp. 52-57, 1997.
- [26] R. M. Redheffer, “The measurement of dielectric constant,” *Techniques of Microwave Measurements*, vol. 2, pp. 591-657, 1966.
- [27] H. L. Bassett, “A free-space focused microwave system to determine the complex permittivity of materials to temperature exceeding 2000° C,” *The Review of Scientific Instruments*, vol. 42, pp. 200-204, 1971.
- [28] D.K Ghodgaonkar, V.V. Vanadan and V.K. Varadan, “A free-space method for measurement of dielectric constants and loss tangents at microwave frequency,” *IEEE Trans. instrum. Mea.*, vol. 38, pp. 789-793, 1989.
- [29] D. M. Pozar, *Microwave Engineering*, New York: John Wiley & Sons, Inc, 2005.
- [30] Rubinger, C. P. L. and Costa, L. C., “Building a resonant cavity for the measurement of microwave dielectric permittivity of high loss materials,” *Microw. Opt. Technol.*

Lett., vol. 49, pp. 1687-1690, 2007.

- [31] Williams T. C., M. A. Stuchly and P. Saville, "Modified transmission-reflection method for measuring constitutive parameters of thin flexible high-loss materials," *IEEE Trans. Microw. Theory Tech.*, vol. 51, pp. 1560-1566, 2003.
- [32] Baker-Jarvis J., M. D. Janezic, J. H. Grosvenor Jr, and R. G. Geyer, "Transmission/reflection and short-circuit line methods for measuring permittivity and permeability," *NIST. Boulder, CO. Tech. Notes*, p. 1335, 1992.
- [33] Decreton M. C. and F. E. Gardiol, "Simple non-destructive method for the measurement of complex permittivity," *IEEE Trans. Instrum. Meas.*, vol. 23, pp. 434-438, 1974.
- [34] Zhang H., S. Y. Tan and H. S. Tan, "An improved method for microwave non destructive dielectric measurement of layered media," *Progress in Electromagnetics Research B*, vol. 10, pp. 145-161, 2008.
- [35] Olmi R., M Tedesco, C. Riminesi, et. al., "Thickness-independent measurement of the permittivity of thin samples in the X band," *Mea. Sci. Technol.*, vol. 13, pp. 503-509, 2002.
- [36] Baker-Jarvis J., M. D. Janezic, P. D. Domich, et. al., "Analysis of an open-ended coaxial probe with lift-off for non destructive testing," *IEEE Trans. Instrum. Meas.*, vol. 43, pp. 711-718, 1994.
- [37] D.K. Ghodgaonkar, V.V. Varadan and V.K. Varadan, "Free-space measurement of complex permittivity and complex permeability of magnetic materials at microwave frequencies," *IEEE Trans. Instrum. Meas.*, vol. 39, pp. 387-394, April 1990.
- [38] G. F. Engen and C. A. Hoer, "Thru-Reflect-Line: An Improved Technique for Calibrating the Dual Six-Port Automatic Network Analyzer," *Microwave Theory and Techniques, IEEE Transactions*, vol. 27, no. 12, pp. 987-993, Dec 1979.

- [39] L. Pentax Precision Co., "Introduction Manual Electronic Total Station R-300 Series," [Online]. Available: <http://www.geosolution.com/download/r300x-quick-basic-english.pdf>. [Accessed 20 Feb 2011].
- [40] Huber+Suhner, 07 Jan 2005. [Online]. Available: <http://www.hubersuhner.com>. [Accessed 01 Feb 2011].
- [41] T. Wendebourg, "Investigation of reflectivity and Attenuation of Microwave-Signals passing through Double Glazed Windows," 2010.
- [42] W. Stutzman, *Antenna theory and design*, New York: Wiley, 1981.
- [43] Y. Liu, "Different definations of Antenna far field boundary," Waterford, 2009.
- [44] R. Bansal, "The Far-Field: How Far is Far Enough?," *Applied Microwave & Wireless*, pp. 58-60, November 1999.
- [45] G. M. Djuknic, "Method of measuring a pattern of electromagnetic radiation". Tenafly, NJ Patent US 6657596 B2, 02 12 2003.
- [46] NIST Construction Automation Program Report No.3, "Electromagnetic Signal Attenuation in Construction Materials," Maryland, 1997.
- [47] UC Hasar, "Two novel amplitude-only methods for complex permittivity determination of medium- and low-loss materials," *Measurement Science and Technology*, vol. 19, 2008.
- [48] Siepel, 02 2008. [Online]. Available: http://www.siepel.com/PDFS/83_BROADBAND_PYRAMIDAL_ABSORBER_HYFRAL_APM_-_12.02.08.pdf.
- [49] "Bundesministerium fuer Verkehr Bau und Stadtentwicklung," 2009.

- [50] D. A. Frickey, "Conversions Between S, Z, Y, h, ABCD, and T Parameters which are Valid for Complex Source and Load Impedances," *IEEE Transactions on Microwave Theory and Techniques*, vol. 42, pp. 205-211, Feb 1994.
- [51] SCHWARZBECK MESS ELEKTRONIK, "Antenna pattern for Double Ridged Broadband Horn Antenna BBHA 9120 LFA 0.7 - 6 GHz,," [Online]. Available: <http://www.schwarzbeck.de/Datenblatt/k9120lf.pdf>. [Accessed 20 Feb 2011].
- [52] M. Hiebel, "Vector Network Analyzer (VNA) Calibration: The Basics," Rohde&Schwarz USA, 2008.
- [53] M. Nakhkash, Y. Huang, W. Al-Nuaimy and M. Fang, "An improved calibration technique for free-space measurement of complex permittivity," *IEEE Trans. Geo. Remote Sensing*, vol. 39, pp. 453-455, February 2011.
- [54] D. Stolhofer, Yaqiang Liu, H. Doecke and P.O'Leary, "RF Propagation Through Transparent Conductors In Energy Efficient Windows," in *European Wireless Conference*, Lucca, Italy, 2010.
- [55] N. Knauer, "Investigation of the Physical Effects when Electromagnetic Waves pass through various Window Types," Germany, 2006.
- [56] R. Gordon, "Criteria for Choosing Transparent Conductors," *MRS Bulletin*, vol. 25, p. 52, August 2000.
- [57] Yaqiang Liu, Praveen Munjampally and P.O'Leary, "Broadband Wireless Propagation through Various Building Materials," in *Royal Irish Academy*, Dublin, 2010.
- [58] Yaqiang Liu, Paul O'Leary, "Broadband wireless access in an energy efficient environment," in *ET Colloquium on Antennas, Wireless and Electromagnetics*, Loughborough, UK, 2013.

- [59] Yaqiang Liu, Paul O'Leary, "Material Moisture Analysis using DC Techniques and Wireless Propagations," in *IEEE International workshop on Electromagnetics: Applications and Student Innovation Competition*, Taipei, Taiwan, 2011.
- [60] "All About Glass," [Online]. Available: <http://www.cmog.org/research/all-about-glass>. [Accessed 22 2014].
- [61] J. C. M. Garnett, "Colors in metal glasses and metal films," *Trans. Roy. Soc.*, vol. 53, pp. 385-420, 1904.
- [62] D. A. G. Bruggeman, "Berechnung verschiedener physikalischer Konstanten von heterogenen Substanzen. I. Dielektrizitätskonstanten und Leitfähigkeiten der Mischkörper aus isotropen Substanzen," *Ann. Phys.*, pp. 636-664, 1935.
- [63] Russell Hornung, insertion Loss and Loss tangent, Arlon: Magnetic for electronic division.
- [64] D Ravindera, Corresponding D Ravinder, G.Ranga Mohan, Prankishan, Nitendarkishan, D.R Sagar, "High frequency dielectric behaviour of aluminium-substituted lithium ferrites," *Materials Letters*, vol. 44, no. 3-4, pp. 256-260, 2000.
- [65] UC Hasar, J José Barrosoc, Y Kayad, M Ertugrulb, M Butea, "Reference-plane invariant transmission-reflection method for measurement of constitutive parameters of liquid materials," *Sensors and Actuators A: Physical*, vol. 203, pp. 346-354, 2013.
- [66] M. R.-V. a. E. Martín, "Contribution to numerical methods for calculation of complex dielectric permittivities," *Electronics letters*, vol. 6, p. 510, August 1970.
- [67] C. Kittel, *Introduction to Solid State Physics*, 6th, Ed., New York: John Wiley, 1986, p. 185.
- [68] J. Singh, *Physics of Semiconductors and Their Heterostructures*, New York: McGraw-Hill, 1993.

- [69] W. Stone, "Electromagnetic Signal Attenuation in Construction Materials," *NIST Construction Automation Program Report No.3*, 1997.
- [70] C. G. Granqvist, in *Transparent conductors as solar energy materials: A panoramic review*, vol. 91, 2007, pp. 1529-1598.
- [71] H. Fröhlich, *Theory of dielectrics : dielectric constant and dielectric loss*, Oxford: Clarendon, 1958.
- [72] WF Hoon, SP Jack, MFA Malek, N Hasssan, "Alternatives for PCB Laminates: Dielectric Properties' Measurements at Microwave Frequencies," Malaysia, 2012.
- [73] C.A.Balanis, *Advanced Engineering Electromagnetics*, Third ed., New York: Wiley, 1989.
- [74] U. C. Hasar, "Thickness-independent complex permittivity determination of partially filled thin dielectric materials into rectangular waveguide," *Progress In Electromagnetics Research*, pp. 189-203, 2009.